Area, Cost and Resilience Targets for Heat Exchanger Networks

Thesis by

Richard Dale Colberg

In Partial Fulfillment of the Requirements

for the Degree of

Doctor of Philosophy

California Institute of Technology

Pasadena, California

1989

(Submitted April 25, 1989)

Dedicated to Mom and Dad, with love.

Acknowledgements

Several people have assisted me during the course of this research. I would like to thank my advisor, Professor Manfred Morari, for his guidance and support; Professor Ignacio Grossmann, of Carnegie Mellon University, for his advice (especially during my job search) and for permission to use the computer program MAGNETS; and Dr. Truls Gundersen, of Norsk Hydro, for his valuable insight and suggestions. I would also like to thank Stratos Pistikopoulos, who has since graduated, for allowing me to stay at his apartment while I visited Carnegie Mellon in November, 1987. Many thanks to Phillipe Engel who, during his sixteen months at Caltech, revamped and debugged much of RESHEX, and who significantly improved the synthesis algorithms in RESHEX. Thanks also to Professor Y. A. Liu, of Virginia Tech, who introduced me to heat exchanger network synthesis, and process synthesis in general. And last, but certainly not least, many thanks to Alok Saboo for the opportunity to spend some time contributing to several of his papers and to RESHEX.

I also appreciate the many friends, postdocs and fellow students in the research group for their comraderie and mutual support. Thanks to Tony Skjellum for the killer croquet games (I still owe you one!); Henrik Andersen, Marc Gelormino and Tony for the late night pinball games; Lionel Laroche, Jay Lee, Tony and Henrik for their late night company, and for lunches at the Ath; Chris and Linda Webb for the Thanksgiving and Christmas dinners; Tyler Holcomb for the interesting (and not too loud) discussions of neural networks; Pete Campo and Frank Doyle for their help with the VAX; and Dan Laughlin for the interesting accounts of his many trips up Mt. Whitney.

Lastly, I wish to thank Caltech and the National Science Foundation for their financial support.

Abstract

This thesis presents improved area and capital cost targets for synthesis of heat exchanger networks (HEN) for fixed operating conditions, and a new resilience target for synthesis of HENs for changing, uncertain operating conditions. In addition, methods are presented to predict, before synthesis, the trade-off between cost and resilience.

A pair of "transshipment" nonlinear programs (NLP) is formulated to calculate the area and capital cost targets for HEN synthesis with unequal heat transfer coefficients and different capital cost laws (for different materials of construction, pressure ratings, etc.) when there are constraints on the number of matches, forbidden matches, and required matches with specified areas (for revamp synthesis). With these NLPs, the trade-off between area and number of units can be evaluated before synthesis. In addition to the targets themselves, solution of the NLPs yields "ideal" temperature profiles (much like the composite curves) for a HEN achieving the targets, and a selection of stream matches and their heat loads which provide an excellent starting point for synthesis of HENs achieving (within a few percent) the area and capital cost targets.

For changing or uncertain operating conditions, a Class 1 resilience target is presented which predicts, given the nominal operating conditions, the largest uncertainty range for which a "practical" HEN (with few more units and stream splits than that required for nominal conditions) can be synthesized. This resilience target also predicts whether trade-offs (in utilities, number of units, or size of uncertainty range) must be made to achieve resilience, and the operating condition and constraint most likely to limit resilience.

A nonlinear program is formulated to calculate the Class 1 HEN resilience target. Trade-offs with minimum approach temperature, utility consumption, and nominal network area are presented. The use of the Class 1 resilience target as a synthesis tool is discussed.

Finally, a simple procedure to predict the trade-off between cost and resilience is introduced so that a process engineer can design for an economically "optimal" amount of resilience.

Contents

List of Figures

List of Tables

Chapter 1

Introduction

1.1 HEN Synthesis Targets

This thesis presents improved area and capital cost targets for synthesis of heat exchanger networks (HEN) for fixed operating conditions, and a resilience target for synthesis of HENs for varying operating conditions. In addition, the use of synthesis targets to predict the trade-off between HEN cost and resilience is presented.

Targets are used in several synthesis areas, including control system synthesis (Morari, 1983) as well as in HEN synthesis. In general, synthesis targets give the process engineer a goal for the best cost or performance achievable for a given synthesis task if all possible design alternatives were to be considered. These targets are a function of the problem specification itself and not of any particular design, and can be calculated before any synthesis work begins. The use of synthesis targets has at least two attractive features:

- Targets allow absolute evaluation of a design with respect to the target itself, in addition to relative evaluation between alternative designs.

- Targets can simplify the search for optimal and reasonable near-optimal designs.

In HEN synthesis, research has been performed by numerous investigators since the late 1960's (Gundersen and Naess, 1988). One key result of this research has been the development of synthesis targets (for fixed operating conditions) to predict:

- minimum utilities, for a specified minimum approach temperature ΔT_m (Hohmann, 1971; Raghavan, 1977; Linnhoff and Flower, 1978; Umeda *et al.*, 1978; Papoulias and Grossmann, 1983; Cerda *et al.*, 1983; O'Young *et al.*, 1988)

- minimum number of units for specified utilities, independent of area (Hohmann, 1971; Cerda and Westerberg, 1983; Papoulias and Grossmann, 1983)

- minimum network area for specified utilities, independent of the number of units (Hohmann, 1971; Nishida *et al.*, 1971; Raghavan, 1977; Nishimura, 1980; Townsend and Linnhoff, 1984)

With these targets, the process engineer can predict the trade-offs between utilities and area, and utilities and number of units (solid lines in Fig. 1.1), and thus roughly predict the trade-off between capital and operating costs (Ahmad and Linnhoff, 1984).

Unfortunately, with existing methods to calculate the HEN synthesis targets, the trade-off between area and number of units cannot be predicted; in addition, the area target cannot be accurately calculated for problems with unequal heat transfer coefficients, except in certain special cases. Chapter 2 presents nonlinear programming

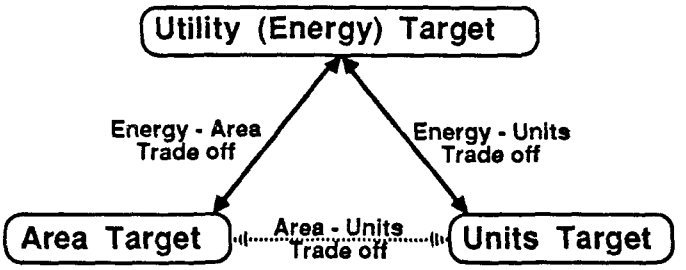

Figure 1.1: Trade-offs between the HEN design targets for minimum utilities, area, and number of units.

(NLP) formulations which can be used to predict the trade-off between area (or capital cost) and the number of units, and the effect of forbidden matches on the area (or capital cost) target (dashed line in Fig. 1.1). With constraints to require the presence of selected matches with specified areas, these NLPs also give area and capital cost targets for revamp synthesis. In addition, with these NLPs, the area and cost targets can be accurately calculated even with unequal heat transfer coefficients.

The economic targets (for minimum utilities, area, and number of units) are valuable tools for synthesizing an optimal network for *fixed* design conditions. However, it is unlikely that a HEN will operate under exactly the conditions for which it is designed, and in fact it is likely to operate under varying operating conditions. Thus a practical HEN should be *resilient* (able to operate in a range of conditions) as well as economically optimal. Chapter 3 reviews recent developments in the analysis and synthesis of resilient HENs. Chapter 4 presents a resilience target which predicts, given the nominal operating conditions, the largest range of operating conditions for which a "practical" HEN (with few more units and stream splits than that required for nominal operating conditions) can be synthesized. This target predicts whether a

resilient HEN can be synthesized for a given operating range, or if trade-offs must be made in utilities, number of units, or resilience. Calculation of the resilience target also identifies the critical operating condition and constraint (e.g., ΔT_m in a particular stream match) most likely to limit resilience.

The resilience target in Chapter 4 relies on a given value (or range) of ΔT_m. The economically optimal value of ΔT_m varies with operating conditions, and ideally should consider the cost of resilience, as well as the cost of not being resilient (e.g., lost production, off-spec product, etc.). However, the optimal range of ΔT_m is difficult to evaluate *a priori* (before calculating the resilience target). Chapter 5 presents a different method for predicting the trade-off between cost and resilience which does not rely on ΔT_m, but instead on HEN area. Finally, Chapter 6 presents conclusions and suggestions for future research.

RESHEX, a computer-aided design package for the synthesis and analysis of resilient HENs (Saboo *et al.*, 1986a,b), has been used to work many examples in this research, to provide initial insight while developing the new area and resilience targets, and to predict the resilience–cost trade-off. During the course of this research, the area targeting and network optimization sections of RESHEX have been completely rewritten; the HEN synthesis algorithms improved; many, many bugs fixed; and the memory and CPU-time requirements reduced. New user's and programmer's guides for RESHEX are available (Colberg and Morari, 1989a,b).

1.2 References

[1] Ahmad, S. and B. Linnhoff, Overall Cost Targets for Heat Exchanger Networks, paper presented at *IChemE Ann. Res. Mtg.*, Bath, U. K. (1984).

[2] Cerda, J. and A. W. Westerberg, Synthesizing Heat Exchanger Networks Having Restricted Stream/Stream Matches Using Transportation Problem Formulations, *Chem. Eng. Sci.*, **38**, 1723 (1983).

[3] Cerda, J., A. W. Westerberg, D. Mason and B. Linnhoff, Minimum Utility Usage in Heat Exchanger Network Synthesis: A Transportation Problem, *Chem. Eng. Sci.*, **38**, 373 (1983).

[4] Colberg, R. D. and M. Morari, RESHEX 1.0 User's Guide, Calif. Inst. of Tech., Pasadena, CA (1989a).

[5] Colberg, R. D. and M. Morari, RESHEX 1.0 Programmer's Guide, Calif. Inst. of Tech., Pasadena, CA (1989b).

[6] Gundersen, T. and L. Naess, The Synthesis of Cost Optimal Heat Exchanger Networks—An Industrial Review of the State of the Art, *Comp. Chem. Eng.*, **12**, 503 (1988).

[7] Hohmann, E. C., Optimum Networks for Heat Exchange, Ph.D. Thesis, Univ. Southern California, Los Angeles (1971).

[8] Linnhoff, B. and J. R. Flower, Synthesis of Heat Exchanger Networks: I. Systematic Generation of Energy Optimal Networks, *AIChE J.*, **24**, 633 (1978).

[9] Morari, M., Design of Resilient Processing Plants—III. A General Framework for the Assessment of Dynamic Resilience, *Chem. Eng. Sci.*, **38**, 1881 (1983).

[10] Nishida, N., S. Kobayashi and A. Ichikawa, Optimal Synthesis of Heat Exchange Systems: Necessary Conditions for Minimum Heat Transfer Area and Their Application to Systems Synthesis, *Chem. Eng. Sci.*, **26**, 1841 (1971).

[11] Nishimura, H., A Theory for the Optimal Synthesis of Heat Exchanger Systems, *J. Opt. Th. Appl.*, **30**, 423 (1980).

[12] O'Young, D. L., D. M. Jenkins and B. Linnhoff, The Constrained Problem Table for Heat Exchanger Networks, *Understanding Process Integration II*, IChemE Symp. Ser. 109, 75 (1988).

[13] Papoulias, S. A. and I. E. Grossmann, A Structural Optimization Approach in Process Synthesis—II. Heat Recovery Networks, *Comp. Chem. Eng.*, **7**, 707 (1983).

[14] Raghavan, S., Heat Exchanger Network Synthesis: A Thermodynamic Approach, Ph.D. Thesis, Purdue Univ., Lafayette, IN (1977).

[15] Saboo, A. K., M. Morari and R. D. Colberg, RESHEX: An Interactive Software Package for the Synthesis and Analysis of Resilient Heat Exchanger Networks—I. Program Description and Application, *Comp. Chem. Eng.*, **10**, 577 (1986a).

[16] Saboo, A. K., M. Morari and R. D. Colberg, RESHEX: An Interactive Software Package for the Synthesis and Analysis of Resilient Heat Exchanger Networks—II. Discussion of Area Targeting and Network Synthesis Algorithms, *Comp. Chem. Eng.*, **10**, 591 (1986b).

[17] Townsend, D. W. and B. Linnhoff, Surface Area Targets for Heat Exchanger Networks, paper presented at *IChemE Ann. Res. Mtg.*, Bath, U. K. (1984).

[18] Umeda, T., J. Itoh and K. Shiroko, Heat Exchange System Synthesis, *Chem. Eng. Prog.*, **74**, 7, 70 (July 1978).

Chapter 2

Area and Capital Cost Targets for Heat Exchanger Networks with Constrained Matches and Unequal Heat Transfer Coefficients

2.1 Introduction

The typical heat exchanger network (HEN) synthesis problem (for fixed design conditions) can be stated as follows:

> For n_h hot streams (to be cooled) and n_c cold streams (to be heated)—with given supply temperatures, target temperatures, heat capacities, flow rates and film heat transfer coefficients—synthesize the HEN with least total (capital plus operating) cost.

To minimize total cost, the "ideal" procedure for solving this synthesis problem should consider all capital cost factors [heat transfer area, number of units (exchangers, heaters and coolers), materials of construction, etc.] and all operating cost factors [types and amount of utilities] *simultaneously.* However, synthesis and sizing of a HEN is a large, combinatorial, nonlinear problem. Because of these difficulties, the ideal synthesis procedure is intractable with current solution methods.

To make the HEN synthesis problem tractable, it is generally decomposed into three steps: (1) minimize utility consumption for given problem data and a given value of minimum approach temperature (ΔT_m); (2) synthesize a minimum-unit HEN structure satisfying minimum utility consumption; and (3) minimize the total area of the synthesized structure. However, this decomposition does *not* necessarily minimize total cost—it does not consider trade-offs between utility consumption, number of units and network area.

Fortunately, in HEN synthesis, design targets area available to guide the process engineer at each of these three steps. Targets are available (for fixed design conditions) to predict, before synthesis, and solely from the problem data:

- minimum utilities, for a specified ΔT_m (Hohmann, 1971; Raghavan, 1977; Linnhoff and Flower, 1978; Umeda *et al.*, 1978; Papoulias and Grossmann, 1983; Cerda *et al.*, 1983; O'Young *et al.*, 1988)

- minimum number of units for specified utilities, independent of area (Hohmann, 1971; Cerda and Westerberg, 1983; Papoulias and Grossmann, 1983)

- minimum network area for specified utilities, independent of the number of units (Hohmann, 1971; Nishida *et al.*, 1971; Raghavan, 1977; Townsend and Linnhoff, 1984)

By varying the value of ΔT_m used for utility targeting and recalculating the units and area targets, the trade-offs between utilities and area, and utilities and number of units, can be predicted (solid lines in Fig. 1.1). Thus the trade-off between capital and operating costs can be roughly predicted before synthesis (Ahmad and Linnhoff, 1984).

In addition, the composite temperature-enthalpy curves provide a model for the ideal temperature profiles in a HEN with equal heat transfer coefficients (cf., temperature driving force plots: Linnhoff and Vredeveld, 1984). If a HEN is synthesized where the temperature profiles of all the hot (cold) streams exactly follow the hot (cold) composite curve, then the HEN will achieve the utility and area targets. However, with a practical number of units, the temperature profiles in the HEN can only approximate the composite curves, and the area target can generally be approached only within a few percent if the utility target is to be met.

There are two difficulties with existing methods to calculate these HEN design targets. First, they cannot consider the trade-off between area and number of units (dashed line in Fig. 1.1). In particular, the area targeting methods—and the composite curves upon which they are based—cannot consider forbidden stream matches or constraints upon the number of units. Second, current area targeting methods cannot rigorously handle unequal heat transfer coefficients except in special cases.

The most common *approximate* method for handling unequal heat transfer coefficients is to modify the area target which is based on the composite curves (Townsend and Linnhoff, 1984). However, this method assumes completely countercurrent stream matching ("vertical" matching on the composite curves), which gives true minimum area only when the heat transfer coefficients are equal. Thus it may overestimate the area target when the heat transfer coefficients are quite different.

Using calculus of variations, Nishimura (1980) developed a rigorous area target for the special case of one hot and several cold streams (or vice versa). Nishimura showed that this area target could be achieved by complex networks in which the approach temperatures are proportional to the square root of the film heat transfer coefficients. Ahmad (1985) extended Nishimura's method to any number of multiple hot and cold streams by assuming that the approach temperatures should be proportional to the square root of the *overall* heat transfer coefficients. However, Ahmad's extension is not rigorous.

Saboo *et al.* (1986) attempted to rigorously treat unequal heat transfer coefficients among any number of hot and cold streams by dividing the area targeting problem into temperature intervals (TI) and formulating a sequence of linear programs (LP). The size of the TIs was decreased from one LP to the next until the area target converged. In practice, however, the number of TIs tended to become prohibitively large before the algorithm converged.[1]

[1]As pointed out to us by Art Westerberg, an alternate approach is to divide each stream into equal-sized elements of heat, and to formulate an ***assignment*** LP to assign heat transfer from each element of heat in a hot stream to an element of heat in a cold stream. This LP can also become very large depending upon the number and size of the heat elements, but assignment LPs can be solved very quickly (compared to the Simplex algorithm used to solve general LPs). This method would be an extension of the early work of Kesler and Parker (1969), Kobayashi *et al.* (1971) and Cena

This chapter presents a pair of nonlinear programs (NLP) to calculate the area target [based on simple countercurrent heat exchangers sized using logarithmic mean temperature differences (ΔT_{LM})] and capital cost target for HEN synthesis problems (for fixed design conditions) given any specified number or set of matches, with different heat transfer coefficients and cost laws (for different materials of construction, pressure ratings, etc.) for each stream match. These NLPs can predict the trade-off between area/cost and number of matches (units), and the effect of forbidden matches upon minimum area/cost. In fact, the cost target considers the optimal distribution of area among the given number or set of matches, rather than assuming an equal distribution of area among all matches (commonly done with current capital cost targeting methods). With constraints to require the presence of selected matches with specified areas, these NLPs also give area and cost targets for revamp synthesis.

To handle unequal heat transfer coefficients, these NLPs merely assume that the area target can be determined by dividing the problem into a finite number of enthalpy intervals (EI). In practice, the number of intervals is very reasonable (roughly twice the number of streams).

In addition to the area or cost target itself, solution of either NLP gives temperature profiles for each stream (much like the composite curves), and a distribution of heat loads and areas among specific matches. By following the temperature profiles given by the area targeting NLP, a HEN can be synthesized which achieves the area

et al. (1977) to synthesize minimum cost HENs. However, this approach cannot be easily extended to area targets for a given number of matches [since, with the introduction of binary variables to count the number of matches, one can no longer take advantage of assignment LP], or to capital cost targets [since summing the capital cost attributed to each element of heat would not consider the economy of scale (i.e., the fact that one large exchanger with area A is less expensive than many small exchangers with the same total area)].

target. But to precisely follow the temperature profiles and thus exactly achieve the area target, many exchangers may be required to represent each stream match.

In general, the area and cost targets can be approached within a few percent with a HEN where each match in the NLP solution is represented by a *single* exchanger. (In fact, the cost target assumes that the area of each match is lumped into a single exchanger.) We show that it is always possible to synthesize a HEN with a one-to-one correspondence between the units and their loads in the HEN and the matches and their loads in the NLP solution. The matches and loads given by the NLPs provide an excellent starting point for synthesis of HENs with a given number of units and achieving within a few percent the area and cost targets.

2.2 Simple Area Target Based on the Composite Curves

The composite temperature-enthalpy curves form the basis for a simple area targeting method which is rigorous when the heat transfer coefficients are equal, and which gives reasonably accurate area targets when the heat transfer coefficients are similar (Townsend and Linnhoff, 1984). The composite curves also provide valuable physical insight into the properties of minimum-area HENs when no constraints are placed upon stream matches. In this section, we review the simple area target based on the composite curves. In later sections, we use the insight provided by the composite curves to formulate the area and cost targeting NLPs.

Consider the stream data given in Table 2.1. For the specified ΔT_m of 10 K, the

Table 2.1: Stream data for Example 2.1.

Stream	*Supply Temperature* (K)	*Target Temperature* (K)	*Heat Capacity Flow Rate* (kW/K)	*Film Heat Transfer Coefficient* ($kW/m^2 K$)
H1	395	343	4.0	2.0
H2	405	288	6.0	0.2
C1	293	493	5.0	2.0
C2	353	383	10.0	0.2
Steam	520	520		2.0
Water	278	288		2.0

$\Delta T_m = 10$ K (for utility targeting).

heating and cooling targets are 620 and 230 kW, respectively. The composite curves for these stream data are shown in Fig. 2.1. This diagram can be divided into seven enthalpy intervals (EI), one under each piecewise linear segment of the composite curves. Two EIs (1.1–1.2) involve heating utility, four EIs (2.1–4.2) involve process heat exchange, and one EI (5.1) involves cooling utility. The solid lines in Fig. 2.1 indicate EI boundaries associated with stream supply temperatures; the dashed lines indicate boundaries associated with target temperatures.

A HEN structure corresponding to these composite curves is shown in Fig. 2.2. Each section of this HEN corresponds to a specific EI in the composite curve diagram, and stream temperatures between HEN sections match those of the composite curves between EIs. Within each HEN section, exchangers are placed in parallel on branches of stream splits; the individual exchanger loads and branch flow rates are chosen to achieve isothermal mixing.

This HEN structure exhibits completely countercurrent stream matching; that is, the temperature profiles of all the hot (cold) streams in the HEN structure follow the temperature profile of the hot (cold) composite curve. Thus if the film heat

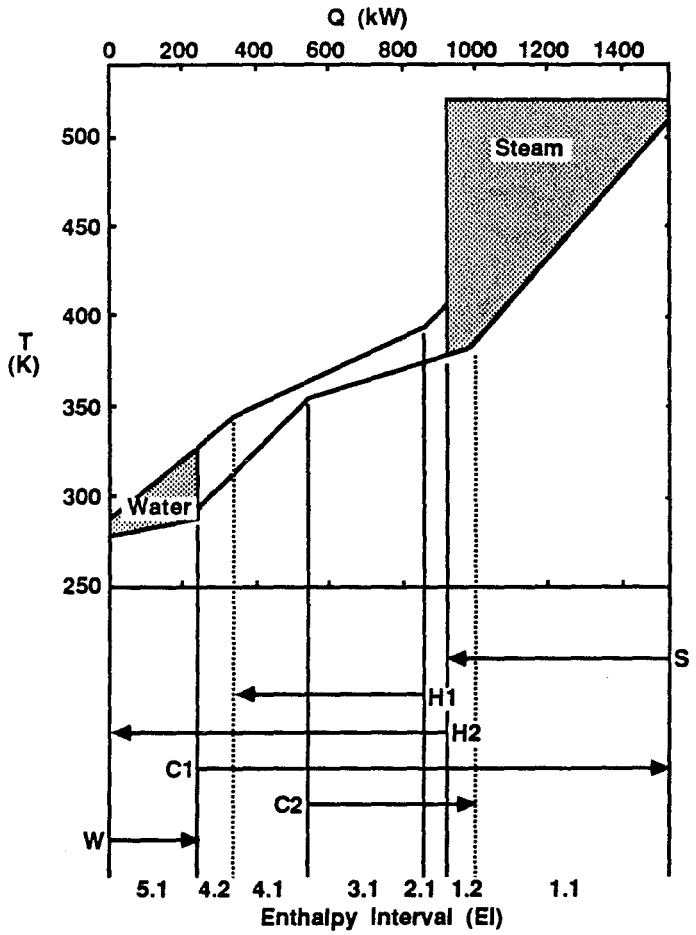

Figure 2.1: Composite curves used to calculate the area target in Section 2.2.

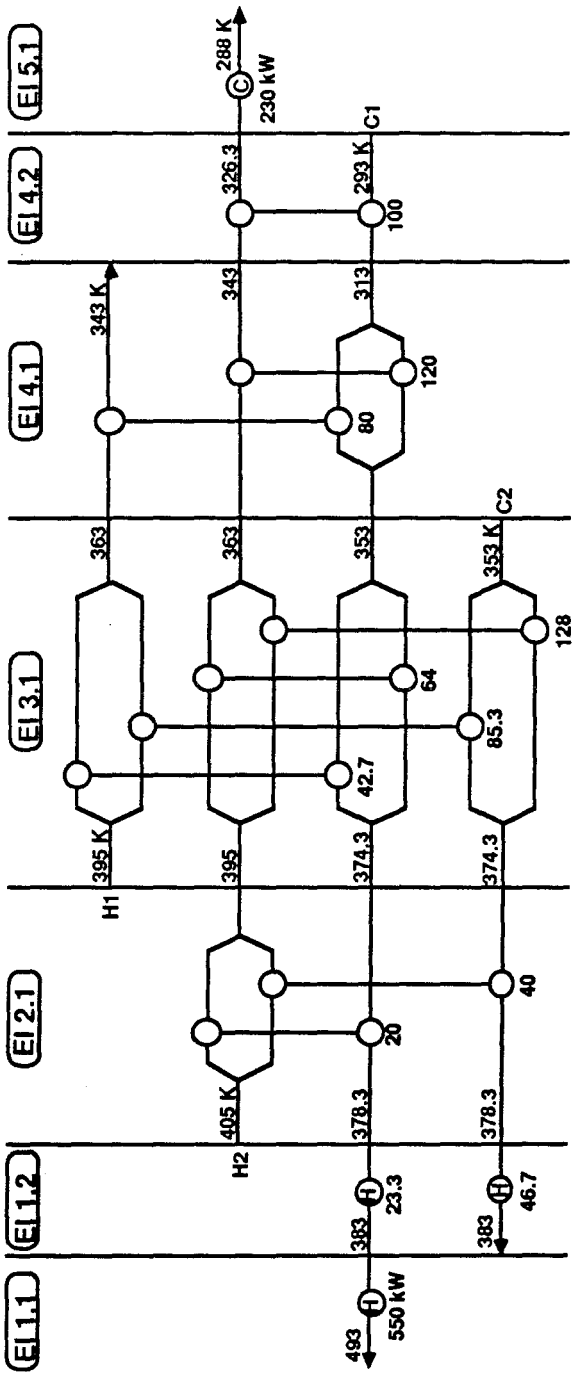

Figure 2.2: Completely countercurrent stream splitting HEN structure (spaghetti structure) represented by the composite curves in Fig. 2.1.

transfer coefficients are equal for all streams, this structure achieves the minimum network area required for the given problem data. The area target is simply the total area required by this or any other completely countercurrent structure (such as an infinitely cyclic HEN structure). Even if the heat transfer coefficients differ somewhat, this network provides a reasonable approximation for the area target.

This type of structure corresponding to the composite curves has been called a "spaghetti" structure by Linnhoff and co-workers. By combining the area calculations for this spaghetti structure into a single algebraic formula, the area target can be calculated directly from the composite curves (Townsend and Linnhoff, 1984):

$$\begin{aligned} A^* &= \sum_{i,j,k} \left(\frac{1}{h_i} + \frac{1}{h_j} \right) \frac{q_{i,j,k}}{\Delta T_{\mathrm{LM}_k}} \\ &= \sum_k \frac{1}{\Delta T_{\mathrm{LM}_k}} \left(\sum_i \frac{q_{i,k}}{h_i} + \sum_j \frac{q_{j,k}}{h_j} \right) \end{aligned} \tag{2.1}$$

where $q_{i,j,k}$ is the amount of heat transferred from hot stream $\mathrm{S_{hi}}$ to cold stream $\mathrm{S_{cj}}$ in EI k, $q_{i,k} = \sum_j q_{i,j,k}$ and $q_{j,k} = \sum_i q_{i,j,k}$ are the total amounts of heat transferred by hot stream $\mathrm{S_{hi}}$ and cold stream $\mathrm{S_{cj}}$ in EI k, h_i and h_j are the film coefficients for streams $\mathrm{S_{hi}}$ and $\mathrm{S_{cj}}$, and ΔT_{LM_k} is the logarithmic mean temperature difference for any pair of streams in EI k. Note that since the temperatures of all the hot and cold streams follow the same profiles, ΔT_{LM} is the same for all stream pairs in each EI.

The full complexity of the spaghetti structure is not really required to achieve the area target. For example, in EI 3.1 in Fig. 2.2, the heat exchanger matching streams $\mathrm{S_{h1}}$ and $\mathrm{S_{c1}}$ can be eliminated by shifting 42.7 kW of heating load around the four exchangers in the EI. However, after this load shift, the same *total* amount of heat

is transferred to and from each stream as before, and the stream temperatures at the hot and cold ends of the EI are unaffected (hence ΔT_{LM} is unaffected). (Only the individual exchanger loads are affected, and the stream split fractions changed to preserve isothermal mixing.) Thus, by applying equation 2.1 to EI 3.1, we see that the total area in the EI does not change. In this manner, exchangers can be eliminated from the spaghetti structure without affecting the area target until a minimum number of units (number of streams + number of utilities − 1) is used in each EI.

2.3 Transshipment Models for HEN Design Targets

Papoulias and Grossmann (1983) developed a pair of linear transshipment models to target the minimum utilities and minimum number of units required to synthesize a HEN. The utility targeting model is essentially a linear programming (LP) implementation of the problem table algorithm of Linnhoff and Flower (1978). The units targeting model is a mixed-integer linear programming (MILP) extension of the utility targeting LP where binary variables are added to count the number of stream matches. Floudas *et al.* (1986) showed that the number of matches counted by the MILP is the units target. In this section, we review the formulation of the utility targeting LP and units targeting MILP. The area and cost targeting NLPs presented later are extensions of these linear transshipment models.

In order to formulate the utility targeting LP, the problem is divided into a series of temperature intervals (TI), where each TI boundary temperature T_l corresponds to

a hot stream supply temperature or to a cold stream supply temperature plus ΔT_m. This division ensures feasible heat transfer (approach temperature $\geq \Delta T_m$) between all hot and cold streams in each TI, and from each hot stream in a TI to all cold streams in colder TIs.

(Note that in order to simplify the area targeting NLP presented later, we choose *not* to shift stream temperatures before defining the TIs. Instead, we essentially maintain two temperature scales for the TI boundaries: hot streams crossing a TI boundary must be hotter than boundary temperature T_l, and cold streams crossing a TI boundary must be colder than $T_l - \Delta T_m$.)

Let T_l be the temperature of the TI boundary at the *cold* end of TI l. Then the following index sets can be defined:

$$
\begin{aligned}
I &= \{i | \mathrm{S_{hi}} \text{ is a hot stream}\} \\
J &= \{j | \mathrm{S_{cj}} \text{ is a cold stream}\} \\
S &= \{s | s \text{ is a hot utility}\} \\
W &= \{w | w \text{ is a cold utility}\} \\
L &= \{l \in (1, 2, \ldots, l_{\max}) | l \text{ is a temperature interval}\} \\
I_l &= \{i \in I | \text{hot stream } \mathrm{S_{hi}} \text{ occurs in or can cascade heat to TI } l\} \\
&= \{i \in I | T_i^S \geq T_{l-1}\} \\
J_l &= \{j \in J | \text{cold stream } \mathrm{S_{cj}} \text{ occurs in TI } l\} \\
&= \{j \in J | T_j^S \leq T_l\} \\
S_l &= \{s \in S | \text{hot utility } s \text{ occurs in or can cascade heat to TI } l\} \\
&= \{s \in S | T_s^S \geq T_{l-1}\} \\
W_l &= \{w \in W | \text{cold utility } w \text{ occurs in TI } l\} \\
&= \{w \in W | T_w^S \leq T_l\} \\
M_{i,j} &= \{(i,j) | i \in I,\ j \in J,\ \mathrm{S_{hi}}\text{–}\mathrm{S_{cj}} \text{ match is allowed (not forbidden)}\} \\
M_{s,j} &= \{(s,j) | s \in S,\ j \in J,\ s\text{–}\mathrm{S_{cj}} \text{ match is allowed (not forbidden)}\} \\
M_{i,w} &= \{(i,w) | i \in I,\ w \in W,\ \mathrm{S_{hi}}\text{–}w \text{ match is allowed (not forbidden)}\}
\end{aligned}
$$

The utility targeting LP is based on a heat cascade from each TI to the next

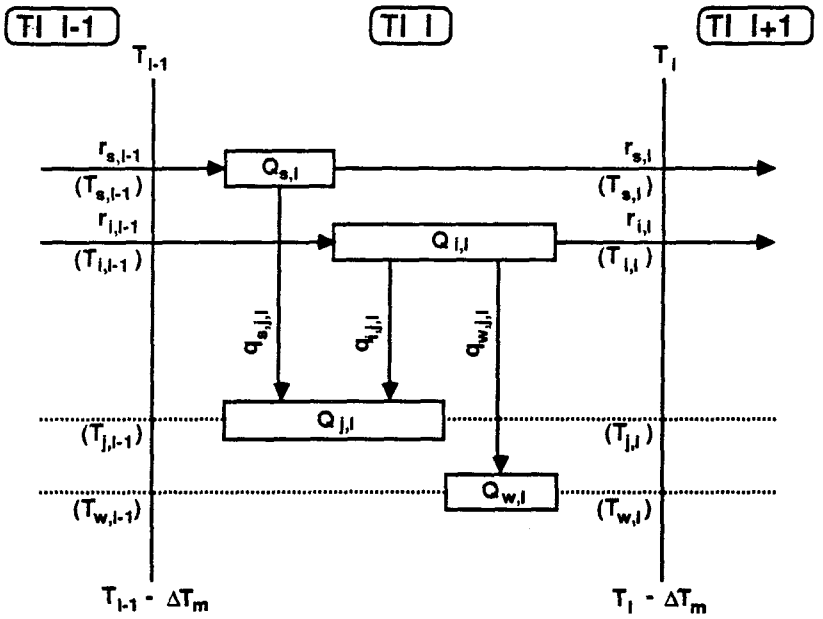

Figure 2.3: Typical temperature interval (TI) for the utility targeting transshipment LP.

colder TI. Figure 2.3 shows a typical TI in the cascade. Heat is transferred from hot streams and utilities to cold streams and utilities in the TI, where $q_{i,j,l}$ is the amount of heat transferred from hot stream S_{hi} to cold stream S_{cj} in TI l, and $q_{s,j,l}$ (and $q_{i,w,l}$) are the amounts of heat transferred from hot utility s to cold stream S_{cj} (and from hot stream S_{hi} to cold utility w) in the TI. Excess heat from the hot streams and utilities is cascaded to the next colder TI via residuals $r_{i,l}$ and $r_{s,l}$. Residual (untransferred) heat causes the temperature of a hot stream crossing a TI boundary to be hotter than the TI boundary temperature:

$$T_{i,l} = \max(T_l, T_i^T) + \frac{r_{i,l}}{w_i} \quad \text{for } i \in I_l,\ l \in L \tag{2.2}$$

Note that the cold streams do *not* cascade heat; thus when a cold stream crosses a TI boundary, its temperature must equal that of the TI boundary (minus ΔT_m):

$$T_{j,l} = \max(T_l - \Delta T_m, T_j^T) \quad \text{for } j \in J_l,\ l \in L \tag{2.3}$$

Within each TI, the heat content of each hot stream and utility is the amount of heat available for transfer before heat is cascaded; the heat content of each cold stream and utility is the amount of heat which can be received. The heat contents of the process streams can be determined from the TIs, before formulating the utility targeting LP, as follows (cf., Fig. 2.4):

$$\begin{aligned} Q_{i,l} &= w_i\,[\max(T_{l-1}, T_i^T) - \max(T_l, T_i^T)] && \text{for } i \in I_l,\ l \in L \\ Q_{j,l} &= w_j\,[\min(T_{l-1} - \Delta T_m, T_j^T) - \min(T_l - \Delta T_m, T_j^T)] && \text{for } j \in J_l,\ l \in L \end{aligned} \tag{2.4}$$

where w_i and w_j are the heat capacity flow rates of hot stream $\mathrm{S_{hi}}$ and cold stream S_{cj}. The heat contents of the utilities are determined by solution of the utility targeting LP:

$$\begin{aligned} Q_{s,l} &= m_s\,\Delta H_{s,k} && \text{for } s \in S_l,\ l \in L \\ Q_{w,l} &= m_w\,\Delta H_{w,k} && \text{for } w \in W_l,\ l \in L \end{aligned} \tag{2.5}$$

where m_s and m_w are the mass flow rates of hot utility s and cold utility w (variables in the LP), and $\Delta H_{s,l}$ and $\Delta H_{w,l}$ are the enthalpy changes of hot and cold utilities s and w in TI l (given parameters).

As an example, Fig. 2.4 shows a full heat cascade for the stream data in Table 2.1. However, for later comparison with an area targeting heat cascade where we relax ΔT_m, the TIs in this figure are based on a ΔT_m of 0.1 K. The amount of heating and

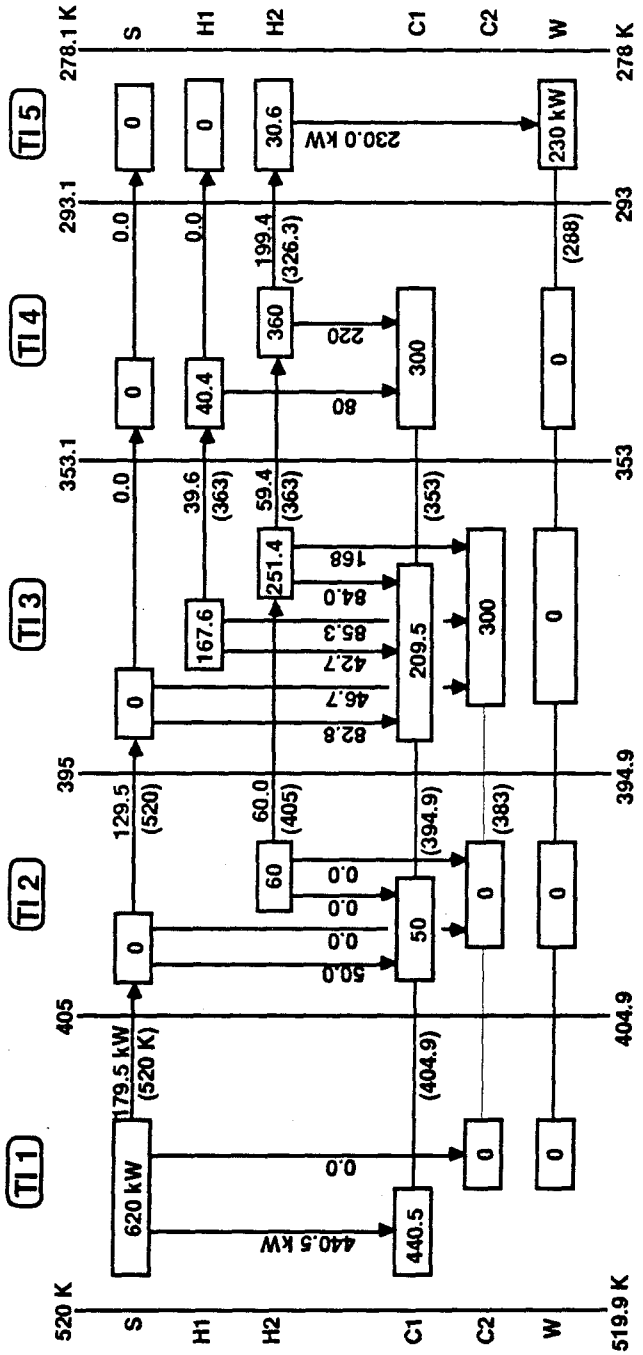

Figure 2.4: Heat cascade for the utility targeting transshipment LP (and the units targeting transshipment MILP).

cooling used correspond to the utility targets for $\Delta T_m = 10$ K.

The utility targeting LP minimizes the total utility cost where c_s and c_w are the unit costs of each hot and cold utility, subject to energy balances on each stream in each TI, where the variables are the utility mass flow rates m_s and m_w, the heat transfer rates $q_{i,j,l}$, $q_{s,j,l}$ and $q_{i,w,l}$, and residuals $r_{i,l}$ and $r_{s,l}$. The LP is formulated as follows:

$$\min \sum_{s \in S} c_s m_s + \sum_{w \in W} c_w m_w \qquad \textbf{(P1)}$$

subject to

(A) Energy balances on hot streams and utilities:

$$Q_{i,l} + r_{i,l-1} = \sum_{j \in (J_l \cup M_{i,j})} q_{i,j,l} + \sum_{w \in (W_l \cup M_{i,w})} q_{i,w,l} + r_{i,l} \quad \text{for } i \in I_l,\ l \in L$$

$$Q_{s,l} + r_{s,l-1} = \sum_{j \in (J_l \cup M_{s,j})} q_{s,j,l} + r_{s,l} \quad \text{for } s \in S_l,\ l \in L$$

where no residuals are cascaded to or from the ends of the heat cascade ($r_{i,0} = r_{i,l_{\max}} = 0$ and $r_{s,0} = r_{s,l_{\max}} = 0$), and no residuals are cascaded from TIs where a stream does not exist ($r_{i,l} = 0$ for $i \notin I_l$, and $r_{s,l} = 0$ for $s \notin S_l$).

(B) Energy balances on cold streams and utilities:

$$Q_{j,l} = \sum_{s \in (S_l \cup M_{s,j})} q_{s,j,l} + \sum_{i \in (I_l \cup M_{i,j})} q_{i,j,l} \quad \text{for } j \in J_l,\ l \in L$$

$$Q_{w,l} = \sum_{i \in (I_l \cup M_{i,w})} q_{i,w,l} \quad \text{for } w \in W_l,\ l \in L$$

(C) Nonnegative utility mass flow rates, heat transfer rates, and residuals:

$$
\begin{aligned}
m_s &\geq 0 \quad \text{for } s \in S \\
m_w &\geq 0 \quad \text{for } w \in W \\
q_{i,j,l} &\geq 0 \quad \text{for } i \in I_l,\ j \in J_l,\ l \in L,\ (i,j) \in M_{i,j} \\
q_{s,j,l} &\geq 0 \quad \text{for } s \in S_l,\ j \in J_l,\ l \in L,\ (s,j) \in M_{s,j} \\
q_{i,w,l} &\geq 0 \quad \text{for } i \in I_l,\ w \in W_l,\ l \in L,\ (i,w) \in M_{i,w} \\
r_{i,l} &\geq 0 \quad \text{for } i \in I_l,\ 1 \leq l < l_{\max} \\
r_{s,l} &\geq 0 \quad \text{for } s \in S_l,\ 1 \leq l < l_{\max}
\end{aligned}
$$

Note that with nonnegative residuals, ΔT_m is automatically satisfied because of the way the TIs are defined. Solution of the utility targeting LP gives the total utility cost, and—if there are multiple hot or cold utilities—the optimal utility distribution.

The MILP to target the minimum number of units is an extension of the utility targeting LP where constraints and binary variables are added to count the number of stream matches. The units targeting MILP minimizes the number of stream matches

$$
\min \sum_{(i,j)\in M_{i,j}} n_{i,j} + \sum_{(s,j)\in M_{s,j}} n_{s,j} + \sum_{(i,w)\in M_{i,w}} n_{i,w} \qquad \textbf{(P2)}
$$

where $n_{i,j} = 1$ if a match between hot stream $\mathrm{S_{hi}}$ and cold stream $\mathrm{S_{cj}}$ exists in any TI, and $n_{i,j} = 0$ if the match does not exist. (Similar comments apply to $n_{s,j}$ and $n_{i,w}$.)

The MILP is formulated subject to the following constraints, in addition to those of LP (P1):

(D) Existence of stream matches:

$$
\sum_{l\in L|(i\in I_l,\, j\in J_l)} q_{i,j,l} \leq Q_{i,j,\max}\, n_{i,j} \quad \text{for } (i,j) \in M_{i,j}
$$

$$\sum_{l \in L | (s \in S_l,\, j \in J_l)} q_{s,j,l} \;\leq\; Q_{s,j,\max}\, n_{s,j} \quad \text{for } (s,j) \in M_{s,j}$$

$$\sum_{l \in L | (i \in I_l,\, w \in W_l)} q_{i,w,l} \;\leq\; Q_{i,w,\max}\, n_{i,w} \quad \text{for } (i,w) \in M_{i,w}$$

(**E**) Binary variables:

$$\begin{aligned} n_{i,j} &= 0,1 \quad \text{for } (i,j) \in M_{i,j} \\ n_{s,j} &= 0,1 \quad \text{for } (s,j) \in M_{s,j} \\ n_{i,w} &= 0,1 \quad \text{for } (i,w) \in M_{i,w} \end{aligned}$$

where $Q_{i,j,\max}$, $Q_{s,j,\max}$ and $Q_{i,w,\max}$ are bounds on the maximum possible heat transfer in each match (which can be determined before formulating the MILP). Note that the logical constraint which determines the existence of matches between hot stream S_{hi} and cold stream S_{cj} forces $n_{i,j}$ to be one if $q_{i,j,l}$ is nonzero in any TI; otherwise, the minimization forces $n_{i,j}$ to be zero. (Similar comments apply to the constraints determining $n_{s,j}$ and $n_{i,w}$.)

Solution of the MILP gives the units target and a set of feasible matches satisfying the target. If the HEN synthesis problem is pinched, the units targeting MILP can be applied separately on each side of the pinch.

2.4 General Area Target (Transshipment NLP)

2.4.1 Formulation of the Area Targeting NLP

The utility targeting LP can be extended to formulate a nonlinear "transshipment" model for the area target. A basic requirement for the area targeting NLP is that it be able to reproduce the composite curve-based area target when the heat transfer coefficients are equal and when no constraints are placed upon stream matches.

However, the utility targeting heat cascade generally cannot represent the composite curves. For example, no matter how the heat loads and residuals are distributed in Fig. 2.4, this heat cascade cannot duplicate the composite curves in Fig. 2.1.

Figure 2.5 shows a heat cascade for the stream data in Table 2.1 (and a relaxed ΔT_m of 0.1 K) which does represent the composite curves (Fig. 2.1). To obtain this new heat cascade, two important extensions are required:

(1) As shown in Fig. 2.1, the stream supply *and target* temperatures divide the composite curves into distinct intervals—one interval for each piecewise linear segment of the composite curves. Thus to represent the composite curves and to reproduce the composite curve-based area target, the heat cascade must be divided into intervals at the stream target temperatures as well as at the supply temperatures.

(2) In the utility targeting cascade, heat is not cascaded by the cold streams or utilities. Thus as discussed in conjunction with equation 2.3, when a cold stream crosses a TI boundary its temperature must equal the boundary temperature [a cold stream supply (or target) temperature, or a hot stream supply (or target) temperature minus ΔT_m]. However, at an interval (EI) boundary on the composite curves (Fig. 2.1), a cold stream might not be at its supply or target temperature (or that of any other cold stream), and might not equal a hot stream supply or target temperature (minus ΔT_m). Thus, we must allow the cold streams and utilities to cascade heat so that their temperatures can vary at the interval boundaries. In particular, we allow the cold streams and utilities to cascade heat "deficits" (the ability to receive heat) from each TI to the next *hotter* TI.

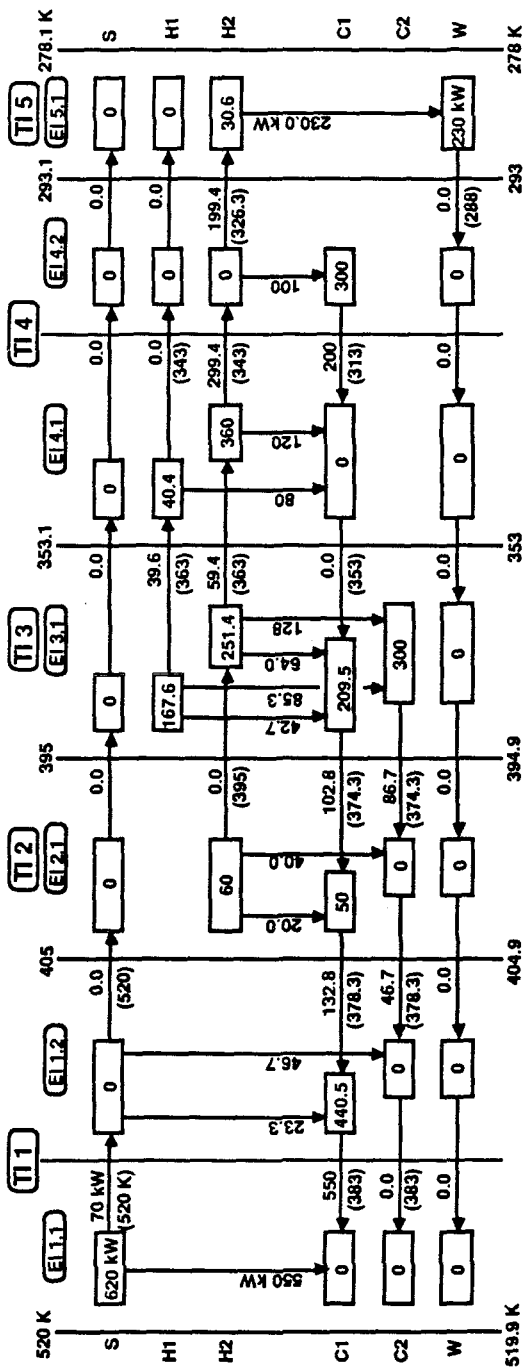

Figure 2.5: Heat cascade corresponding to the composite curves (Fig. 2.1).

Another difficulty is that the utility targeting heat cascade uses temperature intervals (TI), while the composite curve-based area target uses enthalpy intervals (EI). In the utility targeting cascade, TIs are defined to ensure feasible heat transfer between all hot and cold streams in each TI, and to eliminate from the utility targeting LP any match which can never satisfy ΔT_m (e.g., a match between the supply end of a hot stream and the target end of a cold stream where the supply temperature of the hot stream is colder than the target temperature of the cold stream). In the composite curve-based area target, EIs are defined for each piecewise linear segment of the composite curves in order to impose an overall energy balance on the streams in each EI.

In the area targeting heat cascade, we combine the ideas of TIs and EIs. We define TIs l to eliminate from the area targeting NLP those matches which can never satisfy ΔT_m. In particular, we define a TI boundary with boundary temperature T_l (cold end of TI l) at each stream supply, where T_l equals a hot stream supply temperature, or a cold stream supply temperature plus ΔT_m. Then, to be able to reproduce the composite curves, we further subdivide each TI into $k = 1, \ldots, k_{\max_l}$ EIs at the stream targets (Fig. 2.5) and impose energy balances on each EI.

In order to ensure feasible heat transfer between any pair of hot and cold streams in each TI, all hot streams crossing a TI boundary (the cold end of the coldest EI $k_{\max_l}$ in each TI l) must be hotter than the TI boundary temperature ($T_{i,l,k_{\max_l}} \geq T_l$), and all cold streams crossing a TI boundary must be colder than the TI boundary temperature minus ΔT_m ($T_{j,l,k_{\max_l}} \leq T_l - \Delta T_m$). This requirement is satisfied if each heat residual ($r_{i,l,k_{\max_l}}$) and deficit ($d_{j,l+1,1}$, from the first EI in the next colder TI $l+1$)

cascaded across the TI boundary is nonnegative. Note that with this requirement, ΔT_m is automatically satisfied at the TI boundaries. At the EI boundaries ($k < k_{\max_l}$), no special boundary temperatures are needed. However, we must explicitly impose ΔT_m constraints at these boundaries.

In setting up the heat cascade, the entire heat content of a hot stream or utility in a TI is placed in the hottest EI in the TI (Fig. 2.5); excess heat can be cascaded to the colder EIs. Likewise, the entire heat content of a cold stream or utility is placed in the coldest EI in the TI.

Now we have an area targeting heat cascade which can reproduce the composite curves for any set of stream data when no stream match constraints are imposed. This cascade can also be generated when matching constraints are imposed.

The area target is calculated using specified amounts of utilities. However, the area target is *not* calculated for a specific ΔT_m; the NLP determines the optimal approach temperatures to minimize area. To prevent numerical difficulties while calculating ΔT_{LM} and area, we specify a small, positive lower bound ΔT_m^L on the approach temperatures (typically 0.1 K); we use this ΔT_m^L to set up the TIs.

To simplify formulation of the area targeting NLP, the definitions of the stream index sets used earlier are slightly modified: sets I and J should contain nonisothermal ("nonpoint") utilities as well as process streams; sets S and W should contain isothermal ("point") utilities only. The following sets are also defined:

$$K_l = \{k \in (1, 2, \ldots, k_{\max_l}) | \text{ is an enthalpy interval in TI } l\}$$

$$R_{i,j} = \{(i,j) | i \in I,\ j \in J,\ \mathrm{S_{hi}}\text{–}\mathrm{S_{cj}} \text{ match is required}\}$$

$$R_{s,j} = \{(s,j)|s \in S,\ j \in J,\ s\text{–}\mathrm{S}_{cj} \text{ match is required}\}$$

$$R_{i,w} = \{(i,w)|i \in I,\ w \in W,\ \mathrm{S}_{\mathrm{hi}}\text{–}w \text{ match is required}\}$$

For each required match, upper and lower bounds on area ($A^U_{i,j}$, $A^L_{i,j}$, $A^U_{s,j}$, $A^L_{s,j}$, $A^U_{i,w}$ and $A^L_{i,w}$) must be specified.

The variables in the area targeting NLP are the heat transfer rates $q_{i,j,l,k}$, $q_{s,j,l,k}$ and $q_{i,w,l,k}$, cascaded residuals $r_{i,l,k}$ and $r_{s,l,k}$, and the heat deficits $d_{j,l,k}$ and $d_{w,l,k}$ cascaded from EI k (in TI l) to the next hotter EI. However, to calculate area, we need stream temperatures at the cold ($T_{i,l,k}$ and $T_{j,l,k}$) and hot ($T^H_{i,l,k}$ and $T^H_{j,l,k}$) ends of each EI. These are calculated from the optimization variables as follows (for $i \in I_l$, $j \in J_l$):

$$T_{i,l,k} = \max(T_l, T^T_i) + \frac{r_{i,l,k}}{w_i} \quad \text{for } 1 \le k \le k_{\max_l},\ 1 \le l \le l_{\max} \tag{2.6}$$

$$T_{j,l,k} = \begin{cases} \min(T_{l-1} - \Delta T^L_m,\ T^T_j) - \dfrac{d_{j,l,k+1}}{w_j} & \text{for } 1 \le k < k_{\max_l},\ 1 < l \le l_{\max} \\ T^T_j - \dfrac{d_{j,l,k+1}}{w_j} & \text{for } 1 \le k < k_{\max_l},\ l = 1 \\ \min(T_l - \Delta T^L_m,\ T^T_j) - \dfrac{d_{j,l+1,1}}{w_j} & \text{for } k = k_{\max_l},\ 1 \le l \le l_{\max} \end{cases} \tag{2.7}$$

$$T^H_{i,l,k} = \begin{cases} T_{i,l,k-1} & \text{for } 1 < k \le k_{\max_l},\ 1 \le l \le l_{\max} \\ T_{i,l-1,k_{\max_{l-1}}} & \text{for } k = 1,\ 1 < l \le l_{\max} \\ T^S_i & \text{for } k = 1,\ l = 1 \end{cases} \tag{2.8}$$

$$T^H_{j,l,k} = \begin{cases} T_{j,l,k-1} & \text{for } 1 < k \le k_{\max_l},\ 1 \le l \le l_{\max} \\ T_{j,l-1,k_{\max_{l-1}}} & \text{for } k = 1,\ 1 < l \le l_{\max} \\ T^T_j & \text{for } k = 1,\ l = 1 \end{cases} \tag{2.9}$$

where heat is not cascaded from the ends of the problem ($r_{i,0,k} = r_{i,l_{\max},k_{\max_{l_{\max}}}} = 0$ and $d_{j,1,1} = d_{j,l_{\max}+1,k} = 0$), and where heat is not cascaded from TIs where a stream does not exist ($r_{i,l,k} = 0$ for $i \notin I_l$, and $d_{j,l,k} = 0$ for $j \notin J_l$.) Note that for $k < k_{\max_l}$, hot stream temperatures $T_{i,l,k}$ are based on TI boundary temperature T_l at the cold end of the TI, while cold stream temperatures $T_{j,l,k}$ are based on boundary temperature T_{l-1} at the hot end of the TI. This is simply because of the opposite directions of the residual and deficit heat cascades.

To calculate the area target from these loads and temperatures, we must have some HEN structure which corresponds to the area targeting heat cascade. We assume that the area target—with equal or unequal heat transfer coefficients, and with or without stream match constraints—is equal to the area of a "spaghetti" structure (featuring parallel stream splitting and isothermal mixing) corresponding to the heat cascade, just like the composite curve-based area target is equal to the area of a spaghetti structure (e.g., Fig.2.2) corresponding to the composite curves. For a given problem, this assumption can be tested simply by dividing the TIs into more EIs than that suggested by the stream target temperatures; by allowing a larger number of EIs, the resulting structure can be more general (and in fact more closely approaches an infinitely cyclic HEN). In practice, increasing the total number of intervals beyond twice the number of streams (one interval boundary for each stream supply and target, even if some of the supply and target temperatures coincide) has been found to have negligible effect upon the calculated area target.

The area targeting NLP minimizes the total area of the process and utility matches

in the spaghetti structure

$$\min \sum_{(i,j)\in M_{i,j}} A_{i,j} + \sum_{(s,j)\in M_{s,j}} A_{s,j} + \sum_{(i,w)\in M_{i,w}} A_{i,w} \qquad \textbf{(P3)}$$

subject to the following constraints:

(A) Definition of areas:

$$A_{i,j} = \left(\frac{1}{h_i}+\frac{1}{h_j}\right) \sum_{l\in L|(i\in I_l, j\in J_l)} \sum_{k\in K_l} \frac{q_{i,j,l,k}}{\Delta T_{\mathrm{LM}_{i,j,l,k}}} \qquad \text{for } (i,j)\in M_{i,j}$$

$$A_{s,j} = \left(\frac{1}{h_s}+\frac{1}{h_j}\right) \sum_{l\in L|(s\in S_l, j\in J_l)} \sum_{k\in K_l} \frac{q_{s,j,l,k}}{\Delta T_{\mathrm{LM}_{s,j,l,k}}} \qquad \text{for } (s,j)\in M_{s,j}$$

$$A_{i,w} = \left(\frac{1}{h_i}+\frac{1}{h_w}\right) \sum_{l\in L|(i\in I_l, w\in W_l)} \sum_{k\in K_l} \frac{q_{i,w,l,k}}{\Delta T_{\mathrm{LM}_{i,w,l,k}}} \qquad \text{for } (i,w)\in M_{i,w}$$

where ΔT_{LM} is very well approximated by $\frac{2}{3}$ the geometric mean temperature difference + $\frac{1}{3}$ the arithmetic mean temperature difference (Paterson, 1984), while avoiding the singularities occurring when the heat capacities of the hot and cold streams in an exchanger are equal

$$\Delta T_{\mathrm{LM}_{i,j,l,k}} \approx \frac{2}{3}\sqrt{(T^H_{i,l,k}-T^H_{j,l,k})(T_{i,l,k}-T_{j,l,k})} + \frac{1}{3}\left\{\frac{1}{2}\left[(T^H_{i,l,k}-T^H_{j,l,k})+(T_{i,l,k}-T_{j,l,k})\right]\right\}$$

$$\Delta T_{\mathrm{LM}_{s,j,l,k}} \approx \frac{2}{3}\sqrt{(T^S_{s}-T^H_{j,l,k})(T^S_{s}-T_{j,l,k})} + \frac{1}{3}\left\{\frac{1}{2}\left[(T^S_{s}-T^H_{j,l,k})+(T^S_{s}-T_{j,l,k})\right]\right\}$$

$$\Delta T_{\mathrm{LM}_{i,w,l,k}} \approx \frac{2}{3}\sqrt{(T^H_{i,l,k}-T^S_{w})(T_{i,l,k}-T^S_{w})} + \frac{1}{3}\left\{\frac{1}{2}\left[(T^H_{i,l,k}-T^S_{w})+(T_{i,l,k}-T^S_{w})\right]\right\}$$

and where T_s^S and T_w^S are the (supply) temperatures of hot and cold isothermal utilities s and w. In practice, these constraints can be eliminated by substituting the area expressions directly into the objective function.

(B) Energy balances on hot streams and hot isothermal utilities:

$$Q_{i,l} + r_{i,l-1,k_{\max_{l-1}}} = \sum_{j\in(J_l\cup M_{i,j})} q_{i,j,l,k} + \sum_{w\in(W_l\cup M_{i,w})} q_{i,w,l,k} + r_{i,l,k}$$
$$\text{for } k=1,\ i\in I_l,\ l\in L$$

$$r_{i,l,k-1} = \sum_{j\in(J_l\cup M_{i,j})} q_{i,j,l,k} + \sum_{w\in(W_l\cup M_{i,w})} q_{i,w,l,k} + r_{i,l,k}$$
$$\text{for } 1<k\le k_{\max_l},\ i\in I_l,\ l\in L$$

$$Q_{s,l} + r_{s,l-1,k_{\max_{l-1}}} = \sum_{j\in(J_l\cup M_{s,j})} q_{s,j,l,k} + r_{s,l,k} \quad \text{for } k=1,\ s\in S_l,\ l\in L$$

$$r_{s,l,k-1} = \sum_{j\in(J_l\cup M_{s,j})} q_{s,j,l,k} + r_{s,l,k} \quad \text{for } 1<k\le k_{\max_l},\ s\in S_l,\ l\in L$$

(C) Energy balances on cold streams and cold isothermal utilities:

$$d_{j,l,k+1} = \sum_{s\in(S_l\cup M_{s,j})} q_{s,j,l,k} + \sum_{i\in(I_l\cup M_{i,j})} q_{i,j,l,k} + d_{j,l,k}$$
$$\text{for } 1\le k<k_{\max_l},\ j\in J_l,\ l\in L$$

$$Q_{j,l} + d_{j,l+1,1} = \sum_{s\in(S_l\cup M_{s,j})} q_{s,j,l,k} + \sum_{i\in(I_l\cup M_{i,j})} q_{i,j,l,k} + d_{j,l,k}$$
$$\text{for } k=k_{\max_l},\ j\in J_l,\ l\in L$$

$$d_{w,l,k+1} = \sum_{i\in(I_l\cup M_{i,w})} q_{i,w,l,k} + d_{w,l,k} \quad \text{for } 1\le k<k_{\max_l},\ w\in W_l,\ l\in L$$

$$Q_{w,l} + d_{w,l+1,1} = \sum_{i\in(I_l\cup M_{i,w})} q_{i,w,l,k} + d_{w,l,k} \quad \text{for } k=k_{\max_l},\ w\in W_l,\ l\in L$$

In practice, to compensate for round-off error, we allow tolerances in one hot and one cold utility.

(D) ΔT_m constraints:

$$\max(T_l, T_i^T) + \frac{r_{i,l,k}}{w_i} \geq \min(T_{l-1} - \Delta T_m^L, T_j^T) - \frac{d_{j,l,k+1}}{w_j} + \Delta T_m^L$$

$$\text{for } \{(i,j)|i \in I_l, j \in J_l, (i,j) \in M_{i,j}\},\ 1 \leq k < k_{\max_l},\ 1 < l \leq l_{\max}$$

$$\max(T_l, T_i^T) + \frac{r_{i,l,k}}{w_i} \geq T_j^T - \frac{d_{j,l,k+1}}{w_j} + \Delta T_m^L$$

$$\text{for } \{(i,j)|i \in I_l, j \in J_l, (i,j) \in M_{i,j}\},\ 1 \leq k < k_{\max_l},\ l = 1$$

Note that ΔT_m constraints are not imposed upon the isothermal utilities; since TI boundaries are defined at the (supply) temperatures of these utilities, ΔT_m will automatically be satisfied for the utility matches.

(E) Area bounds on required matches:

$$\begin{aligned} A_{i,j}^L \leq A_{i,j} \leq A_{i,j}^U &\quad \text{for } (i,j) \in R_{i,j} \\ A_{s,j}^L \leq A_{s,j} \leq A_{s,j}^U &\quad \text{for } (s,j) \in R_{s,j} \\ A_{i,w}^L \leq A_{i,w} \leq A_{i,w}^U &\quad \text{for } (i,w) \in R_{i,w} \end{aligned}$$

(F) Nonnegative areas, heat loads, residuals and deficits:

$$\begin{aligned} A_{i,j} \geq 0 &\quad \text{for } \{(i,j)|(i,j) \in M_{i,j},\ (i,j) \notin R_{i,j}\} \\ A_{s,j} \geq 0 &\quad \text{for } \{(s,j)|(s,j) \in M_{s,j},\ (s,j) \notin R_{s,j}\} \\ A_{i,w} \geq 0 &\quad \text{for } \{(i,w)|(i,w) \in M_{i,w},\ (i,w) \notin R_{i,w}\} \\ q_{i,j,l,k} \geq 0 &\quad \text{for } \{(i,j)|i \in I_l, j \in J_l, (i,j) \in M_{i,j}\},\ 1 \leq k \leq k_{\max_l},\ l \in L \\ q_{s,j,l,k} \geq 0 &\quad \text{for } \{(s,j)|s \in S_l, j \in J_l, (s,j) \in M_{s,j}\},\ 1 \leq k \leq k_{\max_l},\ l \in L \\ q_{i,w,l,k} \geq 0 &\quad \text{for } \{(i,w)|i \in I_l, w \in W_l, (i,w) \in M_{i,w}\},\ 1 \leq k \leq k_{\max_l},\ l \in L \\ r_{i,l,k} \geq 0 &\quad \text{for } i \in I_l,\ 1 \leq k \leq k_{\max_l},\ l \in L \end{aligned}$$

$$r_{s,l,k} \geq 0 \quad \text{for } s \in S_l,\ 1 \leq k \leq k_{\max_l},\ l \in L$$
$$d_{j,l,k} \geq 0 \quad \text{for } j \in J_l,\ 1 \leq k \leq k_{\max_l},\ l \in L$$
$$d_{w,l,k} \geq 0 \quad \text{for } w \in W_l,\ 1 \leq k \leq k_{\max_l},\ l \in L$$

Note that all the constraints are linear except for the one defining area.

If there are no constraints upon stream matches, the heat cascade corresponding to the composite curves provides a good starting point for the area targeting NLP. When specific stream matches are forbidden [or the number of matches is restricted], solution of utility targeting LP (P1) [or units targeting MILP (P2)] provides a good starting point. As presented, the area targeting NLP can minimize the area required for any given set of allowed matches; section 2.5.2 describes how to minimize the area target for any given number of matches (e.g., corresponding to the units target).

In general, the area targeting NLP can have more than one local optimum. However, for the examples we have studied, the multiple optima all give similar values for the area target (within 3%) even if the temperature distributions ($T_{i,l,k}$ and $T_{j,l,k}$) are quite different. This seems reasonable since the area target is most sensitive to temperatures near the pinch (small driving force), and is relatively insensitive to changes in temperature away from the pinch (large driving force). This result is quite acceptable since HENs with a minimum or near-minimum number of units can generally approach the area target only within a few percent.

Note that the area targeting NLP is formulated for multiple utilities. The area targeting NLP, and the capital cost targeting NLP presented later, are easily extended to piecewise constant heat capacities and film heat transfer coefficients (as a function of temperature) simply by defining a new stream for each piecewise constant

segment. Both NLPs are also easily extended to boiling and condensing streams simply by treating the latent heat of vaporization (condensation) as the heat duty of an isothermal pseudo-utility.

2.4.2 Application of the Area Targeting NLP

Area targeting NLP (P3) offers a number of advantages over current area targeting methods:

- The area target can be calculated with forbidden stream matches, and for revamp problems in which specified areas are required in given matches (Example 2.1).
- The area target can also be calculated for any specified number of matches, including the number of matches corresponding to the minimum units target (Examples 2.3 and 2.4). In fact, we show that it is always possible to synthesize a HEN in which the number of units is the same as the number of matches in the NLP solution (Section 2.5.3).
- The matches and heat loads given by the solution of the NLP with stream match constraints provide an excellent starting point for synthesis of minimum-unit HENs achieving (within a few percent) the area target (Examples 2.3 and 2.4).
- Area targets can now be calculated rigorously for HEN synthesis problems with unequal heat transfer coefficients and any number of hot and cold streams (Examples 2.1, 2.2 and 2.3).

The following two examples begin to illustrate these points.

Example 2.1 This example demonstrates the formulation of area targeting NLP (P3) when specific stream matches are forbidden, or when specific stream matches with given areas are required (for revamp of an existing HEN). In particular, the area target is calculated for the stream data in Table 2.1 where the match between streams S_{h1} and S_{c2} is prohibited, and the match between streams S_{h2} and S_{c1} is required to exist with area 45 $m^2 \leq A_{h2,c1} \leq 50$ m^2.

With the value of ΔT_m (10 K) specified for utility targeting, the heating and cooling targets are 620 and 230 kW, respectively. Note that the condensing steam is an isothermal ("point") utility; however, since the cooling water is a nonisothermal ("nonpoint") utility, we treat it as a third cold stream (S_{c0}) with heat capacity flow rate $w_{c0} = 23$ kW/K.

Figure 2.5 shows the heat cascade corresponding to the composite curves (Fig. 2.1) for these stream data and utility targets, and a ΔT_m^L of 0.1 K. Note that this heat cascade would give the area target if the heat transfer coefficients were equal, and if there were no forbidden or required matches. We use the TIs and EIs in this heat cascade to formulate the area targeting NLP as follows:

$$\min\ A_{h1,c1} + A_{h2,c1} + A_{h2,c2} + A_{s,c1} + A_{s,c2} + A_{h1,c0} + A_{h2,c0}$$

subject to

(A) Definition of areas:

$$A_{h1,c1} = \left(\frac{1}{h_{h1}} + \frac{1}{h_{c1}}\right) \left(\frac{q_{h1,c1,3,1}}{\Delta T_{\mathrm{LM}_{h1,c1,3,1}}} + \frac{q_{h1,c1,4,1}}{\Delta T_{\mathrm{LM}_{h1,c1,4,1}}} + \frac{q_{h1,c1,4,2}}{\Delta T_{\mathrm{LM}_{h1,c1,4,2}}}\right)$$

$$A_{h2,c1} = \left(\frac{1}{h_{h2}} + \frac{1}{h_{c1}}\right) \left(\frac{q_{h2,c1,2,1}}{\Delta T_{\mathrm{LM}_{h2,c1,2,1}}} + \frac{q_{h2,c1,3,1}}{\Delta T_{\mathrm{LM}_{h2,c1,3,1}}} + \frac{q_{h2,c1,4,1}}{\Delta T_{\mathrm{LM}_{h2,c1,4,1}}} + \frac{q_{h2,c1,4,2}}{\Delta T_{\mathrm{LM}_{h2,c1,4,2}}}\right)$$

$$A_{s,c2} = \left(\frac{1}{h_s} + \frac{1}{h_{c2}}\right) \left(\frac{q_{s,c2,1,1}}{\Delta T_{\mathrm{LM}_{s,c2,1,1}}} + \frac{q_{s,c2,1,2}}{\Delta T_{\mathrm{LM}_{s,c2,1,2}}} + \frac{q_{s,c2,2,1}}{\Delta T_{\mathrm{LM}_{s,c2,2,1}}} + \frac{q_{s,c2,3,1}}{\Delta T_{\mathrm{LM}_{s,c2,3,1}}}\right)$$

$$A_{h1,c0} = \left(\frac{1}{h_{h1}} + \frac{1}{h_{c0}}\right) \left(\frac{q_{h1,c0,3,1}}{\Delta T_{\mathrm{LM}_{h1,c0,3,1}}} + \frac{q_{h1,c0,4,1}}{\Delta T_{\mathrm{LM}_{h1,c0,4,1}}} + \frac{q_{h1,c0,4,2}}{\Delta T_{\mathrm{LM}_{h1,c0,4,2}}} + \frac{q_{h1,c0,5,1}}{\Delta T_{\mathrm{LM}_{h1,c0,5,1}}}\right)$$

with similar definitions for $A_{h2,c2}$, $A_{s,c1}$ and $A_{h2,c0}$, where

$$\begin{aligned}
\Delta T_{\mathrm{LM}_{h1,c1,3,1}} &= \tfrac{2}{3}\sqrt{(395 - T_{c1,2,1})(T_{h1,3,1} - T_{c1,3,1})} \\
&\quad + \tfrac{1}{6}[(395 - T_{c1,2,1})(T_{h1,3,1} - T_{c1,3,1})] \\
\Delta T_{\mathrm{LM}_{hi,c1,4,1}} &= \tfrac{2}{3}\sqrt{(T_{hi,3,1} - T_{c1,3,1})(T_{hi,4,1} - T_{c1,4,1})} \\
&\quad + \tfrac{1}{6}[(T_{hi,3,1} - T_{c1,3,1})(T_{hi,4,1} - T_{c1,4,1})] \quad (i = 1, 2) \\
\Delta T_{\mathrm{LM}_{h2,c1,4,2}} &= \tfrac{2}{3}\sqrt{(T_{h2,4,1} - T_{c1,4,1})(T_{h2,4,2} - 293)} \\
&\quad + \tfrac{1}{6}[(T_{h2,4,1} - T_{c1,4,1})(T_{h2,4,2} - 293)]
\end{aligned}$$

and where

$$\begin{aligned}
T_{h1,3,1} &= 353.1 + \tfrac{1}{4}r_{h1,3,1} & T_{h1,4,1} &= 343.0 + \tfrac{1}{4}r_{h1,4,1} \\
T_{h2,3,1} &= 353.1 + \tfrac{1}{6}r_{h2,3,1} & T_{h2,4,1} &= 293.1 + \tfrac{1}{6}r_{h2,4,1} \\
T_{h2,4,2} &= 293.1 + \tfrac{1}{6}r_{h2,4,2} & T_{c1,2,1} &= 394.9 - \tfrac{1}{5}d_{c1,3,1} \\
T_{c1,3,1} &= 353.0 - \tfrac{1}{5}d_{c1,4,1} & T_{c1,4,1} &= 353.0 - \tfrac{1}{5}d_{c1,4,2}
\end{aligned}$$

with similar expressions for the other ΔT_{LM} terms and temperatures.

(B) Energy balances on hot streams and utilities:

$$\begin{aligned}
&\mathrm{S_{h1}},\ \mathrm{TI\ 3},\ \mathrm{EI\ 1}: && 167.6 = q_{h1,c1,3,1} + q_{h1,c0,3,1} + r_{h1,3,1} \\
&\mathrm{S_{h1}},\ \mathrm{TI\ 4},\ \mathrm{EI\ 1}: && 40.4 + r_{h1,3,1} = q_{h1,c1,4,1} + q_{h1,c0,4,1} + r_{h1,4,1} \\
&\mathrm{S_{h1}},\ \mathrm{TI\ 4},\ \mathrm{EI\ 2}: && r_{h1,4,1} = q_{h1,c1,4,2} + q_{h1,c0,4,2} + r_{h1,4,2} \\
&\mathrm{S_{h1}},\ \mathrm{TI\ 5},\ \mathrm{EI\ 1}: && r_{h1,4,2} = q_{h1,c0,5,1} \\
&\qquad\qquad \vdots && \vdots
\end{aligned}$$

$$\begin{aligned}
\text{Steam, TI 1, EI 1:} \quad & 620 = q_{s,c1,1,1} + q_{s,c2,1,1} + r_{s,1,1} \\
\text{Steam, TI 1, EI 2:} \quad & r_{s,1,1} = q_{s,c1,1,2} + q_{s,c2,1,2} + r_{s,1,2} \\
\vdots \quad & \vdots
\end{aligned}$$

(C) Energy balances on cold streams and utilities:

$$\begin{aligned}
\text{S}_{\text{c1}}\text{, TI 1, EI 1:} \quad & d_{c1,1,2} = q_{s,c1,1,1} \\
\text{S}_{\text{c1}}\text{, TI 1, EI 2:} \quad & 440.5 + d_{c1,2,1} = q_{s,c1,1,2} + d_{c1,1,2} \\
\text{S}_{\text{c1}}\text{, TI 2, EI 1:} \quad & 50.0 + d_{c1,3,1} = q_{s,c1,2,1} + q_{h2,c1,2,1} + d_{c1,2,1} \\
\vdots \quad & \vdots \\
\text{S}_{\text{c1}}\text{, TI 4, EI 2:} \quad & 300.0 = q_{s,c1,4,2} + q_{h1,c1,4,2} + q_{h2,c1,4,2} + d_{c1,4,2} \\
\vdots \quad & \vdots \\
\text{Water, TI 4, EI 2:} \quad & d_{c0,5,1} = q_{h1,c0,4,2} + q_{h2,c0,4,2} + d_{c0,4,2} \\
\text{Water, TI 5, EI 1:} \quad & 230.0 = q_{h1,c0,5,1} + q_{h2,c0,5,1} + d_{c0,5,1}
\end{aligned}$$

(D) ΔT_m constraints:

$$\begin{aligned}
\text{S}_{\text{h1}}\text{–S}_{\text{c1}}\text{, TI 4, EI 1:} \quad & 343.0 + \tfrac{1}{4} r_{h1,4,1} \geq 353.0 - \tfrac{1}{5} d_{c1;4,2} + \Delta T_m^L \\
\text{S}_{\text{h2}}\text{–S}_{\text{c1}}\text{, TI 4, EI 1:} \quad & 293.1 + \tfrac{1}{6} r_{h2,4,1} \geq 353.0 - \tfrac{1}{5} d_{c1,4,2} + \Delta T_m^L \\
\text{S}_{\text{h1}}\text{–Water, TI 4, EI 1:} \quad & 343.0 + \tfrac{1}{4} r_{h1,4,1} \geq 288.0 - \tfrac{1}{23} d_{c0,4,2} + \Delta T_m^L \\
\text{S}_{\text{h2}}\text{–Water, TI 4, EI 1:} \quad & 293.1 + \tfrac{1}{6} r_{h2,4,1} \geq 288.0 - \tfrac{1}{23} d_{c0,4,2} + \Delta T_m^L
\end{aligned}$$

Because of the way the TIs are defined, ΔT_m^L will automatically be satisfied at all the other interval boundaries.

(E) Area bounds on required match:

$$45 \leq A_{h2,c1} \leq 50$$

(F) Nonnegative areas, heat loads, residuals and deficits:

$$A_{i,j} \geq 0, \quad A_{s,j} \geq 0, \quad q_{i,j,l,k} \geq 0, \quad q_{s,j,l,k} \geq 0$$
$$r_{i,l,k} \geq 0, \quad r_{s,l,k} \geq 0, \quad d_{j,l,k} \geq 0$$

To obtain a starting point for the area targeting NLP, we solve utility targeting LP (P1) with the S_{h1}–S_{c2} match forbidden. Using this starting point, we calculate an area target of 259.7 m^2. Solution of this NLP using MINOS 5.0 (Murtagh and

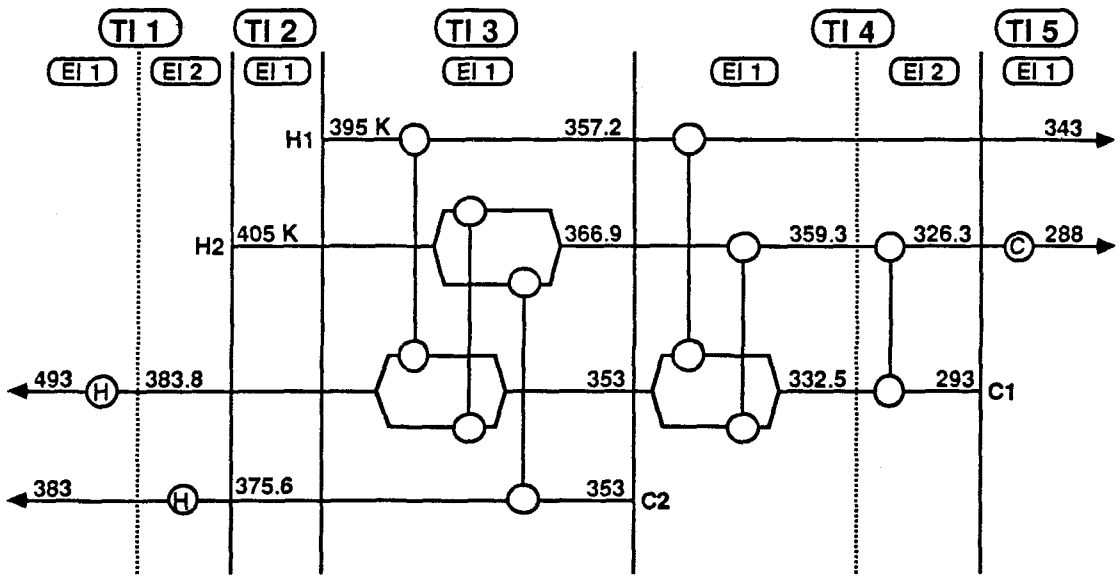

Figure 2.6: Spaghetti structure corresponding to the solution of the area targeting NLP (Example 2.1).

Saunders, 1983) required 23 sec of CPU time on a DEC MicroVAX II computer.

Figure 2.6 shows the spaghetti structure corresponding to the NLP solution; Table 2.2 summarizes the loads, areas and approach temperatures in this structure. Note that the required S_{h2}–S_{c1} match, with an area of 50 m^2, satisfies its area specification. Also note that the optimal value of minimum approach temperature (4.2 K) is *less* than the ΔT_m specified for utility targeting (10 K). To minimize area, smaller approach temperatures are required in matches with good heat transfer coefficients so that larger approach temperatures can be used in matches with poor heat transfer coefficients.

For comparison, when no stream matches are required or forbidden, NLP (P3) yields an area target of 258.8 m^2. However, the simple area targeting method based on the composite curves predicts a target of 295.6 m^2, thus overestimating the area

Table 2.2: Load, approach temperature and area distributions from the solution of the area targeting NLP for Example 2.1.

Match	*TI*	*EI*	*Load*	*Approach Temperature*		*Area*	*Match Area*
				Hot End	*Cold End*		
			(kW)	(K)	(K)	(m^2)	(m^2)
H1-C1	3	1	151.2	11.2	4.2	21.1	
	4	1	56.8	4.2	10.5	8.3	29.4
H2-C1	3	1	2.8	21.2	13.9	0.9	
	4	1	45.6	13.9	26.8	12.8	
	4	2	197.5	26.8	33.3	36.3	50.0
H2-C2	3	1	226.0	29.4	13.9	109.4	109.4
Steam-C1	1	1	546.0	27.0	136.2	8.1	8.1
Steam-C2	1	2	74.0	137.0	144.4	2.9	2.9
H2-Water	5	1	230.0	38.3	10.0	59.9	59.9
Total							259.7

target by 14.2%. ■

Example 2.2 Nishimura (1980) developed a rigorous method to calculate the area target for problems with different heat transfer coefficients, but with only one cold and several hot streams (or vice versa). This example shows that area targeting NLP (P3) can reproduce Nishimura's area target.

The stream data in Table 2.3 is taken from one of Nishimura's examples. Note that the film heat transfer coefficients range over two orders of magnitude, which is not unusual in a HEN with boiling or condensing streams. For the value of ΔT_m specified for utility targeting, the heating and cooling requirements are both zero. The area target for these stream data, calculated by using Nishimura's method, is 29.84 m^2. Figure 2.7 shows the HEN structure obtained with Nishimura's method.

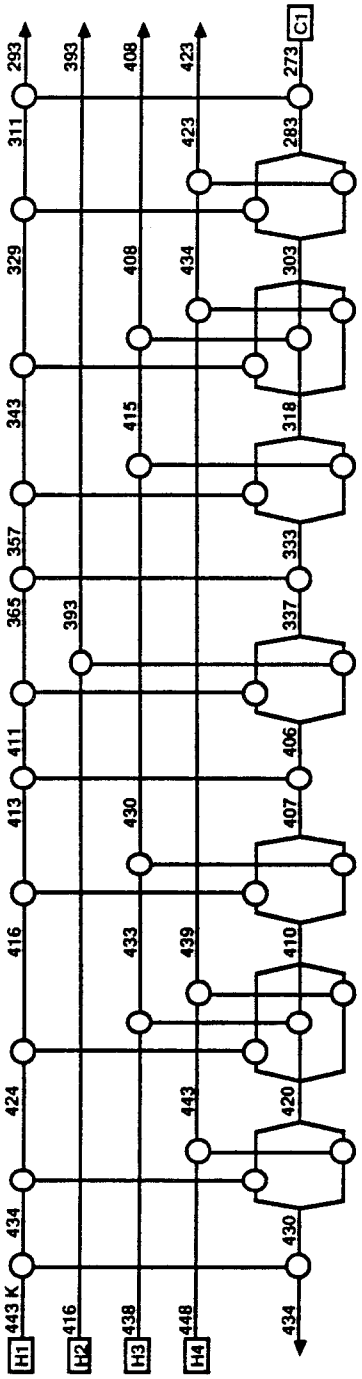

Figure 2.7: HEN structure—determined by using Nishimura's method—which achieves the area target in Example 2.2.

Table 2.3: Stream data for Example 2.2.

Stream	*Supply Temperature* (K)	*Target Temperature* (K)	*Heat Capacity Flow Rate* (kW/K)	*Film Heat Transfer Coefficient* ($kW/m^2 K$)
H1	443	293	0.5	2.0000
H2	416	393	2.0	0.2857
H3	438	408	0.5	0.0645
H4	448	423	1.0	0.0408
C1	273	434	1.0	2.0000
Steam	*none*			
Water	*none*			

$\Delta T_m = 10$ K (for utility targeting).

When using area targeting NLP (P3), we also obtain an area target of 29.84 m^2. Figure 2.8 shows the HEN structure corresponding to the NLP solution. Note that we obtain the area target with a much simpler structure than Nishimura. For comparison, the area target calculated from the composite curves is 47.69 m^2, *60% higher* than the area target from Nishimura's method or from the area targeting NLP. ■

2.5 Capital Cost Target (Transshipment NLP)

There is a trade-off between area and the number of units; that is, the required heat transfer area generally increases as the number of units is reduced. However, capital cost may increase or decrease as the number of units is reduced depending upon whether "fixed" costs (independent of area, but dependent upon the number of units) or variable costs (dependent upon area) dominate. The capital cost targeting NLP introduced in this section can be used to predict the cost trade-off between area and the number of units.

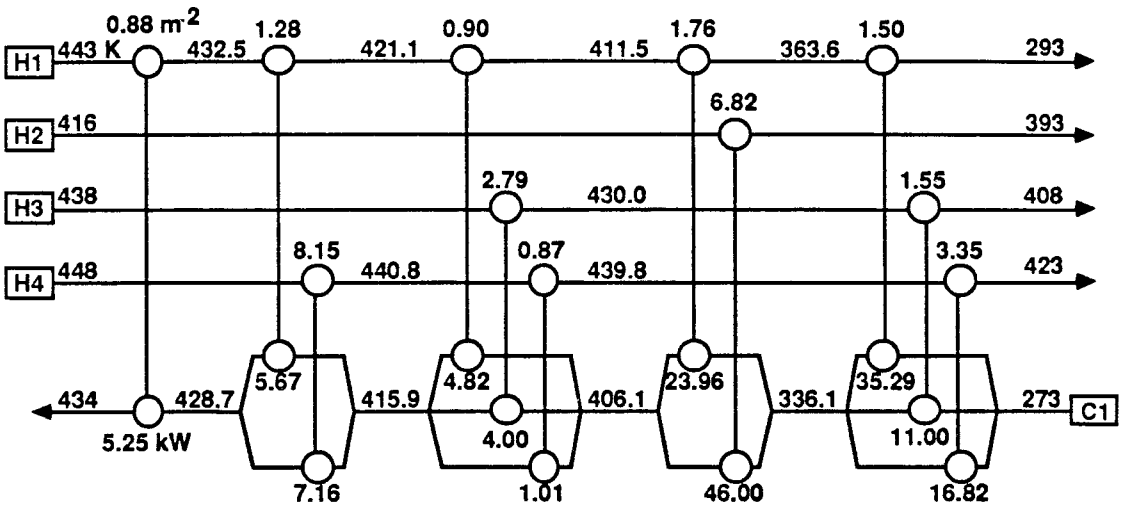

Figure 2.8: HEN spaghetti structure—corresponding to the solution of the area targeting NLP—which achieves the area target in Example 2.2.

2.5.1 Formulation of the Capital Cost Targeting NLP

Area targeting NLP (P3) is easily extended to formulate a capital cost targeting NLP for HEN synthesis. This NLP minimizes the aggregate capital cost of all the process and utility matches, where we assume that the total area of each match is lumped into a single exchanger (even though in the NLP solution, the area of a match may be distributed among several EIs). We assume that the capital cost of each exchanger is given by an exponential cost law, $C_{i,j} = a_{i,j} + b_{i,j}A_{i,j}^{d_{i,j}}$, with similar cost laws for the utility matches. Note that each match can have a different cost law to take into account different materials of construction, pressure ratings, and so on.

The cost targeting NLP is formulated as follows:

$$\sum_{(i,j)\in M_{i,j}} a_{i,j}n_{i,j} + \sum_{(s,j)\in M_{s,j}} a_{s,j}n_{s,j} + \sum_{(i,w)\in M_{i,w}} a_{i,w}n_{i,w}$$

$$+ \min \left(\sum_{(i,j)\in M_{i,j}} b_{i,j}A_{i,j}^{d_{i,j}} + \sum_{(s,j)\in M_{s,j}} b_{s,j}A_{s,j}^{d_{s,j}} + \sum_{(i,w)\in M_{i,w}} b_{i,w}A_{i,w}^{d_{i,w}} \right) \qquad \textbf{(P4)}$$

subject to the same constraints as area targeting NLP (P3), where $n_{i,j}$, $n_{s,j}$ and $n_{i,w}$ are binary "variables" denoting the existence or absence of each match.

Note that the "fixed" capital costs ($\sum a_{i,j}n_{i,j} + \sum a_{s,j}n_{s,j} + \sum a_{i,w}n_{i,w}$) vary with the number of matches, even though they are independent of area. Thus, strictly speaking, we should include the fixed costs along with the variable (area dependent) costs in the minimization. However, we exclude the fixed costs to avoid introducing binary variables in the NLP. Instead, we determine match existence (hence, fixed costs) *after* solving the NLP to minimize variable costs. In general, this does not affect the capital cost target since the NLP itself tends to minimize the number of matches while it minimizes variable costs. This is because the exponential function (with exponent less than 1.0) for the variable costs favors distributing area among a small number of large exchangers rather than among many small exchangers.

2.5.2 Extension of the Area and Capital Cost Targeting NLPs to any Given Number of Matches

As presented, NLPs (P3) and (P4) can calculate the area and capital cost targets for a given *set* of allowed matches. However, these NLPs cannot minimize the area and capital cost targets over all sets of a given *number* of matches (e.g., the number of

matches corresponding to the units target). There are several strategies for extending or otherwise using these NLPs to calculate the targets for a given number of matches:

- Take advantage of the fact that capital cost targeting NLP (P4) tends to minimize the number of matches while it minimizes the variable capital costs. This strategy will generally give the capital cost target (and corresponding match areas) for the number of matches corresponding to the units target.

- Include binary variables to determine the existence or absence of each match, and formulate a mixed-integer nonlinear program (MINLP) to minimize the area or capital cost target subject to a constraint on the number of matches. Recently, Duran and Grossmann (1984) and Kocis and Grossmann (1986) have developed algorithms which should solve this type of MINLP.

- Use a branch-and-bound search where each node of the search tree corresponds to a particular set of forbidden matches (i.e., where the root of the search tree corresponds to no forbidden matches, and where going down a branch of the search tree corresponds to adding one more forbidden match). At each node, the area or capital cost target can be evaluated using NLP (P3) or (P4). Use a depth-first strategy to find a bound on area (or capital cost) for the given number of matches. Then continue searching through the tree for tighter bounds while eliminating any nodes (and their daughter nodes) where prohibiting a particular match causes the area (or capital cost) target to exceed the current bound.

One difficulty with this branch-and-bound procedure is that the area and cost targeting NLPs can have multiple optima, and thus may not give the tightest possible bounds on the targets. However, for the examples we have studied, the multiple optima all give values of the area and capital cost targets within a few percent (e.g., 3%) of each other.

- Use integer cuts with units targeting MILP (P2) to generate all sets of the given number of matches for which a feasible HEN can be synthesized. Then solve area or capital cost targeting NLP (P3) or (P4) for every feasible set to determine the best area or capital cost target for the given number of matches.

For small HEN synthesis problems, it is relatively easy to use integer cuts to enumerate all feasible sets of a given number of matches. Example 2.4 in the next section illustrates this strategy. For larger synthesis problems, the MINLP or branch-and-bound procedures should be more efficient for determining the set of matches (of a given number) with the best area target. For the capital cost target, taking advantage of the fact that NLP (P4) tends to minimize the number of matches while minimizing capital cost should work in most cases.

2.5.3 Application of the Area and Capital Cost Targeting NLPs for HEN Synthesis

With equal heat transfer coefficients and no stream match restrictions, the composite curves provide a model for the "ideal" temperature profiles in a HEN achieving the utility and area targets. Similarly, the solution of area targeting NLP (P3) provides

a model for the "ideal" temperature profiles when synthesizing a HEN *with* unequal heat transfer coefficients and constraints on stream matches. By precisely following the temperature profiles in the NLP solution, one can synthesize a HEN structure (the spaghetti structure corresponding to the NLP solution) which exactly achieves the area and utility targets. The difficulty, of course, is to follow the temperature profiles with a practical number of exchangers.

In the solution of area or capital cost targeting NLP (P3) or (P4), each mathematical heat exchange match might be repeated in several EIs; in terms of the spaghetti structure, each match might be represented by several exchangers. However, it is also always possible to synthesize a HEN in which each match in the NLP solution corresponds to a *single* unit (exchanger, heater or cooler), even if some matches are repeated in several EIs. However, before proving this statement (given formally as Theorem 2.1 below), we need the following lemma:

Lemma 2.1 *While preserving the matches and their heat loads, any feasible solution of area or capital cost targeting NLP (P3) or (P4) can be converted to an equivalent feasible solution of units targeting MILP (P2).*

Proof We prove the lemma for feasible solutions of the area targeting NLP. The same proof also applies to solutions of the capital cost targeting NLP.

Feasible solutions of the area targeting NLP and the units targeting MILP can both be represented by heat cascade diagrams. For example, Fig. 2.4 shows the heat cascade corresponding to a feasible solution of the units targeting MILP (and the utility targeting LP) for the stream data in Table 2.1; Fig. 2.5 shows the heat cascade corresponding to a feasible solution of the area targeting NLP (i.e., the composite

curves) for the same stream data. The area targeting cascade differs from the units targeting cascade in two principal respects: (1) the TIs (defined at the stream supply temperatures) are subdivided into EIs (at the stream target temperatures), and (2) cold streams and utilities are allowed to cascade heat deficits. Thus to convert a feasible solution of the area targeting NLP to an equivalent solution of the units targeting MILP, all the EIs in each TI must be combined into a single interval, and all the heat deficits cascaded by the cold streams and utilities must be eliminated, while preserving the matches and their heat loads.

The cascaded deficits can be eliminated by shifting heat loads around loops in the heat cascade. Figures 2.9–2.11 demonstrate the conversion of the area targeting cascade in Fig. 2.5 to the units targeting cascade in Fig. 2.4. In Fig. 2.9, the EIs in each TI are combined into a single interval per TI; Figs. 2.10–2.11 show how the heat deficits cascaded from TIs 2 and 3 are eliminated. For example, the 132.8 kW heat deficit in Fig. 2.9 cascaded from TI 2 (to TI 1) along stream S_{c1} is eliminated by shifting loads around loop 1 as follows (the result is shown in Fig. 2.10): by *decreasing* the amount of heat transferred from steam to cold stream S_{c1} in TI 1 by 132.8 kW, we (1) *increase* by 132.8 kW the surplus heat which steam can cascade from TI 1 to TI 2, which (2) *increases* by 132.8 kW the amount of heat which steam can transfer to stream S_{c1} in TI 2, which (3) completely satisfies the heat requirement of stream S_{c1} in TI 2, and thus eliminates the 132.8 kW cascaded heat deficit. The net effect of this load shift is to postpone, from TI 1 to TI 2, 132.8 kW of heat transfer between steam and cold stream S_{c1}. The 46.7 kW deficit cascaded from TI 2 to TI 1 along stream S_{c2} is eliminated by shifting loads around loop 2 in a similar manner. The

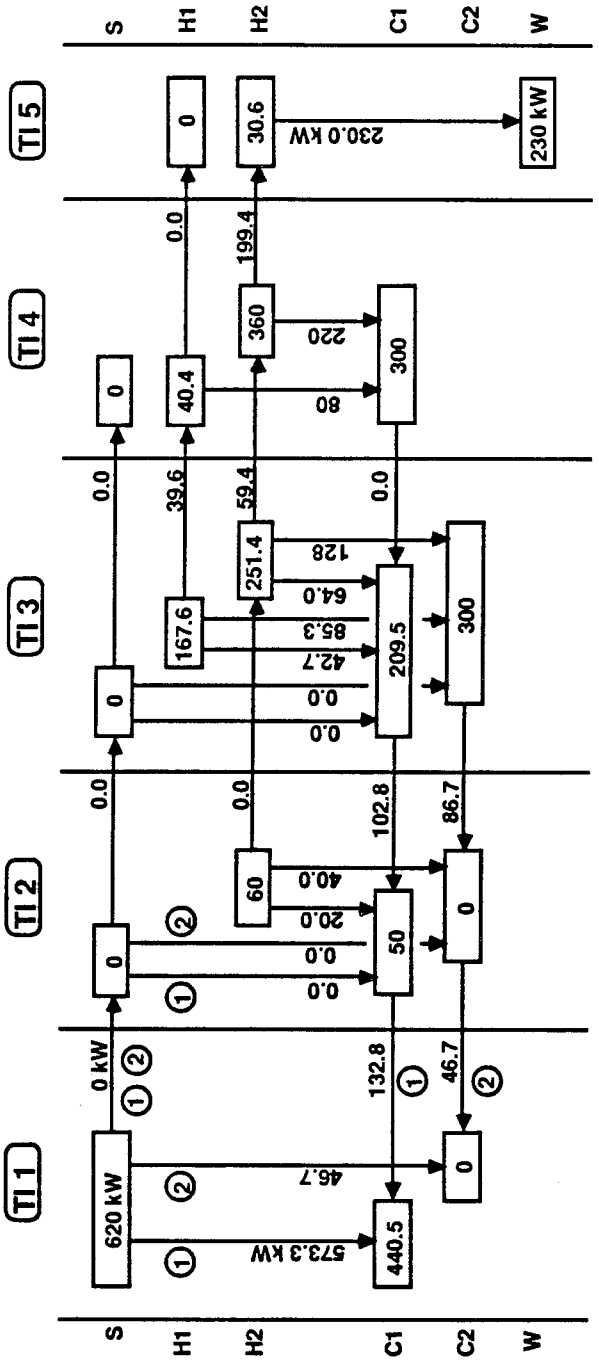

Figure 2.9: Converting an area targeting heat cascade to a units targeting heat cascade—combining the EIs.

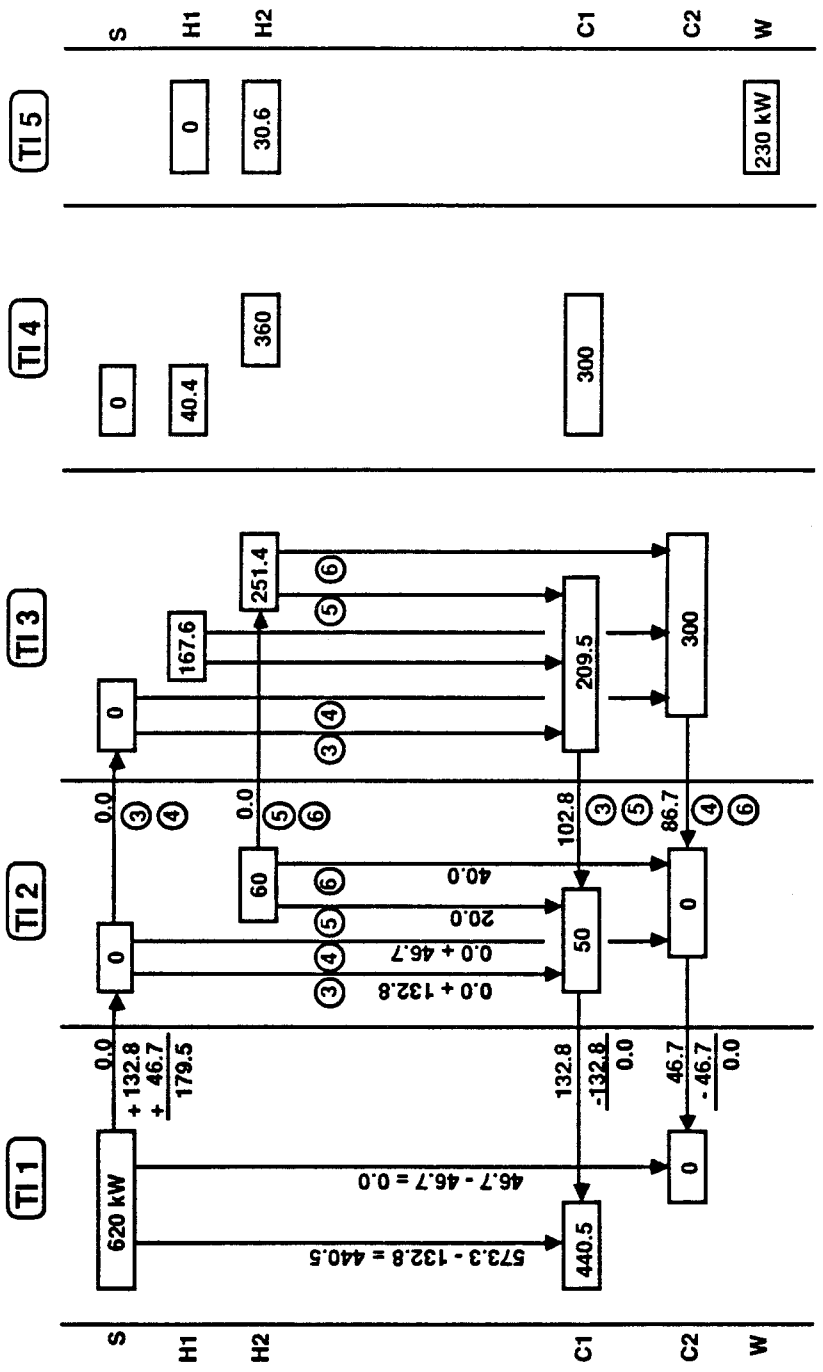

Figure 2.10: Converting an area targeting heat cascade to a units targeting heat cascade—shifting loads to eliminate cascaded heat deficits from TI 2.

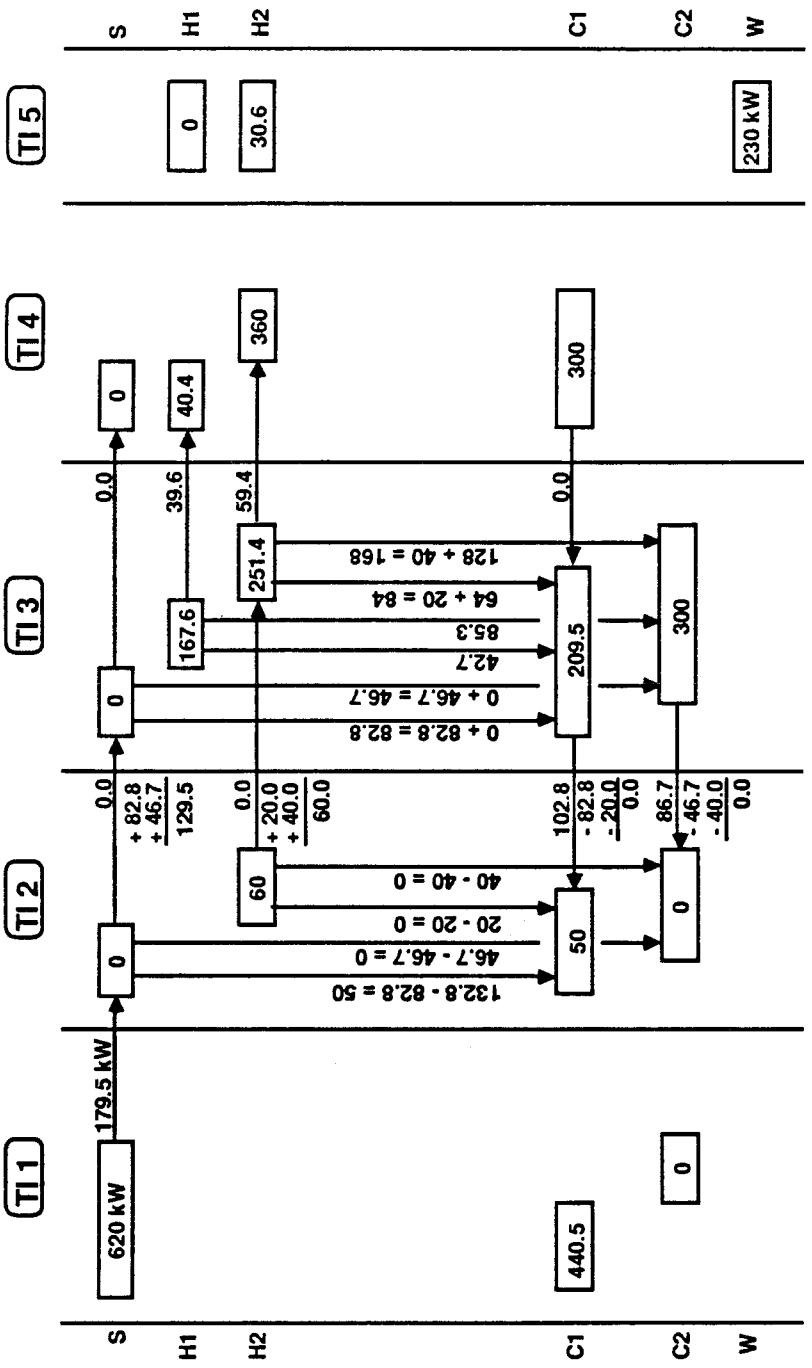

Figure 2.11: Converting an area targeting heat cascade to a units targeting heat cascade—shifting loads to eliminate cascaded heat deficits from TI 3.

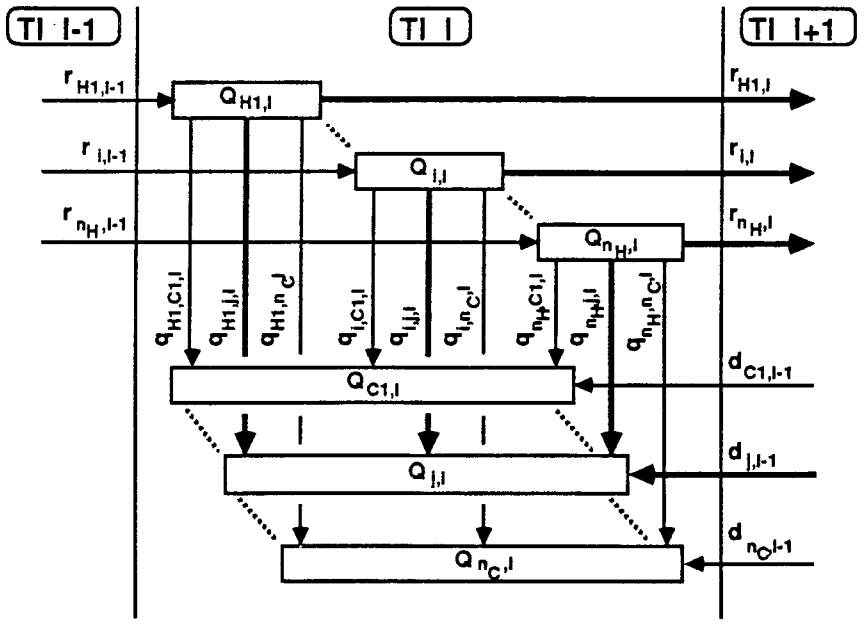

Figure 2.12: Typical temperature interval (TI) in the area targeting heat cascade.

heat deficits cascaded from TI 3 are eliminated by shifting loads around loops 3–6. By proceeding sequentially from TI to TI, all the cascaded deficits can be eliminated to produce the units targeting heat cascade in Fig. 2.4. Note that these load shifts do not create or eliminate any matches, or change the load (summed over all TIs) of any match. Thus the heat deficit cascade is eliminated while preserving the matches and their loads.

By using these types of load shifts, the cascaded deficits can be eliminated given any number of streams, TIs and loops in the heat cascade. Consider the general TI in Fig. 2.12 with an arbitrary number of hot and cold streams. This general TI represents the first (hottest) TI in a heat cascade, or the hottest remaining TI to which cascaded heat deficits have not been eliminated. The cascaded heat deficit

$d_{j,l+1}$ can be eliminated by shifting loads around one or more loops (bold lines in Fig. 2.12) involving heat exchange between cold stream S_{cj} and any hot stream in TI l, including steam. When shifting loads around any of these loops, the amount of heat transfer between stream S_{cj} and the corresponding hot stream is *decreased.* However, the energy balance on stream S_{cj} in TI l

$$\sum_i q_{i,j,l} = Q_{j,l} + d_{j,l+1}$$

guarantees that the total amount of heat transferred to stream S_{cj} in the TI is at least as large as the cascaded heat deficit to be eliminated

$$\sum_i q_{i,j,l} \geq d_{j,l+1}$$

since $Q_{j,l} \geq 0$. Thus, by taking advantage of every loop if necessary, there is always enough heat transfer within a TI to eliminate the heat deficits being cascaded to the TI. Since this is true for all TIs in any heat cascade diagram, the entire heat deficit cascade can be eliminated. Thus, any solution of the area targeting NLP can be converted to an equivalent feasible solution of the units targeting MILP. ■

Note that while the matches and their heat loads are preserved when converting a solution of area or capital cost targeting NLP (P3) or (P4) to an equivalent solution of units targeting MILP (P2), area is not necessarily preserved. In particular, the area changes when the EIs in each TI are combined into a single interval per TI. In addition, the stream temperatures at the TI boundaries change when the cascaded deficits are eliminated.

Theorem 2.1 *For any feasible solution of area or capital cost targeting NLP (P3) or (P4), a HEN can be synthesized with a one-to-one correspondence between each unit (and its load) in the HEN and each match (and its load, summed over all EIs in which the match appears) in the NLP solution.*

Proof From the lemma, any feasible solution of the area or capital cost targeting NLP can be converted to an equivalent solution of the units targeting MILP while preserving the matches and their heat loads. Floudas *et al.* (1986) proved that a one-to-one correspondence exists between the matches and their loads in the units targeting MILP solution and the units and their loads in a physical HEN. Thus, for any feasible solution of the area or capital cost targeting NLP, there exists a HEN with a one-to-one correspondence between the matches and their loads in the NLP solution and the units and their loads in the HEN. ■

Thus each mathematical match in the area or cost targeting NLP solution can be converted to a single exchanger while preserving its load. Unfortunately, area is not necessarily preserved. For example, when the spaghetti structure corresponding to the solution of area or capital cost targeting NLP (P3) or (P4) is simplified by merging exchangers and stream splits, the total load of each match is preserved, but the approach temperature distribution—hence area and capital cost—changes. However, for most problems this change is only a few percent of the corresponding target, especially if matches above and below the pinch are treated separately. As with the composite curve-based area target, the area and capital cost targets given by the NLP solutions are more difficult to achieve with a reasonable number of exchangers if the stream data exhibit multiple or "near" pinches.

The matches and heat loads given by solution of the area and capital cost targeting NLPs provide an excellent starting point for HEN synthesis. In particular, the spaghetti structure provides a good starting point for evolutionary development as long as one takes care to minimize the structural changes where the approach temperatures are tightest. A plot of the temperature profiles in the spaghetti structure, as a function of the cummulative amount of heat transferred by the network, is an especially useful tool to guide the designer during evolutionary development. In the case of equal heat transfer coefficients and no stream match constraints, this plot is the same as the composite curves. The matches and heat loads given by solution of the area or cost targeting NLPs also provide a good starting point for formulation and optimization of a HEN superstructure as used in the computer program MAGNETS (Floudas *et al.*, 1986).

The following example demonstrates that the area target given by NLP (P3) can be achieved (within a few percent) by a network with a reasonable number of units. In fact, this network uses significantly less area than that predicted by the composite curve-based area target. This example also demonstrates how temperature-enthalpy plots can be used as a tool with evolutionary development to synthesize networks approaching the area target.

Example 2.3 Consider the stream data in Table 2.4. (Note that the film heat transfer coefficients range over about two orders of magnitude.) For these data, the heating and cooling targets are 244.2 and 172.6 kW, respectively, where stream S_{c1} causes the pinch. The minimum number of units—when decomposing the problem at the pinch—is 6 units above, and 5 units below the pinch.

Table 2.4: Stream data for Example 2.3.

Stream	*Supply Temperature* (K)	*Target Temperature* (K)	*Heat Capacity Flow Rate* (kW/K)	*Film Heat Transfer Coefficient* ($kW/m^2 K$)
H1	626	586	9.802	1.25
H2	620	519	2.931	0.05
H3	528	353	6.161	3.20
C1	497	613	7.179	0.65
C2	389	576	0.641	0.25
C3	326	386	7.627	0.33
C4	313	566	1.690	3.20
Steam	650	650		3.50
Water	293	308		3.50

ΔT_m = 20 K (for utility targeting).

Table 2.5: Area targets and area of synthesized HEN for Example 2.3.

	Limit on Number of Matches		*Area*
	Above Pinch	*Below Pinch*	(m^2)
Area Targeting NLP	—	—	173.6
	7	5	176.1
	6	5	188.1
Composite Curve-Based Target	—	—	227.0
Synthesized HEN	7	5	188.9

Table 2.5 shows the area targets (1) when no limit is placed upon the number of stream matches, (2) for the best (least area) selection of matches corresponding to the units target, and (3) for the best selection of matches containing one match more than the units target. [The feasible match selections can all be generated by using integer cuts with units targeting MILP (P2). The problem is decomposed at the pinch by first applying area targeting NLP (P3) with no stream match restrictions (but with unequal heat transfer coefficients), and then using as pinch temperatures the temperatures of the streams as they cross the TI boundary associated with the

supply of pinch-causing stream S_{c1}.] As expected, the area target increases as the number of units is reduced. Note that in this example, the composite curve-based method overestimates the area target (with no limit on the number of matches) by 30.8%.

Figures 2.13 and 2.14 show the spaghetti structure corresponding to the best selection of seven matches above and five matches below the pinch. (Above the pinch, we are using one match more than the units target in order to more closely approach the area target obtained with no limit on the number of matches.) By using evolutionary development—with care to limit the structural changes where the approach temperatures are smallest—this spaghetti structure can be simplified to the point where each stream match corresponds to a single exchanger. Temperature-enthalpy plots corresponding to the spaghetti structure, and to the structures at each stage of evolutionary development, are a useful visual tool to quickly show where the approach temperatures are smallest and the exchanger loads are largest, and to show the effects of evolutionary development. Figures 2.15 and 2.16 contain the temperature-enthalpy profiles for the spaghetti structures in Figs. 2.13 and 2.14. These profiles show the temperature of each stream as a function of the *cummulative* amount of heat transferred in the network by all the streams.

The spaghetti structure *below* the pinch can be simplified as follows:

Step 1: In the spaghetti structure (Fig. 2.14), all the exchangers on stream S_{c3} occur in EIs 1.2–2.1, while the only exchanger on stream S_{h2} occurs in EI 2.1. Thus, it seems natural to merge these two EIs. Also, since only a single exchanger occurs in EI 2.2 (between streams S_{h3} and S_{c4}), and since this exchanger is repeated in

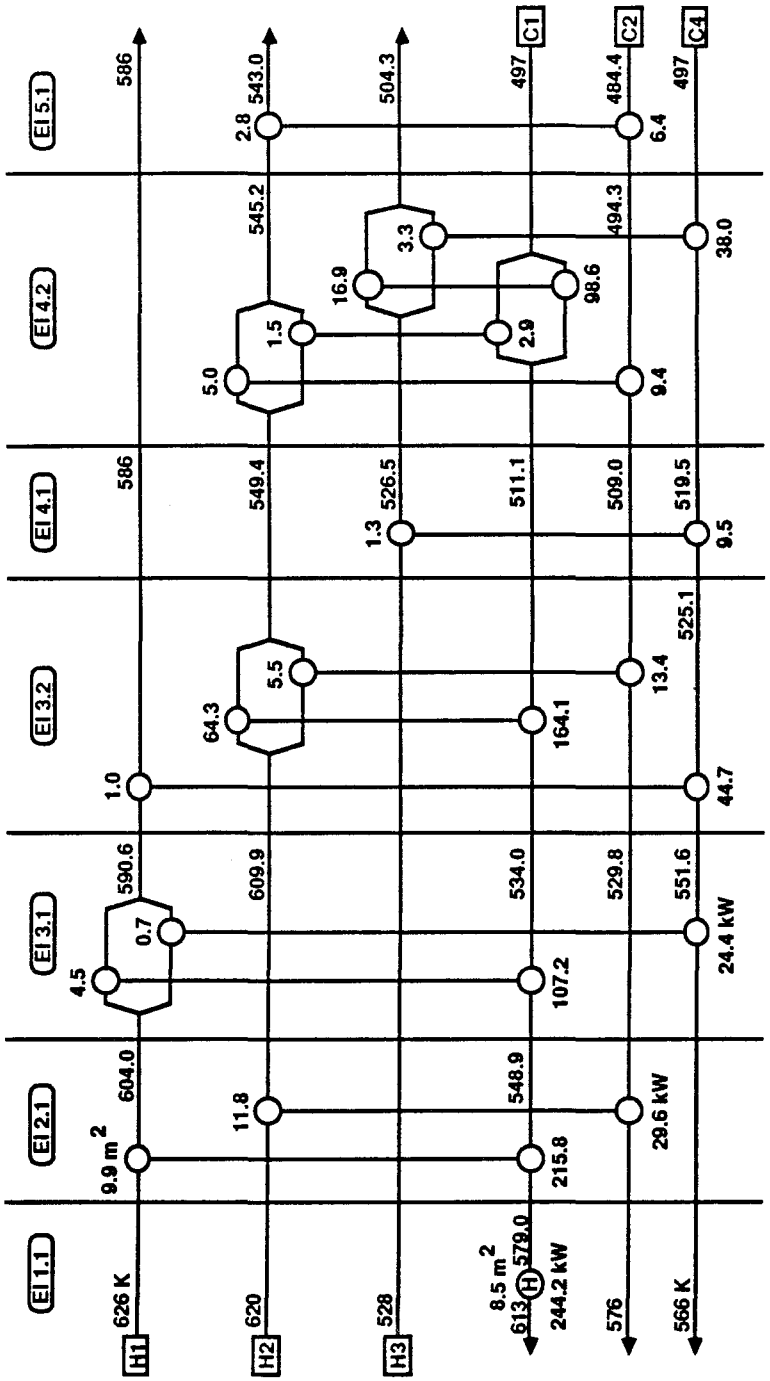

Figure 2.13: Spaghetti structure corresponding to the solution of the area targeting NLP *above* the pinch for Example 2.3.

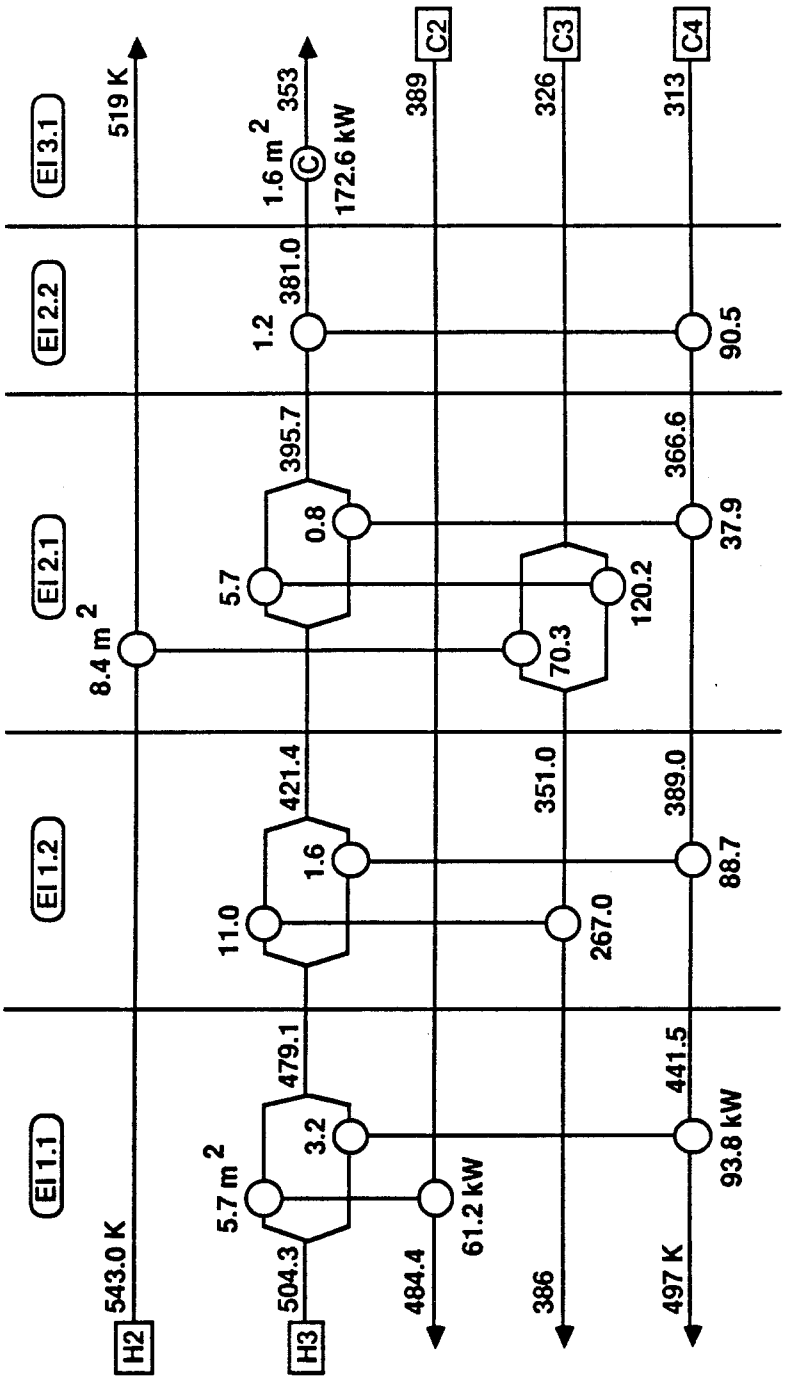

Figure 2.14: Spaghetti structure corresponding to the solution of the area targeting NLP *below* the pinch for Example 2.3.

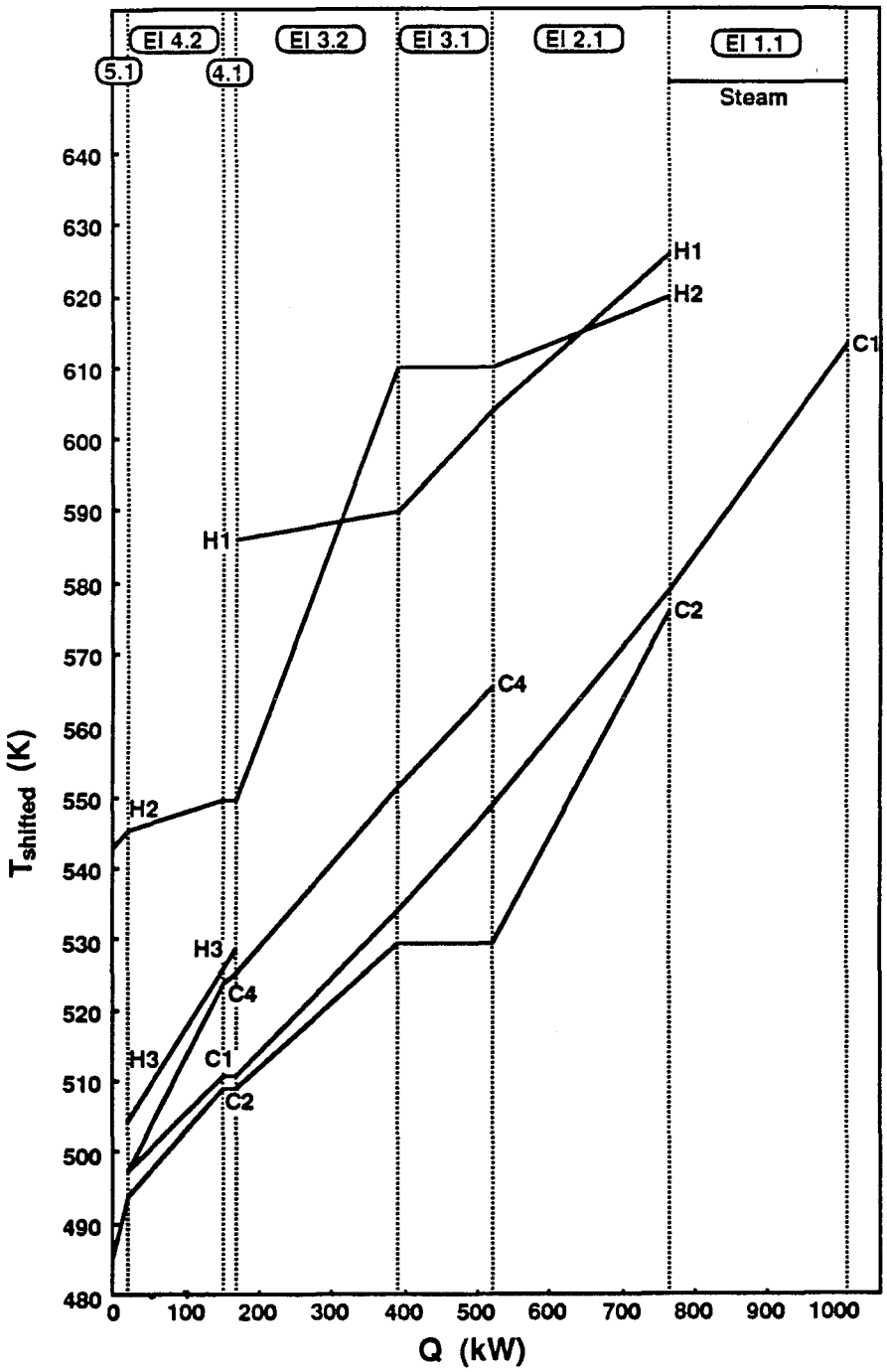

Figure 2.15: Temperature-enthalpy profiles corresponding to the spaghetti structure (Fig. 2.13) *above* the pinch in Example 2.3.

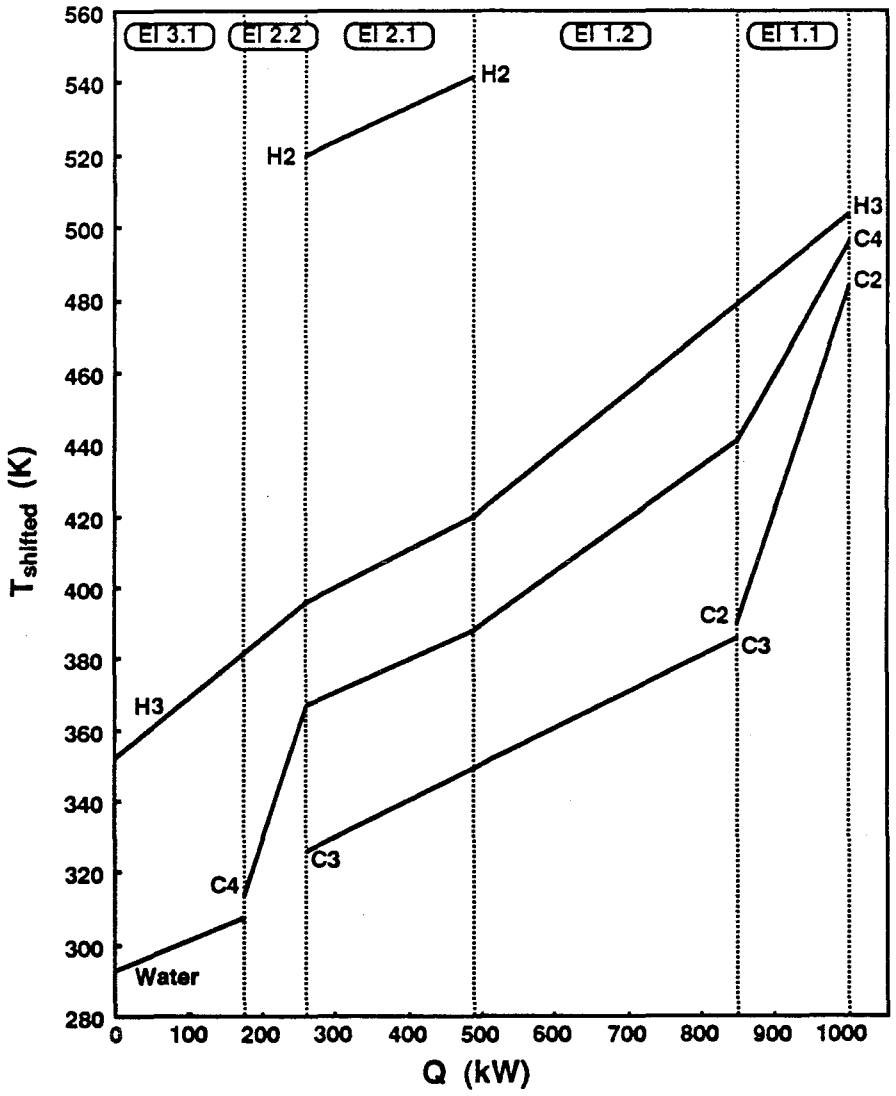

Figure 2.16: Temperature-enthalpy profiles corresponding to the spaghetti structure (Fig. 2.14) *below* the pinch in Example 2.3.

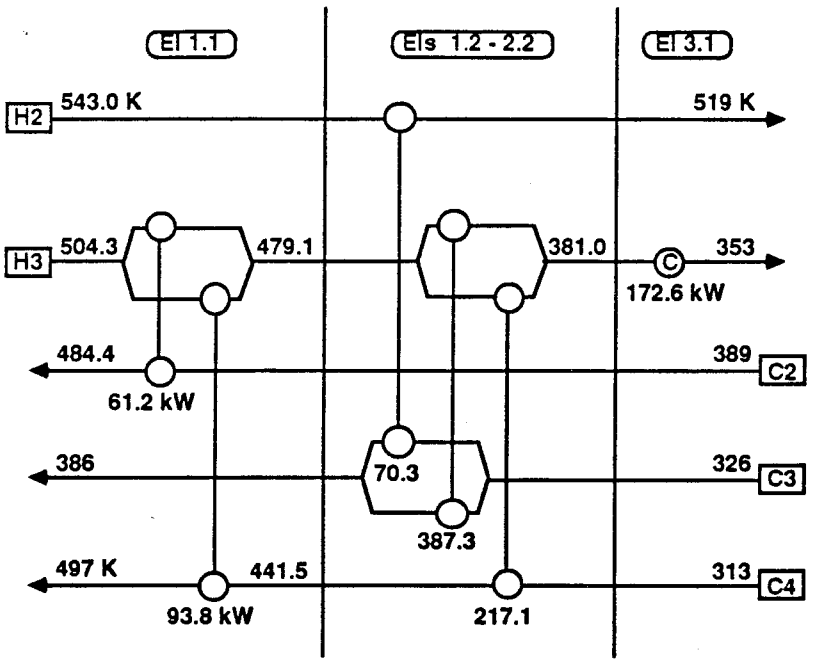

Figure 2.17: HEN structure after step 1 of evolutionary development *below* the pinch in Example 2.3.

EIs 1.2–2.1, we merge this EI (into EIs 1.2–2.1) as well. Figures 2.17 and 2.18 show the HEN structure and corresponding temperature profiles after merging EIs 1.2–2.2 (assuming isothermal stream mixing).

Note from the temperature profiles (Fig. 2.16) corresponding to the initial spaghetti structure (Fig. 2.14) that the approach temperatures are tightest in EI 1.1. This is expected since the hot end of EI 1.1 corresponds to the pinch. Because of the small approach temperatures in this EI, we delay as long as possible making any changes to the HEN structure in this EI (e.g., merging this EI with others).

Step 2: In the HEN structure in Fig. 2.17, stream S_{h3} is matched *in series* with streams S_{c2} (in EI 1.1) and S_{c3} (in EIs 1.2–2.2). [This succession of stream matches can also observed in the initial spaghetti structure (Fig. 2.14), and in the corresponding

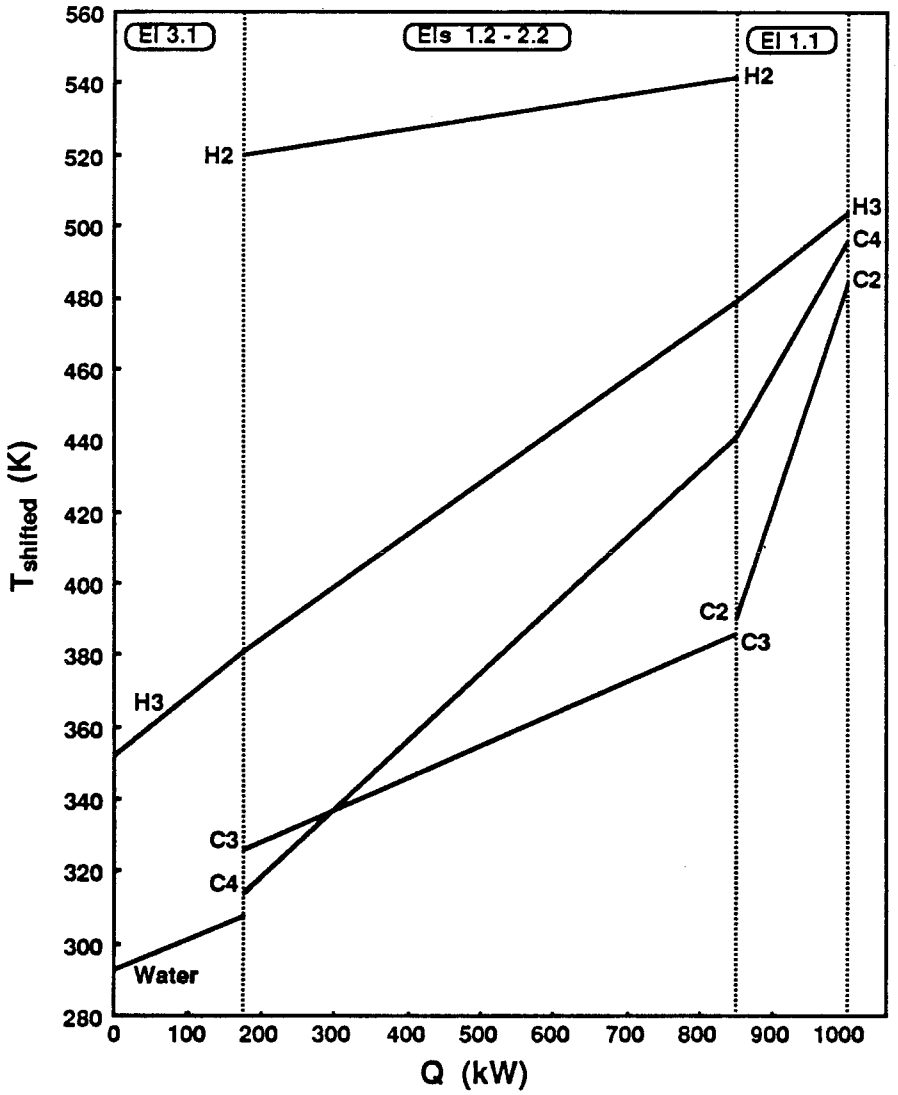

Figure 2.18: Temperature profiles of the HEN structure (Fig. 2.17) after step 1 of evolutionary development *below* the pinch in Example 2.3.

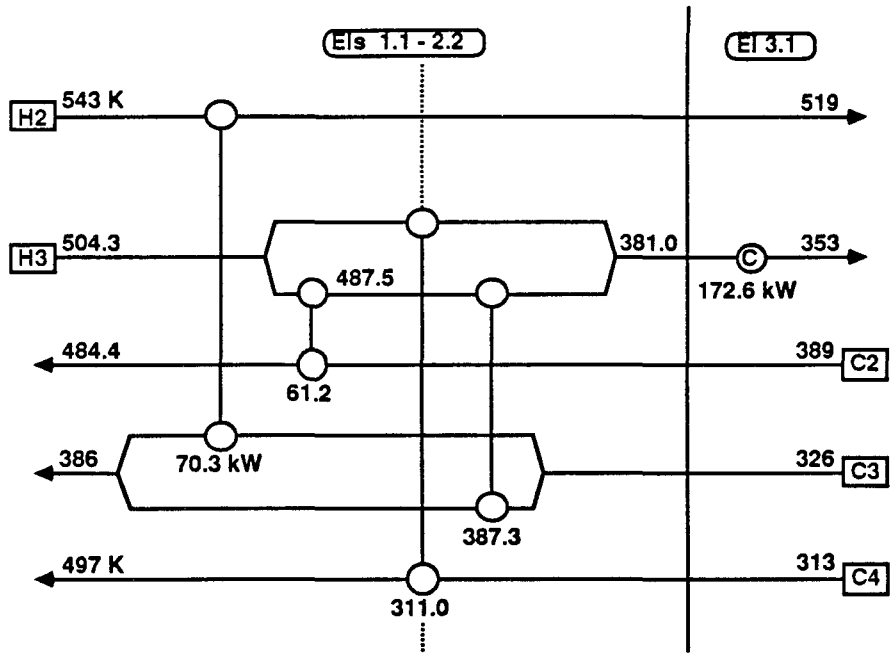

Figure 2.19: HEN structure after step 2 of evolutionary development *below* the pinch in Example 2.3.

temperature profiles.] Thus when merging EI 1.1 with EIs 1.2–2.2, we place the S_{h3}–S_{c3} exchanger in series with the S_{h3}–S_{c2} exchanger on the same branch of the S_{h3} stream split (Fig. 2.19). The corresponding temperature profiles are shown in Fig. 2.20.

Step 3: We now have a structure in which each stream match in the original spaghetti structure is represented by a single exchanger. However, since we reduced the number of exchangers by merging EIs, isothermal stream mixing may no longer be optimal. Minimizing the area required by the HEN structure in Fig. 2.19 produces the temperatures, loads and areas shown in Fig. 2.21. The total area of this network is 40.23 m^2.

In step 3, we finally allowed nonisothermal stream mixing. However, after any

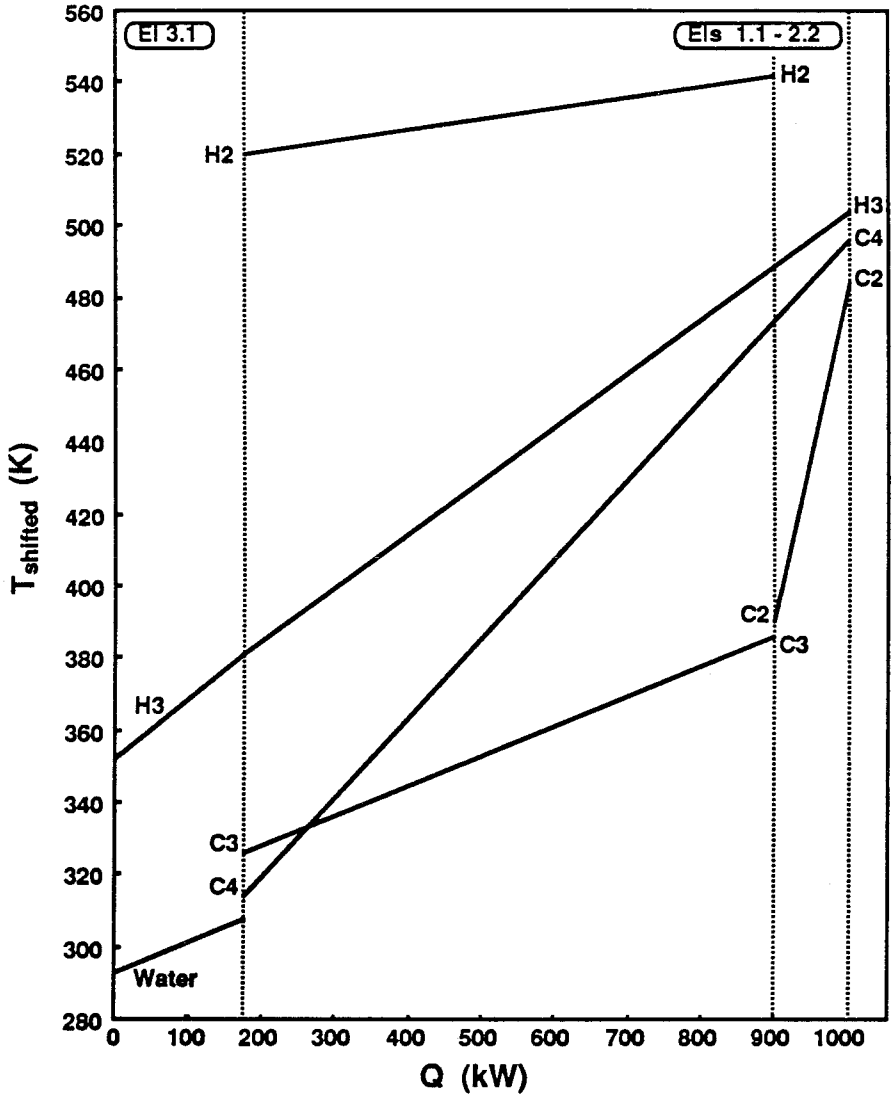

Figure 2.20: Temperature profiles of the HEN structure (Fig. 2.19) after step 2 of evolutionary development *below* the pinch in Example 2.3.

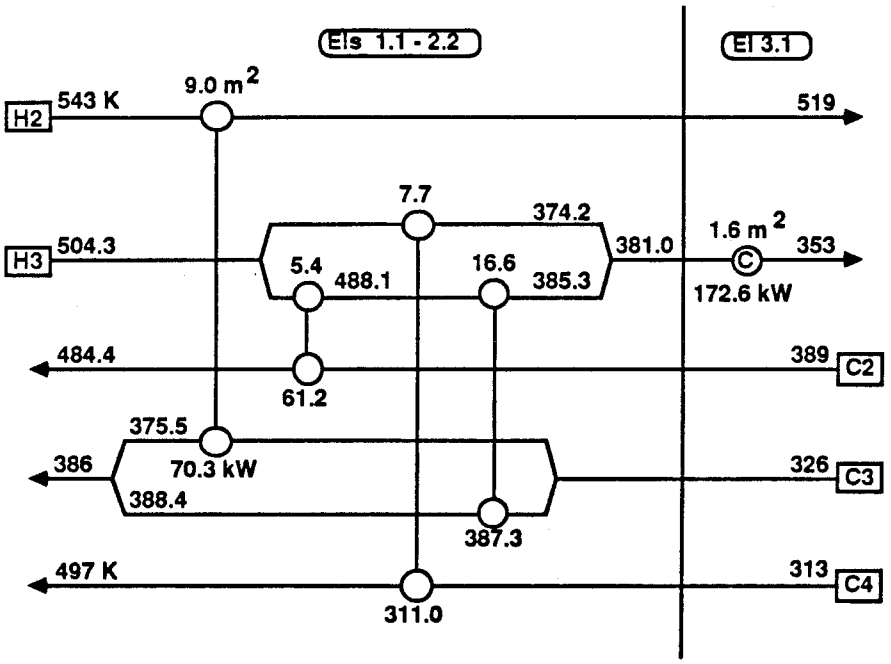

Figure 2.21: HEN structure after step 3 of evolutionary development *below* the pinch in Example 2.3.

evolutionary development step, isothermal stream mixing may no longer be optimal (or even feasible). Thus in general, one might optimize area after each step in order to find suitable stream split fractions. In addition, by optimizing area after each evolutionary step and by comparing this area with the area target (from the area targeting NLP), one can compare the cost (in terms of the additional area required) of different evolutionary changes.

The spaghetti structure *above* the pinch can be simplified as follows:

Step 1: In the spaghetti structure (Fig. 2.13), all the exchangers on stream S_{h1} occur in EIs 2.1–3.2 and, as shown in the temperature profiles in Fig. 2.15, these EIs all have relatively large approach temperatures; thus we merge EIs 2.1–3.2. In addition, EIs 4.1 and 5.1 each contain only one exchanger; the heat loads in these two EIs are small compared to the heat loads in the intervening EI 4.2; and the matches in these two EIs are repeated in EI 4.2. Thus, we also merge EIs 4.1 and 5.1 into EI 4.2. The resulting HEN structure and temperature profiles are shown in Figs. 2.22 and 2.23.

Step 2: In the HEN structure in Fig. 2.22, the exchanger between hot stream S_{h1} and cold stream S_{c1} (in EIs 2.1–3.2) occurs in series with the exchanger between hot stream S_{h3} and the same cold stream (in EIs 4.1–5.1). Thus when merging EIs 2.1–5.1, we place the S_{h1}–S_{c1} exchanger in series with the S_{h3}–S_{c1} exchanger on the same branch of the S_{c1} stream split (Fig. 2.24). The corresponding temperature profiles are shown in Fig. 2.25.

Step 3: The stream split fractions and exchanger loads in Fig. 2.24 are optimized to minimize network area. This yields the temperatures, loads and areas shown in

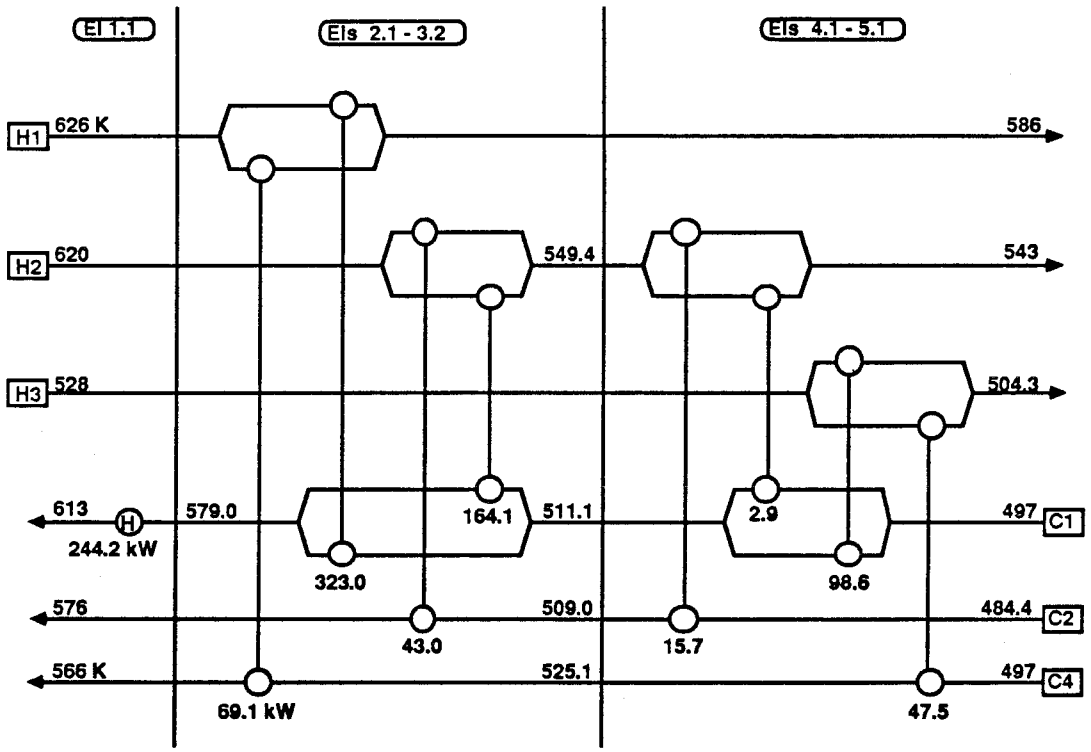

Figure 2.22: HEN structure after step 1 of evolutionary development *above* the pinch in Example 2.3.

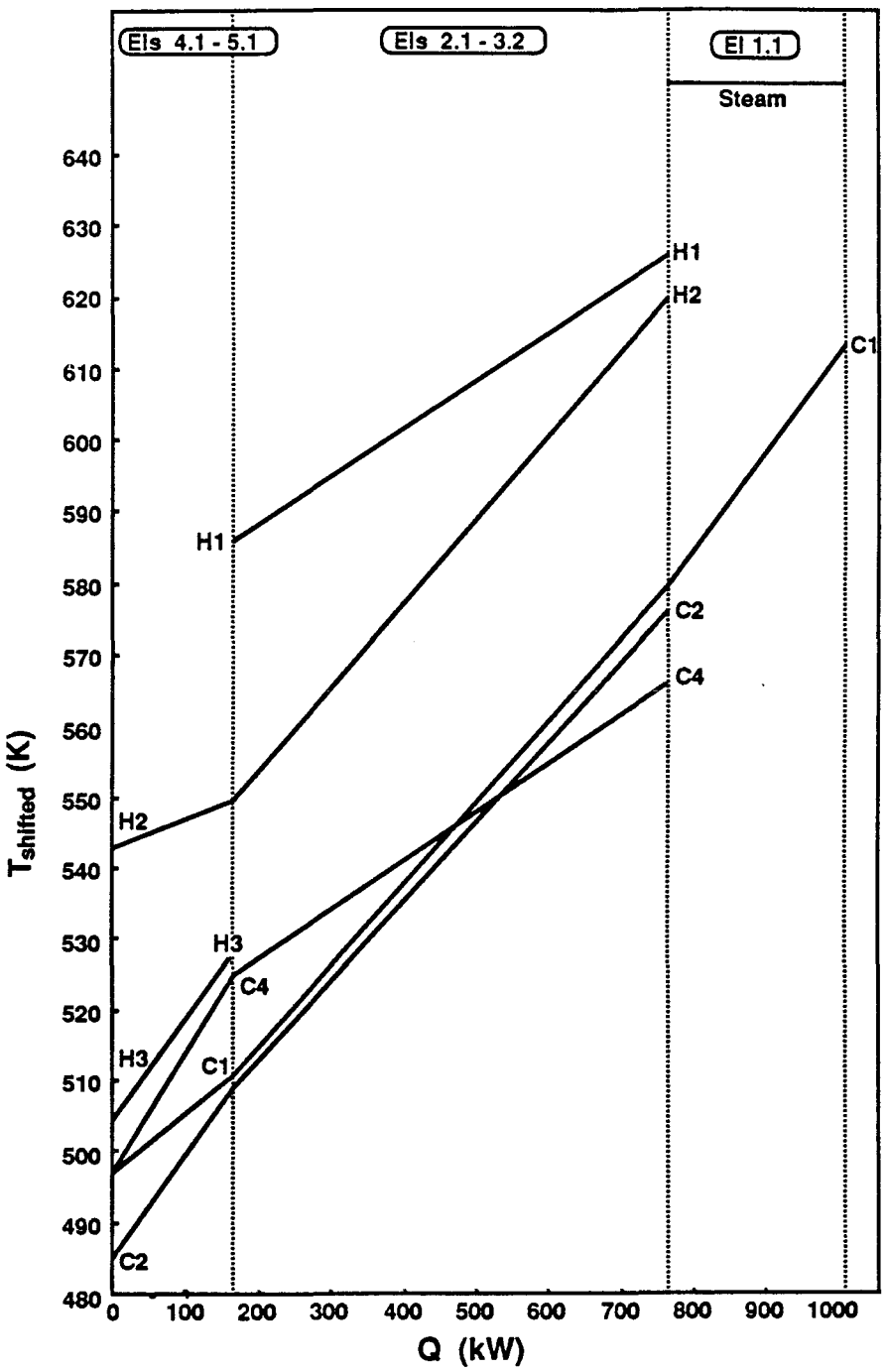

Figure 2.23: Temperature profiles of the HEN structure (Fig. 2.22) after step 1 of evolutionary development *above* the pinch in Example 2.3.

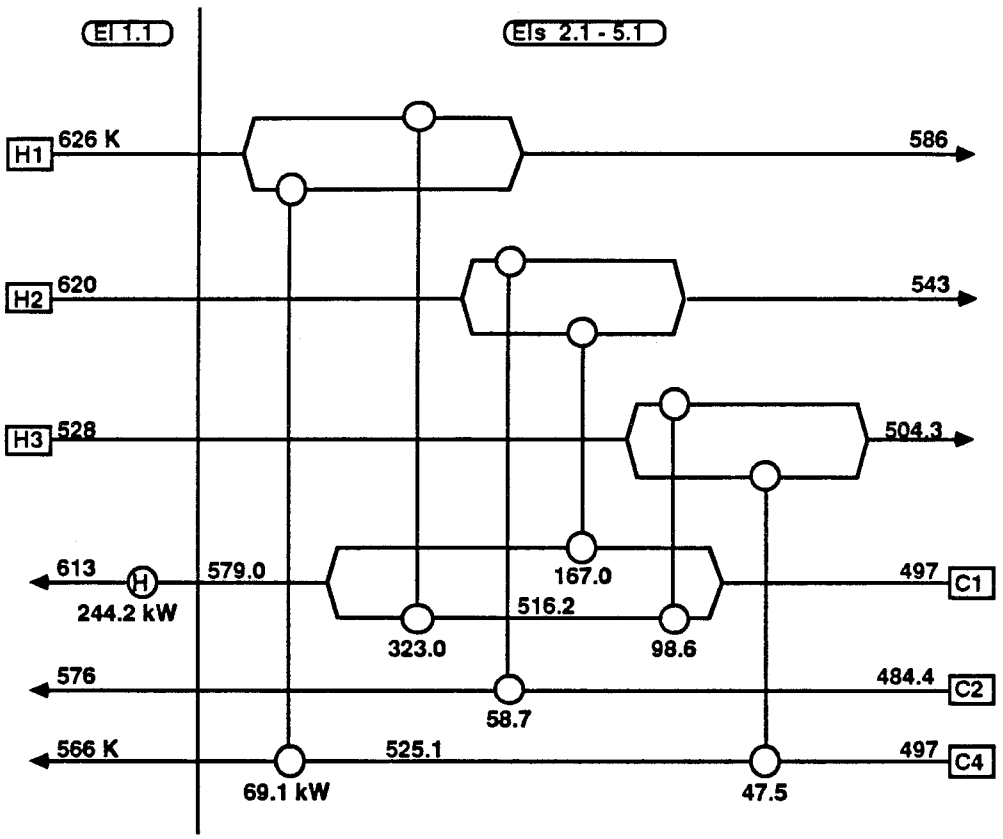

Figure 2.24: HEN structure after step 2 of evolutionary development *above* the pinch in Example 2.3.

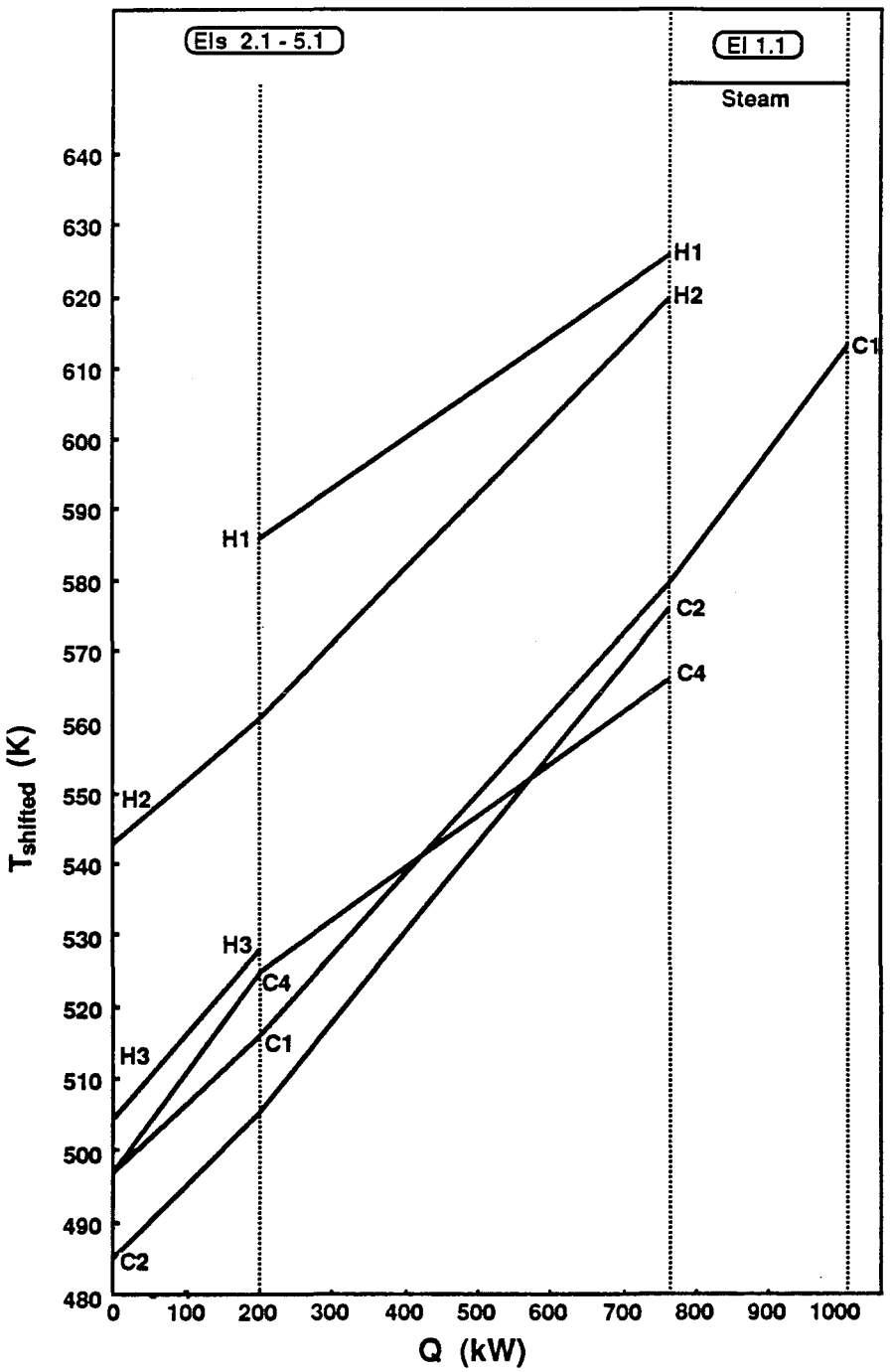

Figure 2.25: Temperature profiles of the HEN structure (Fig. 2.24) after step 2 of evolutionary development *above* the pinch in Example 2.3.

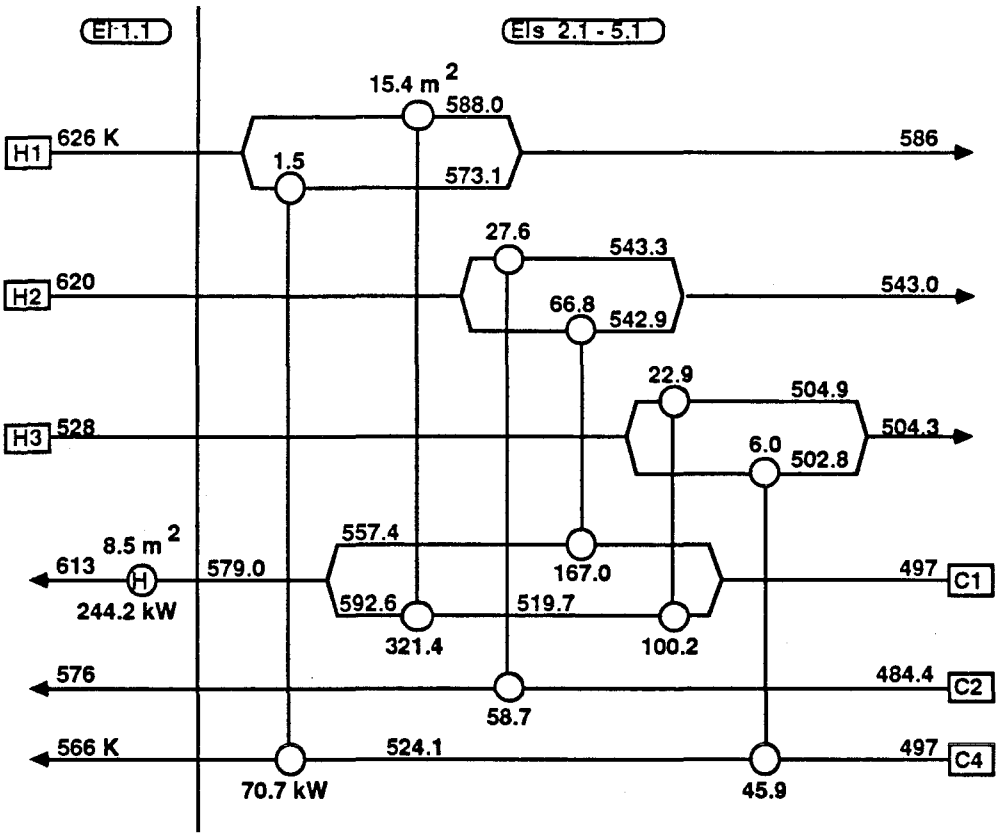

Figure 2.26: HEN structure after step 3 of evolutionary development *above* the pinch in Example 2.3.

Fig. 2.26. The total area of this network is 148.72 m^2.

The final HEN for this example is a combination of the networks shown in Figs. 2.26 (above the pinch) and 2.21 (below the pinch). The total area of this HEN is 188.9 m^2, 7.3% greater than the area target for seven matches above and five matches below the pinch, and *16.8% less* than the composite curve-based area target (Table 2.5). ■

It is common in the HEN synthesis literature to require that the value of ΔT_m used for synthesis [the exchanger minimum approach temperature, EMAT] be the same as that used for utility targeting [the heat recovery approach temperature, HRAT

(Challand *et al.*, 1981)]. However, this yields networks with minimum area (and utilities) only if the heat transfer coefficients are equal and if the synthesis problem is decomposed at the pinch. If the heat transfer coefficients are unequal, EMAT should be less than HRAT—smaller approach temperatures should be allowed in exchangers with good heat transfer coefficients so that one can take advantage of larger approach temperatures in exchangers with poor heat transfer coefficients. If the problem is not decomposed at the pinch (so that the number of units can be reduced), EMAT should be less than HRAT so that more stream matching choices are available (Gundersen and Grossmann, 1988). In fact, EMAT is *not* a parameter which the designer must specify before synthesis; any synthesis or targeting procedure which minimizes area or cost should allow EMAT to vary, and thus choose the appropriate value of EMAT for synthesis (Gundersen and Grossmann, 1988). Area and cost targeting NLPs (P3) and (P4) allow EMAT to vary subject to lower bound ΔT_m^L.

The following example demonstrates the use of the area and capital cost targeting NLPs for HEN synthesis. It illustrates the use of the targets to predict the trade-off between area or capital cost and the number of units, and the fact that EMAT less than HRAT is optimal when reducing the number of units. This example also demonstrates that the NLP solutions provide an excellent starting point for MAGNETS to synthesize HENs with near-minimum area where the units and their loads in the HEN correspond to the matches and their loads in the NLP solution.

Example 2.4 *(adopted from Gundersen and Grossmann, 1988).* Consider the stream data in Table 2.6. For the specified value of HRAT, the heating and cooling targets are 1075 and 400 kW, respectively, where stream S_{h2} causes the pinch.

Table 2.6: Stream and cost data for Example 2.4.

Stream	*Supply Temperature* (K)	*Target Temperature* (K)	*Heat Capacity Flow Rate* (kW/K)	*Film Heat Transfer Coefficient* (kW/m^2 K)
H1	423	333	20	0.1
H2	363	333	80	0.1
C1	293	398	25	0.1
C2	298	373	30	0.1
Steam	453	453		0.1
Water	283	288		0.1

$\Delta T_m = 20$ K (for utility targeting).
Capital cost $= 8600 + 670A^{0.83}$.

The units target is seven if we divide the synthesis problem at the pinch (for EMAT = HRAT = 20 K); however, with fixed amounts of heating and cooling, the number of units can be reduced to five if we do not decompose at the pinch and if we allow EMAT to vary (EMAT $> \Delta T_m^L = 0.1$ K).

For this simple example, it is easy to determine—by using integer cuts with units targeting MILP (P2)—all the sets of five, six, and seven matches for which a feasible HEN can be synthesized. Table 2.7 lists these sets along with their corresponding area and cost targets, and the value of EMAT given by the temperatures from the area targeting NLP solution. The sets are listed in increasing order of area target. Each set of seven matches is determined by decomposing the problem at the pinch (three matches above and four matches below the pinch). Each set of five or six matches is determined without decomposition at the pinch. Note that the optimal value of EMAT for minimizing area *decreases* below the value of HRAT when the number of units is reduced.

The area and capital cost targets for the best (minimum area) sets of matches are

Table 2.7: Area and cost targets for Example 2.4.

Number of Matches	*Matches*								*Area Target* (m^2)	*Cost Target* (1000$)	EMAT (K)
	S C1	S C2	H1 C1	H1 C2	H1 W	H2 C1	H2 C2	H2 W			
7	a		a,b	a		b	b	b	2909	744	20
	a		a	a,b		b	b	b	2910	746	20
	a		a	a,b	b	b	b		2938	742	20
	a		a,b	a	b	b	b		2938	742	20
	a	a	a,b			b	b	b	3122	771	20
	a	a	a	b		b	b	b	3123	773	20
	a	a	a	b	b	b	b		3151	769	20
	a	a	a,b		b	b	b		3151	769	20
6	*		*	*		*	*	*	2919	716	18
	*		*	*	*	*	*		2966	713	18
	*	*	*			*	*	*	3018	726	15
	*	*	*		*	*	*		3076	730	15
		*	*		*	*	*	*	3546	803	13
		*	*	*		*	*	*	3547	824	13
5	*			*		*	*	*	3133	714	8
	*			*	*	*	*		3219	733	8
		*	*			*	*	*	3551	787	13
		*	*		*	*	*		3597	801	13

('a' = above pinch; 'b' = below pinch)

2909 m^2 and \$744,000 (7 matches), 2919 m^2 and \$716,000 (6 matches), and 3133 m^2 and \$714,000 (5 matches). (For comparison, the area and capital cost targets with no stream match restrictions are 2896 m^2 and \$714,000.) As expected, the area target increases when the number of matches is reduced. However, from the capital cost targets, we can see the trade-off between area and the number of units: for HENs with five or six units (one for each match), capital costs should be roughly the same; HENs with seven units will likely be more expensive than those with fewer units.

To our knowledge, no other existing area or capital cost targeting method can predict the trade-off between area and the number of units; in particular, since other methods cannot handle constraints on stream matches, they cannot predict the increase in area as the number of units is reduced. Thus existing capital cost targeting methods use the same amount of area—calculated with no stream match restrictions—for any number of units.

We used the computer program MAGNETS (Floudas *et al.*, 1986)—with the matches and heat loads from the best five-, six- and seven-match area targeting NLP solutions listed in Table 2.7—to synthesize the networks shown in Fig. 2.27. In each of these networks, the units and their loads correspond to the matches and their loads in the NLP solutions. All three HENs have areas and capital costs within 3% of their respective targets (Table 2.8).

If we had not specified the matches and heat loads for MAGNETS, the program would have used the matches and heat loads given by solution of units targeting MILP (P2). The difficulty with this MILP is that it selects the matches and loads with no regard for area. In fact, when we used MILP (P2) to determine all feasible

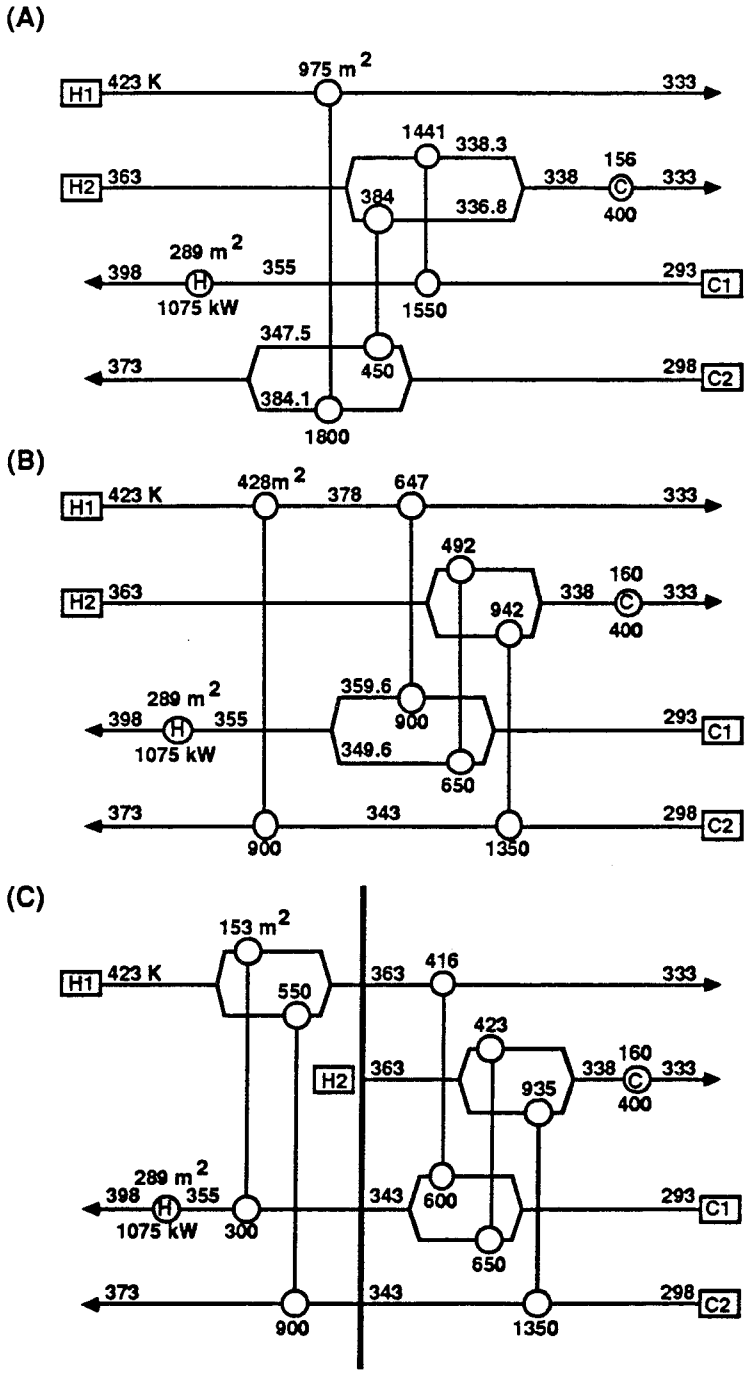

Figure 2.27: HENs obtained with MAGNETS by using the matches and heat loads from the best (a) 5-match, (b) 6-match, and (c) 7-match solutions of the area targeting (Example 2.4).

Table 2.8: Areas and capital costs of the HENs synthesized from the best five-, six- and seven-match solutions of the area targeting NLP (Example 2.4).

Number of Matches	*Area*			*Capital Cost*		
	Network (m^2)	*Target* (m^2)	*% over Target*	*Network* (1000$)	*Target* (1000$)	*% over Target*
5	3215	3133	2.6	732	714	2.5
6	2960	2919	1.4	729	716	1.8
7	2925	2909	0.6	746	744	0.3

sets of matches for this example, it tended to choose the sets of matches in order of decreasing area as we applied integer cuts; in particular, before applying the first integer cut, the MILP tended to choose among the sets of matches requiring *most* area. ■

Gundersen and Grossmann (1988) recently developed a variation of units targeting MILP (P2) where the difference from "vertical" matching (countercurrent matching on the composite curves) is minimized at the same time as the number of units. Since the composite curves yield a rigorous area target when the heat transfer coefficients are equal, this "vertical" units targeting MILP chooses sets of matches leading to good area when the heat transfer coefficients are similar. However, when the heat transfer coefficients differ widely, matching far from vertical is generally required to minimize area, and the area and capital cost targeting NLPs in this chapter will better choose sets of matches leading to lower area and cost.

2.6 Summary

This chapter presents a pair of "transshipment" NLPs to calculate the area and capital cost targets (for fixed design conditions) for HEN synthesis problems with limits on the number of matches/units, forbidden matches, unequal heat transfer coefficients, and different capital cost laws (for different materials of construction, pressure ratings, etc.). With these new targeting NLPs, one can truly predict the trade-off between area and the number of units. In addition, by requiring the presence of selected matches with specified areas, area and capital cost targets can be calculated for revamp synthesis. And since these NLPs allow noncountercurrent stream matching (as opposed to the completely countercurrent stream matching implied by the composite curves), they can rigorously handle problems with unequal heat transfer coefficients among any number of hot and cold streams. For problems with one cold and several hot streams (or vice versa), the area targeting NLP reproduces the rigorous area target of Nishimura (1980).

Just as the composite curves provide a model for the "ideal" temperature profiles in a HEN with no stream match constraints and equal heat transfer coefficients, solution of the area or capital cost targeting NLP provides a model for the "ideal" temperature profiles in a HEN *with* stream match constraints and *unequal* heat transfer coefficients. In addition, the NLP solution gives the proper choice of matches and a good heat load distribution for minimizing area (or capital cost). We show that a HEN can always be synthesized with a one-to-one correspondence between units and loads in the HEN and matches and loads in the NLP solution. These matches and heat loads provide an excellent starting point for synthesis of HENs which achieve

(within a few percent) the area and capital cost targets, while using the same number of units as there are matches in the NLP solution.

2.7 References

[1] Ahmad, S., Heat Exchanger Networks: Cost Trade-offs in Energy and Capital, Ph.D. Thesis, Univ. of Manchester Inst. of Sci. and Tech., U. K. (1985).

[2] Ahmad, S. and B. Linnhoff, Overall Cost Targets for Heat Exchanger Networks, paper presented at *IChemE Ann. Res. Mtg.*, Bath, U. K. (1984).

[3] Cena, V., C. Mustacchi and F. Natali, Synthesis of Heat Exchange Networks: A Non-Iterative Approach, *Chem. Eng. Sci.*, **32**, 1227 (1977).

[4] Cerda, J. and A. W. Westerberg, Synthesizing Heat Exchanger Networks Having Restricted Stream/Stream Matches Using Transportation Problem Formulations, *Chem. Eng. Sci.*, **38**, 1723 (1983).

[5] Cerda, J., A. W. Westerberg, D. Mason and B. Linnhoff, Minimum Utility Usage in Heat Exchanger Network Synthesis: A Transportation Problem, *Chem. Eng. Sci.*, **38**, 373 (1983).

[6] Challand, T. B., R. W. Colbert and C. K. Venkatesh, Computerized Heat Exchanger Networks, *Chem. Eng. Prog.*, **77**, No. 7, 65 (July 1981).

[7] Duran, M. A. and I. E. Grossmann, A Mixed-Integer Nonlinear Programming Algorithm for Process Synthesis, paper presented at *AIChE Ann. Mtg.*, San Francisco (1984).

[8] Floudas, C. A., A. R. Ciric and I. E. Grossmann, Automatic Synthesis of Optimum Heat Exchanger Network Configurations, *AIChE J.*, **32**, 276 (1986).

[9] Gundersen, T. and I. E. Grossmann, Improved Optimzation Strategies for Automated Heat Exchanger Network Synthesis through Physical Insights, paper presented at *AIChE Ann. Mtg.*, Washington, D. C. (1988).

[10] Hohmann, E. C., Optimum Networks for Heat Exchange, Ph.D. Thesis, Univ. Southern California, Los Angeles (1971).

[11] Kesler, M. G. and R. O. Parker, Optimal Networks of Heat Exchange, *Chem. Eng. Prog. Symp. Ser.*, No. 92, **65**, 111 (1969).

[12] Kobayashi, S., T. Umeda and A. Ichikawa, Synthesis of Optimal Heat Exchange Systems—An Approach by the Optimal Assignment Problem in Linear Programming, *Chem. Eng. Sci.*, **26**, 1367 (1971).

[13] Kocis, G. R. and I. E. Grossmann, Relaxation Strategy for the Structural Optimization of Process Flowsheets, paper presented at *AIChE Ann. Mtg.*, Miami (1986).

[14] Linnhoff, B. and J. R. Flower, Synthesis of Heat Exchanger Networks: I. Systematic Generation of Energy Optimal Networks, *AIChE J.*, **24**, 633 (1978).

[15] Linnhoff, B. and D. R. Vredeveld, Pinch Technology Has Come of Age, *Chem. Eng. Prog.*, **80**, No. 7, 33 (July 1984).

[16] Murtagh, B. A. and M. A. Saunders, *MINOS 5.0 User's Guide*, Tech. Rpt. SOL 83-20, Systems Optimization Lab., Dept. Operations Research, Stanford Univ., Palo Alto, CA (1983).

[17] Nishida, N., S. Kobayashi and A. Ichikawa, Optimal Synthesis of Heat Exchange Systems: Necessary Conditions for Minimum Heat Transfer Area and Their Application to Systems Synthesis, *Chem. Eng. Sci.*, **26**, 1841 (1971).

[18] Nishimura, H., A Theory for the Optimal Synthesis of Heat Exchanger Systems, *J. Opt. Th. Appl.*, **30**, 423 (1980).

[19] O'Young, D. L., D. M. Jenkins and B. Linnhoff, The Constrained Problem Table for Heat Exchanger Networks, *Understanding Process Integration II*, IChemE Symp. Ser. 109, 75 (1988).

[20] Papoulias, S. A. and I. E. Grossmann, A Structural Optimization Approach in Process Synthesis—II. Heat Recovery Networks, *Comp. Chem. Eng.*, **7**, 707 (1983).

[21] Paterson, W. R., A replacement for the logarithmic mean, *Chem. Eng. Sci.*, **39**, 1635 (1984).

[22] Raghavan, S., Heat Exchanger Network Synthesis: A Thermodynamic Approach, Ph.D. Thesis, Purdue Univ., Lafayette, IN (1977).

[23] Saboo, A. K., M. Morari and R. D. Colberg, RESHEX: An Interactive Software Package for the Synthesis and Analysis of Resilient Heat Exchanger Networks—II. Discussion of Area Targeting and Network Synthesis Algorithms, *Comp. Chem. Eng.*, **10**, 591 (1986).

[24] Townsend, D. W. and B. Linnhoff, Surface Area Targets for Heat Exchanger Networks, paper presented at *IChemE Ann. Res. Mtg.*, Bath, U. K. (1984).

[25] Umeda, T., J. Itoh and K. Shiroko, Heat Exchange System Synthesis, *Chem. Eng. Prog.*, **74**, 7, 70 (July 1978).

Chapter 3

Analysis and Synthesis of Resilient Heat Exchanger Networks—A Review

ANALYSIS AND SYNTHESIS OF RESILIENT HEAT EXCHANGER NETWORKS

Richard D. Colberg and Manfred Morari

Department of Chemical Engineering
California Institute of Technology
Pasadena, California 91125

I. Introduction

Research on the synthesis of economically optimal heat exchanger networks (HENs) has been performed for over 15 years (Nishida *et al.*, 1981). As a result of this research, two general conclusions have emerged: (1) the optimum network generally features minimum or close to minimum utility consumption, and (2) the optimum network generally has a mini-

mum or close to minimum number of units (exchangers, heaters, and coolers).

As aids in synthesizing economically optimal HENs, targets have been developed to predict *before* synthesis the minimum utilities required (Hohmann, 1971; Raghavan, 1977; Linnhoff and Flower, 1978) and the minimum units required (Hohmann, 1971) for given values of the stream supply and target temperatures and heat capacity flow rates and an assumed value of minimum approach temperature ΔT_m. Thus most recent HEN synthesis algorithms decompose the synthesis problem into at least two stages: (1) targeting of minimum utilities and minimum units and (2) synthesis of a HEN structure with minimum utility consumption and with minimum or close to minimum number of units.

Most recent synthesis algorithms are also based upon the principles of the thermodynamic "pinch" (Linnhoff *et al.*, 1979; Umeda *et al.*, 1978). Recognition of the pinch provided great physical insight into the problem of HEN synthesis. The reader is assumed to be familiar with the principles of the pinch and with general methods for HEN synthesis [e.g., pinch design method (Linnhoff *et al.*, 1982; Linnhoff and Hindmarsh, 1983), structural optimization methods for selection of a minimum set of stream matches (Papoulias and Grossmann, 1983), and determination of the most economical network structure (Floudas *et al.*, 1986) from the predicted matches].

The difficulty with these synthesis methods is that they generate HENs for *fixed* nominal values of the stream supply temperatures and flow rates and for assumed nominal values of the heat transfer coefficients. In an industrial HEN, the supply temperatures and flow rates will vary (because of unpredictable environmental disturbances or because of predictable feedstock and throughput changes), and the heat transfer coefficients are highly uncertain (due to fouling, etc.). The HEN synthesized for nominal conditions must be *resilient* (flexible) to changes in supply temperatures and flow rates and to uncertainties in heat transfer coefficients.

In general, the entire process plant should be resilient. However, in a tightly energy-integrated plant, it is especially important that the HEN be resilient—if the HEN cannot operate, then neither can the plant.

In the past, HEN resilience was often assumed if the HEN could operate for perceived "worst" cases (i.e., combinations of highest and lowest temperatures and flow rates. However, as the next section of this chapter demonstrates, the worst cases for resilience may not agree with intuition (e.g., nonlinearities may cause the worst case for resilience to occur at intermediate values of temperature and flow rate).

A more sophisticated approach to analyzing HEN resilience is to use "shifting" arguments. By considering the effects of temperature and flow

rate disturbances as they are shifted and/or propagated toward the heaters and coolers (which can absorb the disturbances), one can gain physical insight into the problem of HEN resilience. However, the shifting arguments are difficult to apply quantitatively to HENs with several degrees of freedom (several exchangers more than the minimum required and/or stream splits), and it is difficult to study interactions between multiple disturbances.

In this chapter more systematic methods for HEN resilience analysis and three procedures for synthesis of resilient HENs are reviewed. Section II demonstrates how simple, empirical HEN resilience tests can fail and establishes the need for more systematic HEN resilience analysis methods. Section III presents several rigorous analysis methods, states the conditions when they are linear, and includes special nonlinear forms. Section IV reviews three procedures for synthesis of resilient HENs: (1) synthesis based on a resilience target (Colberg *et al.*, 1988); (2) "multiperiod" synthesis–analysis–resynthesis algorithm (Floudas and Grossmann, 1987b), which is an extension of the structural optimization synthesis algorithm for fixed stream conditions; and (3) synthesis using "downstream (disturbance) paths" (Linnhoff and Kotjabasakis 1986).

The scope of this chapter is limited to resilience of HENs in the steady state. Obviously, it is important that a HEN be controllable and that it be resilient to dynamic changes in temperature and flow rate (Morari *et al.*, 1985). However, dynamic resilience will not be addressed. Also, many of the resilience concepts reviewed here were developed for general chemical processes (Grossmann and Morari, 1983; Swaney and Grossmann, 1985a; Grossmann and Floudas, 1987; Linnhoff and Kotjabasakis, 1986). However, in this chapter they will be applied specifically to HENs.

II. Empirical versus Systematic Methods for HEN Resilience

A. Why Empirical Methods Can Fail: Motivating Examples

The conventional procedure for introducing resilience in a HEN (or general process plant) is to use empirical overdesign. That is, a nominal or "conservative" basis is selected for designing and optimizing the HEN. Empirical safety factors based on past experience are applied to the equipment sizes and extra units are also often introduced. However, although this empirical procedure will in general add resilience and

flexibility of operation to a HEN, it has the following drawbacks:

1. Not much insight is gained on how much (if any) resilience is added for a given degree of overdesign.
2. The "most conservative" or "worst case" basis for design may not be the one the designer would intuitively expect.
3. Conditions that give rise to infeasible operation may not be detected since interactions among different exchangers are not explicitly taken into account.
4. The resulting overdesigned network may not operate efficiently and may not be optimal from an economic viewpoint.

The following two examples demonstrate these drawbacks of empirical overdesign.

Example 1 (from Grossmann and Morari, 1983). Traditional industrial practice generates resilient HENs by designing them for what are perceived to be "extreme" operating conditions. Naturally, if these extremes are selected properly, the HEN will perform satisfactorily for the whole range of expected conditions. This example demonstrates that the proper selection of "extremes" is far from trivial and that seemingly logical choices can lead to extremely poor systems.

The HEN shown in Fig. 1a was designed for the problem data shown. There are no other designs with fewer heat transfer units, and the approach temperatures fall nowhere below 10 K; therefore this structure is likely to be close to optimal economically. However, it is known that the heat capacity flow rate of stream S_{h1} can be as large as 1.85 kw/K at times. The natural approach of the design engineer would be to test his design for this extreme condition. The test reveals that the network structure also performs satisfactorily at this flow rate (Fig. 1b). It appears logical to expect that the structure can handle all flow rates in the range 1–1.85 kW/K.

Figure 1c reveals that this is not the case. *Even if exchanger 1 had infinite area* (ie., infinite overdesign factor), for a heat capacity flow rate of 1.359 kW/K the outlet temperature of stream S_{h1} cannot be decreased below 344 K. With a reasonable approach temperature difference of 10 K (Fig. 1d), the minimum attainable outlet temperature for stream S_{h1} is 375.4 K, corresponding to a target temperature violation of 52 K. If S_{h1} were the feed stream to a reactor, this design error could have serious consequences.

By switching the cooler from stream S_{h2} to S_{h1} the network can be made resilient (Fig. 1e). In all exchangers the approach temperatures exceed 10 K over the whole range of flow rate variations $1 \leq w_{h1} \leq 1.85$ kW/K and therefore capital costs remain reasonable. The example shows that

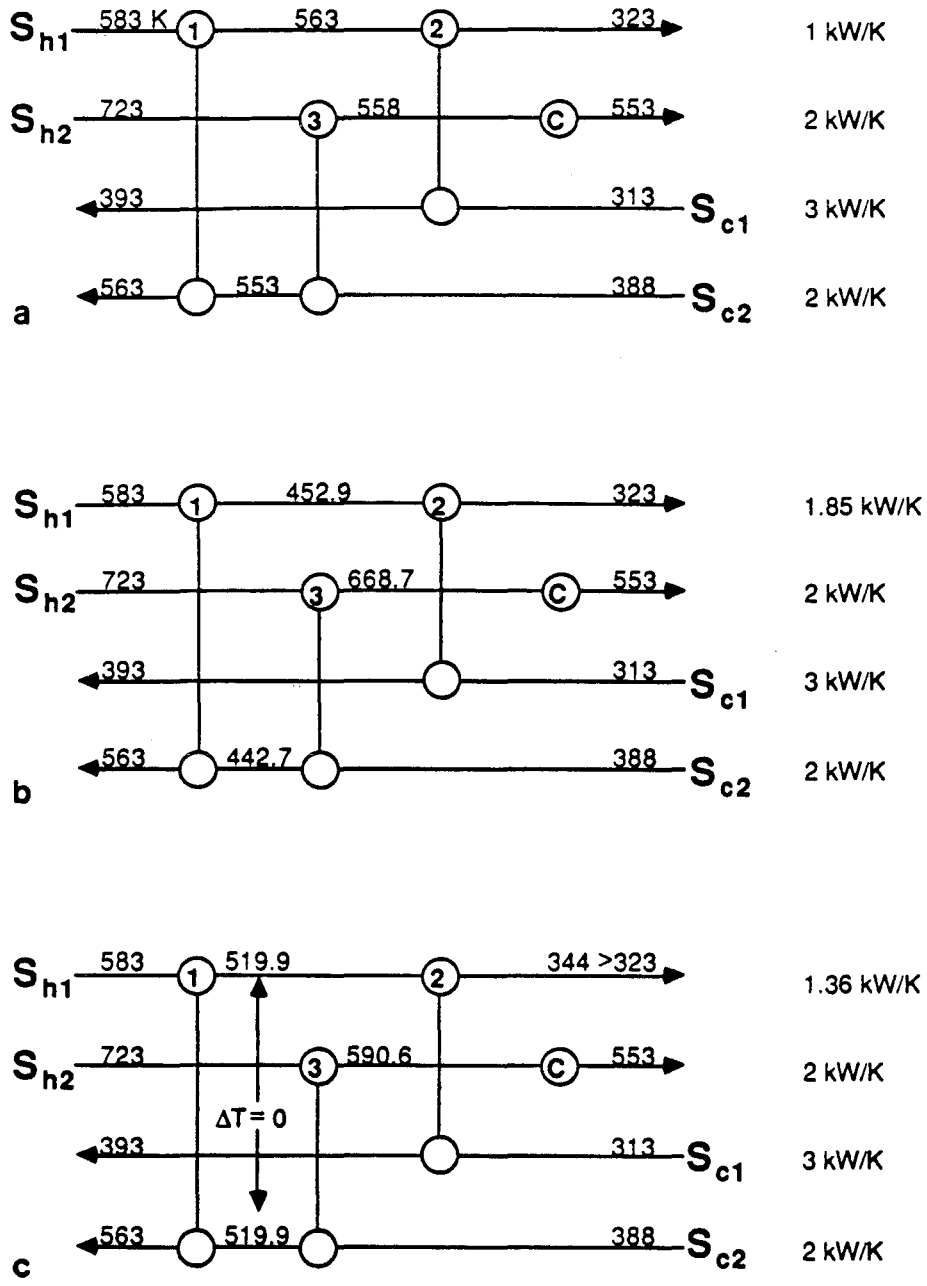

FIG. 1. HEN structures for Example 1: (a) Feasible for nominal flow rate w_{h1} = 1.0 kW/K. (b) Feasible for extreme flow rate w_{h1} = 1.85 kW/K. (c) Target temperature violation of 21 K with intermediate flow rate w_{h1} = 1.359 kW/K (with ΔT_m = 0 K). (d) Target temperature violation of 52 K with intermediate flow rate w_{h1} = 1.359 kW/K (with ΔT_m = 10 K). (e) Resilient for $1.0 \leq w_{h1} \leq 1.85$ kW/K. (f) Resilient for modified example (T^S_{c2} = 393 K).

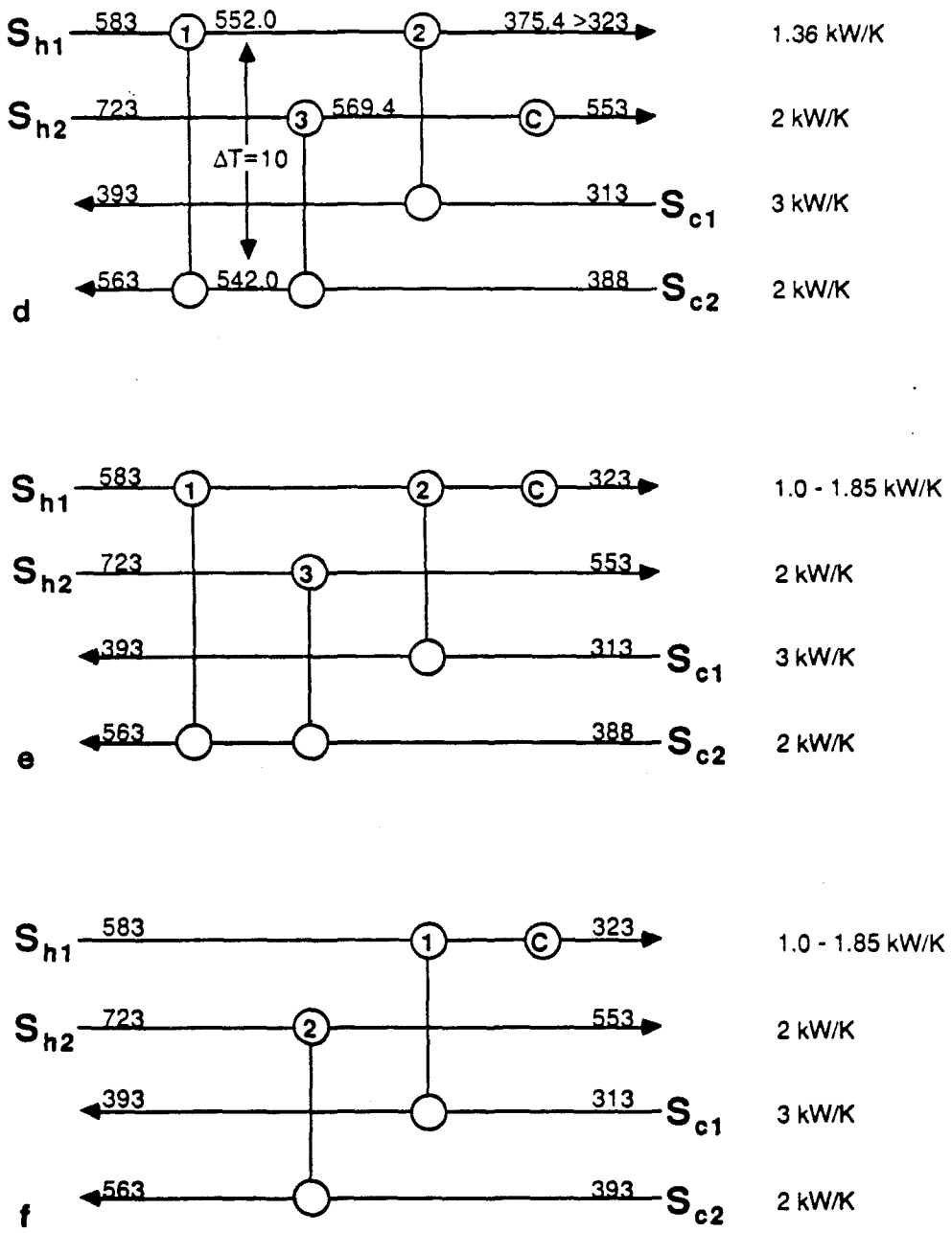

FIG. 1 (*Continued*)

resilience may not be obtained with additional exchangers or excessive oversizing, but simply by a proper redesign of the network structure.

Let us also look at the slightly modified problem in which the inlet temperature of stream S_{c2} is increased to $T^S_{c2} = 393$ K. The network structure in Fig. 1a suffers from the same deficiencies as before. A resilient structure

is shown in Fig. 1f. It involves only three heat exchangers, while the other structure had four. Selecting networks with a larger number of transfer units not only increases capital costs, but can *decrease* resilience. Resilience cannot be achieved by *ad hoc* addition of equipment, but by systematic design techniques based on a thorough understanding of the physicomathematical problem.

Example 2 (from Grossmann and Morari, 1983). In order to illustrate the problem of overlooking effects of interactions, consider the HEN shown in Fig. 2a. Note that in this case the outlet temperatures of streams S_{h1} and S_{c2} have been specified as inequalities: stream S_{h1} must be cooled down to at least 410 K, while stream S_{c2} must be heated up to at least 430 K.

Assume that the areas of exchangers 1 and 2 are sized for nominal values of heat transfer coefficients $U_1 = U_2 = 800$ W/m^2 K and that the resulting areas are oversized by 20%. If such a design were implemented in practice, the following situation might occur.

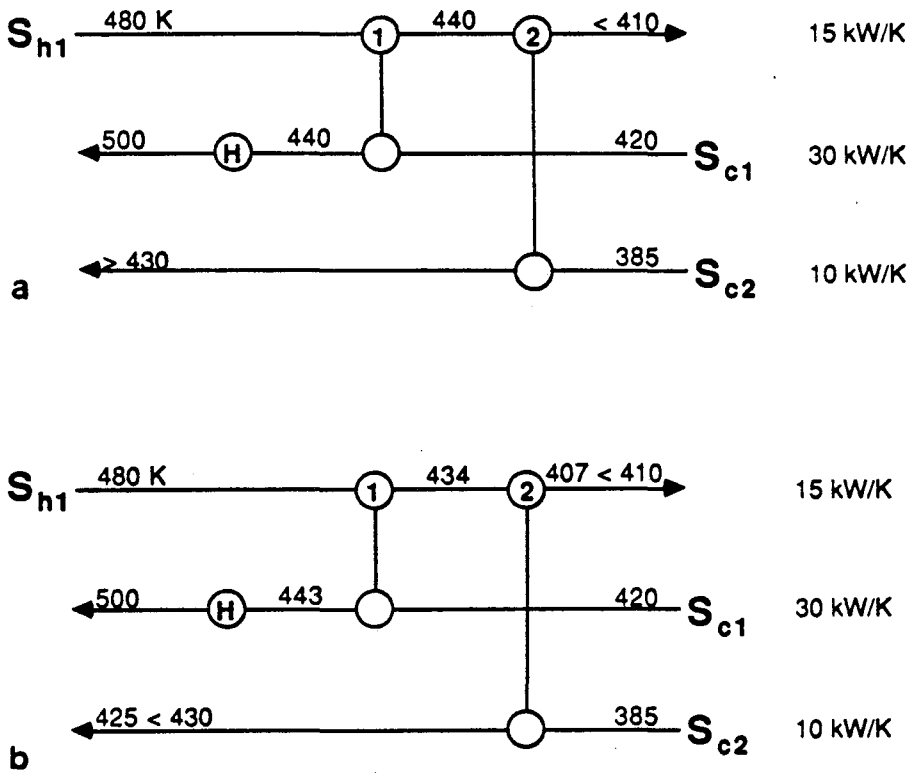

FIG. 2. HEN structure for Example 2: (a) Feasible with nominal heat transfer coefficients. (b) Infeasible with heat transfer coefficients +20% and −20% of their nominal values in exchangers 1 and 2, respectively.

Suppose that U_1 is 20% higher than its nominal value while U_2 is 20% lower. For such a case, as shown in Fig. 2b, the exit temperature of stream S_{h1} from exchanger 1 would drop from the expected 440 K down to 434 K owing to the larger heat transfer coefficient. However, with this change the temperature driving force in exchanger 2 is reduced, which when coupled with the lower heat transfer coefficient causes the outlet temperature of stream S_{c1} from this exchanger to be 425 K, or 5 K below the minimum temperature that was specified. Therefore, for this realization of heat transfer coefficients the network attains infeasible operation since it violates the temperature specification. This example illustrates the danger of overlooking interactions when using empirical overdesign.

It should be noted that this design satisfies the temperature specifications when both heat transfer coefficients are 20% lower than their nominal values, which intuitively would be regarded as the "worst" condition. Thus, this example also shows that identifying "worst" conditions for feasible operation may not always be obvious from intuition.

Another point of the example is related to the choice of areas such that temperature specifications are not violated for any deviation of U_1 and U_2 within $\pm 20\%$ of their nominal values. For instance, if one were to insist on oversizing the area of exchanger 1 by 20%, then the area of exchanger 2 would have to be oversized by 108%. On the other hand, if one were to oversize exchanger 2 by 23%, then exchanger 1 would not have to be oversized, but rather it could be *undersized* by 16%! This shows that the choice of a resilient design which is also economically optimal may not be obvious in general. Hence, the need for a systematic treatment of resilience and flexibility in process design should be evident.

B. Systematic Methods: Basic Problem Descriptions

The previous examples clearly demonstrate the need for more systematic methods to treat HEN resilience. In particular, systematic methods are needed to determine how much, if any, resilience is gained for a given degree of overdesign, or whether resilience can be improved by simple structural changes; to rigorously handle process interactions and to correctly identify "worst case" operating conditions; and to synthesize the structure and determine the minimal amount of oversizing to yield an economically optimal, resilient HEN.

Before describing some basic problems in systematic analysis and synthesis of resilient HENs, we need to establish a common vocabulary of clearly defined terms. (Most of these definitions are adopted from Grossmann and Morari, 1983.)

Analysis means the study of the properties (economics, resilience, etc.) of a given design.

Design is the selection of variables (e.g., heat exchanger areas, maximum heater and cooler loads) which lead a given design structure (HEN topology or general process flow sheet) to have specified properties.

Synthesis is the generation of the process structure. The structural variables (existence or absence of a process unit—e.g., exchanger—or interconnection between process units) can be represented by binary integer variables.

Feasible refers to a process (HEN structure) which satisfies all physical constraints (nonnegative exchanger loads) and performance specifications (target temperatures, minimum approach temperature, specified energy recovery).

Control is the manipulation of a degree of freedom (e.g., heater, cooler or exchanger load, stream split fraction) in order to make a process feasible and/or economically optimal in the steady state. In this chapter, "control" is used in a static sense only; process dynamics are not considered.

Uncertainty range is the range of uncertain variables in a design problem. The uncertainty range can consist of "external" uncertainties (e.g., supply temperatures and flow rates) and/or "internal" uncertainties (e.g., heat transfer coefficients). The uncertainty range is typically specified in terms of finite upper and lower bounds on each of the uncertain variables.[1]

Flexible refers to a process which remains feasible for every value of the uncertain variables in the uncertainty range despite *desired* changes to the process (e.g., supply temperature and flow rate variations due to feedstock changes).

Resilient processes are those which remain feasible for every value of the uncertain variables in the uncertainty range despite *undesired* changes to the process (e.g., environmental disturbances in supply temperatures, fouling of heat transfer surfaces). Mathematically, flexibility and resilience are the same problem; in this chapter, the two terms are used synonymously.

Several types of problems can be defined for the analysis and synthesis of resilient HENs. Some basic problems are verbally described here. In the next section, these problems are defined mathematically and interpreted graphically. In subsequent sections, algorithms are presented for solving these problems.

[1] In all of the resilience analysis techniques reviewed here, the uncertainty range can be extended to include variable target temperatures. In addition, if any of the uncertainties are correlated, then the uncertainty range should include only the independent uncertainties with all the dependent uncertainties expressed in terms of the independent ones.

1. *Feasibility Test*

For assumed, fixed values of the uncertain variables, can the "control variables" (degrees of freedom) be manipulated so as to make the HEN feasible (Saboo *et al.*, 1987a)? Note that feasibility of a HEN depends on several factors: assumed values of the uncertain variables, feasibility constraints (e.g., value of ΔT_m, specified level of energy recovery), values of the design and structural variables chosen by the designer *before* the feasibility test (or analogously before plant operation), and the fact that control variables are allowed to vary *during* the feasibility test (or analogously during plant operation).

Many earlier researchers neglected the fact that degrees of freedom are usually available in a process plant (HEN) which can be manipulated during plant operation so as to maintain feasibility (review by Grossmann *et al.*, 1983). By not allowing the control variables to vary, the feasibility test can be unnecessarily conservative.

2. *Resilience (Flexibility) Test*

Is the HEN feasible for *every* value of the uncertain variables in the expected uncertainty range? Note that whether a HEN is resilient depends upon the size of the expected uncertainty range (which the designer must estimate), in addition to the factors listed earlier which affect HEN feasibility. This test can be used to identify "worst case" values of the uncertain variables and to determine whether design changes make a formerly nonresilient HEN resilient in the specified uncertainty range. [Note that Halemane and Grossmann (1983) and Grossmann and Floudas (1987) call this test a "feasibility test" and that they have no specific name for the test with assumed, fixed values of the uncertain variables. In this chapter, we follow the terminology of Saboo *et al.* (1987)].

3. *Resilience (Flexibility) Index*

The resilience (flexibility) test is a yes–no test of HEN resilience in a specified uncertainty range. A more general problem is to measure the size of the largest uncertainty range for which the HEN is resilient (flexible). The resilience and flexibility indices are two different measures of the largest uncertainties (from assumed nominal values of the uncertain variables) for which a HEN remains feasible (Saboo *et al.*, 1985; Swaney and Grossmann, 1985a). Note that these indices depend upon the choice of nominal values for the uncertain variables. These indices can be used to determine how much resilience (flexibility) is gained for a given design change (overdesign or structural change) and to identify "worst case" values of the uncertain variables which limit HEN resilience.

4. *Synthesis of Resilient HENs*

The problem of synthesizing HENs which are both economically optimal and resilient can be posed in many forms. Should HEN cost be minimized only for "worst case" values of the uncertain variables (minimax strategy), or should the "expected" cost of the HEN—averaged over the expected frequency of occurrence of each value of the uncertain variables—be minimized? Should HEN feasibility be guaranteed only at the values of the uncertain variables which minimize cost or for the whole range of uncertain variables? Grossmann *et al.* (1983) review the approaches of several earlier researchers in uncertain process design. Later in this chapter, methods are presented to synthesize HENs in which the cost is minimized for several values of the uncertain variables (to approximate the minimax strategy) and which are resilient for the entire uncertainty range (Floudas and Grossmann, 1987b; Colberg *et al.*, 1988).

III. Analysis of HEN Resilience

A. General Problem Formulations

In this section, general mathematical formulations and graphic interpretations are presented for several resilience analysis problems: (1) feasibility test, (2) resilience (flexibility) test, (3) flexibility index, and (4) resilience index.

1. *Feasibility Test*

The physical performance of a HEN can be described by the following set of constraints (Grossmann and Floudas, 1987):

$$h(d, z, x, \theta) = 0, \qquad g(d, z, x, \theta) \leq 0 \tag{1}$$

where h is the vector of equations (mass and energy balances, energy recovery specification) which hold for steady-state operation and g is the vector of inequalities (target temperature and ΔT_m specifications; nonnegative load constraints) which must be satisfied if operation is to be feasible. The variables are classified as follows: d is the vector of design variables that define the HEN structure and exchanger sizes. These variables are fixed at the design stage and remain constant during plant operation. Here θ is the vector of uncertain variables (uncertain supply temperatures and flow rates, heat transfer coefficients, etc.). The vector z of control variables stands for the degrees of freedom that are available during operation and

which can be adjusted for different realizations of uncertain variables θ. Finally, x is the vector of state variables which is a subset of the remaining variables and which has the same dimension as h.

For a given HEN design d and for any realization of θ during operation, the state variables can in general be expressed as an implicit function of control variables z using equalities h,

$$h(d, z, x, \theta) = 0 \Rightarrow x = x(d, z, \theta)$$

This allows elimination of the state variables, and the HEN performance specifications can be described with the following reduced set of inequality constraints:

$$g_m[d, z, x(d, z, \theta), \theta] = f_m(d, z, \theta) \leq 0 \qquad (m \in M) \tag{2}$$

where M is the index set for the inequalities. It should be noted that elimination of the state variables is done at this point for the sake of simplicity in presentation; the actual numerical algorithms for analyzing HEN resilience do not require elimination of the equality constraints.

A HEN is feasible for assumed, fixed values of uncertain variables θ if control variables z can be found to satisfy the reduced set of constraints. The HEN feasibility test can be formulated as follows to minimize the maximum constraint violations (Halemane and Grossmann, 1983):

$$\psi(d, \theta) = \min_{z} \max_{m \in M} f_m(d, z, \theta) \tag{3}$$

This minimax problem can be converted to a simpler nonlinear program (NLP) by introducing a slack variable β to measure violations of the inequality constraints:

$$\psi(d, \theta) = \min_{z, \beta} \beta \tag{4}$$

subject to

$$f_m(d, z, \theta) \leq \beta \qquad (m \in M)$$

The HEN is feasible for the assumed values of the uncertain variables θ if and only if $\psi \leq 0$.

In terms of the actual HEN feasibility constraints (including the equality constraints), NLP (4) can be expressed more explicitly as (Saboo *et al.*, 1987a)

$$\psi = \min_{u, v, \beta} \beta \tag{5}$$

subject to:

(A1) Energy balances on all exchangers, heaters, and stream splits:

$$A(u, w)t^S + B(u, v, w)v = b$$

(A2) Specified energy recovery:

$$\sum_k l_k^H = \alpha H(t^S, w)$$

(B1) ΔT_m constraints on all exchangers:

$$C(u, w)t^S + D(u, v, w)v + p \leq \beta e$$

(B2) Nonnegative exchanger and cooler loads:

$$E(u, w)t^S + Gv + r \leq \beta e$$

(B3) Nonnegative heater loads:

$$-l^H \leq \beta e$$

where t^S is the vector of supply temperatures; w the vector of inlet heat capacity flow rates;

$$\theta = \begin{bmatrix} t^S \\ w \end{bmatrix}$$

is the vector of uncertain variables (constant for feasibility test); u the vector of stream split fractions; t^I the vector of intermediate stream temperatures (between exchangers); l^H the vector of heater loads;

$$v = \begin{bmatrix} t^I \\ l^H \end{bmatrix}$$

is the vector of state and control variables (excluding stream split fractions); H the minimum heating requirement; α the factor by which heating target is relaxed from minimum heating requirement;

$$e = [1\ 1 \cdots 1]^T$$

b, G, p, r are constant vectors and matrices; A, C, E are matrices whose elements are functions of u and w; and B, D are matrices whose elements are functions of u, v, and w.

If the HEN has more than the minimum number of exchangers (say n_U more than the minimum) and n_T variable target temperatures, then $n_U + n_T$ of the intermediate stream temperatures and heater loads can be chosen as control variables. Stream split fractions are always available as control variables. These variables are adjusted to try to make the HEN feasible for the assumed, fixed values of the uncertain supply temperatures and flow rates. The HEN is feasible if and only if $\psi \leq 0$.

2. *Resilience (Flexibility) Test*

Resilience of a HEN represents its ability to accommodate uncertainty in a set of selected variables. The resilience properties of a HEN can be

completely described by the feasible region R (Fig. 3) in the space of uncertain variables:

$$R = \{[\theta | \exists\ z] f_m(d, z, \theta) \leq 0\ \forall\ m \in M\}$$

or equivalently

$$R = \{\theta | \psi(d, \theta) \leq 0\}$$

The boundary of R is determined by $\psi = 0$. Individual segments in the boundary of R are determined by $f_m = 0, m \in M$. Values of the uncertain variables θ lying inside feasible region R allow the control variables z to be adjusted so that all the feasibility constraints can be satisfied. For values of θ lying outside the feasible region, the control variables cannot be adjusted to satisfy all the feasibility constraints.

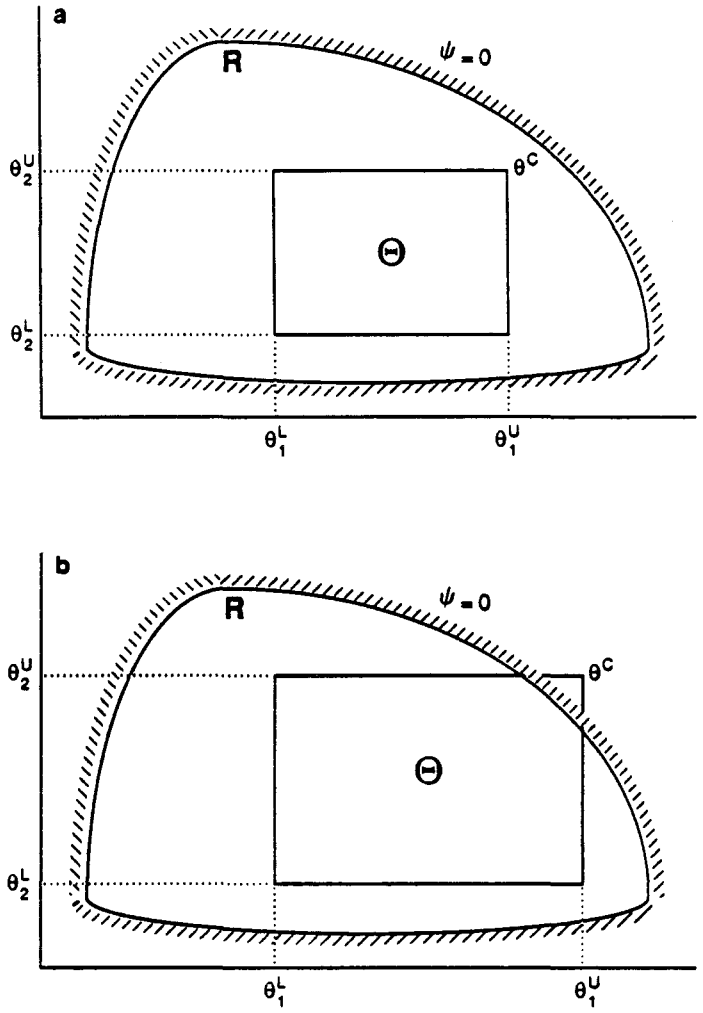

FIG. 3. Feasible region R and uncertainty ranges θ for resilient and nonresilient HENs: (a) Resilient HEN ($\theta \subset R$). (b) Nonresilient HEN ($\theta \not\subset R$).

The resilience (flexibility) test determines whether a HEN is resilient (flexible) throughout a specified uncertainty range Θ,

$$\Theta = \{\theta | \theta^L \leq \theta \leq \theta^U\}$$

where θ^L and θ^U are vectors of lower and upper bounds, respectively, specified by the designer to describe the expected range of uncertainty. (Note that *resilience* and *flexibility* are used synonymously to describe the same test.) In other words, the resilience test determines whether the specified uncertainty range Θ lies entirely within feasible region R (see Fig. 3).

A HEN is resilient throughout uncertainty range Θ if and only if the HEN is feasible ($\psi \leq 0$) for all $\theta \in \Theta$. In mathematical terms, a HEN is resilient in Θ if and only if $\chi(d) \leq 0$, where

$$\chi(d) = \max_{\theta \in \Theta} \psi(d, \theta) \tag{6}$$

(Halemane and Grossmann, 1983). Substituting the definitions of ψ from Eqs. (3) and (4), two equivalent formulations for $\chi(d)$ in terms of the feasibility constraints are

$$\chi(d) = \max_{\theta \in \Theta} \min_{z} \max_{m \in M} f_m(d, z, \theta) \tag{7a}$$

and

$$\chi(d) = \max_{\theta \in \Theta} \min_{z, \beta} \beta \tag{7b}$$

subject to

$$f_m(d, z, \theta) \leq \beta \qquad (m \in M)$$

If $\chi(d) > 0$, then at least one of the feasibility constraints is violated somewhere in the uncertainty range.

In terms of the actual HEN feasibility constraints (including the equality constraints), problem (7b) can be expressed more explicitly as (Saboo *et al.*, 1985a)

$$\chi(d) = \max_{\theta} \min_{u, v, \beta} \beta \tag{8}$$

subject to:

(A1) Energy balances on all exchangers, heaters, and stream splits:

$$A(u, w)t^S + B(u, v, w)v = b$$

(A2) Specified energy recovery:

$$\sum_k l_k^H = \alpha H(t^S, w)$$

(B1) ΔT_m constraints on all exchangers:

$$C(u,w)t^S + D(u,v,w)v + p \leq \beta e$$

(B2) Nonnegative exchanger and cooler loads:

$$E(u,w)t^S + Gv + r \leq \beta e$$

(B3) Nonnegative heater loads:

$$-l^H \leq \beta e$$

(B4) Uncertainty range:

$$\theta^L \leq \theta \leq \theta^U$$

where θ includes the uncertain supply temperature t^S and flow rates w and the control variables z are the degrees of freedom available in the intermediate stream temperatures and heater loads v and stream split fractions u.

The solution θ^C of max–min problem (8) defines a critical point for feasible operation—it is the point where uncertainty range Θ is closest to feasible region R if $\chi(d) \leq 0$ (Fig. 3a), or it is the point where maximum constraint violations occur if $\chi(d) > 0$ (Fig. 3b). In qualitative terms, the critical points in the resilience test are the worst case conditions for feasible operation.

In general, θ^C need not be a vertex of the uncertainty range (e.g., for some nonconvex feasible regions R). An algorithm for finding nonvertex critical points (active constraint strategy; Grossmann and Floudas, 1987) is described later. Swaney and Grossmann (1985a) establish sufficient conditions when the critical point must be a vertex of the uncertainty range. Of course, these conditions include the case when all the feasibility constraints (including the equality constraints) are linear. Section III,B discusses the conditions when the HEN feasibility constraints are linear.

When the critical point must be a vertex of the uncertainty range, the HEN is resilient ($\chi \leq 0$) if and only if it is feasible ($\psi \leq 0$) at every vertex. In mathematical terms, semiinfinite problem (6) reduces to a finite optimization problem

$$\chi(d) = \max_{l \in L_v} \psi(d, \theta^l) \tag{9}$$

where $\psi(d, \theta^l)$ is the value of the feasibility measure at corner point θ^l [obtained by solving problem (4) or (5)], L_v is the index set for the 2^{n_u} vertices, and n_u is the number of uncertain variables. The disadvantage of this approach is the large number of (N)LPs which must be solved (2^{n_u})

even if the number of uncertain variables is reasonably small. Swaney and Grossmann (1985b) and Grossmann and Floudas (1985, 1987) have developed algorithms (including the active constraint strategy for linear problems) which avoid the need to solve an (N)LP for every vertex.

Example 3 (adapted from Grossmann and Floudas, 1987). The HEN in Fig. 4 was designed for the heat capacity flow rates, target temperatures, and nominal stream supply temperatures shown. This HEN is to be tested for resilience in an uncertainty range of ±10 K in all stream supply temperatures.

It can be shown that the resilience test for this HEN is linear (see Section III,B,1). Therefore the HEN is resilient if and only if it is feasible at every vertex of the specified uncertainty range.

The following linear program (LP) can be formulated to check HEN feasibility at specified values of the supply temperatures:

$$\psi = \min \beta$$

subject to the following energy balances,

$$HX\ 1: \quad 1.5(T_1^S - T_5) = 2(T_7 - T_3^S)$$

$$HX\ 2: \quad 1(T_2^S - T_6) = 2(563 - T_7)$$

$$HX\ 3: \quad 1(T_6 - T_2^T) = 3(393 - T_4^S)$$

load constraints,

$$HX\ 1: \quad T_2^S - T_7 \le \beta$$

$$HX\ 2: \quad T_7 - 563 \le \beta$$

$$HX\ 3: \quad T_4^S - 393 \le \beta$$

$$C: \quad 350 - T_5 \le \beta$$

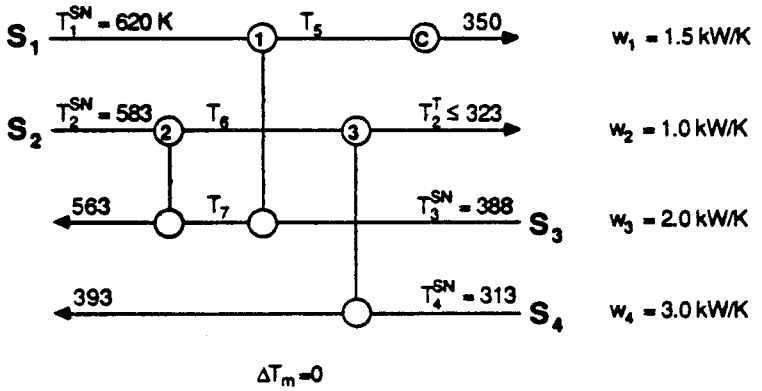

FIG. 4. HEN structure for Examples 3, 4, and 5.

ΔT_m constraints,

$$HX\ 1: \quad T_3^S - T_5 \leq \beta$$

$$HX\ 2: \quad T_7 - T_6 \leq \beta$$

$$HX\ 3: \quad T_4^S - T_2^T \leq \beta$$

and target temperature specification

$$T_2^T \leq 323$$

The energy recovery constraint reduces to $0 = 0$ since there are no heaters.

Application of this LP at each vertex of the uncertainty range yields the results shown in Table I. The HEN is not resilient since it is infeasible at several vertices. In particular, there are four critical vertices where $\psi_{max} = 10.0$. At all four of these critical vertices, HEN feasibility is limited by ΔT_m violations in exchanger 2.

3. *Flexibility Index*

The resilience (flexibility) test is a yes–no test whether or not a HEN is resilient (flexible) in an expected uncertainty range. A more general

TABLE I

RESILIENCE TEST FOR EXAMPLE 3

Vertex							
δT_1^S (K)	δT_2^S (K)	δT_3^S (K)	δT_4^S (K)	ψ	Active constraints		T_2^T (K)
−10	−10	−10	−10	8.8	$HX\ 1\ \Delta T_m$	$HX\ 3\ \Delta T_m$	294.2
			+10[a]	10.0	$HX\ 2\ \Delta T_m$	$T_2^T = 323$	323
		+10	−10	4.8	$HX\ 1\ \Delta T_m$	$HX\ 3\ \Delta T_m$	298.2
			+10[a]	10.0	$HX\ 2\ \Delta T_m$	$T_2^T = 323$	323
	+10	−10	−10	0.8	$HX\ 1\ \Delta T_m$	$HX\ 3\ \Delta T_m$	302.2
			+10	0	$HX\ 2\ \Delta T_m$	$T_2^T = 323$	323
		+10	−10	−3.2	$HX\ 1\ \Delta T_m$	$HX\ 3\ \Delta T_m$	303
			+10	0	$HX\ 2\ \Delta T_m$	$T_2^T = 323$	323
+10	−10	−10	−10	0	$HX\ 2$ load	$HX\ 3\ \Delta T_m$	303
			+10[a]	10.0	$HX\ 2\ \Delta T_m$	$T_2^T = 323$	323
		+10	−10	0	$HX\ 2$ load	$HX\ 3\ \Delta T_m$	303
			+10[a]	10.0	$HX\ 2\ \Delta T_m$	$T_2^T = 323$	323
	+10	−10	−10	−6.7	$HX\ 2$ load	$HX\ 3\ \Delta T_m$	303
			+10	0	$HX\ 3\ \Delta T_m$	$T_2^T = 323$	323
		+10	−10	−6.7	$HX\ 2$ load	$HX\ 3\ \Delta T_m$	303
			+10	0	$HX\ 3\ \Delta T_m$	$T_2^T = 323$	323

[a] Critical corner points.

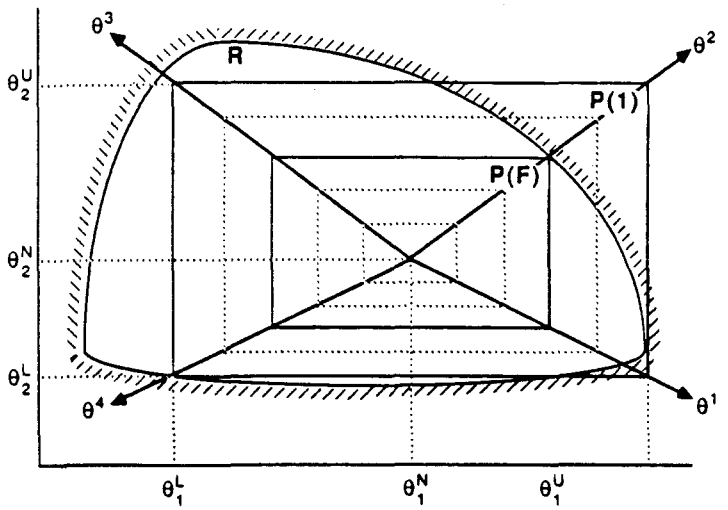

FIG. 5. Flexibility index F defines largest scaled hyperrectangle $\Theta(F)$ for which HEN is resilient.

approach is to measure the size of feasible region R with a numerical flexibility index.

The flexibility index can be defined by considering how much larger (or smaller) the expected uncertainty range Θ must be scaled so that it exactly fits inside feasible region R (Fig. 5). The family of scaled hyperrectangles $\Theta(s)$ can be parameterized by scale factor s as

$$\Theta(s) = \{\theta | (\theta^N - s\,\Delta\theta^-) \leq \theta \leq (\theta^N + s\,\Delta\theta^+)\}$$

where

$$\Delta\theta^+ = \theta^U - \theta^N \qquad \text{and} \qquad \Delta\theta^- = \theta^N - \theta^L$$

and $\Theta(1)$ represents the expected uncertainty range. Then flexibility index F is defined as the value of scale factor s for which the hyperrectangle $\Theta(s)$ exactly fits inside feasible region R[i.e., $\Theta(F)$ is the largest scaled hyperrectangle which can be inscribed in the feasible region (Swaney and Grossmann, 1985a)].

A HEN is resilient in an expected uncertainty range $\Theta(1)$ if and only if $F \geq 1$. This is the same information which the resilience (flexibility) test gives. But the flexibility index tells us even more. For instance if $F = 0.5$, we know that the HEN is not resilient in the specified uncertainty range; in addition, we know that the HEN can tolerate uncertainties only half as large as those expected.

Whether a HEN is resilient in a specified uncertainty range is independent of the choice of nominal values θ^N of the uncertain variables in that range. However, the actual value of the flexibility index F does depend on the choice of θ^N.

The problem of calculating the flexibility index can be mathematically formulated as

$$F(d) = \max_{s} s \qquad \text{subject to} \quad \Theta(s) \subset R \tag{10}$$

In terms of resilience measure χ, this problem is equivalent to (Swaney and Grossmann, 1985a)

$$F(d) = \max_{s} s \qquad \text{subject to} \quad \chi(d, s) \leq 0 \tag{11}$$

Using the definition of χ given by Eq. (7a), a formulation in terms of the feasibility constraints is

$$F(d) = \max_{s} s \qquad \text{subject to} \quad \max_{\theta \in \Theta(s)} \min_{z} \max_{m \in M} f_m(d, z, \theta) \leq 0 \tag{12}$$

and

$$\Theta(s) = \{\theta \,|\, (\theta^N - s\,\Delta\theta^-) \leq \theta \leq (\theta^N + s\,\Delta\theta^+)\}$$

The solution θ^C of problem (12) defines the critical point where the scaled hyperrectangle $\Theta(F)$ meets the boundary of feasible region R (Fig. 5). Note that at the critical point, $\psi(d, \theta) = 0$. In general, θ^C need not correspond to a vertex of the hyperrectangle (e.g., for some nonconvex feasible regions R). An algorithm for finding nonvertex critical points (active constraint strategy; Grossmann and Floudas, 1985a) is described later in this chapter. Swaney and Grossmann (1987) establish sufficient conditions when the critical point must be a vertex of the hyperrectangle. Of course, these conditions include the case when all the feasibility constraints (including the equality constraints) are linear (Section III,B).

When the critical point must be a vertex of the hyperrectangle $\Theta(F)$, the simplest approach to calculating the flexibility index F is to maximize s in each vertex direction θ^l (Fig. 5) by the following (N)LP (Swaney and Grossmann, 1985a):

$$s^{l*}(\theta^l) = \max_{z, s^l} s^l \tag{13}$$

subject to

$$f_m(d, z, \theta) \leq 0 \qquad (m \in M), \qquad \theta = \theta^N + s^l \theta^l$$

Then the flexibility index is the smallest one of these:

$$F = \min_{l \in L_v} s^{l*} \tag{14}$$

The disadvantage of this approach is the large number of (N)LPs which must be solved (2^{n_u}) even if the number of uncertain variables is

reasonably small. Swaney and Grossmann (1985b) and Grossmann and Floudas (1985, 1987) have developed algorithms (including the active constraint strategy for linear problems) which avoid the need to solve an (N)LP for every vertex direction.

In terms of the actual HEN feasibility constraints (including the equality constraints), (N)LP (13) can be expressed more explicity as

$$s^{l*}(\theta^l) = \max_{u,v,s} s^l \tag{15}$$

subject to:

(A1) Energy balances on all exchangers, heaters, and stream splits:

$$A(u,w)t^S + B(u,v,w)v = b$$

(A2) Specified energy recovery:

$$\sum_k l_k^H = \alpha H(t^S, w)$$

(B1) ΔT_m constraints on all exchangers:

$$C(u,w)t^S + D(u,v,w)v + p \leq 0$$

(B2) Nonnegative exchanger and cooler loads:

$$E(u,w)t^S + Gv + r \leq 0$$

(B3) Nonnegative heater loads:

$$-l^H \leq 0$$

(B4) Uncertainty directions:

$$\theta = \theta^N + s^l\theta^l$$

where

$$\theta^1 = \begin{bmatrix} \theta_1^L \\ \theta_2^L \\ \vdots \\ \theta_{n_u-1}^L \\ \theta_{n_u}^L \end{bmatrix} - \theta^N, \quad \theta^2 = \begin{bmatrix} \theta_1^L \\ \theta_2^L \\ \vdots \\ \theta_{n_u-1}^L \\ \theta_{n_u}^U \end{bmatrix} - \theta^N, \quad \ldots, \quad \theta^{2^{n_u}} = \begin{bmatrix} \theta_1^U \\ \theta_2^U \\ \vdots \\ \theta_{n_u-1}^U \\ \theta_{n_u}^U \end{bmatrix} - \theta^N$$

and θ includes the uncertain supply temperatures t^S and flow rates w.

Example 4 (*from Grossmann and Floudas, 1987*). The flexibility index of the HEN structure in Fig. 4 is to be calculated with respect to an expected uncertainty range of + 10 K in all stream supply temperatures.

The supply temperatures shown in Fig. 4 are the assumed nominal values.

The following LP can be formulated to maximize the scale factor s^l in each vertex direction:

$$S^{l*} = \max s^l$$

subject to the following energy balances,

$$HX\ 1: \quad 1.5(T_1^S - T_5) = 2(T_7 - T_3^S)$$

$$HX\ 2: \quad 1(T_2^S - T_6) = 2(563 - T_7)$$

$$HX\ 3: \quad 1(T_6 - T_2^T) = 3(393 - T_4^S)$$

load constraints,

$$HX\ 1: \quad T_3^S - T_7 \leq 0$$

$$HX\ 2: \quad T_7 - 563 \leq 0$$

$$HX\ 3: \quad T_4^S - 393 \leq 0$$

$$C: \quad 350 - T_5 \leq 0$$

ΔT_m constraints,

$$HX\ 1: \quad T_3^S - T_5 \leq 0$$

$$HX\ 2: \quad T_7 - T_6 \leq 0$$

$$HX\ 3: \quad T_4^S - T_2^T \leq 0$$

target temperature specification,

$$T_2^T \leq 323$$

and vertex directions

$$\begin{bmatrix} T_1^S \\ T_2^S \\ T_3^S \\ T_4^S \end{bmatrix} = \begin{bmatrix} 620 \\ 583 \\ 388 \\ 313 \end{bmatrix} + s^l\theta^l, \qquad s^l \geq 0$$

where

$$\theta^1 = \begin{bmatrix} -10 \\ -10 \\ -10 \\ -10 \end{bmatrix}, \quad \theta^2 = \begin{bmatrix} -10 \\ -10 \\ -10 \\ +10 \end{bmatrix}, \quad \ldots, \quad \theta^{16} = \begin{bmatrix} +10 \\ +10 \\ +10 \\ +10 \end{bmatrix}$$

for the directions to the 16 vertices of the expected uncertainty range. Note

that the energy recovery constraint reduces to $0 = 0$ since there are no heaters.

Solution of the 16 LPs yields the results in Table II. The flexibility index is 0.5; thus the HEN can only tolerate uncertainties of ± 5 K in each stream supply temperature instead of the ± 10 K expected. In particular, there are four critical vertices ($s^{l^*}_{\min} = 0.5$). At all four of these critical vertices, HEN flexibility is limited by ΔT_m violations in exchanger 2.

4. *Resilience Index*

A primary disadvantage of the flexibility index is the need to solve 2^{n_u} (N)LPs corresponding to the vertex directions when the critical point must be a vertex of the hyperrectangle $\Theta(F)$. To decrease the required computational effort, Saboo *et al.* (1985) define a different index, the resilience index (RI), to measure the size of feasible region R.

The RI is defined as the largest *total* uncertainty which the HEN can tolerate while remaining feasible:

$$\mathrm{RI} = \max_{\theta \in R} \min_{z} \sum_{l} |\theta_l - \theta_l^{\mathrm{N}}| \tag{16}$$

TABLE II

FLEXIBILITY INDEX FOR EXAMPLE 4

Vertex direction							
δT_1^{S} (K)	δT_2^{S} (K)	δT_3^{S} (K)	δT_4^{S} (K)	s^{l^*}	Active constraints		T_2^{T} (K)
−10	−10	−10	−10	0.56	HX 1 ΔT_m	HX 3 ΔT_m	307.4
			+10[a]	0.5	HX 2 ΔT_m	$T_2^{\mathrm{T}} = 323$	323
		+10	−10	0.7	HX 1 ΔT_m	HX 3 ΔT_m	306
			+10[a]	0.5	HX 2 ΔT_m	$T_2^{\mathrm{T}} = 323$	323
	+10	−10	−10	0.933	HX 1 ΔT_m	HX 3 ΔT_m	303.67
			+10	1.0	HX 2 ΔT_m	$T_2^{\mathrm{T}} = 323$	323
		+10	−10	1.4	HX 1 ΔT_m	HX 3 ΔT_m	299
			+10	1.0	HX 2 ΔT_m	$T_2^{\mathrm{T}} = 323$	323
+10	−10	−10	−10	1.0	HX 2 load	HX 3 ΔT_m	303
			+10[a]	0.5	HX 2 ΔT_m	$T_2^{\mathrm{T}} = 323$	323
		+10	−10	1.0	HX 2 load	HX 3 ΔT_m	303
			+10[a]	0.5	HX 2 ΔT_m	$T_2^{\mathrm{T}} = 323$	323
	+10	−10	−10	3.0	HX 2 load	HX 3 ΔT_m	283
			+10	1.0	HX 2 ΔT_m	$T_2^{\mathrm{T}} = 323$	323
		+10	−10	3.0	HX 2 load	HX 3 ΔT_m	283
			+10	1.0	HX 2 ΔT_m	$T_2^{\mathrm{T}} = 323$	323

[a] Critical corner points.

subject to

$$f_m(d, z, \theta) \leq 0 \qquad (m \in M)$$

Geometrically, the RI defines the largest polytope P which can be inscribed in feasible region R. For example, in Fig. 6 *any* pair of lines drawn from the origin θ^N in the coordinate directions θ_1 and θ_2 to the edge of the polytope will have the same total length

$$\text{RI} = |\theta_1 - \theta_1^N| + |\theta_2 - \theta_2^N|$$

The solution θ^C of max–min problem (16) is the critical point which limits the RI; that is, it is the point where the largest inscribed polytope meets the feasible region R. In general, θ^C need not correspond to a vertex of the polytope (e.g., for some nonconvex feasible regions R). However, to date no general algorithm has been developed to find nonvertex critical points which limit the RI.

A sufficient condition that the RI be determined by a vertex critical point is that the feasible region R be convex. (Of course, a special case of this is when all the feasibility constraints are linear; see Section III,B.) Unfortunately, when flow rates or heat transfer coefficients are included in the uncertainty range, the feasible region can be nonconvex (see Examples 1 and 2 and Section III,C,3). Thus, current algorithms for calculating the RI are limited to temperature uncertainties only.

When the feasible region R is convex, the RI is also the largest *individual* uncertainty which the HEN can tolerate while remaining feasible (in addition to being the largest *total* uncertainty). Thus the simplest algorithm for calculating the RI is to maximize the individual uncertainties which the

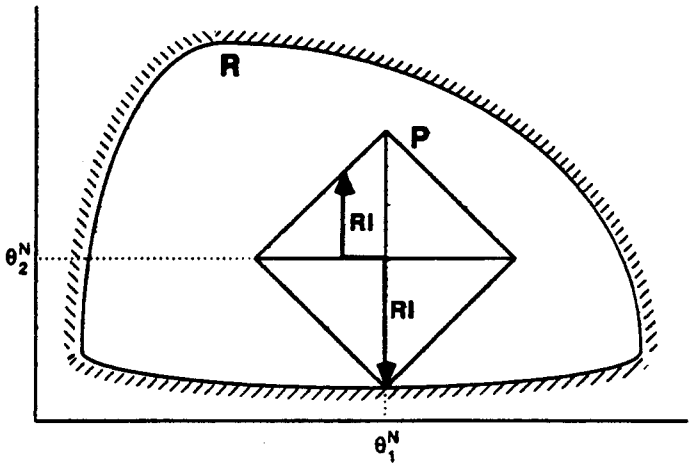

FIG. 6. Resilience index (RI) defines largest polytope P for which HEN is resilient.

HEN can tolerate in each of two directions (Saboo *et al.*, 1985):

$$\delta\theta_{l,\max}^{+} = \max_{z}(\theta_l - \theta_l^{N}) \tag{17a}$$

subject to

$$f_m(d, z, \theta) \leq 0 \qquad (m \in M), \qquad \theta_l \geq \theta_l^{N}$$

and

$$\delta\theta_{l,\max}^{-} = \max_{z}(\theta_l^{N} - \theta_l) \tag{17b}$$

subject to

$$f_m(d, z, \theta) \leq 0 \qquad (m \in M), \qquad \theta_l \leq \theta_l^{N}$$

where θ consists of temperature uncertainties only. Then the RI is the smallest one of these maximum individual uncertainties:

$$\text{RI} = \min_{l}\{\delta\theta_{l,\max}^{+}, \delta\theta_{l,\max}^{-}\} \tag{18}$$

For convex feasible regions, the primary advantage of the resilience index should now be apparent: Only $2n_u$ (N)LPs need to be solved to determine the RI (since a polytope has only $2n_u$ vertices), while 2^{n_u} (N)LPs originally needed to be solved to determine the flexibility index (since a hyperrectangle has 2^{n_u} vertices). However, algorithms developed by Swaney and Grossmann (1985b) and Grossmann and Floudas (1985, 1987) dramatically decrease the number of (N)LPs which must be solved to determine the flexibility index and reduce the advantage of using the resilience index instead of the flexibility index. For nonconvex feasible regions, the active constraint strategy algorithm of Grossmann and Floudas (1987) can locate nonvertex critical points of the flexibility index, while no general algorithm is currently available to locate nonvertex critical points for the RI.

The RI can be scaled in terms of maximum expected uncertainties like the flexibility index. Then the RI would be an upper bound on the flexibility index, since the RI only considers uncertainties in each stream *individually*, while the flexibility index considers uncertainties in all streams *simultaneously*. However, for HENs it seems reasonable to assume that the uncertainty in each stream's supply temperature is roughly inversely proportional to that stream's heat capacity flow rate (i.e., that each stream is subject to roughly the same "load uncertainty"). Thus the RI is calculated in terms of load uncertainty δl_i^{+} or δl_i^{-}, where

$$\delta l_i^{+} = w_i(\delta\theta_i^{+}) = w_i(\delta T_i^{S+}), \qquad \delta l_i^{-} = w_i(\delta\theta_i^{-}) = w_i(\delta T_i^{S-})$$

and w_i is the heat capacity flow rate of stream i and δT_i^{S+} (δT_i^{S-}) is the

positive (negative) uncertainty in the supply temperature of stream S_i relative to its nominal value.

Now in terms of the actual HEN feasibility constraints (including the equality constraints), (N)LPs (17) can be expressed more explicity as (Saboo *et al.*, 1985)

$$\delta l_{i,\max}^{+} = \max_{u,\, v,\, \delta l_i^{+}} \delta l_i^{+} \tag{19}$$

subject to:

(A1) Energy balances on all exchangers, heaters, and stream splits:

$$A(u, w)t^{S} + B(u, v, w)v = b$$

(A2) Energy recovery specification:

$$\sum_{k} l_k^{H} = \alpha H(t^{S}, w)$$

(B1) ΔT_m constraints on all exchangers:

$$C(u, w)t^{S} + D(u, v, w,)v + p \leq 0$$

(B2) Nonnegative exchanger and cooler loads:

$$E(u, w)t^{S} + Gv + r \leq 0$$

(B3) Nonnegative loads in all heaters:

$$-l^{H} \leq 0$$

(B4) Uncertainty directions:

$$t^{S} = t^{SN} + \begin{bmatrix} 1/w_1 & & \\ & \ddots & \\ & & 1/w_{n_s} \end{bmatrix} \delta l^{i+}$$

where

$$\delta l^{i+} = \begin{bmatrix} 0 \\ \vdots \\ 0 \\ \delta l_i^{+} \\ 0 \\ \vdots \\ 0 \end{bmatrix}$$

and n_s is the number of streams. Similar (N)LPs are written for $\delta l_{i,\max}^{-}$.

Then

$$\mathrm{RI} = \min_i \{\delta l^+_{i,\max}, \delta l^-_{i,\max}\} \tag{20}$$

Example 5 (adapted from Grossmann and Floudas, 1987). The resilience index is to be calculated for the HEN shown in Fig. 4. The following series of LPs is formulated to determine the maximum load uncertainty allowed in a positive direction on each stream:

$$\delta l^+_{i,\max} = \max\ \delta l^+_i$$

subject to the same energy balance, ΔT_m, load, and target temperature constraints as in Example 4 and uncertainty directions for the four positive

$$\begin{bmatrix} T_1^S \\ T_2^S \\ T_3^S \\ T_4^S \end{bmatrix} = \begin{bmatrix} 620 \\ 583 \\ 388 \\ 313 \end{bmatrix} + \begin{bmatrix} 1/1.5 & 0 & 0 & 0 \\ 0 & 1/1.0 & 0 & 0 \\ 0 & 0 & 1/2.0 & 0 \\ 0 & 0 & 0 & 1/3.0 \end{bmatrix} \delta l^{i+}$$

where

$$\delta l^{1+} = \begin{bmatrix} \delta l^+_1 \\ 0 \\ 0 \\ 0 \end{bmatrix}, \quad \ldots, \quad \delta l^{4+} = \begin{bmatrix} 0 \\ 0 \\ 0 \\ \delta l^+_4 \end{bmatrix}$$

uncertainty directions along the four streams. Similar LPs are also written for the four negative uncertainty directions. Note that the energy recovery constraint reduces to $0 = 0$ since there are no heaters.

Solution of the eight LPs gives the results in Table III. The RI is 19 kW and is limited by ΔT_m in exchangers 1 and 2 for a positive uncertainty in the supply temperature of stream 2.

In order to compare the resilience index with the flexibility index, suppose that the RI is scaled in terms of temperature rather than load. Then the temperature RI is 6.67 K (Table III), limited by positive uncertainty in the supply temperature of stream 4. (Note that the limiting uncertainty direction changes when the RI is rescaled from load to temperature.) This means that the HEN can tolerate uncertainty of 6.67 K in *any* individual stream supply temperature in either a positive or negative direction. Because of linearity and convexity, it also means that the HEN can tolerate a *total* temperature uncertainty $\Sigma_i |T_i^S - T_i^{SN}|$ of 6.67 K, no matter how the uncertainty is distributed among the streams. Note that this does not mean that the HEN can tolerate uncertainties of 6.67 K in all

TABLE III

RESILIENCE INDEX FOR EXAMPLE 5

Uncertainty direction	$\delta T^{+/-}$ (K)	$\delta l^{+/-}$ (kW)	Active constraints		T_2^{Γ} (K)
l_1^-	18.67	28	HX 1 ΔT_m	HX 3 ΔT_m	313
l_1^+	∞	∞			
l_2^-	19	19[a]	HX 1 ΔT_m	HX 2 ΔT_m	322
l_2^+	330	330	HX 1 load	$T_2^T = 323$	323
l_3^-	42.5	85	C load	HX 3 ΔT_m	313
l_3^+	165	330	HX 1 load	$T_2^T = 323$	323
l_4^-	14	42	HX 1 ΔT_m	HX 3 ΔT_m	299
l_4^+	6.67[b]	20	HX 2 ΔT_m	$T_2^T = 323$	323

[a] Critical point for load RI.
[b] Critical point for temperature RI

four streams *simultaneously*. In fact, the flexibility index (Example 4) tells us that the HEN can only handle uncertainties of ±5 K in all four streams simultaneously.

B. LINEAR RESILIENCE ANALYSIS

Because of the ability of linear programs to guarantee a global optimum and because of the relative ease of solving LPs (as compared to NLPs), we wish to exploit the cases when HEN resilience analysis is linear. This section establishes sufficient conditions for linear HEN resilience analysis.

A type of problem called class 2 is not amenable to straightforward linear analysis. In this type of problem, the form of the energy recovery constraint changes when the stream population at the pinch changes somewhere in the uncertainty range. This section defines and describes the differences betweeen class 1 and class 2 problems.

1. *Sufficient Conditions for Linear Resilience Analysis*

Saboo and Morari (1984) have determined the following sufficient conditions when analysis of HEN resilience is linear:

Theorem 1 (*Corner Point Theorem*). Assume the following: (1) constant heat capacities and no phase change, (2) supply and target temperature uncertainties only (no uncertainties in flow rates or heat transfer coefficients), (3) constant stream split fractions (Saboo *et al.*, 1987b), and

(4) "small" uncertainty range ("class 1" problem defined subsequently). If these assumptions are satisfied, then the HEN resilience analysis problem is linear. [In particular, matrices A, B, C, D, and E are constant in the feasibility test (5), resilience test (8), flexibility index problem (15), and resilience index problem (19).]

As a consequence of linearity (convexity), a HEN is resilient in a specified uncertainty range if and only if it is feasible at every corner point (vertex) of the uncertainty range.

Saboo *et al.* (1985) have shown that under the assumptions of the corner point theorem, HEN resilience analysis problems with specified exchanger areas (rather than specified ΔT_m) are also linear.

2. *Definition of Class 1 and Class 2 Problems*

The assumptions of the corner point theorem are rather restrictive. They are also straightforward except for the meaning of "small" uncertainty range ("class 1" problem).

In HEN synthesis, the pinch occurs at a stream supply, dew point, or bubble point (Saboo and Morari, 1984). A HEN resilience analysis problem is class 1 if the uncertainties are small enough that the stream population at the pinch is constant throughout the uncertainty range. If the uncertainties are too large, then the stream population at the pinch changes and the problem is class 2.

As an example, consider the stream data in Fig. 7, where the only uncertain variable is the supply temperature T^S_{h2} of stream S_{h2}. For an uncertainty range $470 \leq T^S_{h2} \leq 480$ K, the pinch is always caused by the supply of stream S_{h2} (Fig. 7a). Therefore this uncertainty range is class 1. However, if the uncertainty range is expanded to $460 \leq T^S_{h2} \leq 480$ K, then stream S_{h1} causes the pinch for $T^S_{h2} < 470$ (Fig. 7b), while stream S_{h2} still causes the pinch for $T^S_{h2} > 470$ (Fig. 7a). Thus for this larger uncertainty range, the stream population at the pinch changes, and the problem is class 2.

Special cases of class 2 resilience analysis problems include when the problem changes from pinched to unpinched (threshold) or when the problem changes from unpinched heating to unpinched cooling (or vice versa).

Saboo and Morari (1984) give the general test to determine whether a problem is class 1 or class 2. In their test the uncertainty range can include supply temperatures, target temperatures, and flow rates. (It would not matter whether the uncertainty range included heat transfer coefficients.) In this chapter, we restrict their test to problems with constant or piecewise constant heat capacities.

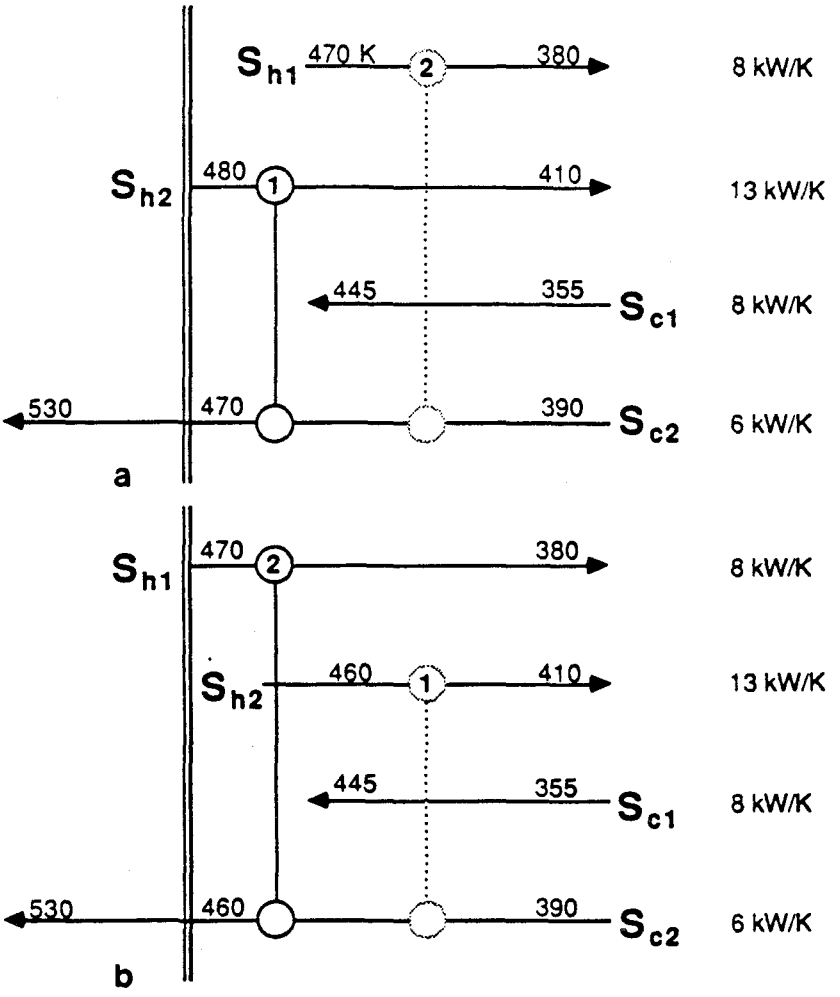

FIG. 7. Class 2 problem—stream population at pinch changes when T^S_{h2} changes: (a) T^S_{h2} = 480 K, (b) T^S_{h2} = 460 K.

Theorem 2. Let *case B* be the point in the uncertainty range which maximizes the HEN's cooling requirement and *case C* be the point which maximizes the HEN's heating requirement. (See Table IV for the supply temperatures, target temperatures, and flow rates corresponding to these two cases.) Then

a. For any point in the uncertainty range, the pinch temperature T_p is between the pinch temperatures for cases B and C:

$$T_p^C \leq T_p \leq T_p^B$$

where hot and cold stream temperatures T are shifted to account for partial contributions to ΔT_m (as in Linnhoff and Flower, 1978).

TABLE IV

SUPPLY TEMPERATURES, TARGET TEMPERATURES, AND FLOW RATES CORRESPONDING TO MAXIMUM HEATING AND MAXIMUM COOLING (WHEN ALL STREAMS HAVE CONSTANT HEAT CAPACITY AND NO PHASE CHANGE

Case	Supply temperatures	Target temperatures	Hot stream flow rates	Cold stream flow rates
Case B (maximum cooling)	Highest	Lowest	Highest	Lowest
Case C (maximum heating)	lowest	highest	lowest	highest

b. The problem is class 1 if (i) the pinch is determined by the supply temperature, dew point, or bubble point of the same stream in both case B and case C (target temperatures cannot cause the pinch) and (ii) for any point in the uncertainty range, no stream supply temperature, target temperature[2], dew point, or bubble point is contained in the open temperature interval (T_p^C, T_p^B), except for the stream supply, dew point, or bubble point temperature associated with the pinch. Otherwise the problem is class 2.

Class 2 problems cause difficulties in HEN resilience analysis because the form of the energy recovery constraint changes as the stream population at the pinch changes. The energy recovery constraint is an energy balance above the pinch limiting the heating used by the network to be less than or equal to the heating required above the pinch (multiplied by some relaxation factor). When the form of the energy recovery constraint changes, the reduced form of the ΔT_m and load constraints also changes. The following example illustrates how the form of the energy recovery, ΔT_m, and loan constraints changes and how this can create nonconvex feasible regions for class 2 problems.

Example 6 (adapted from Saboo et al., 1985). Consider the HEN in Fig. 8. Its resilience is to be tested in the uncertainty range

$$340 \le T_{h2}^S \le 380 \quad \text{K}, \qquad 270 \le T_{c2}^S \le 300 \quad \text{K}$$

Performing a case B–case C analysis for these stream data, we find that for case B (T_{h2}^S = 380 K, T_{c2}^S = 300 K) 140 kW of cooling and no heating are required and that for case C (T_{h2}^S = 340 K, T_{c2}^S = 270 K) 260 kW of heating and no cooling are required. Therefore this problem changes from unpinched cooling to unpinched heating and is class 2.

[2] Saboo and Morari (1984) forgot to include target temperatures in their statement of this theorem. It can be shown by counterexample that target temperatures must be included.

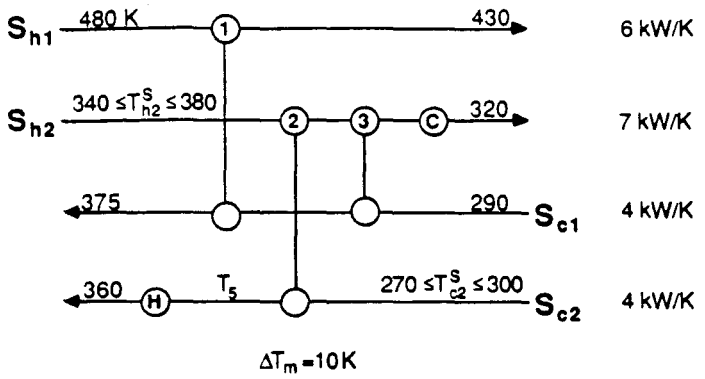

FIG. 8. HEN structure for Examples 6 and 12.

For the case when heating (and no cooling) is required, the energy recovery constraint is the net heating required by the network:

$$\ell^H = 4(375 - 290) + 4(360 - T^S_{h2}) - 6(480 - 430) - 7(T^S_{h2} - 320) \quad \text{(a)}$$

This constraint, along with the energy balances for the exchangers and heater, when substituted into the ΔT_m and load constraints for exchanger 2, yields

$$10 \le T^S_{h2} - T_5 = 570 - 0.75T^S_{h2} - T^S_{c2} \quad \text{(b)}$$

$$0 \le T_5 - T^S_{c2} = 1.75T^S_{h2} - 570 \quad \text{(c)}$$

The feasible region defined by constraints (a)–(c) is the convex region *below* the dashed line in Fig. 9. All other feasibility constraints for the HEN (for the heating only case) lie outside this region.

For the case when cooling (and no heating) is required, the energy recovery constraint reduces to $l^H = 0$. The ΔT_m and load constraints for exchanger 2 become

$$10 \le T^S_{h2} - T_5 = T^S_{h2} - 360 \quad \text{(d)}$$

$$0 \le T_5 - T^S_{c2} = 360 - T^S_{c2} \quad \text{(e)}$$

and the load constraint on the cooler becomes

$$0 \le l^C = 6(480 - 430) + 7(T^S_{h2} - 360) - 4(375 - 290) - 4(360 - T^S_{c2}) \quad \text{(f)}$$

The feasible region defined by constraints (d)–(f) is the convex region *above* the dashed line in Fig. 9. Note that the form of the constraints, and thus the shape of the feasible region, changes between the heating only and cooling only cases.

Now consider the case when the network is allowed to use both heating

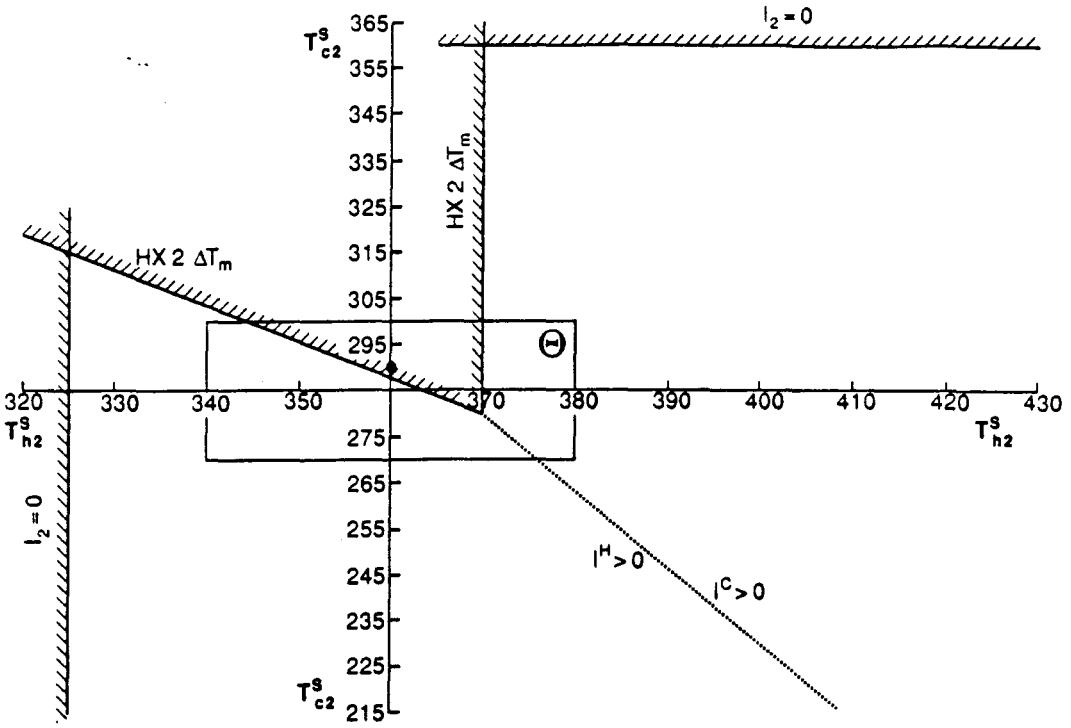

FIG. 9. Nonconvex feasible region for a class 2 problem (Examples 6 and 12).

and cooling. The feasible region for this case is the union of the feasible regions for the heating-only and cooling-only cases. (The dashed line in Fig. 9 is no longer a constraint; it is simply the boundary where the network switches from heating to cooling.) This new feasible region is nonconvex. In particular, the HEN is not feasible for the intermediate case (T^S_{h2} = 360 K, T^S_{c2} = 295 K), while it is feasible for all four corner points of the specified uncertainty range.

C. Nonlinear Resilience Analysis

Heat exchanger network resilience analysis can become nonlinear and nonconvex in the cases of phase change and temperature-dependent heat capacities, varying stream split fractions, or uncertain flow rates or heat transfer coefficients. This section presents resilience tests developed by Saboo *et al.* (1987a,b) for (1) minimum unit HENs with piecewise constant heat capacities (but no stream splits or flow rate uncertainties), (2) minimum unit HENs with stream splits (but constant heat capacities and no flow rate uncertainties), and (3) minimum unit HENs with flow rate and temperature uncertainties (but constant heat capacities and no stream splits).

The nonlinear resilience tests developed by Saboo *et al.* (1987a,b) are each for a rather specific case. A more general resilience analysis technique based on the active constraint strategy of Grossmann and Floudas (1985, 1987) is also presented. The active constraint strategy can be used to test the resilience of a HEN with minimum or more units, with or without stream splits or bypasses, and with temperature and/or flow rate uncertainties (Floudas and Grossmann, 1987b).

1. *Resilience Analysis with Piecewise Constant Heat Capacities*

Most chemical processing plants include pure or multicomponent streams which change phase or which have strongly temperature-dependent heat capacities. Under these conditions the minimum approach temperature in a network can occur *anywhere* inside an exchanger. Therefore integral or differential equations are generally required to locate ΔT_m.

To allow algebraic equations to be used to locate ΔT_m, assume that the heat capacities can be approximated by piecewise constant functions of temperature, with discontinuities at temperature breakpoints T_{BR_i}. Then for each exchanger, ΔT_m can occur only at either end or at a breakpoint location inside the exchanger. However, a remaining difficulty is that since the intermediate stream temperatures are not known before the resilience test, the breakpoint locations are also not known *a priori*.

To deal with this difficulty, the energy balance and ΔT_m constraints are formulated by assuming that *all* breakpoints occur in *every* exchanger. (The energy recovery and load constraints are unaffected by the presence of breakpoints.) Then slack and integer variables are defined to correct the energy balance and ΔT_m constraints for each exchanger in which any temperature breakpoint does not occur (Saboo *et al.*, 1987a).

a. *Energy Balance Constraints.* To demonstrate the energy balance constraint with piecewise constant heat capacities, consider the heat exchanger in Fig. 10, where it is assumed that the hot stream has one tem-

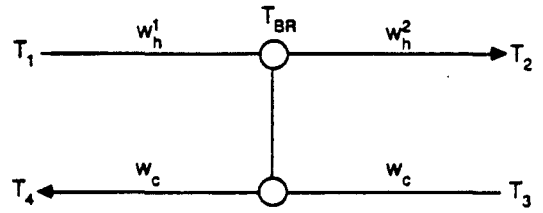

FIG. 10. Heat exchanger with temperature breakpoint in hot stream.

perature breakpoint,

$$w_h = \begin{cases} w_h^1, & T > T_{BR} \\ w_h^2, & T < T_{BR} \end{cases}$$

and that the cold stream has no breakpoint. The energy balance constraint is (Saboo *et al.*, 1987a)

$$w_c(T_4 - T_3) = w_h^1(T_1 - T_{BR}) + w_h^2(T_{BR} - T_2) + (w_h^1 - w_h^2)\,\eta_1 + (w_h^2 - w_h^1)\,\eta_3 \tag{21a}$$

Slack variables η are defined by

$$T_1 - T_{BR} + \eta_1 - \eta_2 = 0 \tag{21b}$$

$$T_{BR} - T_2 + \eta_3 - \eta_4 = 0 \tag{21c}$$

where integer variables m are used to allow only one of η_1 or η_2 (and only one of η_3 or η_4) to be nonzero:

$$\eta_1 \le k m_1 \tag{21d}$$

$$\eta_2 \le k(1 - m_1) \tag{21e}$$

$$\eta_3 \le k m_2 \tag{21f}$$

$$\eta_4 \le k(1 - m_2) \tag{21g}$$

$$\eta_1, \eta_2, \eta_3, \eta_4 \ge 0 \tag{21h}$$

$$m_1, m_2 = 0, 1 \tag{21i}$$

and k is an upper bound on the slack variables (e.g., the difference between the hottest and coldest temperatures in the network).

The energy balance without the slacks ($\eta_1 = \eta_3 = 0$) assumes that the temperature breakpoint occurs inside the exchanger. To demonstrate that the energy balance is correct when the breakpoint occurs outside, consider the case when the breakpoint is upstream of the exchanger ($T_{BR} > T_1 > T_2$). Then constraints (21b)–(21i) give

$$\eta_1 = T_{BR} - T_1, \quad \eta_2 = 0, \quad \eta_3 = 0,$$
$$\eta_4 = T_{BR} - T_2, \quad m_1 = 1, \quad m_2 = 0$$

and Eq. (21a) yields

$$w_c(T_4 - T_3) = w_h^2(T_1 - T_2)$$

which is the correct energy balance for the exchanger.

b. ΔT_m *Constraints.* If T_{BR} occurs inside the heat exchanger in Fig. 10, then ΔT_m can occur at either end or at the breakpoint inside the

exchanger. To set up the ΔT_m constraint at the breakpoint, an energy balance constraint [similar to Eq. (21a)] is first formulated to define temperature T_5 of the cold stream when the hot stream temperature is T_{BR}:

$$w_h^1(T_1 - T_{BR}) = w_c(T_4 - T_5) \tag{22}$$

Temperature T_5 has no physical meaning when the breakpoint occurs outside the exchanger. Then the ΔT_m constraint at the breakpoint is (Saboo *et al.*, 1987a)

$$T_{BR} - T_5 + K(m_1 + m_2) \geq \Delta T_m \tag{23}$$

where K is a sufficiently large positive constant. If the breakpoint occurs inside the exchanger, then both m_1 and m_2 are zero [from constraints (21b–21i)]. If the breakpoint occurs upstream ($m_1 = 1$) or downstream ($m_2 = 1$) of the exchanger, then the ΔT_m constraint at the breakpoint is not physically meaningful, and the term involving m_1 and m_2 forces the constraint to be satisfied.

The energy balance and ΔT_m constraints are easily extended to situations with multiple breakpoints (Saboo *et al.*, 1987a).

c. *Feasibility Test.* If all the restrictions of the corner point theorem are satisfied except that the heat capacities are allowed to be piecewise constant, then the following mixed-integer linear program (MILP) can be formulated to test HEN feasibility for assumed, fixed values of the uncertain temperatures (Saboo *et al.*, 1987a):

$$\psi = \min_{v,\beta,\eta,m} \beta \tag{24}$$

subject to:

(A1) Energy balances on all exchangers and heaters:

$$At^S + Bv + N\eta = b$$

(A2) Specified energy recovery:

$$\sum_k l_k^H = \alpha H$$

(B1) ΔT_m constraints on all exchangers:

$$Ct^S + Dv + O\eta + p \leq \beta e$$

(B2) Nonnegative exchanger and cooler loads:

$$Et^S + Gv + r \leq \beta e$$

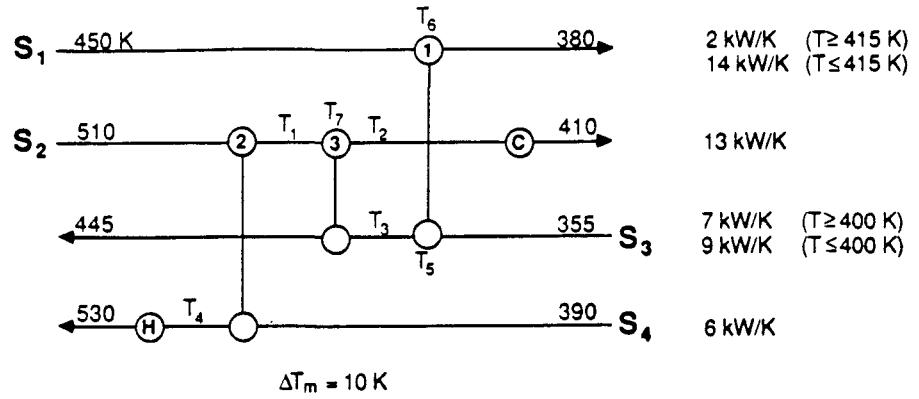

FIG. 11. HEN structure with temperature breakpoints for Example 7 (infeasible).

(B3) Nonnegative heater loads:

$$-l^{H} \leq \beta e$$

(B4) Definition of slack and integer variables:

$$I\eta - km \leq L, \qquad \eta_k \geq 0, \qquad m_k = 0, 1$$

The HEN is feasible if and only if $\psi \leq 0$.

Example 7 (from Saboo et al., 1987a). The HEN structure in Fig. 11 is to be tested if it is feasible for the supply temperatures shown. The heat capacities have two breakpoints: $T_{BR_1} = 415$ K in hot stream S_1 and $T_{BR_3} = 400$ K in cold stream S_3.

In heat exchanger 1, T_5 is the temperature of cold stream S_3 corresponding to hot breakpoint T_{BR_1}. Hot stream temperatures T_6 and T_7 in exchangers 1 and 3, respectively, correspond to potential locations of cold breakpoint T_{BR_3}. The minimum heating requirement is 180 kW for a specified ΔT_m of 10 K.

The constraints for exchanger 1 are formulated as follows. For overall energy balance:

$$2(450 - 415) + 14(415 - 380) = 7(T_3 - 400) + 9(400 - 355) + (7 - 9)\eta_1$$

For energy balance to define temperature T_5 of stream S_3 corresponding to T_{BR_1}:

$$2(450 - 415) = 7(T_3 - 400) + 9(400 - T_5) + (7 - 9)\eta_1 + (9 - 7)\eta_3$$

For energy balance to define temperature T_6 of stream S_1 corresponding to T_{BR_3}:

$$2(450 - 415) + 14(415 - T_6) + (14 - 2)\eta_5 = 7(T_3 - 400) + 7\eta_1$$

For constraints defining slack variables η_i:

$$T_3 - 400 + \eta_1 - \eta_2 = 0, \qquad 400 - T_5 + \eta_3 - \eta_4 = 0$$

$$415 - T_6 + \eta_5 - \eta_6 = 0$$

$$0 \le \eta_1 \le km_1, \qquad 0 \le \eta_2 \le k(1 - m_1)$$

$$0 \le \eta_3 \le km_2, \qquad 0 \le \eta_4 \le k(1 - m_2)$$

$$0 \le \eta_5 \le km_3, \qquad 0 \le \eta_6 \le k(1 - m_3)$$

$$m_1, m_2, m_3 = 0, 1$$

where k is a sufficiently large positive number. For approach temperature constraints:

At hot end:	$450 - T_3 + \beta \ge 10$
At cold end:	$380 - 355 + \beta \ge 10$
At T_{BR_1}:	$415 - T_5 + \beta \ge 10$
At T_{BR_3}:	$T_6 - 400 + Km_1 + \beta \ge 10$

where K is a sufficiently large positive number. For load constraint, the heat load of exchanger 1 will always be positive, since it is the only exchanger on stream 1. Note that the ΔT_m constraint at T_{BR_1} requires no integer variables [as opposed to Eq. (23)] since T_{BR_1} *must* occur inside exchanger 1. The ΔT_m constraint at T_{BR_3} requires only one integer variable since T_{BR_3} can occur only inside or downstream (but not upstream) of exchanger 1. Constraints for the other exchangers are formulated similarly.

Solution of the MILP gives $\psi = 7.2$ K. Therefore the network is infeasible. Both breakpoints T_{BR_1} and T_{BR_2} occur in heat exchanger 1. The corresponding temperatures are

$$T_5 = 412.2 \text{ K} \quad \text{(corresponding to } T_{BR_1} = 415 \text{ K)}$$

$$T_6 = 408.7 \text{ K} \quad \text{(corresponding to } T_{BR_3} = 400 \text{ K)}$$

The ΔT_m violations also occur inside heat exchanger 1:

$$\Delta T_m - (415.0 - 412.2) = 7.2 \text{ K}, \qquad \Delta T_m - (408.7 - 400.0) = 1.3 \text{ K}$$

The structure can be made feasible by shifting the cooler from stream 2 to stream 1 to increase the temperature driving force in exchanger 1.

d. *Resilience Test.* Unfortunately, if the temperature breakpoints move to different exchangers when HEN feasibility is checked at different corner points of the uncertainty range, the corner point theorem may not

hold (Saboo *et al.*, 1987a). However, for HENs with a minimum number of units, an MILP can still be formulated which is a necessary and sufficient resilience test.

In a minimum unit HEN the intermediate stream temperatures and heater loads, and thus the breakpoint locations, are uniquely determined by the energy balance and energy recovery constraints. Thus for given supply temperatures and flow rates, the ΔT_m violations (and surpluses) and load violations (and surpluses) in each exchanger k are also uniquely determined.

The ΔT_m violations (γ_{T_k}) and surpluses (σ_{T_k}) can be defined by

$$T_1 - T_2 + \gamma_{T_k} - \sigma_{T_k} = \Delta T_m \tag{25a}$$

Integer variables m_{T_k} are used as follows to allow only one of γ_{T_k} or σ_{T_k} to be nonzero:

$$0 \leq \gamma_{T_k} \leq k_T m_{T_k} \tag{25b}$$

$$0 \leq \sigma_{T_k} \leq k_T(1 - m_{T_k}) \tag{25c}$$

$$m_{T_k} = 0,\ 1 \tag{25d}$$

where k_T is a sufficiently large number (larger than the maximum possible ΔT_m violation or surplus). Load violations γ_L and surpluses σ_L are defined similarly using integer variables m_L.

By using these definitions for ΔT_m and load violations and surpluses, the following MILP can be formulated to test the resilience of a minimum unit HEN with breakpoints (Saboo *et al.*, 1987a):

$$\chi = \max_{\theta} \sum_{k} (\gamma_{T_k} + \gamma_{L_k}) \tag{26}$$

subject to:

(A1) Energy balances on all exchangers and heaters:

$$At^S + Bv + N\eta = b$$

(A2) Specified energy recovery:

$$\sum_{k} l_k^H = \alpha H$$

(B1) ΔT_m constraints on all exchangers:

$$Ct^S + Dv + O\eta + p = \gamma_T - \sigma_T$$

(B2) Nonnegative exchanger and cooler loads:

$$Et^S + Gv + r = \gamma_L - \sigma_L$$

(B3) Nonnegative heater loads:

$$-l^{H} = \gamma_{L}^{H} - \sigma_{L}^{H}$$

(B4) Definition of slack and integer variables:

$$I\eta - km \le L, \qquad I\gamma_{T} - k_{T}m_{T} \le 0,$$

$$I\sigma_{T} - k_{T}m_{T} \le L_{T}, \qquad I\gamma_{L} - k_{L}m_{L} \le 0$$

$$I\sigma_{L} - k_{L}m_{L} \le L_{L}, \qquad I\gamma_{L}^{H} - k_{L}^{H}m_{L}^{H} \le 0, \qquad I\sigma_{L}^{H} - k_{L}^{H}m_{L}^{H} \le L_{L}^{H}$$

$$m_{k},\ m_{T_k},\ m_{L_k},\ m_{L_k}^{H} = 0,\ 1, \qquad \eta_{k},\ \gamma_{T_k},\ \sigma_{T_k},\ \gamma_{L_k},\ \sigma_{L_k},\ \gamma_{L_k}^{H},\ \sigma_{L_k}^{H} \ge 0$$

(B5) Uncertainty range

$$\theta^{L} \le \theta \le \theta^{U}$$

where θ contains the uncertain supply temperatures. This MILP can be extended to include target temperatures in the uncertainty range. The HEN is resilient in the specified uncertainty range if and only if $\chi = 0$.

2. *Resilience Analysis with Stream Splits*

Resilience analysis for HENS can become nonlinear and nonconvex if varying stream split fractions are allowed. In this section nonlinear feasibility and resilience tests are presented for networks with stream splits, with the assumption that the network has a minimum number of units. This assumption often is not restrictive since many stream split networks do have a minimum number of units.

a. *Stream Split Constraints.* For HENs with a minimum number of units, the heater loads and intermediate stream temperatures are uniquely determined by the energy balance and energy recovery constraints. These equality constraints can be solved simultaneously to obtain explicit expressions for the heater loads and intermediate stream temperatures in terms of the stream supply temperatures and stream split fractions. These expressions can then be substituted into some of the ΔT_{m} constraints to form constraints on the stream split fractions (Saboo *et al.*, 1987b). The following example demonstrates this procedure.

Example 8 (from Saboo et al., 1987b). Resilience of the HEN in Fig. 12 is tested in Example 9. In this example, the constraints on the stream split fractions are formulated.

Note that the energy recovery constraint reduces to $0 = 0$ for this network since there are no heaters. The energy balance constraints for the two exchangers can be solved for intermediate stream temperatures T_5 and

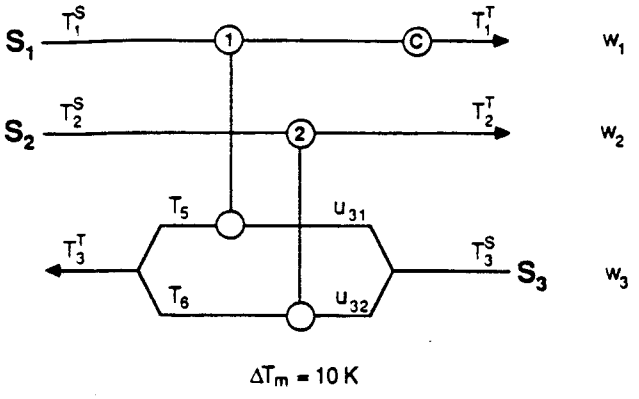

Stream (i)	T_i^S (K)	T_i^T (K)	w_i (kW/K)
1	740	625	2
2	415-515	370	1
3	320	550	1

FIG. 12. Minimum unit HEN structure with stream split (Examples 8, 9, and 11).

T_6 to give

$$HX\,1: \qquad T_5 = T_3^S + \frac{w_3(T_3^T - T_3^S) - w_2(T_2^S - T_2^T)}{u_1 w_3} \tag{a}$$

$$HX\,2: \qquad T_6 = T_3^S + \frac{w_2(T_2^S - T_2^T)}{u_2 w_3} \tag{b}$$

The ΔT_m constraints for this network are

$$HX\,1: \qquad T_1^S - T_5 \geq \Delta T_m; \qquad T_4 - T_3^S \geq \Delta T_m \tag{c}$$

$$HX\,2: \qquad T_2^S - T_6 \geq \Delta T_m; \qquad T_2^T - T_3^S \geq \Delta T_m \tag{d}$$

Substituting for T_5 in $T_1^S - T_5 \geq \Delta T_m$ yields

$$-\frac{w_3(T_3^T - T_3^S) - w_2(T_2^S - T_2^T)}{u_1 w_3} \geq -\left[(T_1^S - \Delta T_m) - T_3^S\right] \tag{e}$$

Note that $T_1^S - \Delta T_m \geq T_5 \geq T_3^S$ for the network to be feasible. Therefore the right side of inequality (e) is negative, and (e) becomes

$$u_{31} \geq g_{31} \triangleq \frac{(w_2 T_2^T + w_3 T_3^T) - w_2 T_2^S - w_3 T_3^S}{(-w_3\,\Delta T_m) + w_3 T_1^S - w_3 T_3^S} \tag{f}$$

Similarly, substituting for T_6 in $T_2^S - T_6 \geq \Delta T_m$ yields

$$u_{32} \geq g_{32} \triangleq \frac{(-w_2 T_2^T) + w_2 T_2^S}{(-w_3 \Delta T_m) + w_3 T_2^S - w_3 T_3^S} \tag{g}$$

These stream split constraints replace the two ΔT_m constraints used in their derivation.

In general, assuming that any exchanger may be connected to *either* a cold stream split or a hot stream split (but not to *both* a cold stream split and a hot stream split), the stream split constraints have the form

$$u_{ij} \geq g_{ij} \triangleq \frac{a_{ijo} + \Sigma_l a_{ijl} T_l^S}{c_{ijo} + \Sigma_l c_{ijl} T_l^S} \tag{27}$$

where u_{ij} is the stream split fraction of branch j in stream i and a_{ijo}, a_{ijl}, c_{ijo}, and c_{ijl} are constants depending on stream target temperatures, flow rates, and ΔT_m (Saboo *et al.*, 1987b). Under the same assumption, the load constraints can always be written in terms of unsplit streams. These results hold for any number of stream splits and for any number of exchangers connected to each branch of a stream split.

b. *Feasibility Test.* If all the restrictions of the corner point theorem are satisfied except that the stream split fractions are allowed to vary, then the following LP can be formulated to test the feasibility of a minimum unit HEN for assumed, fixed values of the uncertain temperatures (Saboo *et al.*, 1987b):

$$\psi = \min_u \beta \tag{28}$$

subject to:

(A1) Mass balance at each stream split:

$$\sum_j u_{ij} = 1 \quad \forall\, i$$

(B1) Constraints on stream split fractions:

$$u_{ij} + \beta \geq g_{ij} \triangleq \frac{a_{ijo} + \Sigma_l a_{ijl} T_l^S}{c_{ijo} + \Sigma_l c_{ijl} T_l^S}$$

(B2) Load and ΔT_m constraints not depending on u:

$$v_k \triangleq v_{ko} + \sum_l v_{kl} T_l^S \leq \beta$$

The minimum unit HEN with stream splits is feasible if and only if $\psi \leq 0$.

For the feasibility test, stream split constraints (B1) are *linear*! In particular, each g_{ij} is constant since the feasibility test is for specified supply temperatures. Also note that the energy balance and energy recovery constraints are not included in this feasibility test; they are used to determine constants a_{ijl}, c_{ijl}, and v_{kl} in the stream split, load, and ΔT_m constraints.

c. *Resilience Test.* For the resilience test, the stream split constraints are *no longer linear* since the supply temperatures are no longer constant but vary within an uncertainty range. In general, the stream split constraints are nonconvex and the corner point theorem cannot be applied. However, it is still possible to develop a sufficient test for HEN resilience.

The critical values of the uncertain supply temperatures limiting HEN resilience are those which maximize constraint functions g_{ij} and v_k. Constraints v_k are linear functions of supply temperatures T_l^S and constraints g_{ij} are monotonic functions of T_l^S (Saboo *et al.*, 1987b). Thus the critical points which maximize g_{ij} and v_k are corner points of the uncertainty range. To identify which of the corner points maximizes each of the constraint functions, one can simply examine the signs of the gradients of g_{ij} and v_k with respect to each of the T_l^S.

A necessary condition for the HEN to be resilient is that $v_{k,\max}$ be nonpositive for every k (Saboo *et al.*, 1987b). This condition is necessary since constraint functions v_k are linear in T_l^S and independent of stream split fractions u. If any of the $v_{k,\max}$ is positive, then one of the ΔT_m or load constraints in problem (28) is violated (at the critical corner point for $v_{k,\max}$) and no choice of stream split fractions u will make the network feasible (at that critical corner point). If all the $v_{k,\max}$ are nonpositive, then all of the ΔT_m and load constraints in problem (28) are satisfied at every corner point, and thus (by linearity in T^S) throughout the entire uncertainty range.

If all the $v_{k,\max}$ are nonpositive, then the ΔT_m and load constraints (which are independent of u) can be deleted from further consideration. The following LP can then be formulated to check whether the remaining constraints (which are functions of u) are satisfied (Saboo *et al.*, 1987b):

$$\chi = \min_{u,\beta} \beta \tag{29}$$

(A1) Mass balance at each stream split:

$$\sum_j u_{ij} = 1 \;\forall\; i; \qquad u_{ij} \geq 0 \;\forall\; i, j$$

(B1) Constraints on stream split fractions:

$$u_{ij} + \beta \geq g_{ij,\max}$$

Note that the uncertain supply temperatures T^S are not included as optimization variables in LP (29), since the uncertainty range was already searched to calculate $g_{ij,\max}$.

The minimum unit HEN with stream splits is resilient if $\chi \leq 0$. This test is sufficient, but not necessary, for HEN resilience. It is necessary only if the same critical corner point maximizes all of the g_{ij} and v_k constraint functions simultaneously.

Example 9. Resilience of the minimum-unit stream-splitting HEN shown in Fig. 12 is to be tested in the uncertainty range 415 K $\leq T_2^S \leq$ 515 K. The stream split constraints were derived in Example 8 from the ΔT_m constraints on the hot ends of the exchangers.

The constraints for the resilience test are the following:

Stream split constraints:

$$HX\,1: \qquad u_{31} \geq g_{31} \triangleq \frac{(600 - T_2^S)}{410}$$

$$HX\,2: \qquad u_{32} \geq g_{32} \triangleq \frac{(T_2^S - 370)}{(T_2^S - 330)}$$

Load constraints:

$$HX\,1: \qquad v_1 \triangleq T_2^S - 600 \leq 0$$

$$HX\,2: \qquad v_2 \triangleq 370 - T_2^S \leq 0$$

$$C: \qquad v_3 \triangleq 370 - T_2^S \leq 0$$

Mass balance at stream split:

$$u_{32} = 1 - u_{31}, \qquad u_{31}, u_{32} \geq 0$$

The remaining ΔT_m constraints ($T_4 - T_3^S \geq 10$, $T_2^T - T_3^S \geq 10$) can be disregarded since for the values of the heat capacity flow rates chosen in this example, ΔT_m will always occur on the hot ends of the exchangers for any value of the stream split fractions.

The feasible region defined by these constraints is plotted in Fig. 13. The feasible region is nonconvex, and thus the corner point theorem does not hold. In particular, the HEN is not feasible for 422 K $\leq T_2^S \leq$ 508 K, even though it is feasible for the corner points of the uncertainty range: T_2^S = 415 K and T_2^S = 515 K.

The resilience test correctly identifies that the HEN is not resilient in the specified uncertainty range. In order to apply the resilience test, the values of $v_{k,\max}$ and $g_{ij,\max}$ shown in Table V are calculated. The values of $v_{k,\max}$ are all nonpositive; thus the load constraints are satisfied throughout the

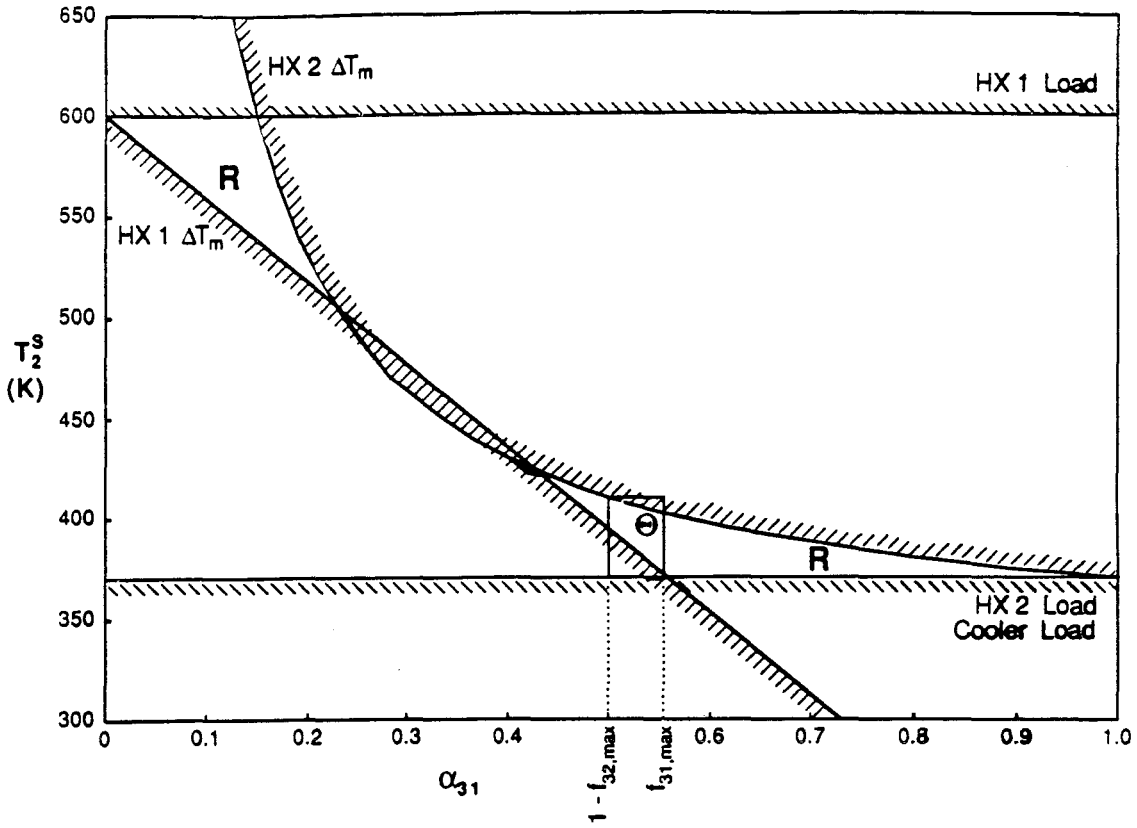

FIG. 13. Feasible region for stream splitting HEN structure (Examples 8, 9 and 11).

TABLE V

MAXIMUM VALUES OF RESILIENCE CONSTRAINT FUNCTIONS $v_{k,max}$ AND $g_{ij,max}$ IN AN UNCERTAINTY RANGE $415 \leq T_2^s \leq 515$ K (EXAMPLE 9)

Constraint function	Maximum value $V_{k,max}$ or $g_{ij,max}$	Critical corner point (K)
v_1	−85	$T_2^s = 515$
v_2	−45	$T_2^s = 415$
v_3	−45	$T_2^s = 415$
g_{31}	0.4512	$T_2^s = 415$
g_{32}	0.7838	$T_2^s = 515$

uncertainty range and can be deleted from further consideration. Now LP (29) is applied to test whether the stream split constraints are satisfied:

$$\chi = \min_{u_{31},\beta} \beta$$

subject to

$$u_{31} + \beta \geq g_{31,\max} = 0.4512, \qquad u_{31} - \beta \leq 1 - g_{32,\max} = 0.2162$$

Solution of this LP yields $\chi = 0.1175$. Since $\chi > 0$, the HEN is not resilient in the uncertainty range 415 K $\leq T_2^S \leq$ 515 K.

To show that this procedure is not a *necessary* test for resilience, consider the uncertainty range 370 K $\leq T_2^S \leq$ 410 K. This uncertainty range is shown in Fig. 13. Obviously, the HEN is resilient in this uncertainty range since for every value of T_2^S in the range, there is a value of u_{31} for which the network is feasible.

The resilience test incorrectly identifies the network as not being resilient. The values of $v_{k,\max}$ and $g_{ij,\max}$ for this uncertainty range are listed in Table VI. Since all the $v_{k,\max}$ are nonpositive, the load constraints are satisfied throughout the uncertainty range. To test the stream split constraints, LP (29) is applied:

$$\chi = \min_{u_{31},\beta} \beta$$

subject to

$$u_{31} + \beta \geq g_{31,\max} = 0.5610, \qquad u_{31} - \beta \leq 1 - g_{32,\max} = 0.5000$$

Solution of this LP yields $\chi = 0.0305$, thus implying that the network is not resilient in the new uncertainty range. The resilience test is conservative because LP (29) looks for values of stream split fractions u which, if held

TABLE VI

MAXIMUM VALUES OF RESILIENCE CONSTRAINT FUNCTIONS $v_{k,\max}$ AND $g_{ij,\max}$ IN AN UNCERTAINTY RANGE 370 $\leq T_2^S \leq$ 410 K (EXAMPLE 9)

Constraint function	Maximum value $v_{k,\max}$ or $g_{ij,\max}$	Critical corner point (K)
v_1	−190	$T_2^S = 410$
v_2	0	$T_2^S = 370$
v_3	0	$T_2^S = 370$
g_{31}	0.5610	$T_2^S = 370$
g_{32}	0.5000	$T_2^S = 410$

constant, would make the HEN resilient for the entire uncertainty range. From Fig. 13, for the uncertainty range 370 K $\leq T_2^S \leq$ 410 K, there is no single value of u_{31} which, if held constant, would make the HEN resilient for the entire uncertainty range.

3. *Resilience Analysis with Flow Rate Uncertainties*

When a HEN resilience problem includes uncertain flow rates, the energy balance, energy recovery, ΔT_m, and load constraints all can become nonlinear. Example 1 demonstrated that this can lead to nonconvex problems and thus that the corner point theorem does not hold for flow rate uncertainties in general.

One reasonable simplifying assumption is a high correlation between the uncertain flow rates. Indeed, it is instructive to study the limiting case when a change in total process throughput changes all the flow rates proportionately. In this case, the changing flow rates simply rescale the resilience problem; that is, the flow rate changes can be factored out of the energy balance and energy recovery constraints and have no effect upon the ΔT_m and load constraints (Saboo *et al.*, 1987b). Therefore if all the flow rates vary proportionately, then the flow rate uncertainties can be ignored while testing the resilience of a HEN to temperature uncertainties. The rating for each heat exchanger is determined by the largest process throughput.

a. ΔT_m *and Load Constraints.* When the uncertain flow rates are not proportionate, the resilience test can still be simplified if the HEN has a minimum number of units. For a minimum unit HEN, the energy balance and energy recovery constraints can be solved simultaneously to give unique expressions for the heater loads and intermediate stream temperatures. Then these expressions can be substituted into the ΔT_m and load constraints to write the constraints explicitly in terms of the supply temperatures T^S and head capacity flow rates w.

Following this procedure, the ΔT_m constraint for an exchanger connected to hot stream S_i and cold stream S_j with uncertain flow rates has the general form (Saboo *et al.*, 1987b)

$$g_{ij}(w, T^S) \triangleq \frac{1}{w_i}\sum_l (a_{ijo} + a_{ijl}T_l^S)w_l - \frac{1}{w_j}\sum_l (c_{ijo} + c_{ijl}T_l^S)w_l - \Delta T_m \geq 0 \qquad (30)$$

where a_{ijo} and c_{ijo} are equal to -1, 0, or $+1$ times a target temperature and

where a_{ijl} and c_{ijl} are equal to -1, 0, or $+1$. If heat capacity flow rates w_i and w_j are constant, then the ΔT_m constraint is required at only one end of the exchanger, depending upon the sign of $(w_i - w_j)$. However, if the flow rates vary enough that the sign of $(w_i - w_j)$ changes in the uncertainty range, then ΔT_m constraints are required at both ends of the exchanger.

The load constraint for an exchanger k with uncertain flow rates has the following general form (Saboo *et al.*, 1987b):

$$v_k(w, T^S) \triangleq \sum_l (v_{ko} + v_{kl} T_l^S) w_l \geq 0 \tag{31}$$

where v_{ko} equals -1, 0, or $+1$ times a target temperature and v_{kl} equals -1, 0, or $+1$.

b. *Resilience Test.* In general, ΔT_m and load constraints (30) and (31) are nonlinear and nonconvex, and the corner point theorem cannot be applied. However, it is still possible to develop a necessary and sufficient resilience test for HENs with a minimum number of units.

A minimum unit HEN with uncertain flow rates is resilient in a specified uncertainty range if and only if ΔT_m and load constraints (30) and (31) are satisfied throughout the uncertainty range; that is, the network is resilient if and only if

$$\min_{i,j,k} (g_{ij,\min}, v_{k,\min}) \geq 0 \tag{32}$$

where

$$g_{ij,\min} = \min_{\theta \in \Theta} g_{ij}, \qquad v_{k,\min} = \min_{\theta \in \Theta} v_k \tag{33}$$

and θ contains the uncertain supply temperatures T^S and flow rates w in the uncertainty range Θ (Saboo *et al.*, 1987b).

Constraint functions v_k are monotonic in supply temperatures T^S and heat capacity flow rates w. Thus the critical point which minimizes v_k is a corner point of the uncertainty range. To identify which of the corner points minimizes each v_k, one can simply examine the signs of the gradients of each v_k with respect to each T_l^S and w_l.

Unfortunately, constraint functions g_{ij} are not necessarily monotonic. However, each g_{ij} has at most one stationary point with respect to flow rates w_i and w_j (Saboo *et al.*, 1987b). Standard nonlinear programming can be used to locate each stationary point. If the stationary point of g_{ij} lies outside the uncertainty range or if the stationary point is a maximum, then $g_{ij,\min}$ occurs at a corner point.

Saboo (1984) has generalized resilience test (32) to class 2 problems. However, his method is still limited to minimum unit HENs with no stream splits.

4. *Active Constraint Strategy for Nonlinear Resilience Analysis*

The nonlinear resilience analysis methods of the previous few sections, although rigorous, are limited to rather specific situations (Saboo *et al.*, 1987a,b): minimum unit HENs with piecewise constant heat capacities (but no stream splits or flow rate uncertainties), minimum unit HENs with stream splits (but constant heat capacities and no flow rate uncertainties), or minimum unit HENs with flow rate and temperature uncertainties (but constant heat capacities and no stream splits). Although it might be possible to combine these resilience analysis methods, the combined method would still be limited to HENs with a minimum number of units, and it would only be a sufficient test for resilience (at least for HENs with stream splits).

A more general algorithm, the active constraint strategy, has been developed by Grossmann and Floudas (1985, 1987) to analyze the resilience of many nonlinear processes in which the critical points limiting resilience need not be corner points of the uncertainty range. The active constraint strategy allows nonlinear resilience analysis of more general HENs than possible by earlier methods. In particular, it can be used to test the resilience of a HEN with minimum or more units, with or without stream splits or bypasses, and with temperature and/or flow rate uncertainties, but with constant heat capacities (Floudas and Grossmann, 1987b).

In addition, the active constraint strategy can save significant computational time in *linear* resilience analysis (86% in one example; Grossmann and Floudas, 1987) by eliminating the need to check HEN feasibility at every corner point. Thus, this strategy makes it practical to analyze the resilience of HENs with a large number of streams.

Grossmann and Floudas (1985, 1987) present both nonlinear and specialized linear forms of the active constraint strategy. Only the nonlinear form is discussed in this chapter.

The active constraint strategy has been developed for both the resilience (flexibility) test and the flexibility index (Grossmann and Floudas, 1985, 1987). However, only the active constraint strategy for the resilience test will be discussed here. Recall that the resilience test is based upon a resilience measure $\chi(d)$:

$$\chi(d) = \max_{\theta \in \Theta} \psi(d, \theta) \tag{6}$$

subject to

$$\Theta = \{\theta | \theta^L \leq \theta \leq \theta^U\}$$

where

$$\psi(d, \theta) = \min_{z,\beta} \beta \tag{4}$$

subject to

$$f_m(d, z, \theta) \leq \beta \qquad (m \in M)$$

A HEN is resilient in a specified uncertainty range Θ if and only if $\chi(d) \leq 0$. If $\chi(d) > 0$, then at least one of the feasibility constraints f_m is violated somewhere in the uncertainty range. Geometrically, the resilience test determines whether uncertainty range Θ lies entirely within feasible region R.

The basic idea of the active constraint strategy is to use the Kuhn–Tucker conditions to identify the potential sets of active constraints at the solution of NLP (4) for feasibility measure ψ. Then resilience test problem (6) [or flexibility index problem (11)] is decomposed into a series of NLPs with a different set of constraints (a different potential set of active constraints) used in each NLP.

Floudas and Grossmann (1987b) have shown that for HENs with any number of units, with or without stream splits or bypasses, and with uncertain supply temperatures and flow rates but with constant heat capacities, the active constraint strategy decomposes the resilience test (or flexibility index) problem into NLPs which have a single local optimum. Thus the resilience test (or flexibility index) also has a single local optimum solution.

a. *Active Constraints in Resilience Analysis.* Resilience measure $\chi(d)$ is determined by the largest value of feasibility measure $\psi(d, \theta)$ in the specified uncertainty range Θ. Feasibility measure $\psi(d, \theta)$ is limited in turn by different sets of reduced inequality constraints f_m which become active at the solution of NLP (4). An understanding of the different sets of active constraints which determine ψ forms the basis of the active constraint strategy. The following example is designed to promote a deeper understanding of feasibility measure ψ and of the active constraints which limit it.

Example 10. Feasibility measure ψ is to be calculated for the HEN in Fig. 14 as a function of uncertain supply temperature T_3^S. Since the HEN

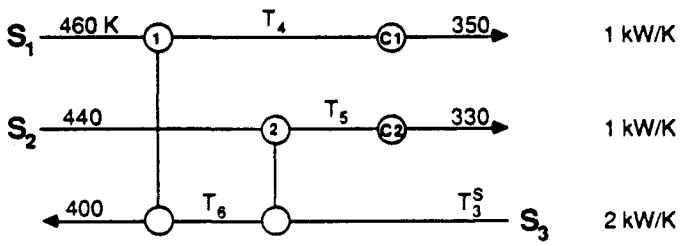

FIG. 14. HEN structure for Example 10.

has one more unit than the minimum required, one degree of freedom (control variable) can be manipulated to satisfy the feasibility constraints. Intermediate stream temperature T_5 is selected as the control variable.

Note that the energy recovery constraint reduces to $0 = 0$ since there is no heater in the network. The energy balances for the two exchangers can be solved simultaneously to yield the following expressions for intermediate stream temperatures T_4 and T_6:

$$T_4 = 2T_3^S - T_5 + 100, \qquad T_6 = T_3^S - 0.5T_5 + 220$$

These expressions can be substituted into the HEN ΔT_m and load constraints to yield the following LP for calculating ψ:

$$\psi(T_3^S) = \min_{T_5,\beta} \beta$$

subject to ΔT_m constraints

$$HX\ 1: \quad f_1 = T_5 - 2T_3^S + 260 \le \beta$$

$$HX\ 2: \quad f_2 = T_3^S - T_5 + 10 \le \beta$$

and load constraints

$$HX\ 1: \quad f_3 = 2T_3^S - T_5 - 360 \le \beta$$

$$HX\ 2: \quad f_4 = T_5 - 440 \le \beta$$

$$C\ 1: \quad f_5 = T_5 - 2T_3^S + 250 \le \beta$$

$$C\ 2: \quad f_6 = 330 - T_5 \le \beta$$

Figure 15 shows the feasible region for this HEN. With appropriate choice of control variable T_5, the HEN is feasible for $295\ \text{K} \le T_3^S \le 400\ \text{K}$. Consider the three points labeled A, B, and C ($T_3^S = 340$ K; $T_5 = 380, 385, 390$ K). Table VII lists the values of f_i and β for each of these points. The value of β is minimized when two of the constraints become simultaneously active ($f_1 = f_2 = \beta_{min} = -35$), which occurs at point B.

Table VII also lists values of $\psi = \beta_{min}$ for other points labeled in Fig. 15. These values of ψ are plotted in Fig. 16. Note that $\psi \le 0$ for $295\ \text{K} \le T_3^S \le 400\ \text{K}$, corresponding to the feasible range of T_3^S. The function $\psi(T_3^S)$ is piecewise linear. For each segment of $\psi(T_3^S)$, a different pair of active constraints (f_i, f_j) determines ψ. The pair of constraints active for each segment is noted on Fig. 16.

b. *Active Constraint Strategy.* In the previous example, different segments of the feasibility function ψ are all characterized by the same number of active constraints. In addition, HEN feasibility is always limited

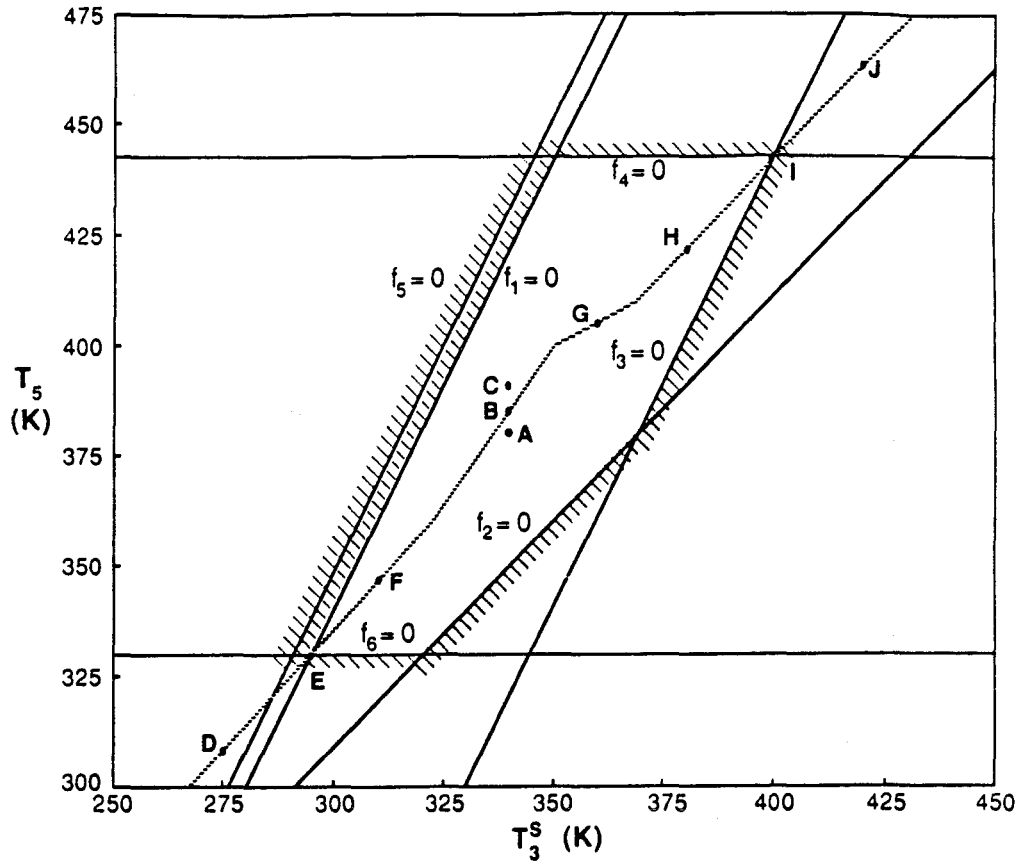

FIG. 15. Feasible region for Example 10.

TABLE VII

CALCULATION OF FEASIBILITY MEASURE ψ FOR EXAMPLE 10

Point	T_3^S	T_5	f_1	f_2	f_3	f_4	f_5	f_6	β
A	340	380	−40	−30	−60	−60	−50	−50	−30
B	340	385	−35	−35	−65	−55	−45	−55	−35
C	340	390	−30	−40	−70	−50	−40	−60	−30
Point	T_3^S	T_5	f_1	f_2	f_3	f_4	f_5	f_6	ψ
D	275	310	20	−25	−120	−130	10	20	20
E	295	330	0	−25	−100	−110	−10	0	0
F	310	345	−15	−25	−85	−95	−25	−15	−15
G	360	405	−55	−35	−45	−35	−65	−75	−35
H	380	420	−80	−30	−20	−20	−90	−90	−20
I	400	440	−100	−30	0	0	−110	−110	0
J	420	460	−120	−30	20	20	−130	−130	20

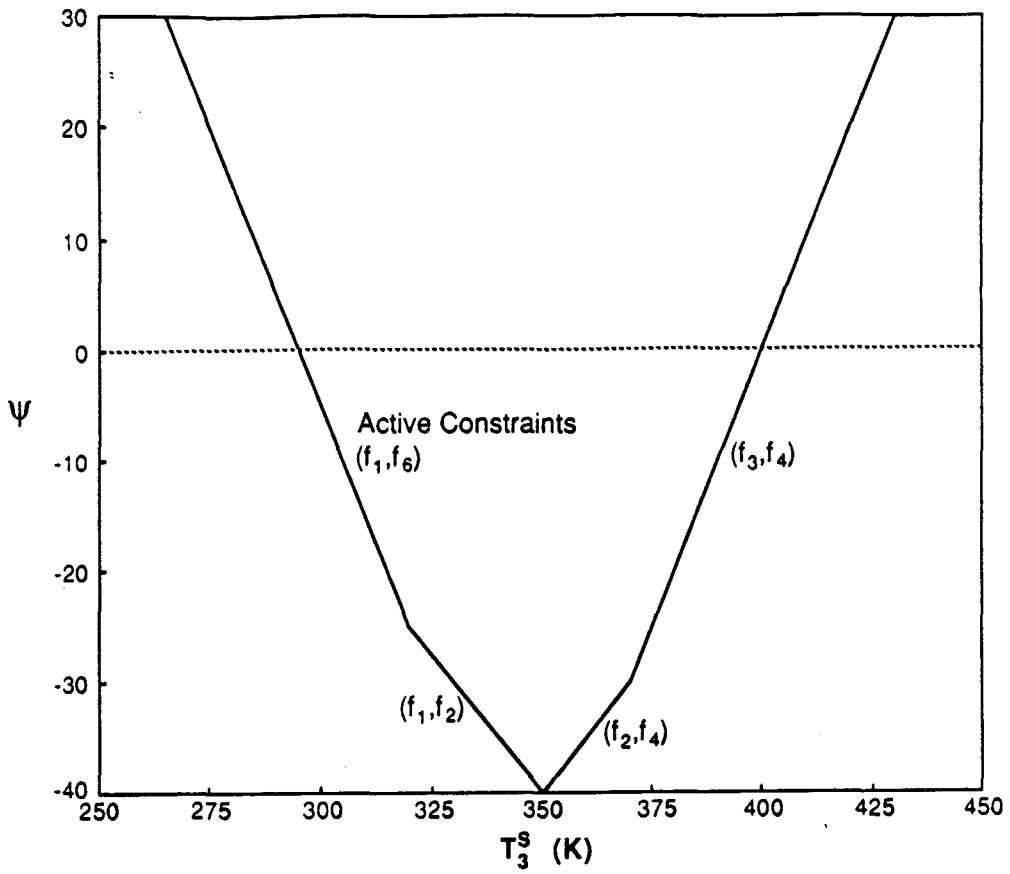

FIG. 16. Feasibility measure ψ for Example 10.

by the same number of active constraints in the resilience test of Example 3 (Table I), the flexibility index of Example 4 (Table II), and the resilience index of Example 5 (Table III). Swaney and Grossmann (1985a) have shown that this observation is general; that is, feasibility function ψ is characterized by a constant number of active constraints.

Theorem 3. Let n_z denote the number of control variables z and n_f the number of reduced inequality constraints f. If each $n_z \times n_z$ square submatrix of the Jacobian of f with respect to z,

$$\begin{bmatrix} \frac{\partial f_1}{\partial z_1} & \frac{\partial f_1}{\partial z_2} & \cdots & \frac{\partial f_1}{\partial z_{n_z}} \\ \frac{\partial f_2}{\partial z_1} & \frac{\partial f_2}{\partial z_2} & \cdots & \frac{\partial f_2}{\partial z_{n_z}} \\ & & \ddots & \\ \frac{\partial f_{n_f}}{\partial z_1} & \frac{\partial f_{n_f}}{\partial z_2} & \cdots & \frac{\partial f_{n_f}}{\partial z_{n_z}} \end{bmatrix}, \qquad n_f \geq n_z + 1$$

is of full rank, then the number of active constraints ($f_m = \beta_{\min} = \psi$, $m \in M_A$) is equal to $n_z + 1$.

Note that this theorem is consistent with the number of active constraints in Examples 3, 4, 5, and 10. (If each square submatrix of the Jacobian is not of full rank, then the number of active constraints may be less than $n_z + 1$.)

Two important consequences leading to the active constraint strategy follow from Theorem 3 (Grossmann and Floudas, 1987). First, for given values of uncertain variables θ, the value of $\psi = \beta_{\min}$ can be uniquely determined from a square system of $n_z + 1$ active constraint equations in $n_z + 1$ unknowns ($z_1, \ldots, z_{n_z}, \beta_{\min}$) rather than having to be determined by optimization. Second, resilience test problem (6) can be reduced to the following much simpler NLP:

$$\chi(d) = \max_{\theta \in \Theta} \beta_{\min} \tag{34}$$

subject to

$$f_m(d, z, \theta) \leq \beta_{\min} \qquad (m \in M_A), \qquad \Theta = \{\theta | \theta^L \leq \theta \leq \theta^U\}$$

where M_A is the set of $n_z + 1$ potentially active constraints at the corresponding value of θ. [The constraints in NLP (34) are written as inequality constraints rather than as equality constraints (as in Grossmann and Floudas, 1987), since all of the constraints may not be active if the submatrix of the Jacobian corresponding to constraint set M_A does not have full rank.]

The difficulty with problem (34) is that the set of active constraint equations M_A can change for different values of uncertain variables θ. The key feature of the active constraint strategy is its ability to identify potential sets of active constraints.

The potential sets of active constraints are identified by applying the Kuhn–Tucker conditions to NLP (4) for feasibility measure ψ (Grossmann and Floudas, 1985, 1987):

$$\sum_{m \in M} \lambda_m = 1 \tag{35a}$$

$$\sum_{m \in M} \lambda_m \frac{\partial f_m}{\partial z} = 0 \tag{35b}$$

$$\xi_m = \beta - f_m(d, z, \theta) \qquad (m \in M) \tag{35c}$$

$$\lambda_m \xi_m = 0 \qquad (m \in M) \tag{35d}$$

$$\lambda_m, \xi_m \geq 0 \qquad (m \in M) \tag{35e}$$

where ξ_m and λ_m are the slack variable and Kuhn–Tucker multiplier, respectively, for constraint m. Equations (35a) and (35b) represent the

stationary points of the Lagrangian with respect to β and z, respectively; (35c) defines the slack variables; and (35d) and (35e) represent the complementary conditions.

Assuming that constraint functions f_m, $m \in M$, are all monotonic in z, the potential sets of active constraints can be determined from Kuhn-Tucker conditions (35b) and (35e) as follows (Grossmann and Floudas, 1987). If the constraint functions f_m are monotonic in z, then every component of $\partial f_m/\partial z$ is one signed for all z for each possible value of θ. Since $\lambda_m \geq 0$ must hold for each constraint $m \in M$ [Eq. (35e)], Eq. (35b) identifies the different sets of $n_z + 1$ constraints which can satisfy the Kuhn–Tucker conditions (different potential sets M_A of $n_z + 1$ active constraints).

To illustrate, reconsider Example 10, which has one control variable $z = T_5$. The reduced constraint functions have the following gradients with respect to z:

$$\frac{\partial f_1}{\partial z} = 1, \quad \frac{\partial f_2}{\partial z} = -1, \quad \frac{\partial f_3}{\partial z} = -1$$

$$\frac{\partial f_4}{\partial z} = 1, \quad \frac{\partial f_5}{\partial z} = 1, \quad \frac{\partial f_6}{\partial z} = -1$$

Since there is one control variable, by Theorem 3 feasibility measure ψ is determined by two active constraints. Since for each pair of active constraints the corresponding Kuhn–Tucker multipliers λ_m must be non-negative [Eq. (35e)], each pair of active constraint functions must have gradients of opposite sign [Eq. (35b)]. Thus the potential sets of active constraints are

$$(f_1, f_2), \quad (f_1, f_3), \quad (f_1, f_6), \quad (f_2, f_4), \quad (f_2, f_5)$$
$$(f_3, f_4), \quad (f_3, f_5), \quad (f_4, f_6), \quad (f_5, f_6)$$

From Example 10 (Fig. 16), the actual sets of active constraints are

$$(f_1, f_2), \quad (f_1, f_6), \quad (f_2, f_4), \quad (f_3, f_4)$$

Now the active constraint strategy for performing the resilience test can be summarized (Grossmann and Floudas, 1987) as follows.

1. Identification of potential sets of active constraints:
   a. For every $m \in M$, compute $\partial f_m/\partial z$ and determine the sign of each component of the gradients.
   b. Using Kuhn–Tucker conditions (35b) and (35e), identify the $k = 1, \ldots, n_A$ potential sets of $n_z + 1$ active constraints, $M_A(k) = \{m \mid m \in M$ and m is one of the $n_z + 1$ active constraints$\}$.

2. Determine the trial resilience measure χ^k for each potential set of active constraints $M_A(k)$.
   a. If $M_A(k)$ involves only upper and lower bound constraints $\theta^L_{l(k)} \leq \theta_{l(k)} \leq \theta^U_{l(k)}$, then

$$\chi^k(d) = \frac{1}{n_k}\left[\sum_{l(k)\in M_A(k)} \theta^L_{l(k)} - \sum_{l(k)\in M_A(k)} \theta^U_{l(k)}\right] \qquad (36)$$

   where index $l(k)$ represents the components of θ involved in the upper and lower bound constraints in $M_A(k)$ and n_k is total number of upper and lower bound constraints (Grossmann and Floudas, 1987).
   b. Otherwise, solve the following version of NLP (34):

$$\chi^k(d) = \max_{\theta\in\Theta, z, \beta_{\min}} \beta_{\min} \qquad (34^k)$$

subject to

$$f_m(d, z, \theta) \leq \beta_{\min} \qquad (m \in M_A(k)), \qquad \Theta = \{\theta | \theta^L \leq \theta \leq \theta^U\}$$

3. Determine the overall resilience measure $\chi(d)$:

$$\chi(d) = \max_{k=1,\ldots,nA} \chi^k(d)$$

4. The HEN is resilient in the specified uncertainty range Θ if and only if $\chi(d) \leq 0$.

It should be noted that the active constraint strategy is equivalent to an explicit enumeration of all potential sets of active constraints. This explicit enumeration could also be performed by a mixed-integer nonlinear program (MINLP), with integer variables denoting whether particular constraints are active. Grossmann and Floudas (1987) present the form of this MINLP, but it is not solvable with current alogrithms. The active constraint strategy decomposes the MINLP into a series of solvable NLPs. In the case of linear constraints, the MINLP reduces to a MILP, which is solvable by standard branch and bound techniques. Grossmann and Floudas (1987) also present forms of the active constraint strategy where the equality constraints are handled explicitly (rather than being substituted into the inequality constraints) and when no control variables are present (e.g., minimum unit HENs with fixed target temperatures and no stream splits).

Example 11. The active constraint strategy is to be used to test the resilience of the same stream splitting HEN as in Example 9 (Fig. 12) in the uncertainty range $\Theta = \{T_2^S | 415 \leq T_2^S \leq 515\ \text{K}\}$.

Note that the energy recovery constraint reduces to $0 = 0$ since there is no heater in this network. The energy balances for both exchangers and the stream split can be solved simultaneously for intermediate stream tempera-

tures T_4, T_5, and T_6 to yield

$$T_4 = 0.5T_2^S + 440, \qquad T_5 = \frac{1}{u_{31}}(600 - T_2^S) + 320,$$

$$T_6 = \frac{T_2^S - 370}{1 - u_{31}} + 320$$

When these expressions for T_4, T_5, and T_6 are substituted into the ΔT_m, load, and stream split constraints, the following NLP can be written for feasibility measure ψ:

$$\psi = \max_{u_{31}, \beta} \beta$$

subject to ΔT_m constraints

$$HX\ 1: \quad f_1 \triangleq \frac{600 - T_2^S}{u_{31}} - 410 \le \beta$$

$$HX\ 2: \quad f_2 \triangleq \frac{T_2^S - 370}{1 - u_{31}} - T_2^S + 330 \le \beta$$

load constraints

$$HX\ 1: \quad f_3 \triangleq 0.5T_2^S - 300 \le \beta$$

$$HX\ 2: \quad f_4 \triangleq 370 - T_2^S \le \beta$$

$$C: \quad f_5 \triangleq 185 - 0.5T_2^S \le \beta$$

and stream split constraints

$$f_6 \triangleq -u_{31} \le \beta, \qquad f_7 \triangleq u_{31} - 1 \le \beta$$

The feasible region determined by these constraints (with $\beta = 0$) is shown in Fig. 13.

The gradients of the constraint functions f_i with respect to control variable u_{31} are

$$\frac{\partial f_1}{\partial u_{31}} = -\frac{600 - T_2^S}{u_{31}^2} < 0 \quad \forall\ T_2^S \in \Theta$$

$$\frac{\partial f_2}{\partial u_{31}} = \frac{T_2^S - 370}{(1 - u_{31})^2} > 0 \quad \forall\ T_2^S \in \Theta$$

$$\frac{\partial f_3}{\partial u_{31}} = \frac{\partial f_4}{\partial u_{31}} = \frac{\partial f_5}{\partial u_{31}} = 0$$

$$\frac{\partial f_6}{\partial u_{31}} = -1, \qquad \frac{\partial f_7}{\partial u_{31}} = 1$$

Thus, from Kuhn–Tucker condition (35b), the potential sets of active constraints are identified as shown in Table VIII. For each potential set of active constraints $M_A(k)$, NLP (34^k) is formulated to determine trial resilience measure $\chi^{(k)}$. For example, for potential set $M_A(1) = \{(f_1, f_2)\}$, the following NLP is solved:

$$\chi^{(1)} = \max_{T_2^S, u_{31}, \beta} \beta$$

subject to

$$f_1 \triangleq \frac{600 - T_2^S}{u_{31}} - 410 \leq \beta, \qquad f_2 \triangleq \frac{T_2^S - 370}{1 - u_{31}} - T_2^S + 330 \leq \beta$$

$$415 \leq T_2^S \leq 515 \text{ K}$$

The solution of NLP (34^k) for each potential set of active constraints is summarized in Table VIII.

The resilience measure for this stream-splitting HEN is

$$\chi = \max_k \chi^k = \chi^1 = 5.7159$$

Thus the HEN is not resilient in the specified uncertainty range. The worst case condition for resilience is given by the solution of NLP (34^k) corresponding to $M_A(1) = \{(f_1, f_2)\}$. At this solution, constraints $f_1 \leq 0$ ($HX\,1\ \Delta T_m$) and $f_2 \leq 0$ ($HX\,2\ \Delta T_m$) are most violated when $T_2^S = 462.2$ K and $u_{31} = 0.3315$ (compare with Fig. 13).

Note that in Table VIII, u_{31} violates the stream split constraints ($0 \leq u_{31} \leq 1$) at some of the solutions of NLP (34^k); for example, $u_{31} < 0$ at the solution of NLP (34^{18}). This means that *potential* set of active constraints $M_A(18) = \{(f_5, f_7)\}$ is *not* active at the solution of the resilience test problem, since u_{31} violates the nonnegativity constraint [which was not included in NLP (34^{18})]. However, u_{31} does satisfy the constraint $u_{31} \leq 1$ ($f_7 \leq 0$), since this constraint was included in NLP (34^{18}).

Note also that some of the gradients $\partial f_i / \partial u_{31}$ are zero and thus that this problem does not strictly satisfy the conditions of Theorem 3. The result of this is either of the following.

1. For given T_2^S, the solution of NLP (34^k) may not be uniquely determined by a system of $n_z + 1$ equality constraints in $n_z + 1$ unknowns (u_{31} and β). For example, in Table VIII, for $M_A(10) = \{(f_3, f_4)\}$ and $M_A(11) = \{(f_3, f_5)\}$, u_{31} is arbitrary at the solution of NLP (34^k). In this case, only a subset of $M_A(k)$ may actually be active.

2. Nonlinear program (34^k) may have no feasible solution [e.g., for $M_A(14) = \{(f_4, f_5)\}$]. If this is the case, then *potential* set $M_A(k)$ *cannot* be active at the solution of the resilience test problem.

TABLE VIII

RESILIENCE TEST WITH ACTIVE CONSTRAINT STRATEGY FOR EXAMPLE 11

	Potential set of active constraints	Solution of NLP (34^k)		
k	M_A(k)	T_2^S (K)	u_{31}	χ^k
1	(f_1, f_2)	462.2	0.3315	5.716
2	(f_1, f_3)	515	0.2313	−42.5
3	(f_1, f_4)	415	0.5068	−45.0
4	(f_1, f_5)	415	0.4774	−22.5
5	(f_1, f_7)	415	0.4519	−0.5482
6	(f_2, f_3)	515	−0.0175[a]	−42.5
7	(f_2, f_4)	415	−0.1250[a]	−45
8	(f_2, f_5)	415	0.2800	−22.5
9	(f_2, f_6)	515	0.2153	−0.2153
10	(f_3, f_4)	446.67	Arbitrary	−76.67
11	(f_3, f_5)	485	Arbitrary	−57.5
12	(f_3, f_6)	415	42.5[a]	−42.5
13	(f_3, f_7)	515	−41.5[a]	−42.5
14	(f_4, f_5)	No feasible solution	No feasible solution	No feasible solution
15	(f_4, f_6)	415	45[a]	−45
16	(f_4, f_7)	415	−44[a]	−45
17	(f_5, f_6)	415	22.5[a]	−22.5
18	(f_5, f_7)	415	−21.5[a]	−22.5
19	(f_6, f_7)	Arbitary	0.5	−0.5

[a] These *potential* sets of active constraints turn out *not* to be active in resilience problem (6) since the constraints on u_{31} $(0 \leq u_{31} \leq 1)$ are violated.

D. CLASS 2 RESILIENCE PROBLEMS

All the resilience analysis methods presented so far require that the form of the energy recovery constraint remain the same throughout the uncertainty range (class 1 problem). If the uncertainty range is sufficiently large, then the stream population at the pinch changes, thus changing the form of the energy recovery constraint (class 2 problem). When the form of the energy recovery constraint changes, then the reduced form of the ΔT_m and load constraints also changes (after the energy recovery and energy balance equality constraints are solved for the state variables and expressions for the state variables are substituted into the ΔT_m and load

constraints). Example 6 earlier in this chapter demonstrated that class 2 problems can be nonconvex even if all the constraints are linear.

A practical disadvantage of class 2 problems is that extra exchangers are often required because of changes in the pinch stream population. For example, reconsider the class 2 problem in Fig. 7. In Fig. 7a, the ΔT_m constraint imposed by the pinch at T_{h2}^S requires the presence of exchanger 1 (matching streams S_{c2} and S_{h2}), while exchanger 2 (matching streams S_{c2} and S_{h1}) can be completely bypassed. However, in Fig. 7b, the new pinch location at T_{h1}^S requires the presence of exchanger 2, while exchanger 1 can be completely bypassed. Thus for the class 2 uncertainty range, both exchangers are required, while for a class 1 uncertainty range ($460 \leq T_{h2}^S \leq 470$ K or $470 \leq T_{h2}^S \leq 480$ K), only one of the two exchangers is required. As a result, requiring strict resilience for class 2 problems (including that the energy recovery specification be satisfied throughout the uncertainty range) can make a HEN's capital cost quite high.

For quality control or safety considerations, it is essential that a HEN meet specified target temperatures, whether or not it achieves specified energy recovery. Thus for industrial problems with large uncertainty ranges, it may be desirable to design networks which are merely *operable*, rather than resilient, that is, to require that the network meet all target temperatures while satisfying the ΔT_m and load constraints, but allowing the energy recovery constraint to be violated at some points in the uncertainty range. Requiring that a HEN be operable rather than strictly resilient allows some extra heating to be used occasionally in order to lower capital costs.

Assuming that all the restrictions of the corner point theorem are satisfied except that class 2 problems are allowed, HEN resilience analysis without the energy recovery constraint is convex even for class 2 problems, since all the other constraints are still linear. This leads to the following modification of the corner point theorem (Saboo *et al.*, 1987b).

Theorem 4. Assume that all the restrictions of the corner point theorem are satisfied except that class 2 problems are allowed.

a. Then a HEN is operable in a specified uncertainty range if and only if it is operable at every corner point of the uncertainty range.

b. An upper bound on the minimum heating necessary for the HEN to be operable at a specified point θ in the uncertainty range is given by a linear combination of the minimum heating targets at all the corner points:

$$H_{min} \leq \sum_{l \in L_v} y^l H^l \tag{37}$$

where y^l are determined such that

$$\theta = \sum_{l \in L_v} y^l \theta^l \tag{38}$$

Here θ^l are the values of the uncertain variables and H^l the minimum heating target at corner point l and L_v is the index set for the corner points.

Example 12 (from Saboo et al., 1987b). For the HEN structure in Fig. 8, the problem of analyzing resilience in an expected uncertainty range of

$$340 \leq T^S_{h1} \leq 380 \quad \text{K}, \qquad 270 \leq T^S_{c2} \leq 300 \quad \text{K}$$

is class 2 (Example 6). However, the HEN is operable at all four corner points (Fig. 9) and thus is operable throughout the uncertainty range.

The minimum heating requirement at each corner point is

$$\begin{aligned} H^1 &= 260 \quad \text{kW} \qquad \text{at} \quad \theta^1 = (340, 270) \\ H^2 &= \quad 0 \quad \text{kW} \qquad \text{at} \quad \theta^2 = (380, 270) \\ H^3 &= 140 \quad \text{kW} \qquad \text{at} \quad \theta^3 = (340, 300) \\ H^4 &= \quad 0 \quad \text{kW} \qquad \text{at} \quad \theta^4 = (380, 300) \end{aligned}$$

Thus at the intermediate uncertainty point

$$\theta = \begin{bmatrix} 360 \\ 295 \end{bmatrix} = y^1 \begin{bmatrix} 340 \\ 270 \end{bmatrix} + y^2 \begin{bmatrix} 380 \\ 270 \end{bmatrix} + y^3 \begin{bmatrix} 340 \\ 300 \end{bmatrix} + y^4 \begin{bmatrix} 380 \\ 300 \end{bmatrix} \tag{a}$$

an upper bound on the minimum heating requirement is

$$H_{\min} \leq y^1(260) + y^2(0) + y^3(140) + y^4(0) \tag{b}$$

However, since there are four unknowns (y^1, y^2, y^3, y^4) and only two equations in system (a), the choice of the unknowns is not unique. The following LP is formulated to find the choice of y^1, y^2, y^3, y^4 which minimizes the upper bound on $H_{\min}$:

$$H_{\min} \leq \min_{y^1,\, y^2,\, y^3,\, y^4,\, H} H$$

subject to

$$\begin{aligned} H &= 260y^1 + 0y^2 + 140y^3 + 0y^4 \\ 360 &= 340y^1 + 380y^2 + 340y^3 + 380y^4 \\ 295 &= 270y^1 + 270y^2 + 300y^3 + 300y^4 \\ y^1, y^2, y^3, y^4 &\geq 0 \end{aligned}$$

Solution of this LP yields $H_{min} \leq 47.8$ kW, with $y^1 = y^2 = 0$, $y^3 = 0.3417$, and $y^4 = 0.6417$. The actual heating requirement at this intermediate uncertainty point is $H_{min} = 20$ kW.

The preceding theorem describes an *operability test* for class 2 HENs. Similarly, by omitting the energy recovery constraint from flexibility index problem (15) or resilience index problem (19), an *operability index* could be defined for class 2 HENs.

To rigorously analyze the resilience of class 2 HENs, and not just the operability, requires more complicated algorithms that are beyond the scope of this chapter. Saboo (1984) presents a mixed-integer linear program (MILP) for testing the resilience of minimum unit HENs to temperature uncertainties and a quadratic program (QP) for testing the resilience of HENs with more than minimum units. In addition, he presents an algorithm (based on solving a series of NLPs) for testing the resilience of minimum unit HENs with both temperature and flow rate uncertainties. Saboo (1984) also presents an algorithm for calculating the resilience index of class 2 HENs. However, all of these algorithms are limited to HENs with constant heat capacities and no phase change and constant stream split fractions.

E. Summary of HEN Resilience Analysis Techniques; Areas for Future Research

Several HEN resilience analysis techniques have been reviewed in this chapter. These techniques are all variations of three basic problems.

1. The resilience (flexibility) test determines whether a HEN structure is resilient (flexible) in a given uncertainty range.
2. The flexibility index determines the largest uncertainty range (scaled hyperrectangle) for which the HEN is resilient. The flexibility index is scaled in terms of an expected uncertainty range ($\theta^N - F\,\Delta\theta^- \leq \theta \leq \theta^N + F\,\Delta\theta^+$).
3. The resilience index, another measure of the largest uncertainties for which the HEN remains feasible, is the size of the largest *total* uncertainty load (polytope region) which the HEN can tolerate.

Different algorithms are required to solve these three basic resilience analysis problems depending on whether the problem is linear, nonlinear, or class 2. A HEN resilience problem is linear under the following conditions (corner point theorem, Saboo and Morari, 1984): (1) constant heat capacities and no phase change, (2) temperature uncertainties only

(no uncertain flow rates or heat transfer coefficients), (3) constant stream split fractions, and (4) class 1 uncertainty range.

If the HEN resilience problem is linear, then the three basic analysis techniques can be implemented as follows.

1. For the resilience (flexibility) test, a HEN is resilient (flexible) in a specified uncertainty range if and only if it is feasible at every corner point of the uncertainty range.
2. The flexibility index can be calculated by determining the largest scaled uncertainty s^k which the network can tolerate in the direction of each of the k corner points of the uncertainty range. Then the flexibility index is

$$F = \min_k s^k$$

3. The resilience index can be determined by maximizing the load uncertainty l_i which the network can tolerate in either a positive or negative direction in each stream supply temperature. Then the resilience index is

$$\text{RI} = \min_i \left(l_{i,\max}^-, l_{i,\max}^+\right)$$

Different algorithms are required if the HEN resilience problem is nonlinear. Special algorithms were presented for testing the resilience of minimum unit HENs with piecewise constant heat capacities, stream splits, or simultaneous flow rate and temperature uncertainties. A more general algorithm, the active constraint strategy, was also presented which can test the resilience or calculate the flexibility index of a HEN with minimum or more units, stream splits and/or bypasses, and temperature and/or flow rate uncertainties, but with constant heat capacities.

In the case of class 2 resilience problems, the temperature or flow rate uncertainties are large enough that the stream population at the pinch changes somewhere in the uncertainty range, thus changing the form of the energy recovery constraint. More complicated algorithms (Saboo, 1984) are required to rigorously analyze resilience for these problems. However, for class 2 problems it may be more practical to require that the HEN merely be operable rather than strictly resilient. A HEN is operable throughout a specified uncertainty range if and only if it is operable at every corner point of the uncertainty range.

Several powerful HEN resilience analysis algorithms have been reviewed in this chapter, including the active constraint strategy (Grossmann and Floudas, 1985, 1987) which can test the resilience of the most general HEN. However, many common industrial HENs still cannot be analyzed with present techniques. For example, no technique has been

reported which can analyze the resilience of a HEN with uncertain flow rates and temperatures *and* phase change. Also, no *rigorous* technique (with a single local optimum) has been reported which can analyze HEN resilience with respect to *area* constraints (rather than ΔT_m constraints), except when the HEN satisfies all the restrictions of the corner point theorem (Saboo *et al.*, 1985).

In order to extend present resilience analysis techniques to more general HENs, the following areas of research seem useful.

1. Develop more general techniques to analyze the resilience of HENs with minimum or more units, stream splits and/or bypasses, temperature and/or flow rate uncertainties, *and* temperature-dependent heat capacities and phase change. It may be possible to extend the active constraint strategy to heat capacities with a specific temperature dependence (e.g., $C_p = a + bT + cT^2$). It might also be possible to handle phase change with the active constraint strategy (e.g., by using breakpoints as in Section III,C,1) if this approach will lead to mixed-integer nonlinear programs which are solvable (e.g., by the outer approximation algorithm of Duran and Grossmann, 1986).

2. Develop more general techniques to test the resilience of HENs with area constraints instead of (or in addition to) ΔT_m constraints. It is possible to include area constraints in the active constraint strategy. However, the active constraint strategy for the resilience test may not satisfy the (sufficient) conditions for a single local optimum when logarithmic mean ΔT (ΔT_{LM}) is used. It may have a single optimum when arithmetic mean ΔT is used or when a Taylor series approximation of ΔT_{LM} is used. These approximations could be used to find a starting point to initialize the NLPs of the active constraint strategy with ΔT_{LM}.

3. Develop techniques to test the resilience of HENs with uncertain heat transfer coefficients (e.g., heat transfer coefficients as a function of flow rate, but with uncertain function parameters). It is possible to extend the active constraint strategy to heat transfer coefficients with bounded uncertainties (not as a function of flow rate), but then the active constraint strategy may not have a single local optimum solution.

4. Develop techniques to test the resilience of class 2 HENs with stream splits and/or bypasses, temperature and/or flow rate uncertainties, and temperature-dependent heat capacities and phase change. It may be possible to extend the active constraint strategy to class 2 problems. This would allow resilience testing of class 2 problems with stream splits and/or bypasses and temperature and/or flow rate uncertainties. However, the uncertainty range would still have to be divided into "pinch regions" (as in Saboo, 1984).

IV. Synthesis and Design of Resilient HENs

Research on the synthesis of economically optimal HENs has been performed by various investigators for over 15 years (Nishida *et al.*, 1981). Several powerful synthesis methods have evolved, including the pinch design method (Linnhoff *et al.*, 1982; Linnhoff and Hindmarsh, 1983) and methods based on structural optimization [to predict a minimum set of stream matches (Papoulias and Grossmann, 1983) and to determine the most economical network structure (Floudas *et al.*, 1986) from the predicted matches]. However, these methods synthesize networks only for fixed, assumed nominal values of any uncertain supply temperatures and flow rates and uncertain heat transfer coefficients.

The analysis techniques presented earlier in this chapter can be used to test the resilience of a synthesized network, and evolutionary changes can be made to the network, if necessary, to improve its resilience. However, this type of procedure may require many evolutionary synthesis–analysis iterations, and it may not be obvious which evolutionary changes are required to improve a network's resilience. Obviously, better methods are needed which incorporate resilience into the synthesis procedure itself.

Two such methods to synthesize HENs, which are both economically optimal and resilient, have evolved from the resilience analysis techniques reviewed. These methods are (1) synthesis of HEN structure based on a flexibility index (FI) target (Colberg *et al.*, 1988) and (2) synthesis of HEN structure and design (sizing) of individual exchangers based on structural optimization algorithms for multiperiod operation (e.g., for multiple critical points which limit resilience) (Floudas and Grossmann, 1987b). In addition, Linnhoff and Kotjabasakis (1986) have introduced the simple but intuitively appealing concept of "downstream (disturbance) paths" for synthesis of resilient HENs. All these methods are discussed here. However, emphasis is on how resilience aspects are incorporated into the synthesis algorithms rather than on the mechanics of the synthesis algorithms themselves.

A. HEN Synthesis Based on a Flexibility Index Target

Just as targets for minimum required utilities, units, and heat transfer area can guide a designer in synthesizing an economically optimal HEN, a target for maximum possible resilience (flexibility) can guide the designer in synthesizing a resilient HEN. And just as the economic targets simplify the search for an economically optimal HEN (by restricting the search to networks with minimum utility consumption), the flexibility index target

simplifies the search for a resilient HEN [by identifying the "critical" operating condition (supply temperatures and flow rates) and constraint (e.g., appearance of a new pinch) most likely to limit resilience].

1. *Flexibility Index Target*

Colberg *et al.* (1988) define the "general" resilience (flexibility) target as the maximum amount of resilience that could be incorporated into a HEN structure synthesized for given nominal stream data if the designer were to consider *all* possible HENs synthesized for that stream data. They show that such a target is arbitrarily large (i.e., for *any* given nominal values of uncertain stream data, it is *always* possible to synthesize a HEN structure which is resilient for *all* physically meaningful combinations of the uncertain supply temperatures, target temperatures, and heat capacity flow rates). In particular, infinitely cyclic HEN structures (or finite ones with a sufficient number of stream splits) can achieve this general resilience target. These particular structures can mimic the composite curves for any set of supply and target temperatures and flow rates [i.e., the temperature–enthalpy profile of each hot (cold) stream in the structure can always mimic the temperature–enthalpy profile of the hot (cold) composite curve]. And since the composite curves can be constructed for all physically possible temperatures and flow rates, the structures are resilient for all such temperatures and flow rates.

This general resilience target is not very practical. (1) Complex, costly HEN structures are generally required to achieve it; and (2) designing for *all* physically possible uncertainties is unrealistic (overly ambitious). A practical resilience target should be achievable with reasonable HEN structures (i.e., structures with few more units or stream splits than the number required for nominal stream data). A practical resilience target can be defined by restricting the target to class 1 uncertainty ranges (Colberg *et al.*, 1988). Larger, class 2 uncertainty ranges generally require HEN structures with a greater number of exchangers in order to satisfy ΔT_m at a number of different pinches (see Section III,D).

In order to quantify this resilience (flexibility) target, it can be defined in terms of the flexibility index. Then the resilience target—the class 1 flexibility index target—is the flexibility index of the largest possible class 1 uncertainty range (scaled with respect to the designer-specified expected uncertainty range) for the given nominal stream data (Colberg *et al.*, 1988).

For simple problems with a small number of streams and a small number of uncertain parameters, the class 1 FI target can be determined simply by trial-and-error plotting of the composite curves (Colberg *et al.*, 1988). The size of a class 1 uncertainty range is generally limited by its case B

(maximum cooling) and case C (maximum heating) corner points (see Theorem 3 in Section III,B,2). Starting from the nominal stream data, one can vary the uncertain supply temperatures and flow rates in the direction of the case B and case C corner points of the expected uncertainty range (see Table IV) and plot several sets of composite curves as the uncertain parameters vary. If a problem is pinched for the nominal stream data, the scaled uncertainty range is class 1 as long as (1) the pinch-causing stream is the same for the case B and case C corner points of the scaled uncertainty range, as well as for the nominal operating point; (2) the stream populations above and below the pinch are the same for the case B, case C, and nominal operating points; and (3) none of the stream supply, target, dew point, or bubble point temperatures (or breakpoint temperatures in the case of piecewise constant heat capacities) overlaps the range of pinch temperatures. If a problem is threshold heating (cooling) for the nominal stream data, the scaled uncertainty range is class 1 as long as the problem is also threshold heating (cooling) for both the case B and case C corner points of the scaled uncertainty range.

Trial-and-error plotting of composite curves is impractical for problems with a large number of streams, a large number of uncertain parameters, or correlated uncertainties. Colberg *et al.*, (1988) present a nonlinear program (NLP) to calculate the class 1 FI target for these (and simpler) problems.

Example 13 (*from Colberg et al., 1988*). Consider the nominal stream data given in Table IX. Stream S_{c2} causes the pinch for these data.

Assume that the supply temperature T^S_{h2} and heat capacity flow rate w_{h2} of hot stream S_{h2} are uncertain. Figure 17 shows a "pinch behavior diagram" as T^S_{h2} and w_{h2} vary. The nominal stream data are indicated with an asterisk. For every combination of uncertain parameters T^S_{h2} and w_{h2} in

TABLE IX

NOMINAL STREAM DATA FOR EXAMPLES 13 AND 14.[a]

Stream	T^S (K)	T^T (K)	w (kW/K)
S_{h1}	390	338	4.0
S_{h2}	400	283	6.0
S_{c1}	298	498	5.0
S_{c2}	358	388	10.0

[a] After shifting to account for ΔT_m = 10 K.

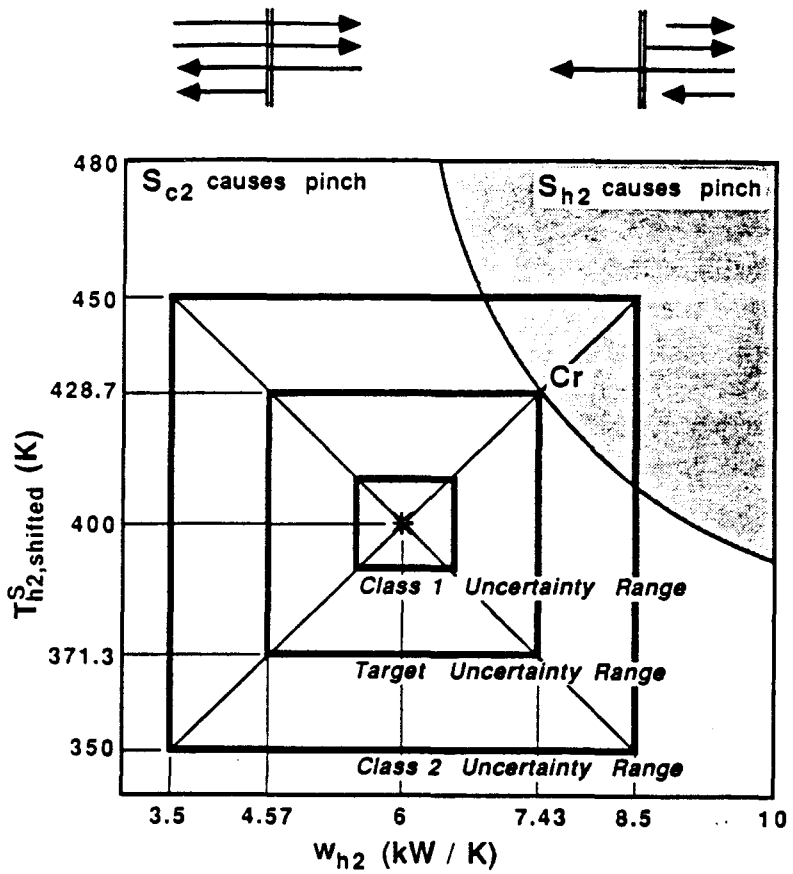

FIG. 17. "Pinch behavior diagram" illustrating class 1, class 2, and target uncertainty ranges for Example 13.

the unshaded portion of this diagram, stream S_{c2} causes the pinch. For all values of T^S_{h2} and w_{h2} in the shaded portion of this diagram, stream S_{h2} causes the pinch. If an uncertainty range includes both shaded and unshaded regions of this diagram, then it is class 2; otherwise it is class 1.

Figure 17 shows an uncertainty range as it increases in size. The smallest uncertainty range is class 1—for every combination of T^S_{h2} and w_{h2} in the range, stream S_{c2} causes the pinch, and the stream populations above the pinch (S_{h1}, S_{h2}, S_{c1}, S_{c2}) and below the pinch (S_{h1}, S_{h2}, S_{c1}) are constant. The largest uncertainty range is class 2—in one corner of the uncertainty range stream S_{h2} causes the pinch, while in the remainder of the uncertainty range stream S_{c2} causes the pinch. The middle-size uncertainty range (the "target uncertainty range") corresponds to the resilience target—it is at the transition between class 1 and class 2. If the uncertainties were any larger (in the direction of increasing T^S_{h2} or increasing w_{h2}), then this uncertainty range would become class 2. The point labeled "Cr" in Fig. 17 limits the size of the target operating range; this point is called the

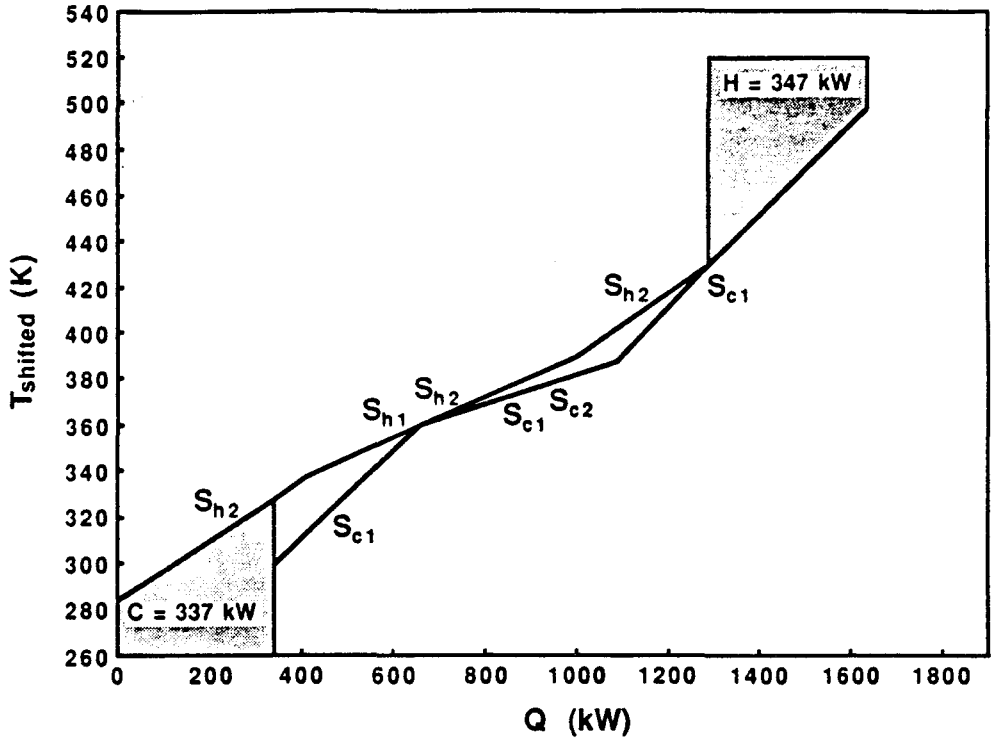

FIG. 18. Composite temperature–enthalpy curves for the critical uncertainty point of Example 13.

"critical uncertainty point." At this point, *both* stream S_{h2} *and* stream S_{c2} cause pinches, as shown in the composite curves in Fig. 18. Thus the "critical constraint" which limits resilience in this example is the appearance of a new pinch at the supply of stream S_{h2}.

Suppose that the designer specifies as the expected uncertainty range the smallest uncertainty range shown in Fig. 17 ($\Delta T^S_{h2} = \pm 10$ K; $\Delta w_{h2} = \pm 0.5$ kW/K). Then the class 1 FI target (F^*) has the value 2.87 ($F^*\ \Delta T^S_{h2} = \pm 28.7$ K; $F^*\ \Delta w_{h2} = \pm 1.44$ kW/K); the size of the target uncertainty range is scaled relative to the size of the expected uncertainty range. Note that the class 1 FI target can also have a value less than 1.0 if the expected uncertainty range specified by the designer is class 2.

2. *Use of the Class 1 Flexibility Index Target in HEN Synthesis*

In the synthesis of resilient HENs, use of the class 1 flexibility index target offers two important features (Colberg *et al.*, 1988):

1. The size of the target (compared to 1) tells the process engineer if the expected uncertainty range is class 1 or class 2, and thus predicts (in a qualitative sense) how difficult it is to synthesize a resilient HEN for the expected uncertainty range.

2. Calculation of the FI target identifies the critical uncertainty point and constraint most likely to limit resilience, and thus identifies the supply temperatures and flow rates (in addition to the nominal ones) to which the process engineer should pay special attention.

To use the size of the class 1 FI target F^* to judge the difficulty of synthesizing a HEN resilient in a specified expected uncertainty range, consider three cases.

(1) $F^* \gg 1$. In this case, the expected uncertainty range is class 1 and is *much* smaller in size than the target uncertainty range. Since the uncertainties in the expected uncertainty range are relatively small (compared to the largest uncertainties in the target uncertainty range), traditional synthesis methods for fixed (nominal) stream conditions should be sufficient. Of course after designing the HEN, the designer should verify whether or not it is resilient in the desired expected uncertainty range.

(2) $F^* \gtrsim 1$. Now the expected uncertainty range is class 1 but is close in size to the target uncertainty range. Since the expected uncertainty range is class 1, one can still "have it all;" that is, one can still synthesize a HEN structure with a "practical" number of units (qualitatively, few more units than the number required for nominal conditions) which is resilient—while using minimum utilities—throughout the expected uncertainty range. However, since the expected uncertainty range is close in size to the target uncertainty range, synthesis may be more difficult (Colberg *et al.*, 1988). Example 14 below illustrates one crude procedure for synthesizing a resilient HEN in this case. This procedure uses the critical uncertainty point as well as the nominal stream data to synthesize the HEN structure.

(3) $F^* < 1$. Now the expected uncertainty range is class 2 and one can no longer "have it all"—some trade-off must be made (Colberg *et al.*, 1988). The most common trade-off is to require minimum utility consumption only at the nominal operating point and at the corner points of the uncertainty range, and to allow extra utility consumption for other points in the uncertainty range. Alternatively, the designer could require minimum utility consumption throughout the uncertainty range, with a consequent increase in the number of units. Or the designer could decrease the size of the expected uncertainty range (e.g., by imposing tighter control on the surrounding process).

Unlike the economic HEN synthesis targets (for nominal stream conditions), the class 1 FI target is a "soft" target—the process engineer can actually exceed the target (i.e., design for class 2 uncertainty ranges by making one of the trade-offs discussed above). Whether the process engineer chooses to meet, not meet, or even exceed the resilience target

depends upon economic factors, including the cost of *not* being resilient (e.g., lost production). Likewise, whether or not the engineer chooses to meet the (nominal) economic targets depends upon resilience (as well as safety, controllability, and so on).

By calculating the class 1 FI target, the process engineer can identify the critical uncertainty point and critical constraint (appearance of new pinches, nonnegative heating or cooling, and so on). This uncertainty point and constraint limit the resilience of a completely countercurrent (e.g., infinitely cyclic) HEN structure able to mimic the composite curves; thus they seem the *most likely* uncertainty point and constraint to limit the resilience of a practical but well-designed (almost completely countercurrent) HEN structure.

The following example demonstrates, by means of a crude synthesis procedure, how the class 1 FI target can be used as a synthesis tool. By using the target to identify the critical uncertainty point and constraint, the process engineer can consider resilience *during* the early stages of synthesizing a resilient, economic HEN, rather than adding resilience *after* synthesis of an economic (for nominal conditions) HEN. Knowledge of the critical constraint (e.g., appearance of a second pinch) tells the process engineer exactly where to place exchangers and stream splits in order to best achieve resilience.

Example 14 (from Colberg et al., 1988). For the nominal stream data of Example 13 (Table IX), synthesize a "practical" HEN structure which is as resilient as possible for uncertainties in the supply temperature and heat capacity flow rate of stream S_{h2}, based on "expected" uncertainties of $\Delta T_{h2}^{S} = \pm 10$ K and $\Delta w_{h2} = \pm 0.5$ kW/K. In other words, synthesize a HEN structure to achieve the class 1 FI target based on this expected uncertainty range. [Note that here we have specified the "expected" uncertainties to establish the relative sizes of the two uncertainties (i.e., to establish the aspect ratio of the rectangular expected uncertainty range), rather than to specify absolute sizes of the uncertainties for which to design].

Step 1. Calculate the class 1 FI target. The target was determined graphically in Example 13. The target, $F^* = 2.87$, is limited by a critical uncertainty point of $F^* \Delta T_{h2}^{S} = +28.7$ K, $F^* \Delta w_{h2} = +1.43$ kW/K (i.e., $T_{h2}^{S} = 428.7$ K after shifting to account for ΔT_m, and $w_{h2} = 7.43$ kW/K), and a critical constraint involving the appearance of a second pinch at the supply of stream S_{h2} (Fig. 17).

Step 2. Synthesize a HEN structure for the critical uncertainty point. Since the critical uncertainty point limits resilience, it is the uncertainty

point with the tightest design constraints (in this case due to the appearance of simultaneous pinches at S_{c2} and S_{h2}). Thus we synthesize for this point before considering the nominal stream data. A structure [obtained by the pinch design method (Linnhoff and Hindmarsh, 1983)] is shown in Fig. 19a. The four shaded exchangers are required to satisfy ΔT_m at the pinch caused by S_{c2}; the blackened exchanger and heater are required to satisfy ΔT_m at the pinch caused by S_{h2}.

Step 3. Synthesize a HEN structure for the nominal stream data as similar as possible to the structure synthesized for the critical uncertainty point. Such a structure is shown in Fig. 19b. The shaded exchangers are required to satisfy ΔT_m at the pinch.

Step 4. Merge the two separate structures into a single structure. In this case, merging is trivial because of the strong similarity between the two designs; we merely add the heater on S_{c2} for the nominal structure to the structure synthesized for the critical uncertainty point. The resulting structure is shown in Fig. 19c.

Step 5. Test the resilience of the merged structure. (Before this test we only know that the merged structure is feasible for both the nominal stream data and the critical uncertainty point. We do not know yet if the structure is resilient throughout the desired uncertainty range.) The flexibility index of the merged HEN structure is 2.87. Thus the structure achieves the class 1 FI target and is resilient throughout the target uncertainty range.

Step 6. Try to reduce the number of units in the merged HEN structure (e.g., by loop-breaking; Su and Motard, 1984). The only loop in this structure is shown by the dashed lines in Fig. 19c. (Since the pinch caused by stream S_{c2} occurs for every point in the uncertainty range, we are not considering loops which straddle this pinch so that we can maintain minimum utility consumption throughout the uncertainty range.) Eliminating any unit in this loop except the match between streams S_{h2} and S_{c1} reduces the flexibility index to zero (i.e., the structure becomes infeasible even for nominal conditions); eliminating the S_{h2}–S_{c1} match reduces the flexibility index to 0.57. Thus no unit can be deleted from the merged HEN structure without a loss of resilience.

B. Multiperiod HEN Synthesis Using Structural Optimization

To automatically synthesize HENs operable ("resilient" without any constraint on energy recovery; see Section III,D) in a specified range of uncertain temperatures and flow rates, Floudas and Grossmann (1987b) have developed computer algorithms which iteratively synthesize a HEN, analyze its operability, and resynthesize a more operable HEN if neces-

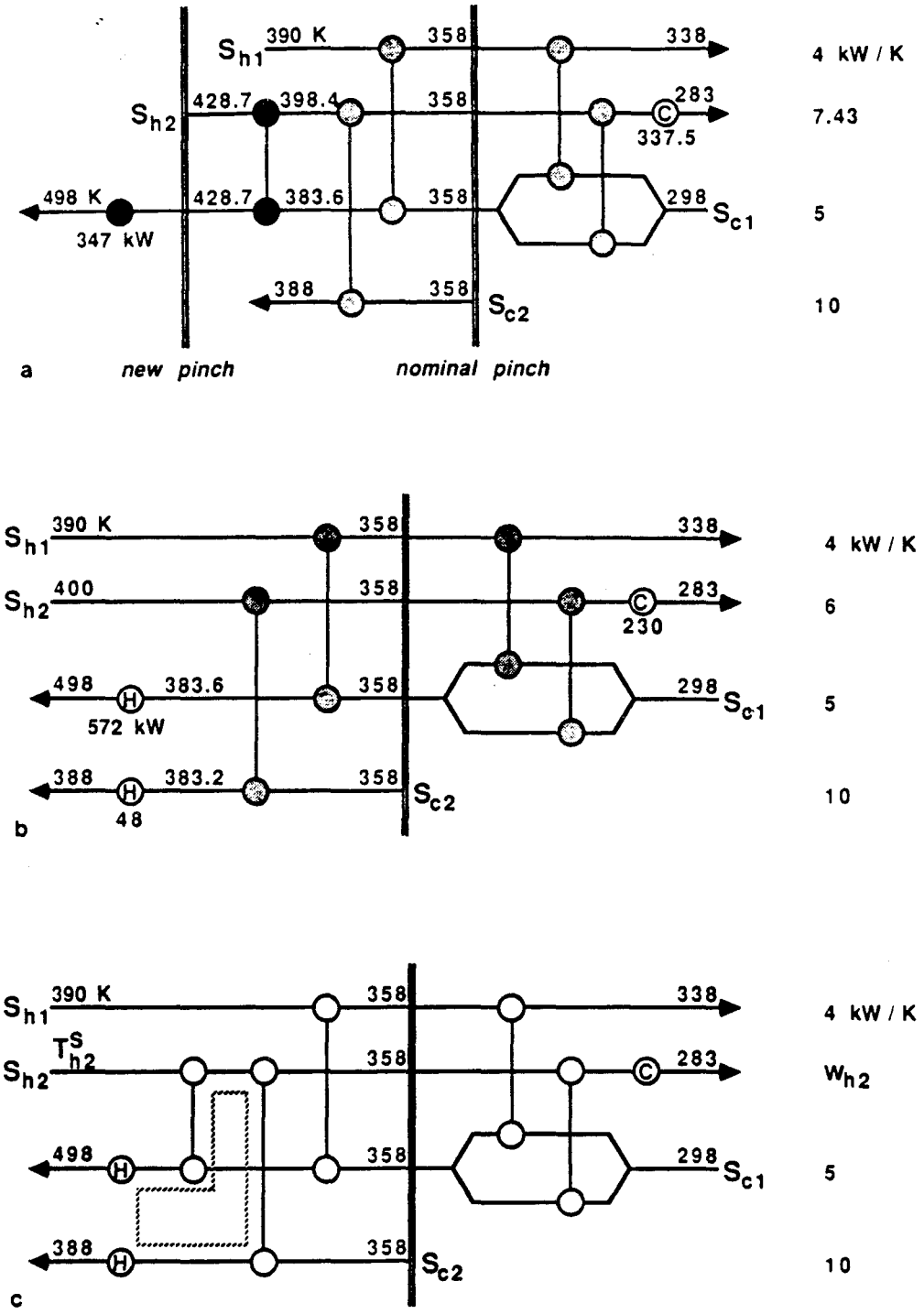

FIG. 19. HEN structures for Example 14: (a) Synthesized for critical uncertainty point, (b) synthesized for nominal stream data, and (c) merged structure which achieves the class 1 FI target.

sary. In particular, they have combined the multiperiod synthesis algorithm of Floudas and Grossmann (1986, 1987a) with special forms of the operability test and flexibility index (without the energy recovery constraint) reviewed earlier in this chapter. By requiring operability in the specified uncertainty range rather than strict resilience, Floudas and Grossmann (1987b) avoid the issue of class 1–class 2 problems. They also restrict their synthesis procedure to constant heat capacities.

The multiperiod synthesis algorithm of Floudas and Grossmann (1986, 1987a) generates HENs which are feasible for each of several periods of operation (i.e., for each of several critical points which may limit operability) and which have a minimum number of units, a minimum investment cost (given the predicted minimum number of units), and a minimum utility cost for each period. The multiperiod synthesis algorithm guarantees HEN feasibility (operability) only at the discrete periods of operation. The operability test (or the flexibility index without the energy recovery constraint) ensures that the HEN is operable throughout the entire uncertainty range. (Note that maximum energy recovery—minimum utility consumption—is also guaranteed only for the discrete periods of operation, and not for the entire uncertainty range.) If the HEN is not operable throughout the uncertainty range, then the critical point for operability (i.e., the combination of uncertain supply temperatures and flow rates where the HEN feasibility constraints are most violated) is added as a new period of operation, and the multiperiod synthesis algorithm is applied again to generate a more operable HEN.

The multiperiod synthesis–analysis–resynthesis algorithm is actually decomposed into two stages (Floudas and Grossmann, 1987b):

1. The stage of matches includes the following.
   a. Synthesis: Predict a minimum set of stream matches, and the heat transferred in each match, which will lead to a minimum unit HEN feasible for each period of operation and which has minimum utility cost during each period (Floudas and Grossmann, 1986).
   b. Analysis: Apply the active constraint strategy to the "operability[3] test at the stage of matches" to determine whether the predicted set of matches can lead to an operable HEN.
   c. Iteration: If the predicted set of matches can lead to an operable HEN, then proceed to stage 2. Otherwise, add the critical point for operability as a new period of operation and repeat stage 1.

[3] Floudas and Grossmann (1987b) actually call this the *feasibility test at the stage of matches*. However, since Floudas and Grossmann do not include an energy recovery constraint, we are calling this the *operability test at the stage of matches* in order to remain consistent with the terminology of Saboo *et al.* (1987b).

2. The stage of structure includes the following.
   a. Synthesis: Derive the HEN superstructure from the predicted set of stream matches. (The HEN superstructure consists of the predicted stream matches and mathematical "piping" connecting the matches in all possible series, parallel, and bypass combinations.) Optimize the superstructure to determine the actual structure and exchanger areas which minimize total investment cost[4] (Floudas and Grossmann, 1987a).
   b. Analysis: Apply the active constraint strategy to the "flexibility index at the stage of structure" to determine whether the actual HEN is operable.
   c. Iteration: If the HEN is operable in the specified uncertainty range, then stop. Otherwise, add the critical point for operability as a new period of operation and repeat stage 2.

Decomposition of the multiperiod synthesis–analysis–resynthesis algorithm into these two stages is possible because any feasible (operable) set of matches predicted by the first stage can always be translated into a feasible (operable) HEN in the second stage (Floudas and Grossmann, 1987b). The operability test in stage 1 ensures that the set of matches can lead to an operable HEN. However, even if a set of matches does pass the operability test in stage 1, an operability test (or corresponding flexibility index) is still necessary in stage 2. This is because even though the operable set of matches can always be translated into an operable HEN, not all HENs translated from the set of matches will necessarily be operable; that is, operability of a HEN depends upon the details of its structure (the order in which the matches are connected) as well as upon the set of matches themselves.

The steps of the multiperiod synthesis–analysis–resynthesis algorithm can now be summarized as follows (Floudas and Grossmann, 1987b).

Step 1. Select a finite number of periods of operation (i.e., sets of values of the uncertain supply temperatures and flow rates). Typically, the nominal operating point is selected, as well as some combinations of upper and lower bounds on the uncertain variables [e.g., bounds corresponding to maximum heating, maximum cooling, maximum heat exchange, and maximum required heat transfer area, as suggested by Marselle *et al.* (1982)].

[4] Note that the investment cost is minimized for a HEN superstructure with a fixed number of units (matches). If the number of units could vary, then the investment cost might be minimized even further.

Step 2. Formulate and solve the LP transshipment model of Papoulias and Grossmann (1983) for each period of operation to determine the minimum utility cost and pinch location for each period.

Step 3. Formulate and solve the multiperiod MILP transshipment model of Floudas and Grossmann (1986) to determine a minimum set of stream matches for feasible operation in all the periods and the heat transferred in each match in each period.

Step 4. Apply the operability test at the stage of matches (with the active constraint strategy). The form of this operability test is described in the next section. (a) If the set of matches cannot lead to an operable HEN, then add the critical point for operability as another period of operation and return to step 2. (b) If the set of matches can lead to a HEN operable in the specified uncertainty range, then go to step 5.

Step 5. Derive the multiperiod superstructure based upon the matches and heat transferred in each match predicted by the multiperiod MILP transshipment model. Formulate an NLP to optimize the superstructure (Floudas and Grossmann, 1987a) to give the HEN structure and exchanger sizes which minimize investment cost.

Step 6. Apply the active constraint strategy to the flexibility index (F) at the stage of structure (without the energy recovery constraint). The form of this flexibility index problem is described in a later section. (a) If $F \geq 1$, then the HEN is operable in the specified uncertainty range. Stop. (b) If $F < 1$, then add the critical point for operability as another period of operation and return to step 5.

1. *Operability Test at the Stage of Matches*

The operability test (resilience test in Section III,A,2, but without the energy recovery constraint) is applied at the stage of matches to determine whether the predicted stream matches can lead to an operable HEN. The general form of this operability test is

$$\chi(d) = \max_{\theta \in \Theta} \psi(d, \theta) \tag{39}$$

where $\psi(d, \theta)$ is determined by the LP

$$\psi(d, \theta) = \min_{z, \beta} \beta \tag{40}$$

subject to:

Equality constraints

(A1) Energy balances on each hot process and utility stream in each "temperature interval" (TI) of the multiperiod MILP transshipment model. Each energy balance involves the "residuals" (heat cascaded) to and from the TI and the heat transferred in each stream match in the TI.

(A2) Energy balances on each cold process and utility stream in each TI.
(A3) Zero residual to the hottest TI and from the coldest TI.

Inequality constraints

(B1) Residuals of $-\beta$ or more
(B2) Heat loads in each stream match of $-\beta$ or more

where θ contains the uncertain supply temperatures and flow rates and z the control variables. Note that ΔT_m will automatically be satisfied if all the residuals are nonnegative (because of the way the TIs are defined). The matches lead to an operable HEN if and only if $\chi \leq 0$. Floudas and Grossmann (1987b) give the specific form of the constraints in this operability test. The constraints are nonlinear in general; however, they are linear for fixed values of the uncertain supply temperatures and flow rates.

Floudas and Grossmann (1987b) show that the solution (critical point) of problem (39) must be a corner point of the uncertainty range. Thus operability test (39) can be simplified to

$$\chi(d) = \max_{l \in L_v} \psi(d, \theta^l) \tag{41}$$

where $\psi(d, \theta^l)$ is calculated at corner point θ^l of the uncertainty range and L_v is the index set of all the corner points. Problem (41) can be solved by a series of LPs (40) for $\psi(d, \theta^l)$, one at each corner point of the uncertainty range. Alternatively, to avoid exhaustive evaluation of all the corner points, the active constraint strategy can be applied directly to operability test (39).

2. *Flexibility Index at the Stage of Structure*

The flexibility index at the stage of structure ensures that the HEN translated from the operable matches is itself operable in the specified uncertainty range. A yes–no operability test at the stage of structure could be used to ensure operability of the HEN. Instead, Floudas and Grossmann (1987b) choose to use the more general flexibility index (as reviewed in Section III,A,3, but without the energy recovery constraint) since it also provides information on the largest scaled uncertainty range in which the HEN remains operable.

The general form of the flexibility index at the stage of structure (without the energy recovery constraint) is

$$F(d) = \max_{s} s \tag{42}$$

subject to

$$h(d, z, \theta) = 0$$

$$\max_{\theta \in \Theta(s)} \min_{z} \max_{m \in M} g_m(d, z, \theta) \leq 0$$

$$\Theta(s) = \{\theta \mid \theta^N - s\,\Delta\theta^- \leq \theta \leq \theta^N + s\,\Delta\theta^+\}, \qquad s \geq 0$$

where equality constraints $h(d, z, \theta)$ consist of

(A1) Mass balances for each splitter
(A2) Mass balances for each mixer
(A3) Energy balances for each mixer
(A4) Energy balances for each exchanger
(A5) Area constraints for each exchanger without bypass

and inequality constraints $g(d, z, \theta)$ consist of

(B1) Area constraints for each exchanger with bypass
(B2) ΔT_m constraints for each exchanger
(B3) Nonnegative loads for each exchanger, heater, and cooler
(B4) Nonnegative flow rates

Floudas and Grossmann (1987b) give the specific form of these constraints. The energy balance and area constraints are, in general, nonlinear.

The critical point for the flexibility index is, in general, not a corner point of the uncertainty range (e.g., see Section III,C,2 on stream splits or Section III,C,3 on flow rate uncertainties). Thus, Floudas and Grossmann (1987b) use the active constraint strategy to solve problem (42). Floudas and Grossmann (1987b) show that the active constraint strategy applied to the flexibility index at the stage of structure has a single local optimum if area constraints (A5) and (B1) are excluded. When the area constraints are included, the active constraint strategy may have multiple local optima.

Example 15 (*from Floudas and Grossmann, 1987b*). A HEN is to be designed for the nominal stream data shown in Table X. Due to changes in the process feedstocks, an uncertainty range is defined for the flow rates (i.e., ±0.4 kW/K of the nominal point) and supply temperatures of hot

TABLE X

NOMINAL STREAM CONDITIONS FOR EXAMPLE 15

Stream	w (kW/K)	T^S (K)	T^T (K)
S_{h1}	1.4	583	323
S_{h2}	2	723	553
S_{c1}	3	313	393
S_{c2}	2	388	553

stream S_{h1} (± 10 K) and cold stream S_{c2} (± 5 K). The objective is to design a HEN which is operable for the specified uncertainty range and which features the minimum investment cost, fewest number of units, and minimum utility cost.

Suppose that only two periods of operation are considered in the first iteration of the synthesis procedure. The selected periods correspond to (1) maximum total heat exchange (i.e., w_{h1}^{U}, w_{c2}^{U}, T_{h1}^{U}, T_{c2}^{L}, and (2) maximum cooling (i.e., w_{h1}^{U}, w_{c2}^{L}, T_{h1}^{U}, T_{c2}^{U}). Solving the LP transshipment model for each period with a specified ΔT_m of 10 K yields

Period 1	Period 2
$H_{min} = 0$	$H_{min} = 0$
$C_{min} = 178$ kW	$C_{min} = 330$ kW
No pinch	No pinch

By formulating and solving the multiperiod MILP transshipment model for these two periods of operation, the following set of matches is identified:

$$S_{h1}\text{–}S_{c2},\quad S_{h2}\text{–}S_{c1},\quad S_{h2}\text{–}S_{c2},\quad S_{h1}\text{–CW}$$

where CW denotes cooling water. The solution of this model was obtained by using the computer code LINDO (Schrage, 1981) and required 2.4 sec (DEC-20). By applying the operability test at the stage of matches and solving LP (40) at each of the 16 corner points, the operability measure was found to be $\chi(d) = 128$. This solution was obtained by using the computer code LINDO in 20.5 sec. Positive $\chi(d)$ implies that the preceding selection of matches cannot result in an actual operable network.

The critical uncertainty point for $\chi(d) = 128$ is introduced (i.e., w_{h1}^{L}, w_{c2}^{L}, T_{h1}^{L}, T_{c2}^{U}) as a third period of operation, which in fact corresponds to the condition of maximum heating. This third period features utility loads of $H_{min} = 58$ kW and $C_{min} = 0$, with no pinch point. Then by formulating and solving the multiperiod MILP transshipment model for the three periods of operation, the following set of matches is predicted:

$$H\text{–}S_{c2},\quad S_{h1}\text{–}S_{c1},\quad S_{h1}\text{–}S_{c2},\quad S_{h2}\text{–}S_{c2},\quad S_{h2}\text{–CW}$$

where H denotes steam. This solution was obtained by using the computer code LINDO in 2.76 sec. The corresponding heat exchanged at each match is shown in Table XI. By applying the operability test in the stage of matches, it was found that $\chi(d) = 0$. This required the solution of LP (40) at each of 16 corner points (21 sec). Since the operability measure $\chi(d)$ is zero, this implies that the preceding selection of matches predicted by the multiperiod MILP transshipment model can result in an operable HEN.

TABLE XI

MATCHES AND HEAT EXCHANGED IN EACH OPERATING PERIOD IN EXAMPLE 15

		Heat exchanged (kW)		
Unit	Match	Period 1	Period 2	Period 3
1	$H-S_{c2}$	0	0	58
2	$S_{h1}-S_{c1}$	240	240	240
3	$S_{h1}-S_{c2}$	246	246	10
4	$S_{h2}-S_{c2}$	162	10	340
5	$S_{h2}-CW$	178	330	0

To automatically determine the network structure that is feasible for these three periods of operation and that features minimum investment cost, as well as minimum utility cost for each period, the automatic synthesis approach for multiperiod networks by Floudas and Grossmann (1987a) is utilized. The value of ΔT_m was relaxed to 1 K for this design stage. In the first step of this approach, the multiperiod superstructure is derived by using the five predicted matches. Then by formulating the superstructure as an NLP and using the values of the overall heat transfer coefficients and cost data shown in Table XII, the resulting NLP is solved by using the computer code MINOS/AUGMENTED (Murtagh and Saunders, 1981). This NLP features 108 variables, 57 nonlinear constraints, and 60 linear constraints. The CPU time for solving this NLP was 24.8 sec.

TABLE XII

OVERALL HEAT TRANSFER COEFFICIENTS AND COST DATA FOR EXAMPLE 15[a]

Match	U_{ij} (kW/m^2 K)	A_{ij} (m^2)
$H-S_{c2}$	0.08	23.77
$S_{h1}-S_{c1}$	0.08	103.83
$S_{h1}-S_{c2}$	0.08	56.583
$S_{h2}-S_{c2}$	0.08	23.315
$S_{h2}-CW$	0.08	13.013

[a] $C_{ij} = 4333A_{ij}^{0.6}$ (\$), A in m^2. Steam cost (573 K): 171.428×10^{-4} (\$/kW hour). Cooling water cost (303–323 K): 60.576×10^{-4} (\$/kW hour)

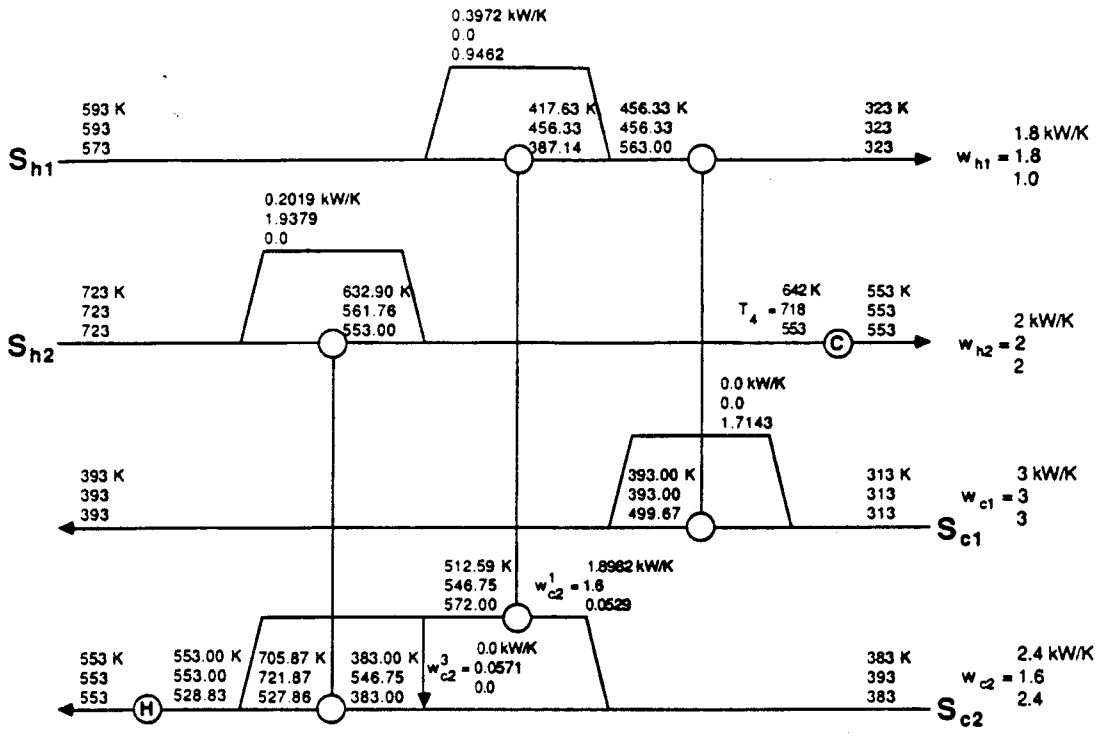

FIG. 20. Operable HEN synthesized for Example 15.

The solution of this optimization problem provides the HEN shown in Fig. 20, where flow rates and temperatures are listed for the three operating periods. The areas of the heat exchangers are given in Table XII. Notice that there is splitting of cold stream S_{c2} into two branches. Bypasses are also involved in stream S_{c1} (match S_{h1}–S_{c1}), stream S_{h1} (match S_{h1}–S_{c2}), and stream S_{h2} (match S_{h2}–S_{c2}). This network, which is feasible for the three operating periods that are considered, features a minimum investment cost of \$196,900 and a minimum utility cost of \$1.078/hour for operating period 1, \$1.999/hour for period 2, and \$0.9943/hour for period 3.

To test for operability of the HEN in the specified uncertainty range, the active constraint strategy is applied to the flexibility index at the stage of structure (without the energy recovery constraint). First, constraints (A1)–(A5) and (B1)–(B4) are developed for this network. Since there are nine equations and 12 unknowns, there exist three control variables which have been selected to be $z_1 = w^1_{c2}$, $z_2 = w^3_{c2}$, $z_3 = T_4$ (see Fig. 20). Using the information from the gradients of the feasibility constraints with respect to the control variables, four active sets of constraints are identified. Then, solving an NLP for each active set of constraints, it was found

that the flexibility index is $F = 1$, which implies that the network configuration derived in the preceding step is not only economical and energy efficient, but also operable for the full uncertainty range. The solution of the four NLPs required 22.4 sec. Hence, the total computer time that was required to solve this problem was 94 sec.

C. HEN Synthesis Using "Downstream (Disturbance) Paths"

Kotjabasakis and Linnhoff (1986) introduced the concept of "downstream (disturbance) paths" for synthesis of resilient HENs (or more general processes). This simple concept provides an excellent physical understanding of structural HEN resilience. It also can be used to study the qualitative effects of varying an uncertain parameter (e.g., a supply temperature and/or flow rate) upon specified fixed parameters (e.g., target temperatures) and to suggest design changes to eliminate or counteract these effects early in the structural design stage. The concept of downstream paths is best illustrated by example.

Example 16 (from Linnhoff and Kotjabasakis, 1986). Consider the HEN structure in Fig. 21. Based on a physical understanding of the HEN structure and without the need to solve any linear programs, we wish to investigate two questions. (1) Will varying a specified uncertain supply temperature and/or flow rate affect a given fixed target temperature? (2) What design changes might be used to eliminate these effects?

In the HEN structure in Fig. 21, all the streams except S_{c1} have heaters or coolers which can be used to control their target temperatures (though extra utility may be required to do so). Thus in this example we will concentrate on maintaining the target temperature of stream S_{c1}.

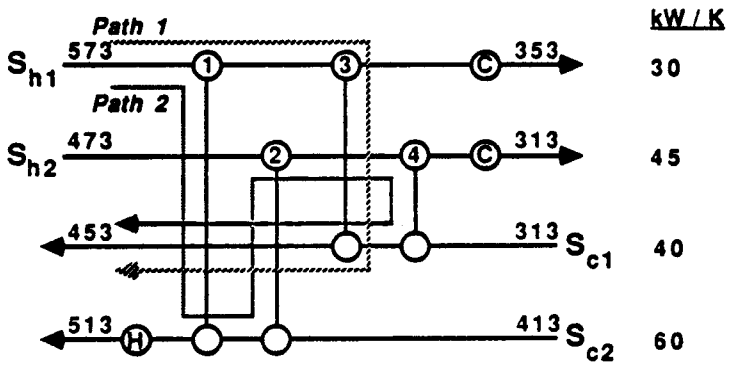

FIG. 21. Two paths from T^S_{h1} to T^T_{c1}, (1) Completely downstream and (2) partially upstream.

Consider the effect of varying T^S_{h1} upon T^T_{c1}. Figure 21 shows two "paths" from the supply of S_{h1} to the target of S_{c1}. A "path" is an unbroken connection between any two points in the HEN grid diagram. It seems obvious that a varying supply temperature or flow rate can affect a (fixed) target temperature only if they are physically connected by a "path" through streams and heat exchangers. Path 1 in Fig. 21 carries a change in T^S_{h1} downstream along S_{h1}, through exchanger 3, and downstream along S_{c1}. Path 2 carries the change downstream along S_{h1}, through exchanger 1, and *upstream* S_{c2}. However, the effect of a changing supply temperature or flow rate *cannot* travel upstream. Thus a changing supply temperature or flow rate can affect a (fixed) target temperture only if there is a path connecting the two which is completely downstream.

Now consider the effect of varying T^S_{c2} upon (fixed) T^T_{c1}. Figure 22a shows two completely downstream paths between T^S_{c2} and T^T_{c1}. We wish to consider possible design changes which can eliminate the effect of varying T^S_{c2} upon T^T_{c1}.

(1) *Break downstream path.* If the ΔT_m (or area) and load constraints of the remaining exchangers allow it, removing exchanger 3 will break path 1 between T^S_{c2} and T^T_{c1}, as shown in Fig. 22b.

(2) *Insert upstream element.* If the ΔT_m (or area) and load constraints allow it, exchangers 2 and 4 can be interchanged to block path 2, as shown in Fig. 22c. Here we have inserted exchanger 4 *upstream* of exchanger 2. If the changes in Figs. 22b and 22c are possible, then we can eliminate the effect of varying T^S_{c2} upon (fixed) T^T_{c1} *without* the need for any overdesign.

(3) *Apply manipulation.* If ΔT_m (or area) and load constraints do not allow the changes in Figs. 22b and 22c, then manipulation (of an exchanger bypass) might be used to counteract the effect of changing T^S_{c2} upon (fixed) T^T_{c1}. Figure 23 shows that there are downstream paths from all four exchangers to the target of stream S_{c1}. Thus a bypass around any one of the four exchangers can be used to counteract the effect of changing T^S_{c2} upon T^T_{c1}. Of course the effect of manipulating the chosen bypass upon the other target temperatures must also be considered.

In the previous example, several design changes were considered in order to eliminate or counteract the effect of a changing supply temperature upon a fixed target temperature. The best choice of design change depends on trade-offs between capital and energy costs; that is, removing exchanger 3 to give Fig. 22b might require adding area to the other exchangers and/or increasing heating and cooling, while the changes in Fig. 23 (adding an exchanger bypass) require adding area.

Kotjabasakis and Linnhoff (1986) demonstrate the use of sensitivity tables for a quick (but qualitative) means of evaluating these trade-offs and

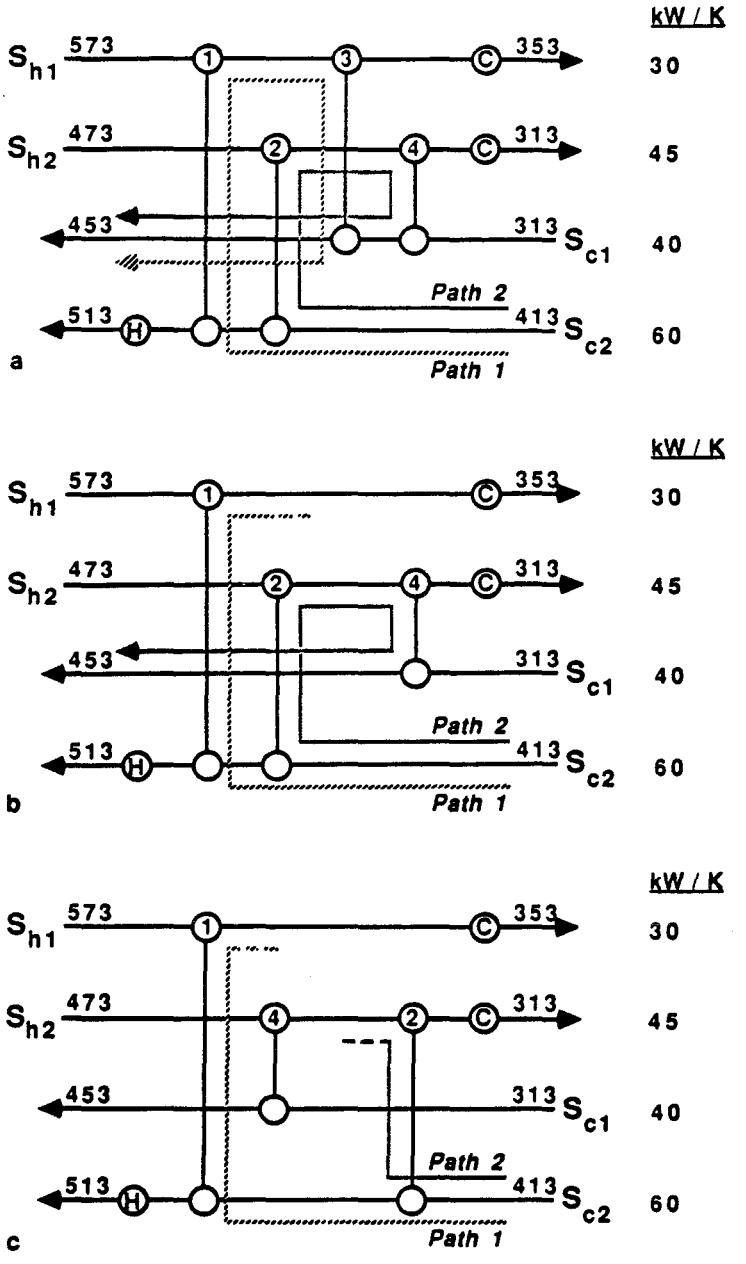

FIG. 22. Two design changes to block downstream paths. (a) Original design, (b) remove exchanger 3 to break path 1, and (c) insert exchanger 4 upstream of exchanger 2 to block path 2.

eliminating obviously expensive design choices. However, these sensitivity tables do not consider the nonlinearity of area (capital cost) as a function of the uncertain supply temperatures and flow rates, and they do not consider interactions between two simultaneously varying supply temperatures or between two paths connecting the same supply and target temperatures.

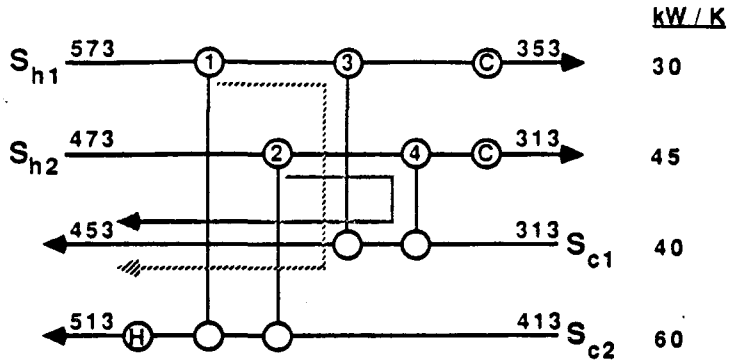

FIG. 23. Downstream paths from all four exchangers allow manipulation of T_{c1}^{T}.

Thus simulation (e.g., the feasibility test in Section III,A,1 with area constraints replacing the ΔT_m constraints) and costing should be used to evaluate the final design choices.

In addition, the sensitivity tables do not consider the inherent nonlinearity of the HEN resilience problem. Thus while the use of downstream paths and sensitivity tables may guarantee feasible HEN operation for specified discrete values of supply temperatures and flow rates, they do not guarantee feasible HEN operation for intermediate supply temperatures and flow rates [unless *all* paths between varying and fixed parameters have been blocked, as in Fig. 22b, or unless the assumptions of the corner point theorem (Section III,B,1) are satisfied]. More rigorous testing (e.g., using one of the techniques discussed in Section III) may be necessary to guarantee resilience for intermediate supply temperatures and flow rates.

D. Summary of Resilient HEN Synthesis Procedures; Areas for Future Research

Three methods for synthesis of HENs which are economically optimal and resilient have been reviewed in this chapter: (1) synthesis of HEN structure based on a class 1 flexibility index (FI) target (Colberg *et al.*, 1988); (2) synthesis of HEN structure and design (sizing) of individual exchangers using mixed-integer optimization algorithms for multiperiod operation (Floudas and Grossmann, 1987b); and (3) synthesis of HEN structure based on "downstream (disturbance) paths" (Linnhoff and Kotjabasakis, 1986).

The class 1 FI target is the flexibility index of the largest possible class 1 uncertainty range for given nominal stream data. For simple problems it can be calculated by trial-and-error plotting of the composite curves. For larger problems, or problems with correlated uncertainties, the target can be calculated with a NLP (Colberg *et al.*, 1988).

The class 1 FI target serves two important uses during synthesis of resilient HENs.

1. The size of the target (relative to 1) tells the designer if the expected uncertainty range is class 1 or class 2, and thus whether trade-offs must be made to achieve resilience in the expected uncertainty range.
2. Calculation of the target identifies the critical uncertainty point and constraint most likely to limit resilience.

Use of the class 1 FI target as a HEN synthesis tool offers a number of attractive features.

1. Knowledge of the critical uncertainty point and constraint allows the designer to strategically place exchangers and stream splits where they will most improve resilience. This feature tends to minimize the number of synthesis–analysis iterations required to achieve a resilient HEN.
2. The class 1 FI target can be used to predict the trade-off between a *constant* value of ΔT_m and resilience, and energy and resilience (Colberg *et al.*, 1988).
3. The target attempts to consider economics, albeit indirectly (Colberg *et al.*, 1988). It indirectly limits the number of exchangers (by limiting the target to class 1 uncertainty ranges), and places bounds on utility consumption and network area (implicitly through use of the composite curves, or by constraints in the NLP).

The class 1 FI target also suffers a few disadvantages.

1. It is limited to class 1 problems.
2. It cannot handle uncertain heat transfer coefficients.
3. Although the FI target can consider ΔT_m varying as a function of uncertain supply temperatures and flow rates (e.g., by using the *nominal* energy, area, and units targets to predict an economic optimum ΔT_m), this dependence must be specified *before* plotting any composite curves or solving the NLP. Thus the trade-off between cost and resilience is not accurately considered (i.e., ΔT_m should reflect the cost of overdesign to achieve resilience as well as the cost of energy, units, and area for nominal operating conditions).

The second synthesis procedure reviewed in this chapter, based on mixed-integer optimization, iteratively synthesizes a HEN, analyzes its operability, and resynthesizes a more operable HEN if necessary (Floudas and Grossmann, 1987b). In particular, this procedure combines the multiperiod, mixed-integer synthesis algorithm of Floudas and Grossmann (1986, 1987a) with specific forms of the operability test at the stage of matches

and flexibility index at the stage of structure (with active constraint strategy) developed by Floudas and Grossmann (1987b).

The synthesis procedure of Floudas and Grossmann (1987b) is one of the most powerful in the open literature for solving practical HEN synthesis problems and has a number of attractive features.

1. It synthesizes a HEN which is resilient *and* which has the minimum number of units required for resilience, minimum investment cost, and minimum utility cost for each period of operation.
2. It not only synthesizes the HEN structure, but also designs (sizes) the individual exchangers.
3. It synthesizes and designs the HEN automatically from given stream and cost data.
4. By decomposing the synthesis problem into the "stage of matches" and the "stage of structure," the synthesis procedure can handle large problems with reasonable computational effort.

However, these same features also have the following drawbacks.

1. Although HENs with reasonable cost should be obtained by separately minimizing energy cost, number of units, and investment cost, this procedure does not necessarily minimize total cost. In particular, the choice of ΔT_m for energy targeting and for predicting the stream matches is not optimized to consider the trade-off between energy and capital costs (as in Ahmad and Linnhoff, 1984). Even more important, different values of ΔT_m will generally be optimal for different periods of operation in the synthesis procedure. Also, investment cost is minimized only for a fixed set of matches.
2. By decomposing the HEN synthesis problem into the stages of matches and structure, this procedure might make it difficult for the designer to directly influence the shape of the synthesized network (i.e., how should the stage of matches be influenced in order to achieve a desired change at the stage of structure?). For example, this procedure does not seem to allow the designer to easily constrain stream splitting (like Saboo *et al.*, 1986) and might be difficult to apply in revamp synthesis.
3. The synthesis procedure guarantees minimum energy cost only for the discrete periods of operation considered, and not for the whole uncertainty range (especially for class 2 problems).
4. The analysis portion fo the procedure is limited to constant heat capacities.

The concept of "downstream (disturbance) paths" (Linnhoff and Kotjabasakis, 1986) is a simple and intuitively appealing tool for evolutionary synthesis of resilient HENs. It can be used to identify the qualitative effects of varying uncertain supply temperatures and flow rates upon (fixed) target

temperatures, and to identify potential design changes to eliminate or counteract these effects. The qualitative use of downstream paths has several attractive features.

1. It is simple (no calculations required).
2. It provides great physical insight into the structural resilience of a HEN.

However, the quantitative use of downstream paths suffers several disadvantages.

1. It is difficult to consider interactions among two or more supply temperatures or flow rates changing simultaneously.
2. It is difficult to consider interactions among two or more paths between the same supply temperature (or flow rate) and target temperature.
3. It is difficult to consider nonlinear effects on HEN resilience.

These disadvantages are apparent in the use of sensitivity tables (Kotjabasakis and Linnhoff, 1986) combined with downstream paths.

In addition, both the FI target-based synthesis procedure and the multiperiod synthesis procedure suffer from the fact that they synthesize a HEN for a *specified* uncertainty range and cannot directly consider the trade-off between resilience and total HEN cost. At present, the best way of evaluating this trade-off with these methods is to synthesize HENs for several different sizes of the uncertainty range and then to compare the HENs. The downstream path method (combined with sensitivity tables) evaluates this trade-off much more easily and directly (subject to the quantitative limitations discussed above).

The class 1 FI target (Colberg *et al.*, 1988) combined with the pinch design method (Linnhoff *et al.*, 1982; Linnhoff and Hindmarsh, 1983) for synthesis of an initial HEN, and the use of downstream paths (Linnhoff and Kotjabasakis, 1986) to improve resilience (or reduce cost), yields a very flexible synthesis method with great physical insight into structural HEN resilience (both through the use of downstream paths and knowledge of the critical uncertainty point and constraint). This combined method allows the designer to evaluate trade-offs between capital and energy, but can be difficult to apply to problems with many streams or where several or dissimilar designs must be merged (Example 14). The multiperiod synthesis–analysis–resynthesis algorithm of Floudas and Grossmann (1987b) is easy to apply even to large problems with many critical uncertainty points (periods of operation), but cannot directly evaluate trade-offs between capital and energy (unless one iterates ΔT_m), and is not flexible enough to allow the designer to influence the synthesized HEN (e.g., to constrain

stream splitting or to perform revamp synthesis). The "ideal" algorithm for resilient HEN synthesis should combine the desirable features of both of these algorithms. Possible areas of research to develop a more ideal synthesis algorithm include the following.

1. Develop methods for predicting energy–capital–resilience trade-offs by use of the energy, units, area, and FI targets. In particular, develop an area target which considers the total *installed* HEN area required for resilience, including the area which might be bypassed for nominal stream conditions.
2. In the multiperiod synthesis–analysis–resynthesis algorithm of Floudas and Grossmann (1987b), minimize the total HEN cost rather than separately minimizing energy and capital costs. This can be accomplished at least at the stage of structure by treating utility loads and loads of the stream matches as variables in the superstructure, rather than as constants predicted by the LP transshipment model (Papoulias and Grossmann, 1983) and the multiperiod MILP transshipment model (Floudas and Grossmann, 1986).
3. In order to properly consider the trade-offs between capital, energy, and resilience at the stage of matches, investigate the "optimum" choice of ΔT_m. Actually, in an ideal synthesis algorithm, these trade-offs should be evaluated directly and not by means of a possibly artificially chosen value of ΔT_m.
4. In order to make the multiperiod synthesis–analysis–resynthesis algorithm more flexible (and to extend it later to revamp synthesis), investigate how to constrain stream splitting.
5. Extend the multiperiod synthesis–analysis–resynthesis algorithm to handle temperature-dependent heat capacities and phase change and uncertain heat transfer coefficients.

Nomenclature

a Constant used in stream split constraint (27)[5] or constant used in ΔT_m constraint with uncertain flow rates (30)
A Matrix used in general form of energy balance constraint (5)
b Vector used in general form of energy balance constraint (5)
B Matrix used in general form of energy balance constraint (5)
c Constant used in stream split constraint (27) or constant used in ΔT_m constraint with uncertain flow rates (30)
c_p Heat capacity, kJ/kg K

[5] Numbers in parentheses refer to the first equation in which a symbol is used.

C Matrix used in general form of ΔT_m constraint (5)

C_{min} Minimum cooling requirement, kW

d Vector of design variables (1)

D Matrix used in general form of ΔT_m constraint (5)

e Vector of ones, $[1\ 1 \cdots 1\ 1]^T$ (5)

E Matrix used in general form of load constraint (5)

f Vector of reduced inequality constraints (2)

F Flexibility index, dimensionless (10)

g_{ij} Constraint on split fraction of branch j on stream i (27) or ΔT_m constraint on exchanger connected to streams S_i and S_j with uncertain flow rates (30)

G Matrix used in general form of load constraint (5)

h Vector of equality constraints (1)

H Minimum heating requirement, kW (5)

I Identity matrix

k Upper bound on slack variables η (21)

k_L Upper bound on slack variables γ_L and σ_L (25)

k_T Upper bound on slack variables γ_T and σ_T (25)

l^H Vector of heater loads, kW (5)

L Matrix used to define integer variables m (24)

L_L Matrix used to define integer variables m_L (26)

L_T Matrix used to define integer variables m_T (26)

m Integer variables determining in which exchanger each temperature breakpoint occurs (21)

m_L Integer variables used in equality form of load constraint with temperature breakpoints (26)

m_T Integer variables used in equality form of ΔT_m constraint with temperature breakpoints (25)

M Index set for reduced inequality constraints (2)

M_A Index set for active reduced inequality constraints (34)

n_A Number of potential sets of active constraints M_A

n_f Number of reduced inequality constraints f

n_z Number of control variables (degrees of freedom) z

n_θ Number of uncertain variables θ

N Matrix used in general form of energy balance constraint with temperature breakpoints (24)

O Matrix used in general form of ΔT_m constraint with temperature breakpoints (24)

p Vector used in general form of ΔT_m constraint (5)

P Polytope region defined by resilience index

r Vector used in general form of load constraint (5)

R Region for feasible operation of a HEN

RI Resilience index, kW (16)

s Scale factor for family of hyperrectangles used to define the flexibility index, dimensionless (10)

t Vector of temperatures

T Temperature, K

u_{ij} Split fraction of branch j on stream i, dimensionless

U Heat transfer coefficient, kW/m^2 K

v Vector of state and control variables $[t^I, l^H]$ (5)

v_k Kth load or ΔT_m constraint function not depending on any stream split fractions (28) or load constraint function for exchanger k with uncertain flow rates (31)

w_i Heat capacity flow rate of stream S_i, kW/K

x Vector of state variables

z Vector of control variables (degrees of freedom) (1)

Greek Letters

α Factor by which to relax minimum heating target, dimensionless (5)

β Slack variable for measuring worst violation of feasibility constraints (4)

γ_L Load violation, kW (26)
γ_T ΔT_m violation, K (25)
δl Supply temperature uncertainty expressed in terms of load, kW (19)
δT Uncertainty in (supply) temperature, K (19)
$\delta\theta$ Uncertainty (in any uncertain variable) (17)
ΔT Approach temperature, K
ΔT_m Minimum approach temperature allowed in a HEN, K
ΔT_s Smallest approach temperature actually occurring in a HEN, K
$\Delta\theta$ Expected uncertainty (in any uncertain variable) (12)
η Slack variables for determining in which exchangers each temperature breakpoint occurs, K ((21)
θ Vector of uncertain variables (supply temperatures, flow rates, and/or heat transfer coefficients)
Θ Hyperrectangular uncertainty range
λ Kuhn–Tucker multiplier (35)
ξ Kuhn–Tucker slack variables (35)
σ_L Load surplus, kW (26)
σ_T ΔT_m surplus, K (25)
χ Resilience measure (6)
ψ Feasibility measure (3)

Subscripts

BR Breakpoint (discontinuity in piecewise constant heat capacity)
i Stream index
j Stream index
k Exchanger (or heater) index
l Uncertainty direction (along a single stream)
L Load constraint
m Index for reduced inequality constraints

Superscripts

C Critical (uncertainty point)
H Heater (load)
I Intermediate (stream temperature)
l Uncertainty direction (toward a vertex of the uncertainty range)
L Lower bound (on uncertain variable)
N Nominal (value of uncertain variable)
S Supply (temperature)
T Target (temperature)
U Upper bound (on uncertain variable)
+ Positive uncertainty direction
− Negative uncertainty direction

References

Ahmad, S., and Linnhoff, B., Overall cost targets for heat exchanger networks. *IChemE Annu. Rese. Meet.*, Bath, Apr. (1984).

Colberg, R. D., Morari, M., and Townsend, D. W., A resilience target for heat exchanger network synthesis. *Comp. Chem. Eng.*, in press (1988).

Duran, M. A., and Grossmann, I. E., A mixed-integer nonlinear programming algorithm for process systems synthesis. *AIChE J.* **32,** 592 (1986).

Floudas, C. A., and Grossmann, I. E., Automatic generation of multiperiod heat exchanger network configurations. *Comp. Chem. Eng.* **11,** 123 (1987a).

Floudas, C. A., and Grossmann, I. E., Synthesis of flexible heat exchanger networks for multiperiod operation. *Comp. Chem. Eng.* **10,** 153 (1986).

Floudas, C. A., and Grossmann, I. E., Synthesis of flexible heat exchanger networks with uncertain flowrates and temperatures. *Comp. Chem. Eng.* **11,** 319 (1987b).

Floudas, C. A., Ciric, A. R., and Grossmann, I. E., Automatic synthesis of optimum heat exchanger network configurations. *AIChE J.* **32,** 276 (1986).

Grossmann, I. E., and Floudas, C. A., Active constraint strategy for flexibility analysis in chemical processes. *Comp. Chem. Eng.* **11**, 675 (1987).

Grossmann, I. E., and Floudas, C. A., A new approach for evaluating flexibility in chemical process design. *Proc. Process Syst. Eng. PSE '85, Cambridge, IChemE Symp. Ser.* **92**, 619 (1985). *Process Syst. Eng.* (1985b).

Grossmann, I. E., and Morari, M., Operability, resiliency and flexibility—process design objectives for a changing world. *Int. Conf. Found. Computer-Aided Process Design, 2nd, Snowmass, CO* (1983).

Grossmann, I. E., Halemane, K. P., and Swaney, R. E., Optimization strategies for flexible chemical processes. *Comp. Chem. Eng.* **7**, 439 (1983).

Halemane, K. P., and Grossmann, I. E., Optimal process design under uncertainty. *AIChE J.* **29**, 425 (1983).

Hohmann, E. C., Optimum networks for heat exchange. Ph.D. thesis, Univ. of So. Calif. (1971).

Kotjabasakis, E., and Linnhoff, B., Sensitivity tables for the design of flexible processes (1)—How much contingency in heat exchanger networks is cost effective? *Chem. Eng. Res. Des.* **64** (1986).

Linnhoff, B., and Flower, J. R., Synthesis of heat exchanger networks: I. Systematic generation of energy optimal networks. *AIChE J.* **24**, 633 (1978).

Linnhoff, B., and Hindmarsh, E., The pinch design method for heat exchanger networks. *Chem. Eng. Sci.* **38**, 745 (1983).

Linnhoff, B., and Kotjabasakis, E., Downstream paths for operable process design. *Chem. Eng. Prog.* **82** (5), 23 (1986).

Linnhoff, B., Mason, D. R., and Wardle I., Understanding heat exchanger networks. *Comp. Chem. Eng.* **3**, 295 (1979).

Linnhoff, B., Townsend D. W., Boland, D., Hewitt, G. F., Thomas, B. E. A., Guy, A. R., and Marsland R. H., "A User Guide on Process Integration for the Efficient Use of Energy." IChemE, available from Pergamon, Oxford, 1982.

Marselle, D. F, Morari, M., and Rudd, D. F., Design of resilient processing plants—II. Design and control of energy management systems. *Chem. Eng. Sci.* **37**, 259 (1982).

Morari, M., Grimm, W., Oglesby, M. J., and Prosser, I. D., Prosser, Design of resilient processing plants—VII. Design of energy management system for unstable reactors—new insights. *Chem. Eng. Sci.* **40**, 187 (1985).

Murtagh, B. A., and Saunders, M. A., A projected Lagrangian algorithm and its implementation for sparse nonlinear constraints, and MINOS/AUGMENTED user's manual, Technical Reports SOL 80-1R and SOL 80-14, Systems Optimization Laboratory, Dept. of Operations Research, Stanford Univ., CA (1981).

Nishida, N., Stephanopoulos, G., and Westerberg, A. W., A review of process synthesis. *AIChE J.* **27**, 321 (1981).

Papoulias, S. A., and Grossmann, I. E., A structural optimization approach in process synthesis. II: Heat recovery networks. *Comp. Chem. Eng.* **7**, 707 (1983).

Raghavan, S., Heat exchanger network synthesis: a thermodynamic approach. Ph.D. thesis, Purdue Univ. (1977).

Saboo, A. K., Synthesis and analysis of resilient heat exchanger networks. Ph.D. thesis, Univ. of Wisc., Madison (1984).

Saboo, A. K., and Morari, M., Design of resilient processing plants—IV. Some new results on heat exchanger network synthesis. *Chem. Eng. Sci.* **39**, 579 (1984).

Saboo, A. K., Morari, M., and Colberg, R. D., Resilience analysis of heat exchanger networks—Part I: Temperature dependent heat capacities. *Comp. Chem. Eng.*, **11**, 399 (1987a).

Saboo, A. K., Morari, M., and Colberg, R. D., Resilience analysis of heat exchanger networks—Part II: Stream splits and flowrate variations. *Comp. Chem. Eng.*, **11**, 457 (1987b).

Saboo, A. K., Morari, M., and Colberg, R. D., RESHEX—an interactive software package for the synthesis and analysis of resilient heat exchanger networks. Part II: Discussion of area targeting and network synthesis algorithms. *Comp. Chem. Eng.* **10**, 591 (1986).

Saboo, A. K., Morari, M. and Woodcock, D. C., Design of resilient processing plants—VIII. A resilience index for heat exchanger networks. *Chem. Eng. Sci.* **40**, 1553 (1985).

Schrage, L., "User's Manual—Linear, Integer and Quadratic Programming with LINDO." Scientific Press, Palo Alto, California, 1981.

Swaney, R. E., and Grossmann, I. E., An index for operational flexibility in chemical process design. Part II: Computational algorithms. *AIChE J.* **31**, 631 (1985b).

Umeda, T., Itoh, J., and Shiroko, K., Heat exchange system synthesis. *Chem. Eng. Prog.* **74**, (7), 70 (1978).

Chapter 4

A Resilience Target for Heat Exchanger Network Synthesis

4.1 Introduction

The economic targets for HEN synthesis (minimum utilities, area, and number of units) are valuable tools for designing an optimal network for *fixed* operating conditions. However, previous papers (Marselle *et al.*, 1982; Grossmann and Morari, 1983; Saboo and Morari, 1984) have shown what industrial process engineers have long realized—a practical HEN must not only be economical, but also resilient and flexible. Grossmann and Morari (1983) define *resilience* as "the ability of the plant to tolerate and recover from undesirable changes and upsets." For example, a HEN should be able to tolerate uncertainties and static (long-term) changes in supply temperatures, flow rates and heat transfer coefficients, and be able to respond smoothly to dynamic (short-term) upsets in temperature and flow rate. The new target

presented in this chapter deals with the static aspect of resilience—the ability to tolerate static change and uncertainty, and the ability to operate at a new steady state after an upset.

Similarly, Grossmann and Morari (1983) define *flexibility* as "the [static] ability to readily adjust to meet the requirements of changing conditions. For example, a flexible plant can be adapted to different feedstocks, product specifications or process conditions. ... The main difference is that resilience refers to the maintenance of satisfactory performance despite adverse conditions, while flexibility is the ability to handle alternate (desirable) operating conditions." Grossmann and Morari (1983) admit that the distinction between flexibility and static resilience is not always clear, and they treat the two as the same mathematical problem.

However, we would like to suggest a distinction. Flexibility deals with planned, desirable changes (e.g., feedstock changes) which often have a *discrete* set of magnitudes; static resilience deals with unplanned, undesirable changes (e.g., fouling, the effect of rain on an air-cooled condenser) which often have a *continuous* range of magnitudes. Thus flexibility should consider problems with multiple, discrete "periods of operation;" static resilience should consider problems with a continuous range of operating conditions surrounding some nominal operating point. The most general resilience-flexibility problem would consider continuous operating ranges surrounding each of several nominal operating points. In this chapter, we consider an operating range (uncertainty range) surrounding a single nominal operating point.

In general, several economically optimal or near-optimal HENs can be designed for given nominal operating conditions (supply temperatures and flow rates). One

criterion for selecting among these networks is to choose the most resilient [e.g., by using the resilience analysis techniques of Saboo *et al.* (1985, 1987a,b), Swaney and Grossmann (1985a,b), or Grossmann and Floudas (1987)]. But having done so, the process engineer may wonder if there is a more resilient network which he has not considered, which is also economically attractive. By having a resilience target with which to compare the resilience of the best network, the engineer can determine if there is scope for improving resilience.

This chapter presents two resilience targets[1] and shows how one of these targets can be used as a synthesis tool. The "general" resilience target—where no constraints are imposed upon the size (number of units) and complexity (number of stream splits) of a HEN—is arbitrarily large; given any nominal stream data, a HEN structure can always be synthesized which is resilient for *all* physically meaningful combinations of uncertain supply temperatures, target temperatures and heat capacity flow rates, while using minimum utilities. However, this general resilience target is not very practical since (1) large, expensive HEN structures are generally required to achieve it; and (2) designing for all physically meaningful supply temperatures and flow rates is unrealistic (overly ambitious).

A "practical" resilience target—achievable with practical HEN structures with few more units or stream splits than the number required for nominal operating conditions—can be defined by restricting the range of uncertain supply temperatures and flow rates such that the same stream inlet always causes the pinch (assuming

[1]To be consistent with the suggested distinction between resilience and flexibility introduced in this chapter, the flexibility index (FI) target described in Section 3.4.1 is now being called a resilience target.

constant heat capacities). This resilience target can be used to predict whether a practical HEN structure can be synthesized for a specified uncertainty range, or if trade-offs must be made in utilities, number of units, or resilience. Calculation of the resilience target also identifies the operating point and constraint (e.g., appearance of a new pinch) most likely to limit resilience.

4.2 General Resilience Target

Previous investigators have developed methods to synthesize resilient HENs (Saboo and Morari, 1984; Floudas and Grossmann, 1987b) and flexible HENs (Linnhoff and Kotjabasakis, 1986; Floudas and Grossmann, 1987a), and to quantify the resilience of an existing design (Saboo *et al.*, 1985; Swaney and Grossmann, 1985a,b). Now that one can synthesize resilient HENs and can quantify the resilience of alternative designs, it is natural to ask "What is the most resilient design I can achieve?"

In order to develop a resilience target to answer this question, we need a more specific definition of resilience for HENs. Consider an *uncertainty range* of uncertain parameters (supply temperatures and flow rates) over which a HEN is expected to operate. A HEN structure is *resilient* in the given uncertainty range if for every combination of supply temperatures and flow rates in the uncertainty range it (1) achieves the specified target temperature of each stream; (2) satisfies the specified minimum approach temperature (ΔT_m) in each exchanger; while (3) satisfying a specified utility consumption constraint (minimum utility consumption, or some relaxation factor times minimum utility consumption) (Saboo and Morari, 1984).

Note that since we are interested in the effects of HEN *structure* (topology) upon resilience *before* sizing individual exchangers, we define HEN resilience with respect to ΔT_m rather than area. Of course, the economically optimal value of ΔT_m varies with operating conditions, and ideally should consider the cost of *not* being resilient (e.g., lost production). However, for ease of presentation, the majority of this chapter assumes constant ΔT_m. Section 4.3.3 discusses extension of the resilience target to varying ΔT_m.

Also note that we include a utility consumption constraint for every point in the uncertainty range; other authors (e.g., Swaney and Grossmann, 1985b; Floudas and Grossmann, 1987b) constrain utility consumption only at the corner points (vertices) of the uncertainty range.

As defined, the uncertainty range includes uncorrelated supply temperatures and flow rates. The uncertainty range and the resilience target can be extended to varying target temperatures as well as correlated uncertainties.

Now, we can define a target for HEN resilience. It seems natural to define the resilience target in a manner similar to the economic targets:

> *For given nominal supply temperatures, target temperatures, heat capacities and flow rates, what is the largest amount of resilience which could be incorporated into a HEN if the process engineer were to consider all possible designs, with no constraints upon the complexity of the design? In other words, what is the largest possible uncertainty range for which the process engineer can synthesize a HEN?*

It turns out that this is not a very practical definition for the resilience target. Given

any nominal values of supply temperatures, target temperatures, heat capacities and flow rates, a HEN can be synthesized which is resilient not only for any arbitrarily large uncertainty range, but for *all* physically meaningful operating conditions. However, such a HEN is generally very complex and very costly.

For example, consider the HEN structure in Fig. 4.1 synthesized for a problem with two hot and two cold streams. This complex "spaghetti" structure is resilient for all uncertainty ranges no matter how large, surrounding any nominal operating point, while using minimum utilities. In fact, it is resilient for all supply temperatures, target temperatures, (constant) heat capacities and flow rates for *any* problem involving two hot and two cold streams.[2] The reason that this spaghetti structure is so resilient is that it can mimic the composite temperature-enthalpy curves for any set of operating conditions; that is, the temperature-enthalpy profiles of each hot/cold stream in the structure can always follow the temperature-enthalpy profile of the hot/cold composite curve. And since the composite curves can represent any physically meaningful combination of supply temperatures, target temperatures, heat capacities and flow rates, this structure is resilient for all such combinations.

To demonstrate how this structure can mimic the composite temperature-enthalpy curves, consider the composite curves in Fig. 4.2, which correspond to the temperatures and heat capacity flow rates in Fig. 4.1. (Note that for all the composite curve and HEN diagrams in this chapter, the temperatures are shifted to account for ΔT_m. For example, if $\Delta T_m = 10$ K, then a partial ΔT_m contribution of 5 K is

[2]If the heat capacities are taken as piecewise constant, then the structure in Fig. 4.1—with one additional stream split section for each discontinuity in heat capacity—is equally resilient. For temperature-dependent heat capacities not taken as piecewise constant, an infinitely cyclic HEN structure is resilient for all physically meaningful operating conditions.

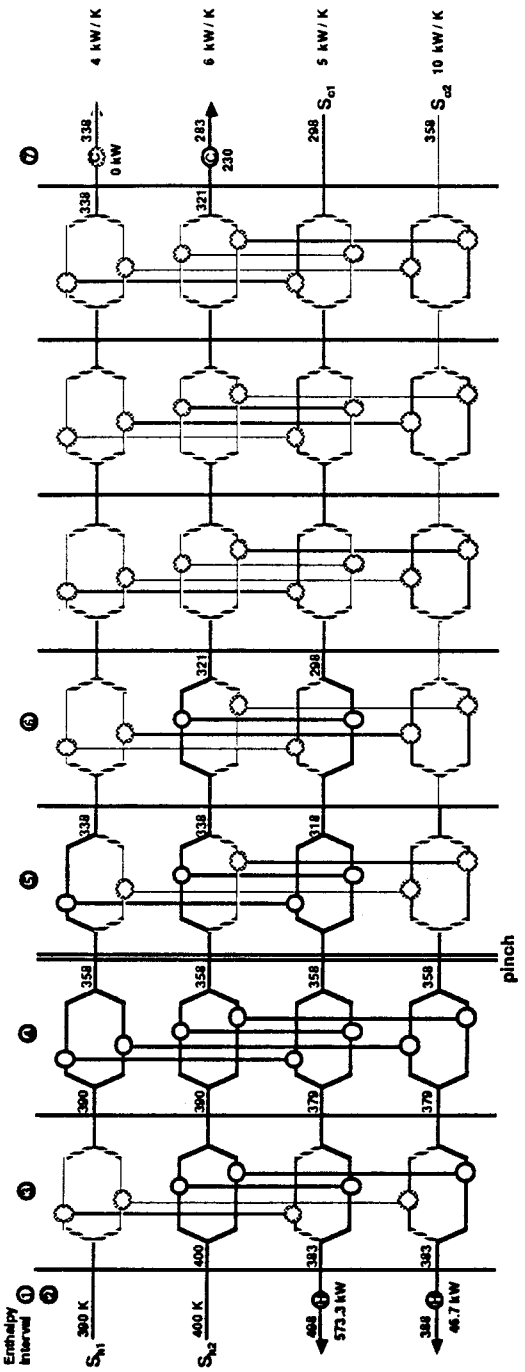

Figure 4.1: "Spaghetti" structure mimicking the nominal composite temperature-enthalpy curves of Example 4.1 (temperatures shifted to account for ΔT_m).

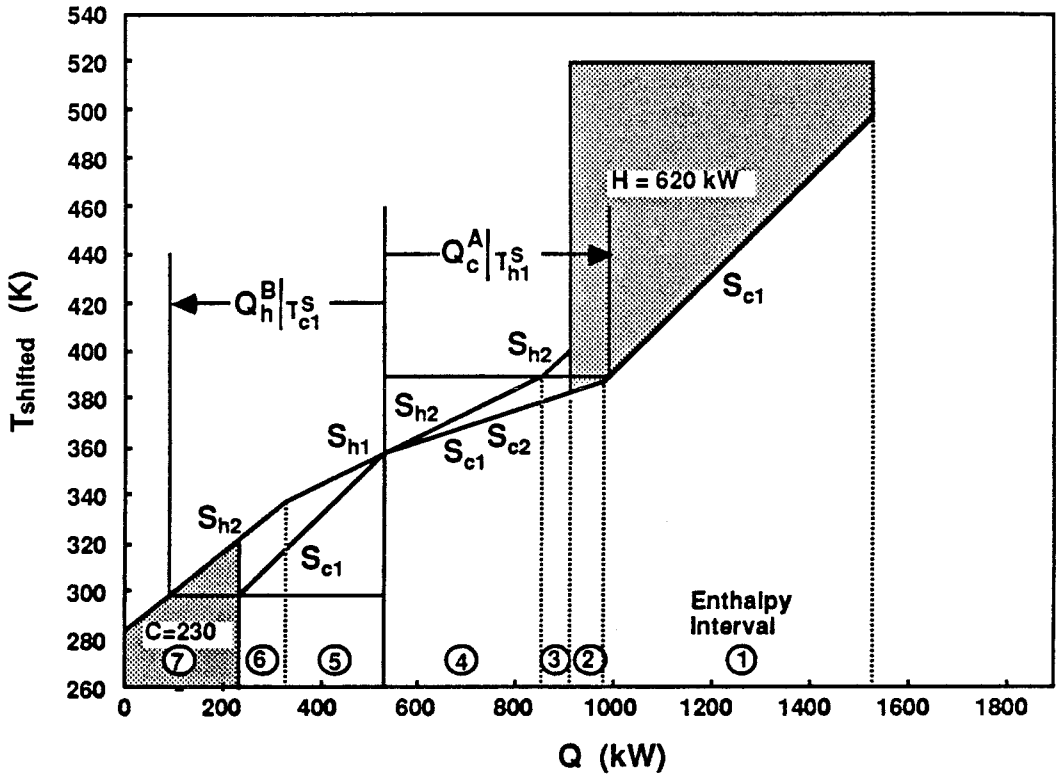

Figure 4.2: Composite temperature-enthalpy curves for nominal stream data (Example 4.1).

subtracted from all hot stream temperatures and added to all cold stream temperatures.) There are seven enthalpy intervals (EIs) under the piecewise linear segments of these composite curves. Four EIs involve heat exchange between process streams; three EIs involve utility heating or cooling. In the most general case, all seven EIs could involve heat exchange between process streams.

The HEN structure in Fig. 4.1 contains seven stream split sections, corresponding to the maximum possible number of EIs in the composite curves. The structure also contains a heater on each cold stream and a cooler on each hot stream. The exchangers drawn with solid lines have positive heat duty for the operating condition shown; the exchangers drawn with dashed lines exchange no heat and are completely bypassed. Four of the seven stream split sections have heat exchange corresponding to the four EIs in the composite curves with process heat exchange; the exchangers in the other three stream split sections are all bypassed. The flow rates in each branch of a stream split are chosen such that the HEN structure mimics the composite curves. For example, in EI 5, cold stream S_{c1} exchanges heat with hot streams S_{h1} and S_{h2}, while the exchangers on cold stream S_{c2} are completely bypassed. The flow rates through each branch of the split on stream S_{c1} (2 and 3 kW/K through the upper and lower branches, respectively) are chosen such that the ratio of the branch flow rates is equal to the ratio of stream S_{h1}'s heat capacity flow rate to that of stream S_{h2}. This yields the temperatures shown in Fig. 4.1, which are the same as the temperatures in the composite curves of Fig. 4.2.

The HEN structure in Fig. 4.1 contains a large number of bypassed exchangers. These exchangers are not required for the operating condition shown, but are required

as changing supply temperatures and flow rates cause the "kinks" (changes in slope) in the hot composite curve to shift past the kinks in the cold composite curve. As the kinks shift past each other, different streams exchange heat in some EIs, and some exchangers which were bypassed no longer can be. All the exchangers in Fig. 4.1 are required for this structure to be able to mimic the composite curves for any combination of supply temperatures, target temperatures, heat capacities and flow rates. All seven stream split sections are required for the rare case when no utility heating or cooling is required, and process streams exchange heat in every EI on the composite curves.

4.3 Class 1 Resilience Target

The resilience target presented in the last section is not very practical: (1) the HENs required to achieve it are generally very complex and costly; and (2) it is unrealistic (overly ambitious) to design a HEN for all physically meaningful operating conditions. A practical resilience target should be achievable with reasonable HENs (qualitatively, HENs with only a few more units and stream splits than that required for nominal operating conditions). In addition, a practical target should be easily computed and should be a useful tool for HEN synthesis.

4.3.1 A Target Based on the Thermodynamic Pinch and Class 1 and Class 2 Uncertainty Ranges

We can define a practical HEN resilience target based on the thermodynamic pinch. Basically, we examine the composite curves for secondary or "near" pinches. One approach would be to examine the composite curves just for the nominal supply temperatures and flow rates and to look for the second closest approach temperature at a kink in the composite curves (if the problem is pinched). However, new pinches can appear as the operating conditions are varied. So instead, we examine the behavior of the composite curves as the supply temperatures and flow rates vary, and determine the operating conditions when a new pinch appears or when the problem becomes unpinched (threshold).

To be more precise, we examine the behavior of the composite curves for the supply temperatures and flow rates throughout an uncertainty range as the uncertainty range expands in size. The resilience target corresponds to the uncertainty range at the transition between "Class 1" and "Class 2." A Class 1 uncertainty range is one in which the uncertainties are small enough that (1) the pinch-causing stream, and the stream populations above and below the pinch, are constant throughout the uncertainty range if the problem is pinched; or (2) the problem remains threshold heating (or cooling) throughout the uncertainty range if the problem is unpinched. If the uncertainties are too large, then the uncertainty range is Class 2.[3]

[3]The original definition of a Class 1 uncertainty range requires that the uncertainties be small enough for a "unique, explicit expression" to exist for the energy recovery (utility heating) constraint throughout the uncertainty range (Saboo and Morari, 1984). The definition in this chapter is a physical interpretation of the original mathematical definition.

Table 4.1: Nominal stream data for Examples 4.1, 4.2 and 4.4 (after shifting to account for $\Delta T_m = 10$ K).

Stream	*Supply Temperature* (K)	*Target Temperature* (K)	*Heat Capacity Flow Rate* (kW/K)
H1	390	338	4.0
H2	400	283	6.0
C1	298	498	5.0
C2	358	388	10.0

Thus, the resilience target corresponds to the largest possible Class 1 uncertainty range. Restricting the resilience target to Class 1 uncertainty ranges results in practical HENs with a reasonable number of units and stream splits. The following example illustrates graphically the difference between Class 1 and Class 2 uncertainty ranges, and demonstrates the meaning of the resilience target. The example also illustrates why Class 2 uncertainty ranges generally require more complex HENs than Class 1 uncertainty ranges.

Example 4.1 Consider the nominal stream data given in Table 4.1 and the corresponding composite curves in Fig. 4.2. As the composite curves indicate, stream S_{c2} causes the pinch for these nominal stream data.

Assume that the supply temperature T_{h2}^S and heat capacity flow rate w_{h2} of hot stream S_{h2} are uncertain. Figure 4.3 shows a "pinch behavior diagram" as T_{h2}^S and w_{h2} vary. The nominal stream data are indicated with an asterisk. For every combination of uncertain parameters T_{h2}^S and w_{h2} in the unshaded portion of this diagram, stream S_{c2} causes the pinch. For all values of T_{h2}^S and w_{h2} in the shaded portion of this diagram, stream S_{h2} causes the pinch (cf., composite curves in Fig. 4.4, which

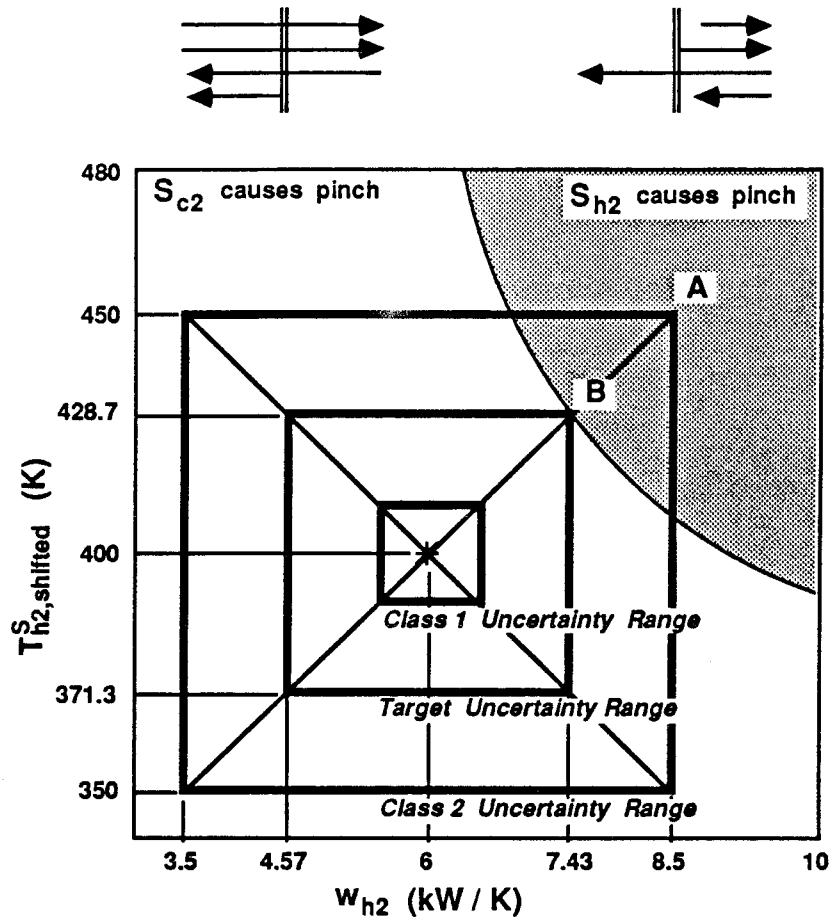

Figure 4.3: Pinch behavior diagram illustrating Class 1, Class 2, and target uncertainty ranges (Example 4.1).

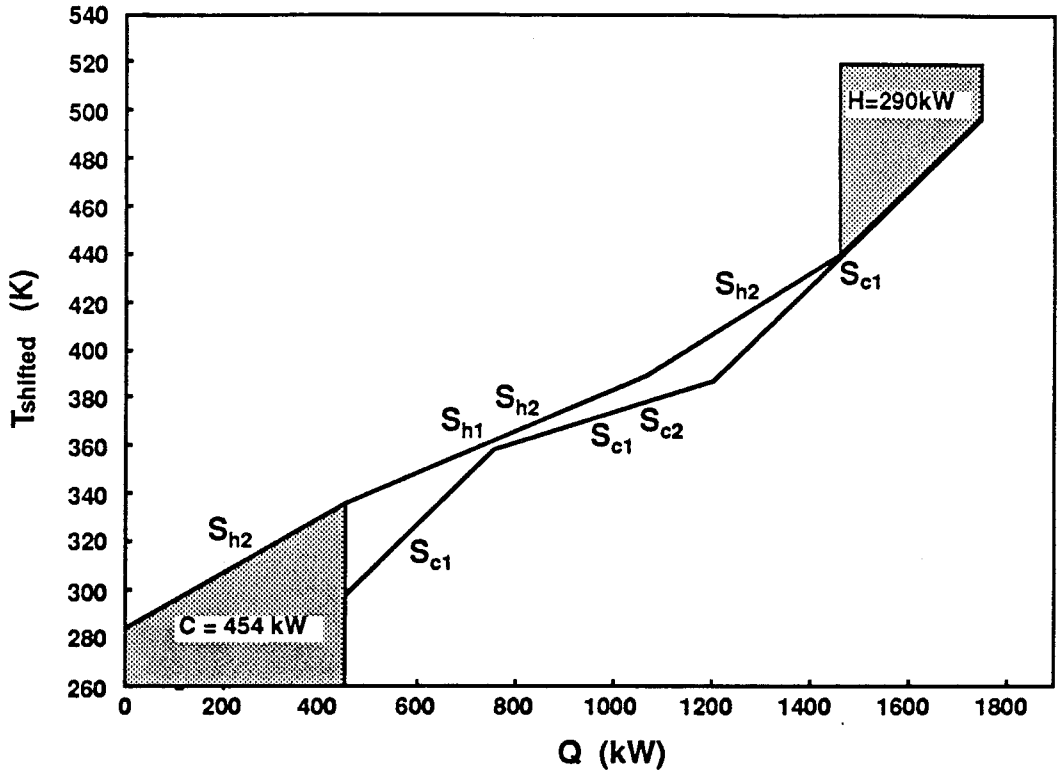

Figure 4.4: Composite temperature-enthalpy curves for point "A" in Fig. 4.3 (Example 4.1).

correspond to point "A" in Fig. 4.3). If an uncertainty range includes both shaded and unshaded regions of this diagram, then it is Class 2; otherwise the uncertainty range is Class 1.

Figure 4.3 shows three different size uncertainty ranges. The smallest uncertainty range is Class 1—for every combination of T_{h2}^S and w_{h2} in the range, stream S_{c2} causes the pinch and the stream populations above the pinch (S_{h1}, S_{h2}, S_{c1}, S_{c2}) and below the pinch (S_{h1}, S_{h2}, S_{c1}) are constant. The largest uncertainty range is Class 2—in one corner of the uncertainty range stream S_{h2} causes the pinch, while in the remainder of the uncertainty range stream S_{c2} causes the pinch. The middle-size uncertainty

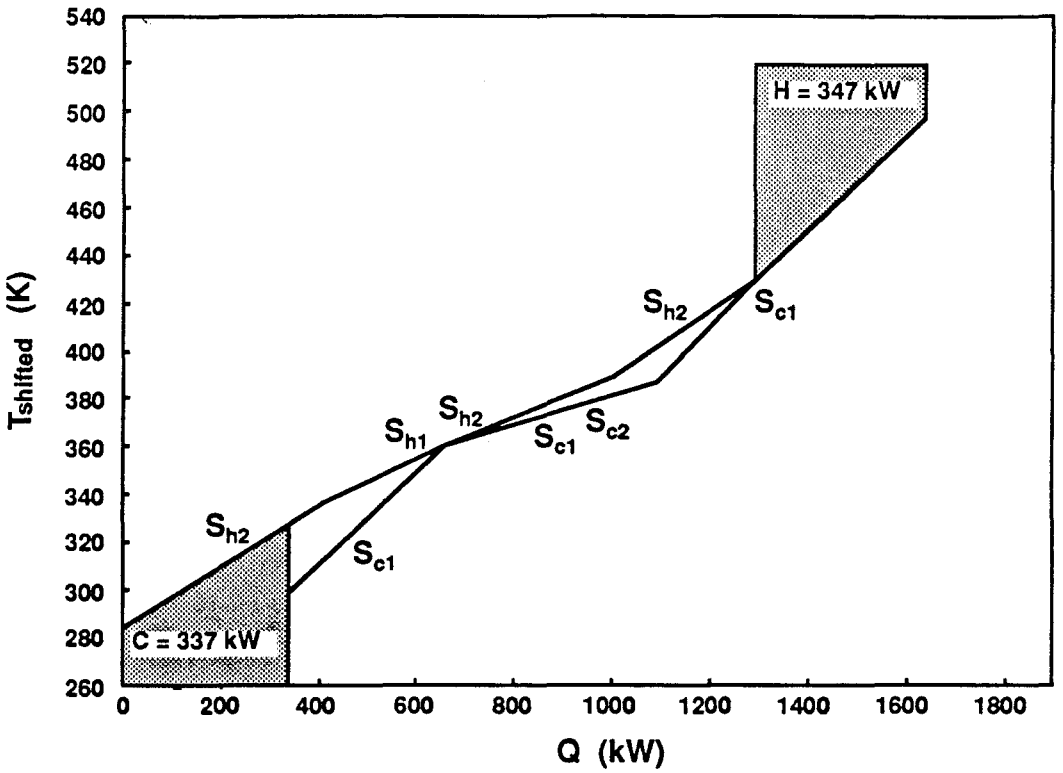

Figure 4.5: Composite temperature-enthalpy curves for critical uncertainty point in Fig. 4.3 (Example 4.1).

range corresponds to the resilience target—it is the target uncertainty range at the transition between Class 1 and Class 2. If the uncertainties were any larger (in the direction of increasing T_{h2}^{S} or increasing w_{h2}), this uncertainty range would become Class 2. The point labeled "B" in Figure 4.3 limits the size of the target uncertainty range; this point is called the "critical uncertainty point." At this point, both stream S_{h2} and stream S_{c2} cause pinches as shown in the composite curves in Fig. 4.5.

More complicated HENs with a larger number of units are generally required for Class 2 uncertainty ranges in order to satisfy ΔT_m at a larger number of pinches (especially if minimum utility consumption is required throughout the uncertainty range).

Throughout the Class 1 uncertainty range shown in Fig. 4.3, only one pinch occurs (at the supply of stream S_{c2}) and the four shaded exchangers shown in Fig. 4.11(b) are required in order to satisfy ΔT_m at this pinch. For the Class 2 uncertainty range shown in Fig. 4.3, pinches can occur at the supply of either stream S_{h2} or S_{c2}. In fact, at the critical uncertainty point (point "B"), pinches occur at both S_{h2} and S_{c2}. At this point, the two blackened units in Fig. 4.11(a) (a heater and an exchanger) are required to satisfy ΔT_m at the new pinch caused by stream S_{h2} *in addition to* the four shaded exchangers required to satisfy ΔT_m at the original pinch caused by stream S_{c2}. ■

In defining a practical resilience target, we have tried to consider economics, albeit indirectly. In restricting the resilience target to Class 1 uncertainty ranges, we have limited the number of units required in the network. By defining resilience with respect to ΔT_m and by including a constraint on utility consumption (Section 4.2)—note the composite curves were shifted to account for ΔT_m and that they assume minimum utility consumption—we have included implicit bounds on area and utility costs. Sections 4.3.3 and 4.3.4 below discuss trade-offs between the resilience target and ΔT_m and utility consumption, and show how the resilience target can be extended to nonminimum utility consumption and to varying ΔT_m.

The previous example illustrated one type of transition between Class 1 and Class 2 uncertainty ranges—a pinch "shift" (or "jump") from one stream supply to another, with the appearance of two or more simultaneous pinches at the transition. There are two other types of Class 1–Class 2 transitions as well: (1) changing stream populations above or below the pinch, with two or more streams

simultaneously causing the same pinch at the transition (Fig. 4.6); and (2) the transition from a pinched to an unpinched (threshold) problem, or vice versa.

In order to assign a numerical value to the resilience target, the uncertainty ranges are assumed to be scaled proportional in size relative to a reference uncertainty range specified by the process engineer. The resilience target is simply the size ratio s of the target uncertainty range relative to the reference uncertainty range.[4]

Example 4.1 *(continued).* Suppose that the process engineer specifies as a reference uncertainty range the smallest uncertainty range shown in Fig. 4.3 ($\Delta T_{h2}^S = \pm 10$ K; $\Delta w_{h2} = \pm 0.5$ kW/K). (Note that in general, the positive and negative magnitudes of the uncertainties need not be the same.) Then the resilience target s^* has a value of 2.87 ($s^* \Delta T_{h2}^S = \pm 28.7$ K; $s^* \Delta w_{h2} = \pm 1.44$ kW/K), the size of the target uncertainty range scaled relative to the size of the reference uncertainty range.

The resilience target can also have a value less than 1.0 if the reference uncertainty range specified by the process engineer is Class 2. Suppose that the largest uncertainty range in Fig. 4.3 is specified as a reference uncertainty range ($\Delta T_{h2}^S = \pm 50$ K; $\Delta w_{h2} = \pm 2.5$ kW/K). Then the resilience target has a value of $s^* = 0.72$ ($s^* \Delta T_{h2}^S = \pm 28.7$ K; $s^* \Delta w_{h2} = \pm 1.44$ kW/K). The fact that the resilience target is less than 1.0 means that the reference uncertainty range has to be scaled *down* to match the size of the target uncertainty range. ■

The choice of the reference uncertainty range is entirely that of the process engineer. It might represent absolute sizes of (or bounds on) uncertainties the engineer

[4]This size ratio is based on the "flexibility index" introduced by Swaney and Grossmann (1985a) for quantifying the resilience (using our proposed distinction between resilience and flexibility in Section 4.1) of an *existing* HEN structure.

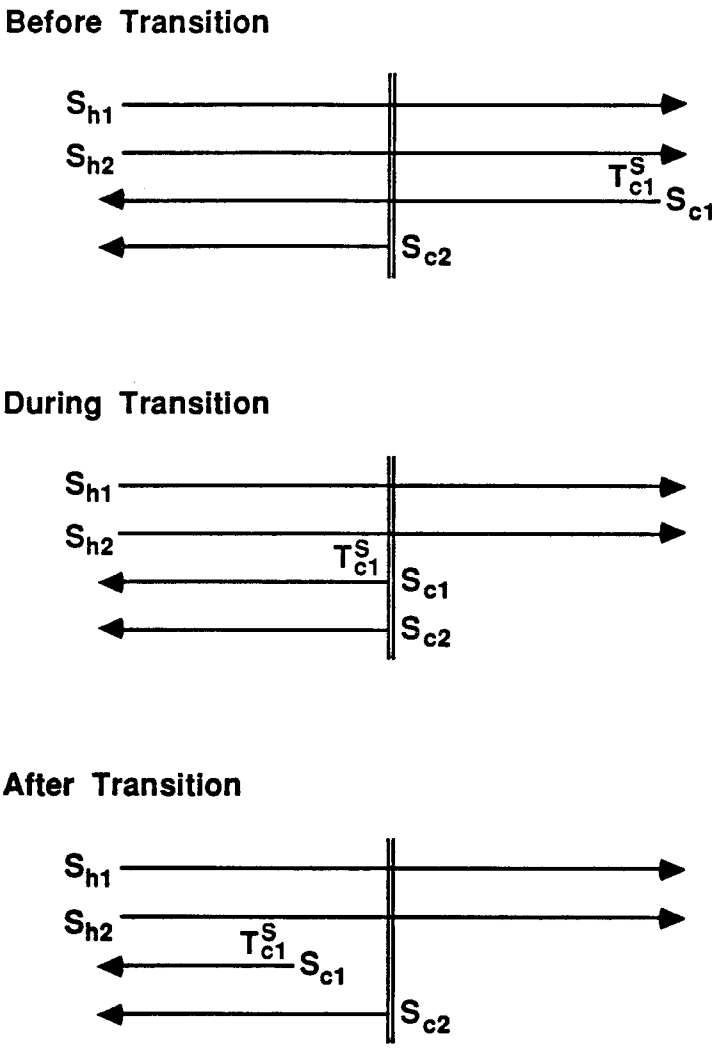

Figure 4.6: Transition between Class 1 and Class 2 uncertainty ranges where the stream population changes below the pinch.

realistically expects. Or it might represent relative sizes between various uncertainties; that is, the engineer might specify only the general shape (aspect ratio) of the rectangular reference uncertainty range. In the absence of reliable uncertainty estimates, the engineer might choose symmetric ($\Delta T_i^S = \pm 1$ K for all uncertain supply temperatures; $\Delta w_j = \pm 1$ kW/K for all uncertain heat capacity flow rates) or one-dimensional ($\Delta T_i^S = \pm 1$ K for one uncertain supply temperature; $\Delta T_j^S = 0$ K for all other supply temperatures) reference uncertainty ranges in order to probe the amount of uncertainty allowed before an uncertainty range becomes Class 2.

4.3.2 Calculation of the Class 1 Resilience Target

For problems with more than two uncertain parameters, it is difficult to determine the Class 1 HEN resilience target simply by plotting a pinch behavior diagram such as Fig. 4.3. Also, for problems with a large number of uncertainties or with correlated uncertainties, it becomes unwieldly to determine the resilience target by trial-and-error plotting of the composite curves. For these (and simpler) problems, a nonlinear program (NLP) can be used to model the composite curves and to calculate the resilience target.

Marselle *et al.* (1982) defined four specific uncertainty directions (away from the nominal values of the uncertain parameters) upon which they based a heuristic procedure for synthesizing resilient HENs. The NLP presented below is based on two of these four uncertainty directions. The following theorem from Saboo and Morari (1984) shows that these two directions (the "Case B" and "Case C" directions) are important in determining when an uncertainty range changes from Class 1 to Class 2.

Table 4.2: Supply temperatures, target temperatures, and flow rates corresponding to Case B (maximum cooling) and Case C (maximum heating).

	Supply Temperatures	*Target Temperatures*	*Hot Stream Flow Rates*	*Cold Stream Flow Rates*
Case B (maximum cooling)	highest	lowest	highest	lowest
Case C (maximum heating)	lowest	highest	lowest	highest

We restate their theorem subject to the restriction of constant heat capacities and no phase change.[5]

Theorem 4.1 *Let* Case B *be the uncertainty direction which maximizes the HEN's cooling requirement, and* Case C *be the uncertainty direction which maximizes the HEN's heating requirement. (See Table 4.2 for the supply temperatures, target temperatures and flow rates corresponding to these two cases.)*

a. *For any point in the uncertainty range, the pinch temperature T_p^S (i.e., the supply temperature of pinch-causing stream* S_p*) is between the pinch temperatures for Cases B and C ($T_p^{SC} \leq T_p^S \leq T_p^{SB}$) where hot and cold stream temperatures T are shifted to account for partial contributions to ΔT_m.*

b. *The uncertainty range is Class 1 if*

   i. *the pinch is determined by the supply temperature of the same stream for both the Case B and Case C corner points; and*

   ii. *for any point in the uncertainty range, no stream supply or target*

[5]The resilience target in this chapter can be extended to piecewise constant heat capacities and phase change as long as one remembers the additional potential pinch point locations (Saboo and Morari, 1984) at the heat capacity discontinuities, boiling points, dew points, and/or bubble points.

temperature[6] *is contained in the open temperature interval* (T_p^{SC}, T_p^{SB}) *except for the supply temperature associated with the pinch.*

Otherwise the uncertainty range is Class 2.

As given, Theorem 4.1 is restricted to problems with a single pinch (and possibly a second pinch at the transition between Class 1 and Class 2, such as in Fig. 4.5). Except for rare degenerate cases, this restriction is satisfied for problems with single hot and cold utilities. This theorem and the Class 1 resilience target can be extended to multiple utilities if multiple pinches are explicitly considered.

In terms of the pinch behavior diagram, condition b(i) of Theorem 4.1 implies that if the pinch-causing stream changes in an uncertainty range as the uncertainty range increases in size, it must change first at either the Case B or Case C corner point [e.g., in Fig. 4.3, as the uncertainty range increases in size, the Case B corner point (the upper right corner point in Fig. 4.3) is the first point of the uncertainty range to cross into the shaded region, where stream S_{h2} becomes the new pinch-causing stream]. Thus condition b(i) prevents the type of pinch transition demonstrated in Example 4.1 (i.e., a pinch shift from one stream to another, with two simultaneous pinches at the transition). Condition b(ii) prevents the type of Class 1–Class 2 transition illustrated in Fig. 4.6 (i.e., changing stream populations above or below the pinch, with two streams simultaneously causing the same pinch at the transition).

The NLP to calculate the resilience target maximizes the size ratio s of uncertainty ranges relative to a reference uncertainty range specified by the process engineer,

[6]Saboo and Morari (1984) forgot to include target temperatures in their statement of this theorem. It can be shown by counterexample that target temperatures are required.

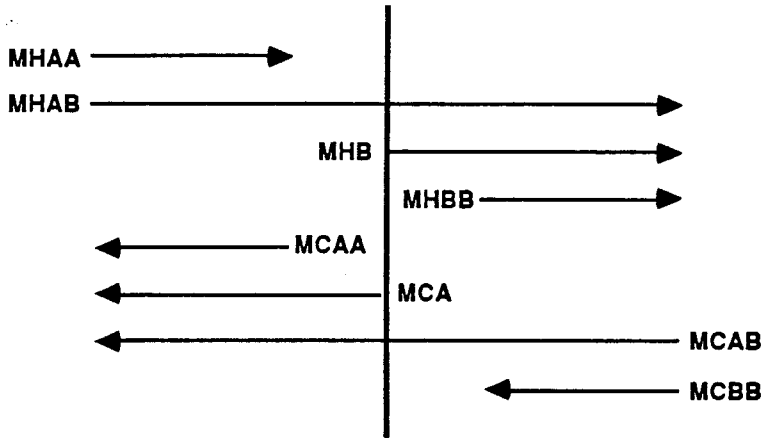

Figure 4.7: Stream index sets used to formulate the NLP to calculate the Class 1 resilience target.

subject to constraints which limit the uncertainty range to Class 1. The reference uncertainty range is specified with upper and lower bounds on all uncertain supply temperatures T_i^S and heat capacity flow rates w_i,

$$T_i^{SN} - \Delta T_i^{S-} \leq T_i^S \leq T_i^{SN} + \Delta T_i^{S+}$$
$$w_i^N - \Delta w_i^- \leq w_i \leq w_i^N + \Delta w_i^+$$

where T_i^{SN} is the nominal supply temperature of stream S_i, w_i^N is the nominal heat capacity flow rate of stream S_i, ΔT_i^{S+} and ΔT_i^{S-} are the positive and negative reference uncertainties in T_i^S, and Δw_i^+ and Δw_i^- are the positive and negative reference uncertainties in w_i.

In order to formulate the NLP, the following index sets are useful (Fig. 4.7):

$$\begin{aligned}
\text{MH} &= \{i|\text{S}_\text{i} \text{ is a hot stream}\} \\
\text{MC} &= \{i|\text{S}_\text{i} \text{ is a cold stream}\} \\
\text{MHAA} &= \{i|\text{hot stream S}_\text{i} \text{ is completely } \textit{above} \text{ the pinch}\} \\
&= \{i \in \text{MH}|T_i^T \geq T_p^S\} \\
\text{MHAB} &= \{i|\text{hot stream S}_\text{i} \text{ straddles (i.e., is } \textit{above} \text{ and } \textit{below}\text{) the pinch}\} \\
&= \{i \in \text{MH}|T_i^S > T_p^S > T_i^T\} \\
\text{MHB} &= \{i|\text{hot stream S}_\text{i} \text{ causes (and is } \textit{below}\text{) the pinch}\} \\
&= \{i \in \text{MH}|T_i^S = T_p^S\} \\
\text{MHBB} &= \{i|\text{hot stream S}_\text{i} \text{ is completely } \textit{below} \text{ the pinch}\} \\
&= \{i \in \text{MH}|T_p^S > T_i^S\} \\
\text{MCAA} &= \{i|\text{cold stream S}_\text{i} \text{ is completely } \textit{above} \text{ the pinch}\} \\
&= \{i \in \text{MC}|T_i^S > T_p^S\} \\
\text{MCA} &= \{i|\text{cold stream S}_\text{i} \text{ causes (and is } \textit{above}\text{) the pinch}\} \\
&= \{i \in \text{MC}|T_i^S = T_p^S\} \\
\text{MCAB} &= \{i|\text{cold stream S}_\text{i} \text{ straddles (i.e., is } \textit{above} \text{ and } \textit{below}\text{) the pinch}\} \\
&= \{i \in \text{MC}|T_i^T > T_p^S > T_i^S\} \\
\text{MCBB} &= \{i|\text{cold stream S}_\text{i} \text{ is completely } \textit{below} \text{ the pinch}\} \\
&= \{i \in \text{MC}|T_p^S > T_i^T\}
\end{aligned}$$

Note that the pinch-causing stream must be known (by energy targeting for the nominal stream data) before these index sets can be defined and the NLP formulated.

Also note that if a hot stream causes the pinch, then MHB contains that stream index and MCA is an empty set; if a cold stream causes the pinch, then MHB is an empty set.

With these stream index sets, the NLP to calculate the Class 1 resilience target s^* can be formulated as follows after shifting all temperatures to account for ΔT_m:

$$s^* = \max_s s \qquad \textbf{(P1)}$$

subject to

(A) Nonnegative heating:

$$\begin{aligned} 0 \leq H_{\min} = & \sum_{i \in \text{MCAA}} (w_i^N - s\,\Delta w_i^-)\,[T_i^T - (T_i^{SN} + s\,\Delta T_i^{S+})] \\ & + \sum_{i \in \text{MCA,MCAB}} (w_i^N - s\,\Delta w_i^-)\,[T_i^T - (T_p^{SN} + s\,\Delta T_p^{S+})] \\ & - \sum_{i \in \text{MHAA}} (w_i^N + s\,\Delta w_i^+)\,[(T_i^{SN} + s\,\Delta T_i^{S+}) - T_i^T] \\ & - \sum_{i \in \text{MHAB}} (w_i^N + s\,\Delta w_i^+)\,[(T_i^{SN} + s\,\Delta T_i^{S+}) - (T_p^{SN} + s\,\Delta T_p^{S+})] \end{aligned}$$

where $H_{\min}$ is the minimum heating utility required for a given ΔT_m, obtained by overall energy balance above the pinch.

(B) Nonnegative cooling:

$$
\begin{aligned}
0 \le C_{\min} = & \sum_{i \in \text{MHBB}} (w_i^N - s\,\Delta w_i^-)\,[(T_i^{SN} - s\,\Delta T_i^{S-}) - T_i^T] \\
& + \sum_{i \in \text{MHAB,MHB}} (w_i^N - s\,\Delta w_i^-)\,[(T_p^{SN} - s\,\Delta T_p^{S-}) - T_i^T] \\
& - \sum_{i \in \text{MCBB}} (w_i^N + s\,\Delta w_i^+)\,[T_i^T - (T_i^{SN} - s\,\Delta T_i^{S-})] \\
& - \sum_{i \in \text{MCAB}} (w_i^N + s\,\Delta w_i^+)\,[(T_p^{SN} - s\,\Delta T_p^{S-}) - (T_i^{SN} - s\,\Delta T_i^{S-})]
\end{aligned}
$$

where $C_{\min}$ is the minimum cooling utility required for a given ΔT_m, obtained by overall energy balance below the pinch.

(C) Stream existence:

$$
\left.
\begin{aligned}
T_i^{SN} - s\,\Delta T_i^{S-} &\ge T_i^T \\
w_i^N - s\,\Delta w_i^- &\ge 0
\end{aligned}
\right\} \quad \text{for } i \in \text{MHAA, MHBB}
$$

$$
\left.
\begin{aligned}
T_i^{SN} + s\,\Delta T_i^{S+} &\le T_i^T \\
w_i^N - s\,\Delta w_i^- &\ge 0
\end{aligned}
\right\} \quad \text{for } i \in \text{MCAA, MCBB}
$$

$$
w_i^N - s\,\Delta w_i^- \ge 0 \qquad \text{for } i \in \text{MHAB, MHB, MCA, MCAB}
$$

(D) Prevent T_p^S from crossing any supply or target temperature:

$$
\begin{aligned}
T_p^{SN} + s\,\Delta T_p^{S+} &\le T_i^{SN} - s\,\Delta T_i^{S-} && \text{for } i \in \text{MHAB, MCAA} \\
T_p^{SN} - s\,\Delta T_p^{S-} &\ge T_i^{SN} + s\,\Delta T_i^{S+} && \text{for } i \in \text{MHBB, MCAB} \\
T_p^{SN} + s\,\Delta T_p^{S+} &\le T_i^T && \text{for } i \in \text{MHAA, MCA, MCAB} \\
T_p^{SN} - s\,\Delta T_p^{S-} &\ge T_i^T && \text{for } i \in \text{MHAB, MHB, MCBB}
\end{aligned}
$$

These constraints prevent changing stream populations above or below the pinch:

that is, they require that condition b(ii) of Theorem 4.1 be satisfied.

(E) Prevent pinch shifts (jumps):

$$Q_h^A|_{T_i^S} \leq Q_c^A|_{T_i^S} \quad \text{for } i \in \text{MHAA, MHAB, MCAA}$$

$$Q_h^B|_{T_i^S} \leq Q_c^B|_{T_i^S} \quad \text{for } i \in \text{MHBB, MCAB, MCBB}$$

where

$Q_h^A|_T$, $Q_c^A|_T$ = enthalpy of the hot (cold) composite curve at temperature T *above* the pinch ($T > T_p^S$) based on a reference enthalpy of zero at the pinch (see Fig. 4.2)

$Q_h^B|_T$, $Q_c^B|_T$ = enthalpy of the hot (cold) composite curve at temperature T *below* the pinch ($T < T_p^S$) based on a reference enthalpy of zero at the pinch (see Fig. 4.2)

These constraints prevent the pinch from shifting (jumping) from one stream to another; that is, they require that condition b(i) of Theorem 4.1 be satisfied. In terms of the composite curves, these constraints require that at any potential pinch location (i.e., at all stream supply temperatures) the hot composite curve lie to the left of the cold composite curve ($Q_h < Q_c$), as in Fig. 4.2. The functional form of Q_h^A, Q_h^B, Q_c^A and Q_c^B is described below.

(F) Nonnegative size ratio: $s \geq 0$

All the constraints in NLP (P1) are linear in s except for the nonnegative heating and cooling constraints and the pinch shift constraints. [The form of the pinch shift constraints is motivated by the pinch location method of Duran and Grossmann (1986).] The nonlinearity of the pinch shift constraints arises from the functional

form of Q_h^A, Q_c^A, Q_h^B and Q_c^B:

$$
\begin{aligned}
Q_h^A|_T &= \sum_{i\in\text{MHAA}} w_i\,[\max(0,T-T_i^T)-\max(0,T-T_i^S)] \\
&\quad + \sum_{i\in\text{MHAB}} w_i\,[\max(0,T-T_p^S)-\max(0,T-T_i^S)] \qquad (4.1)\\
Q_c^A|_T &= \sum_{i\in\text{MCAA}} w_i\,[\max(0,T-T_i^S)-\max(0,T-T_i^T)] \\
&\quad + \sum_{i\in\text{MCA,MCAB}} w_i\,[\max(0,T-T_p^S)-\max(0,T-T_i^T)] \qquad (4.2)\\
Q_h^B|_T &= \sum_{i\in\text{MHBB}} w_i\,[\max(0,T_i^T-T)-\max(0,T_i^S-T)] \\
&\quad + \sum_{i\in\text{MHB,MHAB}} w_i\,[\max(0,T_i^T-T)-\max(0,T_p^S-T)] \qquad (4.3)\\
Q_c^B|_T &= \sum_{i\in\text{MCBB}} w_i\,[\max(0,T_i^S-T)-\max(0,T_i^T-T)] \\
&\quad + \sum_{i\in\text{MCAB}} w_i\,[\max(0,T_i^S-T)-\max(0,T_p^S-T)] \qquad (4.4)
\end{aligned}
$$

where T is some stream supply temperature T_j^S ($j \in$ MH,MC) parametrized in terms of size ratio s (e.g., $T_j^S = T_j^{SN} + s\,\Delta T_j^{S+}$). Note from equations (4.1)–(4.4) that enthalpies above the pinch ($Q_h^A|_T$ and $Q_c^A|_T$) are defined to be positive, while enthalpies below the pinch ($Q_h^B|_T$ and $Q_c^B|_T$) are defined to be negative.

The max operators in equations (4.1)–(4.4) cause the enthalpy functions to include only the portions of the hot or cold streams occurring between temperatures T and T_p^S. To illustrate, consider the calculation of $Q_h^B|_{T_{c1}^S}$ for the hot composite curve in Fig. 4.2:

$$
\begin{aligned}
Q_h^B|_{T_{c1}^S} &= w_{h1}\,[\max(0,T_{h1}^T-T_{c1}^S)-\max(0,T_{c2}^S-T_{c1}^S)] \\
&\quad + w_{h2}\,[\max(0,T_{h2}^T-T_{c1}^S)-\max(0,T_{c2}^S-T_{c1}^S)] \\
&= w_{h1}\,[(T_{h1}^T-T_{c1}^S)-(T_{c2}^S-T_{c1}^S)] + w_{h2}\,[0-(T_{c2}^S-T_{c1}^S)]
\end{aligned}
$$

$$= \quad -w_{h1}\,(T^S_{c2} - T^T_{h1}) - w_{h2}\,(T^S_{c2} - T^S_{c1})$$

$$< \quad 0$$

which is the correct expression for $Q^B_h|_{T^S_{c1}}$ since streams S_{h1} and S_{h2} both straddle the pinch (i.e., h1,h2 $\in$ MHAB), and we want to include in $Q^B_h|_{T^S_{c1}}$ all of stream S_{h1} below the pinch, but only the portion of stream S_{h2} below the pinch and hotter than T^S_{c1}.

Since the objective function in NLP (P1) is linear, the solution of the NLP lies on a constraint. And since NLP (P1) has no degrees of freedom other than s (i.e., no "control variables"), then in general only one constraint is active (cf., active constraint strategy: Grossmann and Floudas, 1987). An efficient way to solve the NLP is to examine the constraints one-by-one, solving each constraint for the value of size ratio s which would make it active if none of the other constraints were violated. Then the resilience target s^* is determined by the constraint which most limits s.

Since the constraints in NLP (P1) can be examined one-by-one, it is necessary to evaluate each constraint only in its own worst case uncertainty direction. The worst cases for the nonnegative heating and cooling constraints are the Case B (minimum heating/maximum cooling) and Case C (minimum cooling/maximum heating) directions, respectively. For each pinch shift constraint, the worst uncertainty direction is either Case B or Case C [according to Theorem 4.1, condition b(i)]; since the worse of these two directions is not known *a priori*, each pinch shift constraint is evaluated in both directions. The worst case uncertainty directions for the remaining constraints are obvious by inspection. For example when $T^S_i > T^S_p$ (i.e., $i \in$ MHAB,MCAA), constraint (D) to prevent pinch temperature T^S_p from crossing supply temperature T^S_i

is most likely to be violated when T_p^S increases (ΔT_p^{S+}) and T_i^S decreases (ΔT_i^{S-}). Example 4.2 below illustrates the formulation of the constraints in their worst case uncertainty directions.

For uncorrelated uncertainties, NLP (P1) is restricted to problems with a single pinch-causing stream (and possibly two or more simultaneous pinch-causing streams at the transition between Class 1 and Class 2, such as in Fig. 4.6). However, if the supply temperatures of two streams are identical and perfectly correlated (e.g., the liquid and vapor exit streams from an equilibrium flash drum), then NLP (P1) allows both streams to simultaneously cause the pinch throughout the Class 1 uncertainty range.

NLP (P1) can also be applied to threshold problems. The constraints collapse to the proper form for threshold heating problems if all streams are considered to occur above the pinch ($i \in$ MHAA, MCAA), and for threshold cooling problems if all streams are considered to occur below the pinch ($i \in$ MHBB, MCBB). One additional constraint is also required for threshold problems. For threshold heating problems, a constraint is required to ensure that at least one cold stream is colder than all the hot streams (or else cooling utility will be required):

$$T_j^S \leq \min_{i \in \mathrm{MH}} T_i^T \quad \text{for some } j \in \mathrm{MC} \tag{4.5}$$

where temperatures T_i^T and T_j^S are shifted to account for ΔT_m. Note that the set of one or more cold streams which satisfies this inequality can change as the uncertain stream supply temperatures vary. Similarly, for threshold cooling problems a

constraint is required to ensure that at least one hot stream is hotter than all the cold streams (or else heating utility will be required):

$$T_i^S \geq \max_{j \in \mathrm{MC}} T_j^T \quad \text{for some } i \in \mathrm{MH} \tag{4.6}$$

Example 4.2 NLP (P1) will be applied to calculate the Class 1 resilience target for the same nominal supply temperatures and flow rates as Example 4.1 (Table 4.1), with the smallest uncertainty range in Fig. 4.3 used as the reference uncertainty range:

$$\begin{aligned}
&\Delta T_{h1}^{S+} = \Delta T_{h1}^{S-} = 0 \qquad \Delta w_{h1}^{+} = \Delta w_{h1}^{-} = 0 \\
&\Delta T_{h2}^{S+} = \Delta T_{h2}^{S-} = 10\ \mathrm{K} \qquad \Delta w_{h2}^{+} = \Delta w_{h2}^{-} = 0.5\ \mathrm{kW/K} \\
&\Delta T_{cj}^{S+} = \Delta T_{cj}^{S-} = 0 \qquad \Delta w_{cj}^{+} = \Delta w_{cj}^{-} = 0 \qquad (j = 1, 2)
\end{aligned}$$

Stream S_{c2} causes the pinch for the nominal stream data.

Resilience targeting NLP (P1) is formulated as follows:

$$s^* = \max_s s$$

subject to

(A) Nonnegative heating:

$$\begin{aligned}
0 \leq H_{\min} = {} & (5 - s\,\Delta w_{c1}^{-})\,[498 - (358 + s\,\Delta T_{c2}^{S+})] \\
& + (10 - s\,\Delta w_{c2}^{-})\,[388 - (358 + s\,\Delta T_{c2}^{S+})] \\
& - (4 + s\,\Delta w_{h1}^{+})\,[(390 + s\,\Delta T_{h1}^{S+}) - (358 + s\,\Delta T_{c2}^{S+})] \\
& - (6 + s\,\Delta w_{h2}^{+})\,[(400 + s\,\Delta T_{h2}^{S+}) - (358 + s\,\Delta T_{c2}^{S+})]
\end{aligned}$$

(B) Nonnegative cooling:

$$\begin{aligned}
0 \leq C_{\min} = {} & (4 - s\,\Delta w_{h1}^{-})\,[(358 - s\,\Delta T_{c2}^{S-}) - 338] \\
& + (6 - s\,\Delta w_{h2}^{-})\,[(358 - s\,\Delta T_{c2}^{S-}) - 283] \\
& - (5 + s\,\Delta w_{c1}^{+})\,[(358 - s\,\Delta T_{c2}^{S-}) - (298 - s\,\Delta T_{c1}^{S-})]
\end{aligned}$$

(C) Stream existence:

$$\begin{aligned}
\mathrm{S_{h1}}: &\quad 4 - s\,\Delta w_{h1}^{-} \geq 0 \\
\mathrm{S_{h2}}: &\quad 6 - s\,\Delta w_{h2}^{-} \geq 0 \\
\mathrm{S_{c1}}: &\quad 5 - s\,\Delta w_{c1}^{-} \geq 0 \\
\mathrm{S_{c2}}: &\quad 10 - s\,\Delta w_{c2}^{-} \geq 0
\end{aligned}$$

(D) Prevent $T_p^S = T_{c2}^S$ from crossing any T_i^S or T_i^T:

$$\begin{aligned}
T_{h1}^S: &\quad 358 + s\,\Delta T_{c2}^{S+} \leq 390 - s\,\Delta T_{h1}^{S-} \\
T_{h1}^T: &\quad 358 - s\,\Delta T_{c2}^{S-} \geq 338 \\
T_{h2}^S: &\quad 358 + s\,\Delta T_{c2}^{S+} \leq 400 - s\,\Delta T_{h2}^{S-} \\
T_{h2}^T: &\quad 358 - s\,\Delta T_{c2}^{S-} \geq 283 \\
T_{c1}^S: &\quad 358 - s\,\Delta T_{c2}^{S-} \geq 298 + s\,\Delta T_{c1}^{S+} \\
T_{c1}^T: &\quad 358 + s\,\Delta T_{c2}^{S+} \leq 498 \\
T_{c2}^T: &\quad 358 + s\,\Delta T_{c2}^{S+} \leq 388
\end{aligned}$$

(E) Prevent pinch shifts to T_i^S:

Case B:

$$\begin{aligned}
T_{h1}^S: &\quad w_{h1}\left[\max(0, T_{h1}^S - T_{c2}^S) - \max(0, T_{h1}^S - T_{h1}^S)\right] \\
&\quad + w_{h2}\left[\max(0, T_{h1}^S - T_{c2}^S) - \max(0, T_{h1}^S - T_{h2}^S)\right] \\
&\leq w_{c1}\left[\max(0, T_{h1}^S - T_{c2}^S) - \max(0, T_{h1}^S - 498)\right] \\
&\quad + w_{c2}\left[\max(0, T_{h1}^S - T_{c2}^S) - \max(0, T_{h1}^S - 388)\right] \\
T_{h2}^S: &\quad w_{h1}\left[\max(0, T_{h2}^S - T_{c2}^S) - \max(0, T_{h2}^S - T_{h1}^S)\right] \\
&\quad + w_{h2}\left[\max(0, T_{h2}^S - T_{c2}^S) - \max(0, T_{h2}^S - T_{h2}^S)\right] \\
&\leq w_{c1}\left[\max(0, T_{h2}^S - T_{c2}^S) - \max(0, T_{h2}^S - 498)\right] \\
&\quad + w_{c2}\left[\max(0, T_{h2}^S - T_{c2}^S) - \max(0, T_{h2}^S - 388)\right] \\
T_{c1}^S: &\quad w_{h1}\left[\max(0, 338 - T_{c1}^S) - \max(0, T_{c2}^S - T_{c1}^S)\right] \\
&\quad + w_{h2}\left[\max(0, 283 - T_{c1}^S) - \max(0, T_{c2}^S - T_{c1}^S)\right] \\
&\leq w_{c1}\left[\max(0, T_{c1}^S - T_{c1}^S) - \max(0, T_{c2}^S - T_{c1}^S)\right]
\end{aligned}$$

where

$$\begin{aligned}
T_{h1}^S &= 390 + s\,\Delta T_{h1}^{S+} & \qquad w_{h1} &= 4 + s\,\Delta w_{h1}^{+} \\
T_{h2}^S &= 400 + s\,\Delta T_{h2}^{S+} & \qquad w_{h2} &= 6 + s\,\Delta w_{h2}^{+} \\
T_{c1}^S &= 298 + s\,\Delta T_{c1}^{S+} & \qquad w_{c1} &= 5 - s\,\Delta w_{c1}^{-} \\
T_{c2}^S &= 358 + s\,\Delta T_{c2}^{S+} & \qquad w_{c2} &= 10 - s\,\Delta w_{c2}^{-}
\end{aligned}$$

Case C: Same constraints as Case B, except

$$\begin{aligned} T_{h1}^S &= 390 - s\,\Delta T_{h1}^{S-} & w_{h1} &= 4 - s\,\Delta w_{h1}^- \\ T_{h2}^S &= 400 - s\,\Delta T_{h2}^{S-} & w_{h2} &= 6 - s\,\Delta w_{h2}^- \\ T_{c1}^S &= 298 - s\,\Delta T_{c1}^{S-} & w_{c1} &= 5 + s\,\Delta w_{c1}^+ \\ T_{c2}^S &= 358 - s\,\Delta T_{c2}^{S-} & w_{c2} &= 10 + s\,\Delta w_{c2}^+ \end{aligned}$$

(F) Nonnegative scale factor:

$$s \geq 0$$

The NLP is solved by examining the constraints one-by-one to determine the value of size ratio s when each constraint becomes active. The smallest value of s for which any constraint becomes active gives the resilience target. This procedure yields the results in Table 4.3. The resilience target is $s^* = 2.87$; the pinch shifts from the supply of stream S_{c2} to the supply of stream S_{h2} at a critical uncertainty of $s^*\Delta T_{h2}^{S+} = +28.7$ K and $s^*\Delta w_{h2}^+ = +1.43$ kW/K (i.e., at $T_{h2}^S = 428.7$ K after shifting to account for ΔT_m, and $w_{h2} = 7.43$ kW/K). This agrees with the graphical demonstration of the resilience target in Example 4.1 (Fig. 4.3). ■

4.3.3 Extension to Varying Minimum Approach Temperature

The economically optimal value of ΔT_m generally varies with the operating conditions in an uncertainty range. This section shows how the Class 1 resilience target can be extended to varying ΔT_m. In order to motivate this extension, we first consider the trade-off between the resilience target and *fixed* ΔT_m (i.e., ΔT_m fixed throughout the uncertainty range, but varied as a parameter while calculating the resilience target).

Figure 4.8 shows the resilience target as a function of ΔT_m for the stream data and reference uncertainty range of Example 4.2 (Table 4.1). Depending upon which

Table 4.3: Solution of the NLP for the Class 1 resilience target (Example 4.2).

Constraint	*Bound on Resilience Target*
A. Nonnegative Heating	5.67
B. Nonnegative Cooling	6.13
C. Stream Existence	
S_{h1}	∞
S_{h2}	12.00
S_{c1}	∞
S_{c2}	∞
D. Prevent T_p^S from crossing	
T_{h1}^S	∞
T_{h1}^T	∞
T_{h2}^S	4.20
T_{h2}^T	∞
T_{c1}^S	∞
T_{c1}^T	∞
T_{c2}^T	∞
E. Prevent pinch shift to	
Case B:	
S_{h1}	8.75
S_{h2}	2.87
S_{c1}	∞
Case C:	
S_{h1}	17.13
S_{h2}	4.20
S_{c1}	4.67

Resilience target = 2.87

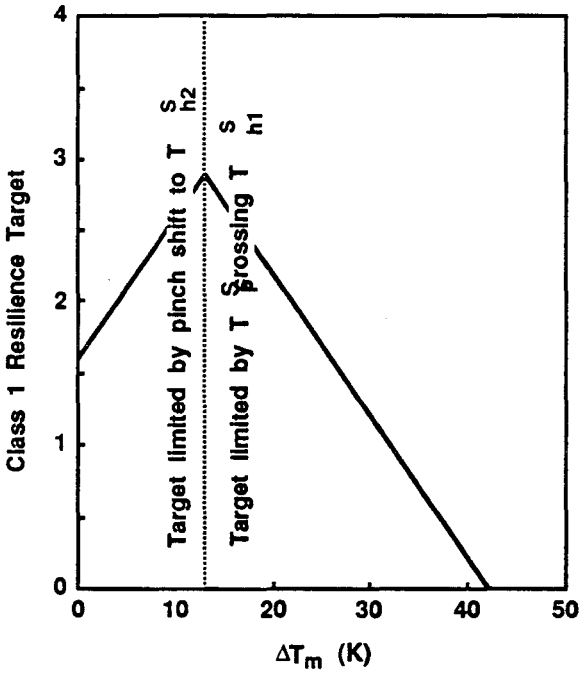

Figure 4.8: Trade-off between minimum approach temperature and the Class 1 resilience target (for data of Examples 4.1 and 4.2).

constraint is limiting, the resilience target increases or decreases linearly with increasing ΔT_m. For $\Delta T_m < 13$ K, the resilience target is limited by the pinch shifting from stream S_{c2} to stream S_{h2} for uncertainties in the Case B direction (cf., Fig. 4.3 for $\Delta T_m = 10$ K), and the resilience target increases with increasing ΔT_m. In this case, increasing ΔT_m moves the composite temperature-enthalpy curves apart, and larger uncertainties are required to cause the pinch shift. For $\Delta T_m > 13$ K, the resilience target is limited by pinch temperature T_p^S (p $\in$ MCA) crossing supply temperature T_{h1}^S (h1 $\in$ MHAB), and the target decreases with increasing ΔT_m. In this case increasing ΔT_m *decreases* the shifted supply temperature of hot stream S_{h1} ($T_{\mathrm{h1,shifted}}^S = T_{h1}^S - \frac{1}{2}\Delta T_m$), while *increasing* the shifted supply temperature of cold pinch-causing stream S_{c2} ($T_p^S = T_{\mathrm{c2,shifted}}^S = T_{c2}^S + \frac{1}{2}\Delta T_m$). This decreases the interval ($T_{\mathrm{h1,shifted}}^S - T_p^S$) over which the supply temperatures can vary before T_p^S crosses $T_{\mathrm{h1,shifted}}^S$, thus decreasing the resilience target.

In general, the Class 1 resilience target increases when increasing the value of ΔT_m used throughout the uncertainty range (i.e., as the composite temperature-enthalpy curves are shifted apart, larger uncertainties are required to cause zero heating or cooling, or a pinch shift). But when stream existence limits the resilience target, it is independent of ΔT_m (until another constraint becomes active). And when the resilience target is limited by pinch temperature T_p^S crossing a stream supply or target temperature, the target can increase or decrease with increasing ΔT_m depending upon which stream is limiting.

By using a worst case analysis, the Class 1 resilience target can be extended when ΔT_m varies with the operating conditions in an uncertainty range. In particular, since

the constraints in NLP (P1) can be examined one-by-one, they can each be evaluated for their worst case value of ΔT_m.

For Class 1 uncertainty ranges, each constraint in NLP (P1) either varies monotonically with ΔT_m, or is independent of ΔT_m. For the nonnegative heating and cooling constraints, the worst case value of ΔT_m is the smallest one associated with the uncertainty range since the minimum heating and cooling requirements decrease with decreasing ΔT_m. For the pinch shift constraints, the smallest value of ΔT_m is also the worst case since pinch shifts are more likely to occur when the composite curves are closer together. For the constraints to prevent pinch temperature T_p^S from crossing any supply or target temperature, the worst case ΔT_m may be the smallest or largest value of ΔT_m in the uncertainty range; which value of ΔT_m is worse can be determined by inspection, and may change if the uncertainty range becomes Class 2. For the stream existence constraints, any value of ΔT_m can be used since these constraints are independent of ΔT_m.

For a given size uncertainty range, reasonable bounds on ΔT_m can be determined by economic targeting for selected discrete points in the uncertainty range. The difficulty is that the ΔT_m bounds should correspond to the target uncertainty range, which is not known *a priori*. Thus calculating the Class 1 resilience target with varying ΔT_m requires iteration: (1) assume a size for the target uncertainty range; (2) determine ΔT_m bounds for the assumed uncertainty range; (3) with these bounds on ΔT_m, calculate the Class 1 resilience target by examining one-by-one each of the constraints of NLP (P1) for its worst case value of ΔT_m; (4) determine ΔT_m bounds for the new target uncertainty range and repeat. By calculating the Class 1 resilience

target for different *fixed* values of ΔT_m, one can obtain a good initial guess for the size of the target uncertainty range with varying ΔT_m.

4.3.4 Extension to Nonminimum Utilities

The Class 1 resilience target can be extended to relaxed (nonminimum) utility consumption. In this chapter, we follow Saboo *et al.* (1985) in using a factor to relax the utility requirement:

$$H = (1 + \alpha)H_{\min} \tag{4.7}$$

where $H_{\min}$ is the minimum heating required for given nominal or uncertain stream data [NLP (P1), constraint (A)], α is a nonnegative factor by which $H_{\min}$ is to be relaxed, and H is the total (relaxed) heating allowed for the given stream data.

For the nominal stream data of Examples 4.1 and 4.2 (Table 4.1), Fig. 4.9 shows how the pinch behavior diagram changes as α is increased. (Fig. 4.3 shows the pinch behavior diagram for $\alpha = 0$.) The Class 1 region expands in certain directions as α is increased. Thus as utility consumption is relaxed, the Class 1 resilience target increases—or is constant—depending upon which constraint limits the target.

The meaning of a pinch shift with increased utility consumption deserves some explanation. Allowing increased heating moves the hot and cold composite curves apart from each other by $\alpha H_{\min}$ kW; in particular, the composite curves are separated from each other by $\alpha H_{\min}$ kW at the original pinch. We say that the pinch shifts if a new pinch appears with 0 kW separation between the hot and cold composite curves (i.e., the composite curves touch at the new pinch).

In general, the nonnegative cooling and pinch shift constraints are relaxed as α

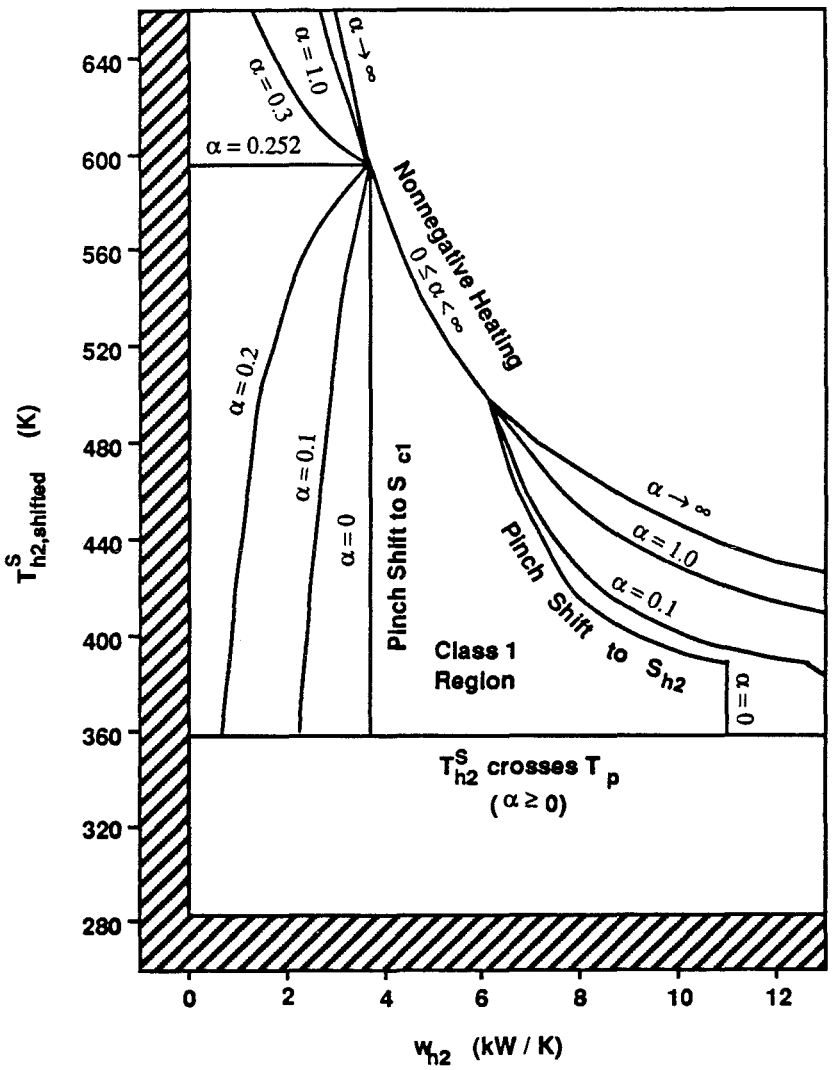

Figure 4.9: Class 1 region expands as utility requirement is relaxed (data of Examples 4.1 and 4.2).

is increased (since the composite curves are shifted apart by $\alpha H_{\min}$ kW, and larger uncertainties are required to eliminate the cooling requirement or to cause a new pinch). The nonnegative heating constraint and the constraints preventing pinch temperature T_p^S from crossing any supply or target temperature are independent of α. The nonnegative heating constraint is *not* relaxed as α is increased because as $H_{\min}$ goes to zero, allowed heating H (equation 4.7) also goes to zero independent of (finite) α. If extra heating were limited by an additive factor ($H = H_{\min} + \beta$), then the nonnegative heating constraint would be relaxed with increasing β. The nonnegative cooling constraint does relax as α is increased because extra cooling *is* limited by an additive factor ($C = C_{\min} + \alpha H_{\min}$).

NLP (P1) for calculating the Class 1 resilience target can be extended to relaxed utility consumption as follows:

$$s^*(\alpha) = \max_s s \qquad \textbf{(P2)}$$

subject to

(A) Nonnegative heating: $(1 + \alpha)H_{\min} \geq 0$

(B) Nonnegative cooling: $C_{\min} + \alpha H_{\min} \geq 0$

(C) Stream existence: same as NLP (P1)

(D) Prevent T_p^S from crossing any supply or target temperature: same as NLP (P1)

(E) Prevent pinch shifts to any supply temperature:

$$\begin{aligned} Q_h^A|_{T_i^S} &\leq Q_c^A|_{T_i^S} + \alpha H_{\min} \quad \text{for } i \in \text{MHAA, MHAB, MCAA} \\ Q_h^B|_{T_i^S} &\leq Q_c^B|_{T_i^S} + \alpha H_{\min} \quad \text{for } i \in \text{MHBB, MCAB, MCBB} \end{aligned}$$

(F) Nonnegative scale factor: $s \geq 0$

where expressions for $H_{\min}$ and $C_{\min}$ are given in constraints (A) and (B) of NLP (P1), and Q_h^A, Q_h^B, Q_c^A and Q_c^B are defined by equations (4.1)–(4.4).

4.4 Synthesis of Resilient Heat Exchanger Networks

As mentioned before, previous investigators have developed analytic tools to quantify the resilience of a HEN structure *after synthesis.* The Class 1 resilience target presented in Section 4.3 is an analytical device for predicting *before synthesis* the maximum resilience achievable by practical HENs. In this section, we discuss two issues important *during synthesis* of resilient HENs:

- the observation that HEN structures requiring minimum or near-minimum area for *nominal* stream conditions provide a good starting point for synthesizing resilient HENs;
- implications of the Class 1 resilience target for synthesis of resilient HENs, and use of the Class 1 resilience target as a synthesis tool.

4.4.1 Minimum - Nominal - Area Structures — A Good Starting Point for Synthesizing Resilient Networks

Townsend and Morari (1984) observed that maximum resilience is an objective compatible with minimum *nominal* area—similar HEN structures can achieve both. We wish to clarify this observation.

For fixed stream conditions, a minimum-area HEN structure can be synthesized by mimicking the composite curves (assuming identical heat transfer coefficients in all exchangers). For example, for the nominal stream data of Example 4.1 (Table 4.1), a simplified version of the HEN structure in Fig. 4.1 (i.e., Fig. 4.1 *without* the bypassed exchangers indicated by dashed lines) mimics the nominal composite curves (Fig. 4.2) and thus achieves the minimum area target calculated for the *nominal* stream data. However, this simplified structure is also the basis for a more resilient HEN; by adding the bypassed exchangers shown in Fig. 4.1, resilience is achieved for *all* physically meaningful supply temperatures, target temperatures, heat capacities and flow rates. A good distribution of temperature driving forces in the simplified HEN structure leads to minimum area, and makes the simplified structure a good starting point for synthesizing the more resilient HEN.

This observation suggests that resilient HENs more practical than that in Fig. 4.1 can be synthesized with a two stage strategy:

1. With no regard for resilience, synthesize a HEN structure for fixed (e.g., nominal) stream data which, when sized, requires minimum or near-minimum area for the *fixed* stream conditions.

Table 4.4: Resilience measures, area requirements (for *nominal* stream conditions), and their corresponding targets for the three HEN structures in Fig. 4.10.

HEN Structure	*Resilience Measure* (—)	*Percent of Resilience Target*	ΣUA kW/K	*Percent over Area Target*
1	0.47	28.3	59.9	25.5
2	1.55	93.4	56.2	17.6
3	1.66	100.0	52.4	9.7
Target	1.66		47.8	

2. Oversize and add bypasses to some of the exchangers in this structure (or to new exchangers added to this structure) to achieve the desired amount of resilience.

While this strategy gives resilient HEN structures with minimum or near-minimum area for *fixed* stream conditions, this strategy does not necessarily minimize the area of the network after overdesigning it to achieve resilience. And since this strategy tries to achieve a uniform driving force distribution throughout the network rather than just for matches with a particular stream, it tends to give more resilient HEN structures when the uncertainties in supply temperatures and flow rates are distributed somewhat uniformly among all streams rather than just in one stream.

Example 4.3 *(adopted from Townsend and Morari, 1984).* Three different HEN structures synthesized for the same nominal stream data are shown in Fig. 4.10. Each of these structures requires less area for *nominal* stream conditions than the previous one—25.5%, 17.6% and 9.7% excess area, respectively, compared to the nominal area target (Table 4.4). Based on the observation discussed above, we expect structure 3 to be the best starting point for synthesizing a resilient HEN. To test this expectation, we can calculate a "resilience measure" for each structure with respect to a ΔT_m of

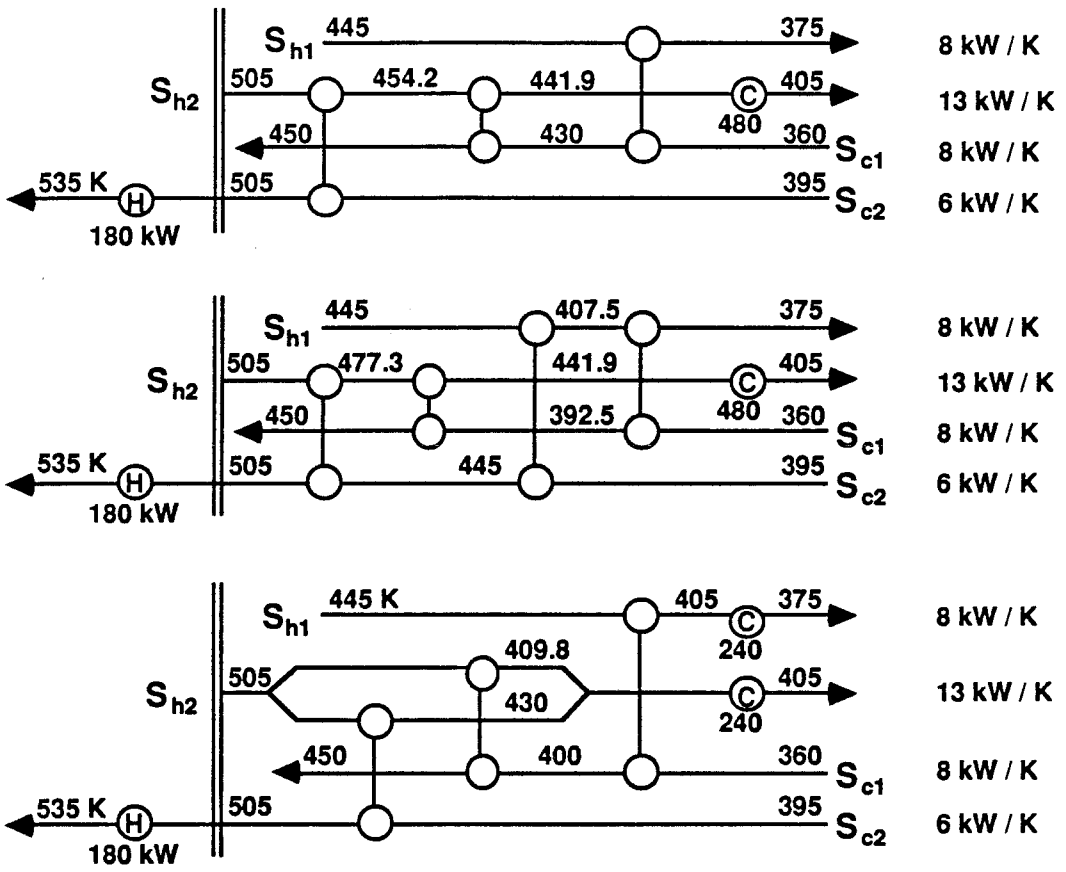

Figure 4.10: HEN structures 1, 2, and 3 for Example 4.3 (ΔT_m = 10 K; steam available at 570 K; cooling water range 290–300 K).

10 K and a reference uncertainty range of ± 10 K in every stream supply temperature. This resilience measure is the size ratio of the largest uncertainty range, relative to the reference uncertainty range, for which the given structure is resilient.[7] The resilience measure is used to quantify *after synthesis* the resilience of a given structure; the Class 1 resilience target is used *before synthesis* to predict the maximum resilience measure achievable with "practical" HEN structures.

The resilience measure for each of the three HEN structures in Fig. 4.10 is listed in Table 4.4. As expected, structure 3 is most resilient—it achieves 100% of the Class 1 resilience target. Structures 1 and 2 achieve 28.3% and 93.4% of the resilience target, respectively.

The individual exchangers in these structures must still be sized to achieve the desired amount of resilience. But structure 1 requires the most overall area for nominal stream conditions and, based on its low resilience measure, is likely to require excessive area in order to achieve resilience throughout the specified reference uncertainty range. Either structure 2 or structure 3 should be a good starting point for designing a (sized) HEN resilient in the reference uncertainty range. Note that both of these structures contain one extra unit compared to structure 1. In this example, the extra unit is needed in order to reduce the overall area required for *nominal* stream conditions and to improve the resilience measure. ■

[7]This "resilience measure" is actually the "flexibility index" defined by Swaney and Grossmann (1985a) with the utility consumption constraint applied at every point in the uncertainty range instead of just at the corner points. However, we are calling it a resilience measure instead of the flexibility index to be consistent with the distinction between resilience and flexibility proposed in Section 4.1.

4.4.2 Use of the Class 1 Resilience Target as a Synthesis Tool

In the synthesis of resilient HENs, use of the Class 1 resilience target offers two important features:

- The size of the resilience target (compared to 1.0) tells the process engineer if the reference uncertainty range is Class 1 or Class 2, and thus predicts qualitatively the difficulty of synthesizing a resilient HEN for the reference uncertainty range.
- Calculation of the resilience target identifies the critical uncertainty point most likely to limit resilience, and thus identifies those supply temperatures and flow rates (in addition to the nominal ones) to which the process engineer should pay special attention.

To use the size of the Class 1 resilience target s^* to judge the difficulty of synthesizing a HEN resilient in a specified reference uncertainty range, consider three cases: (1) $s^* \gg 1$, (2) $s^* \gtrsim 1$, and (3) $s^* < 1$.

(1) $s^* \gg 1$. In this case, the reference uncertainty range is Class 1 and is much smaller in size than the target uncertainty range. Since the uncertainties in the reference uncertainty range are relatively small (compared to the largest uncertainties in the target uncertainty range), traditional synthesis methods for fixed (nominal) stream conditions should be sufficient. Of course, after designing the HEN, one should verify whether or not it is resilient in the desired uncertainty range.

(2) $s^* \gtrsim 1$. Now the reference uncertainty range is Class 1, but is close in size to the target uncertainty range. Since the reference uncertainty range is Class 1, one

can still "have it all;" that is, one can still synthesize a HEN structure with a "practical" number of units (qualitatively, few more units than the number required for nominal conditions) which is resilient—while using specified utilities—throughout the reference uncertainty range. However, since the reference uncertainty range is close in size to the target uncertainty range, synthesis may be more difficult. Example 4.4 below illustrates one crude procedure for synthesizing a resilient HEN in this case. This procedure uses the critical uncertainty point as well as the nominal stream data to synthesize the HEN structure.

(3) $s^* < 1$. Now the reference uncertainty range is Class 2 and one can no longer "have it all"—some trade-off must be made. The most common trade-off is to require minimum utility consumption at the nominal operating point and at the corner points of the uncertainty range, but to allow extra utility consumption at other points in the uncertainty range. Alternatively, one could require minimum utility consumption throughout the uncertainty range, with a consequent increase in the number of units (as demonstrated in Example 4.1). Or one could decrease the size of the reference uncertainty range (e.g., by imposing tighter control on the surrounding process).

Unlike the economic HEN synthesis targets for nominal stream conditions, the Class 1 resilience target is a "soft" target—the process engineer can actually exceed the target by making one of the trade-offs discussed above. Whether the process engineer chooses to meet, not meet, or exceed the resilience target depends upon economic factors, including the cost of *not* being resilient (e.g., lost production). Likewise, whether or not the engineer chooses to meet the (nominal) economic targets depends upon resilience (as well as safety, controllability, etc.).

By calculating the Class 1 resilience target, the process engineer can identify the critical uncertainty point and critical constraint (nonnegative heating or cooling, pinch shift, etc.). This uncertainty point and constraint limit the resilience of a completely countercurrent HEN structure able to mimic the composite curves; thus they seem the most likely uncertainty point and constraint to limit the resilience of a practical but well designed (almost completely countercurrent) HEN structure.

The following example demonstrates, by means of a crude synthesis procedure, how the Class 1 resilience target can be used as a synthesis tool. By using the Class 1 resilience target to identify the critical uncertainty point and constraint, the process engineer can consider resilience *during* the early stages of synthesizing a resilient, economic HEN, rather than adding resilience *after* synthesis of an economic (for nominal conditions) HEN. Knowledge of the critical uncertainty point makes synthesis easier; by synthesizing a base case design (the "merged" HEN structure in the following example) which is feasible for the critical uncertainty point as well as for the nominal stream data, the number of iterations (evolutionary network modifications) to synthesize a HEN structure resilient throughout the specified uncertainty range is generally reduced. Knowledge of the critical constraint (e.g., appearance of a second pinch) tells the process engineer exactly where to place exchangers and stream splits in order to best achieve resilience.

Example 4.4 For the nominal stream data of Examples 4.1 and 4.2 (Table 4.1), synthesize a "practical" HEN *structure* which is as resilient as possible for uncertainties in the supply temperature and heat capacity flow rate of stream S_{h2}, based on reference uncertainties of $\Delta T_{h2}^{S} = \pm 10$ K and $\Delta w_{h2} = \pm 0.5$ kW/K. In other words,

synthesize a HEN structure to achieve the Class 1 resilience target based on these uncertainties. [Note that here we have specified the reference uncertainties to establish the relative sizes of the two uncertainties (i.e., to establish the aspect ratio of the rectangular reference uncertainty range), rather than to specify absolute sizes of the uncertainties for which to design.]

Step 1: Calculate the Class 1 resilience target. The target was determined graphically in Example 4.1 and calculated with an NLP in Example 4.2. The target, s^* = 2.87, is limited by a critical uncertainty point of $s^*\Delta T_{h2}^S$ = +28.7 K and $s^*\Delta w_{h2}$ = +1.43 kW/K (i.e., T_{h2}^S = 428.7 K after shifting to account for ΔT_m, and w_{h2} = 7.43 kW/K), and a critical constraint involving a pinch shift from stream S_{c2} to stream S_{h2} (Figs. 4.3 and 4.5).

Step 2: Synthesize a HEN structure which would require minimum or near-minimum area for the critical uncertainty point. Since the critical uncertainty point limits resilience, it is the uncertainty point with the tightest design constraints (in this case due to the appearance of simultaneous pinches at streams S_{c2} and S_{h2}). Thus we synthesize for this point before considering the nominal stream data. A structure obtained by the pinch design method (Linnhoff and Hindmarsh, 1983; Linnhoff *et al.*, 1982) is shown in Fig. 4.11(a). The four shaded exchangers are required to satisfy ΔT_m at the pinch caused by stream S_{c2}; the blackened exchanger and heater are required to satisfy ΔT_m at the pinch caused by stream S_{h2}.

Step 3: Synthesize a near-minimum-area HEN structure for the nominal stream data as similar as possible to the structure synthesized for the critical uncertainty point. Such a structure is shown in Fig. 4.11(b). The shaded exchangers are required

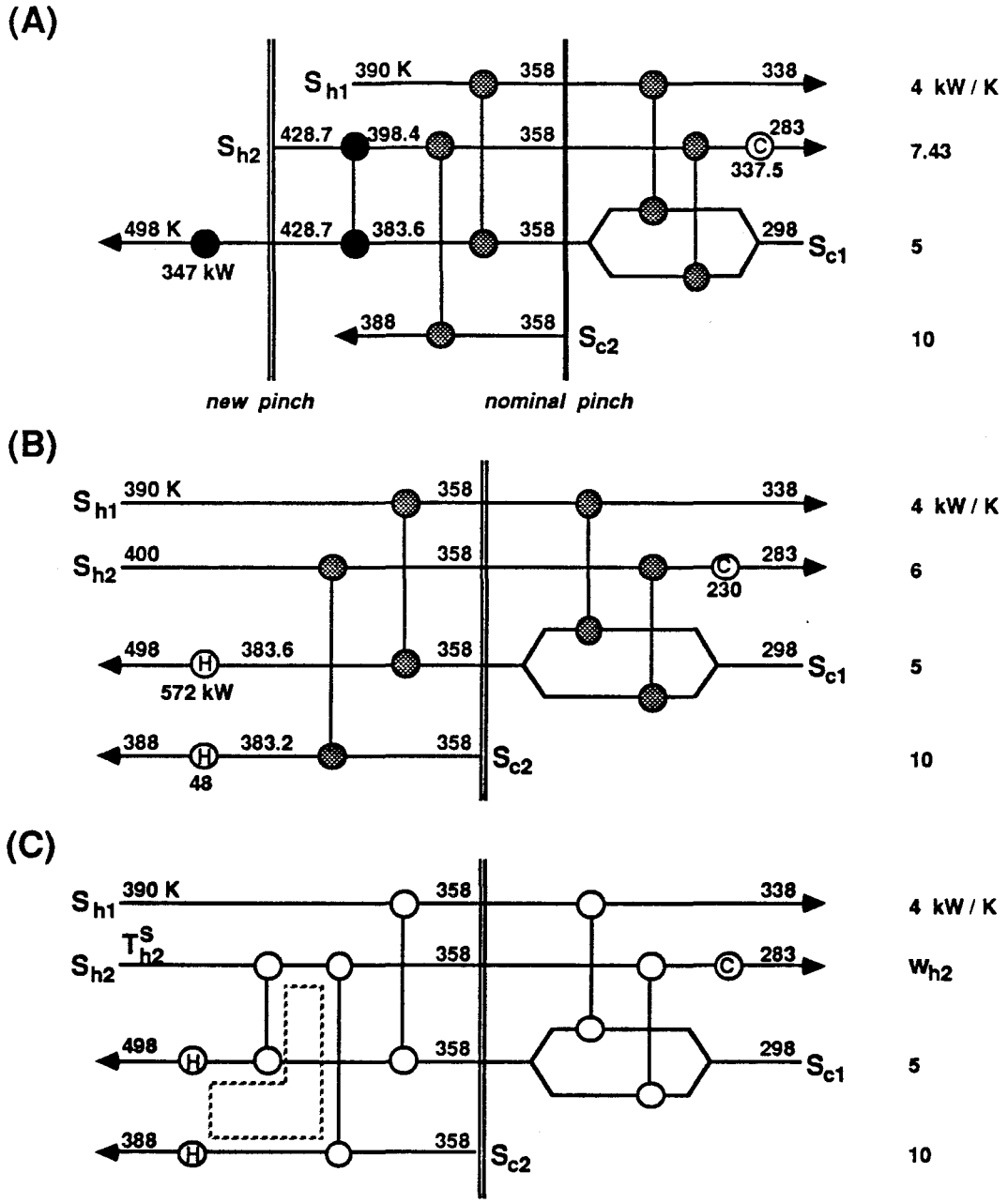

Figure 4.11: HEN structures for Example 4.4: (a) synthesized for critical uncertainty; (b) synthesized for nominal stream data; (c) merged structure which achieves the Class 1 resilience target.

to satisfy ΔT_m at the pinch.

Step 4: Merge the two separate structures into a single one. In this case, merging is trivial because of the strong similarity between the two designs; we merely add the heater on stream S_{c2} in the nominal structure to the HEN synthesized for the critical uncertainty point. The resulting structure is shown in Fig. 4.11(c).

Step 5: Test the resilience of the merged structure. (Before this test, we only know that the merged structure is feasible for both the nominal stream data and the critical uncertainty point. We do not know yet if it is resilient throughout the desired uncertainty range.) The resilience measure of the merged HEN structure is 2.87. Thus the structure achieves the Class 1 resilience target and is resilient throughout the target uncertainty range.

Step 6: Try to reduce the number of units in the merged HEN structure (e.g., by loop breaking: Su and Motard, 1984; Engel and Morari, 1988). The only loop in this structure is shown by the dashed lines in Fig. 4.11(c). (The pinch caused by stream S_{c2} occurs for every point in the uncertainty range. We are not considering loops which straddle this pinch so that we can maintain minimum utility consumption throughout the uncertainty range.) Eliminating any unit in this loop except the exchanger matching streams S_{h2} and S_{c1} reduces the resilience measure to zero (i.e., the structure becomes infeasible even for nominal conditions); eliminating the S_{h2}–S_{c1} match reduces the resilience measure to 0.57. Thus no unit can be deleted from the merged HEN structure without a loss of resilience. ■

4.5 Summary

Two resilience targets are presented. The general resilience target—where no constraints are placed upon the size (number of units) or complexity (number of stream splits) of a HEN—is arbitrarily large; given any nominal stream data, a HEN structure can always be synthesized which is resilient for *all* physically meaningful operating conditions (supply temperatures, target temperatures and heat capacity flow rates) while using minimum utilities. However, this general resilience target is not very practical: (1) large, complex, costly HEN structures are generally required to achieve it; and (2) designing for all physically meaningful operating conditions is unrealistic (overly ambitious).

A more practical resilience target—one which is achievable with practical HEN structures with few more units or stream splits than that required for nominal stream conditions—is defined by restricting it to Class 1 (Saboo and Morari, 1984) uncertainty ranges. An uncertainty range is Class 1 if the uncertainties are small enough that (1) the pinch-causing stream, and the stream populations above and below the pinch, are constant throughout the uncertainty range if the problem is pinched; or (2) the problem remains threshold heating (or cooling) throughout the uncertainty range if the problem is unpinched. The Class 1 resilience target corresponds to the largest possible Class 1 uncertainty range.

For simple problems with few uncertain supply temperatures and flow rates, the Class 1 resilience target can be determined by plotting the composite curves for different values of the uncertain parameters. For more complicated problems, NLP (P1) can be formulated to model the composite curves and to calculate the resilience

target. NLP (P1) is easily solved by examining the constraints one-by-one in their worst case uncertainty directions.

The Class 1 resilience target predicts (qualitatively) the difficulty of synthesizing a HEN structure resilient in a specified uncertainty range. If the specified uncertainty range is Class 1 (smaller than the target uncertainty range), then a resilient minimum-utilities HEN structure with a "practical" number of units can be synthesized for the specified range. If the specified uncertainty range is Class 2 (larger than the target uncertainty range), then some trade-offs must be made: (1) minimum utility consumption might be required only at the corner points of the uncertainty range instead of throughout the uncertainty range; (2) a larger number of units might be allowed; or (3) the size of the uncertainties might be reduced by imposing tighter control on the surrounding process.

By calculating the Class 1 resilience target, the process engineer can identify the critical uncertainty point (supply temperatures and flow rates) and constraint (e.g., appearance of a new pinch) most likely to limit resilience. A good starting point for synthesis of a resilient HEN structure is to synthesize minimum or near-minimum area structures for the nominal stream data and the critical uncertainty point, and then to merge these structures. Knowledge of the critical constraint tells the process engineer exactly where to place exchangers and stream splits in order to best achieve resilience.

4.6 References

[1] Duran, M. A. and I. E. Grossmann, Simultaneous Optimization and Heat Integration of Chemical Processes, *AIChE J.*, **32**, 123 (1986).

[2] Engel, P. and M. Morari, Limitations of the Primary Loop-Breaking Method for Synthesis of Heat Exchanger Networks, *Comp. Chem. Eng.*, **12**, 307 (1988).

[3] Floudas, C. A. and I. E. Grossmann, Automatic Generation of Multiperiod Heat Exchanger Network Configurations, *Comp. Chem. Eng.*, **11**, 123 (1987a).

[4] Floudas, C. A. and I. E. Grossmann, Synthesis of Flexible Heat Exchanger Networks with Uncertain Flow Rates and Temperatures, *Comp. Chem. Eng.*, **11**, 319 (1987b).

[5] Grossmann, I. E. and C. A. Floudas, Active Constraint Strategy for Flexibility Analysis in Chemical Processes, *Comp. Chem. Eng.*, **11**, 675 (1987).

[6] Grossmann, I. E. and M. Morari, Operability, Resiliency and Flexibility—Process Design Objectives for a Changing World, paper presented at *2nd Int. Conf. on Found. of Computer-Aided Process Design*, Snowmass, CO (1983).

[7] Linnhoff, B. and E. Hindmarsh, The Pinch Design Method for Heat Exchanger Networks, *Chem. Eng. Sci.*, **38**, 745 (1983).

[8] Linnhoff, B. and E. Kotjabasakis, Downstream Paths for Operable Process Design, *Chem. Eng. Prog.*, **82** (5), 23 (May 1986).

[9] Linnhoff, B., D. W. Townsend, D. Boland, G. F. Hewitt, B. E. A. Thomas, A. R. Guy and R. H. Marsland, *A User Guide on Process Integration for the Efficient Use of Energy*, Pergamon Press, Elmsford, NY (1982).

[10] Marselle, D. F., M. Morari and D. F. Rudd, Design of Resilient Processing Plants—II. Design and Control of Energy Management Systems, *Chem. Eng. Sci.*, **37**, 259 (1982).

[11] Saboo, A. K. and M. Morari, Design of Resilient Processing Plants—IV. Some New Results on Heat Exchanger Network Synthesis, *Chem. Eng. Sci.*, **39**, 579 (1984).

[12] Saboo, A. K., M. Morari and R. D. Colberg, Resilience Analysis of Heat Exchanger Networks—I. Temperature Dependent Heat Capacities, *Comp. Chem. Eng.*, **11**, 399 (1987a).

[13] Saboo, A. K., M. Morari and R. D. Colberg, Resilience Analysis of Heat Exchanger Networks—II. Stream Splits and Flow Rate Variations, *Comp. Chem. Eng.*, **11**, 457 (1987b).

[14] Saboo, A. K., M. Morari and D. C. Woodcock, Design of Resilient Processing Plants—VIII. A Resilience Index for Heat Exchanger Networks, *Chem. Eng. Sci.*, **40**, 1553 (1985).

[15] Su, J. L. and R. L. Motard, Evolutionary Synthesis of Heat Exchanger Networks, *Comp. Chem. Eng.*, **8**, 67 (1984).

[16] Swaney, R. E. and I. E. Grossmann, An Index for Operational Flexibility in Chemical Process Design—I. Formulation and Theory, *AIChE J.*, **31**, 621 (1985a).

[17] Swaney, R. E. and I. E. Grossmann, An Index for Operational Flexibility in Chemical Process Design—II. Computational Algorithms, *AIChE J.*, **31**, 631 (1985b).

[18] Townsend, D. W. and M. Morari, Resiliency of Heat Exchanger Networks: An Objective Compatible with Minimum Cost, paper presented at *AIChE Ann. Mtg.*, San Francisco (1984).

Chapter 5

Use of HEN Synthesis Targets to Predict the Resilience–Cost Trade-off

5.1 Introduction

Chapter 4 presented a resilience target, the Class 1 resilience target, to predict the largest uncertainty range, scaled with respect to a reference uncertainty range, for which a "practical" HEN can be synthesized. This resilience target can be used to roughly predict the trade-off between resilience and utilities, and resilience and ΔT_m (constant throughout an uncertainty range, but varied parametrically while calculating the resilience target).

In addition, previous investigators have developed methods which can predict the trade-off between cost and *flexibility* [the ability to operate for multiple, discrete

"periods of operation" (Section 4.1)]. Floudas and Grossmann (1986) developed a procedure for synthesis of flexible HENs using several optimization steps. Two of these steps involve utility and units targeting for multiple periods of operation. By repeating these utility and units targeting algorithms for more widely spaced operating points, the trade-offs between utilities and flexibility, and units and flexibility, can be predicted. Floudas' and Grossmann's algorithms, however, require the same value of ΔT_m for each operating point. Jones (1987) presented a method to minimize a total (annualized) cost target for flexible HENs, where for each period of operation the optimal utilities are determined as a function of area (rather than ΔT_m).

To synthesize *resilient* HENs [able to operate in a continuous range of operating conditions (Section 4.1)], Floudas and Grossmann (1987) combined the synthesis procedure of Floudas and Grossmann (1986) with an active contraint strategy to identify the critical points (analogous to "periods of operation") which limit resilience. By applying their utility and units targeting algorithms (along with the active constraint strategy at the "stage of matches") for several different size uncertainty ranges, one can predict the trade-off between utilities and resilience, and units and resilience. [However, Floudas and Grossmann (1987) require minimum utilities only for specified discrete points in each uncertainty range, rather than throughout the uncertainty range.]

The application of Floudas' and Grossmann's algorithms (1987) to predict the trade-offs between resilience and utilities, and resilience and units, is limited to a single, fixed value of ΔT_m for all uncertainty ranges. However, the economically optimal value of ΔT_m varies with operating conditions (Ahmad and Linnhoff, 1984),

even if one does not consider the effect of resilience upon cost. In addition, with the Class 1 resilience target the process engineer cannot specify how ΔT_m should vary with operating conditions—ΔT_m must be fixed throughout the uncertainty range, or allowed to vary between some upper and lower bounds with no specification on how ΔT_m should vary between these bounds (Section 4.3.3). (Another problem with the Class 1 resilience target is that it is difficult to determine reasonable bounds on ΔT_m before calculating the target.)

For fixed operating conditions, it is common to parameterize the HEN synthesis targets in terms of ΔT_m. By doing this, one can evaluate the trade-offs between utilities, area, and number of units, and can combine the utility, area and units targets to predict an overall cost target (Ahmad and Linnhoff, 1984) as in Fig. 5.1. However, since the optimum value of ΔT_m changes with operating conditions, this parameterization causes difficulties when evaluating the economic (and resilience) trade-offs for varying conditions. To avoid this difficulty, we parameterize the HEN synthesis targets in terms of area rather than ΔT_m. This is based on the fact that an installed HEN must operate with fixed total area as conditions change, rather than with fixed (or controlled) ΔT_m.

This chapter introduces a procedure for using the HEN synthesis targets, parameterized in terms of area, to predict the trade-off between cost and resilience. However, the goal of this chapter is not to present the "ultimate" tractable procedure for predicting the trade-off, but merely to show—by example—one simple procedure in order to present some initial ideas and to motivate some suggestions for future research.

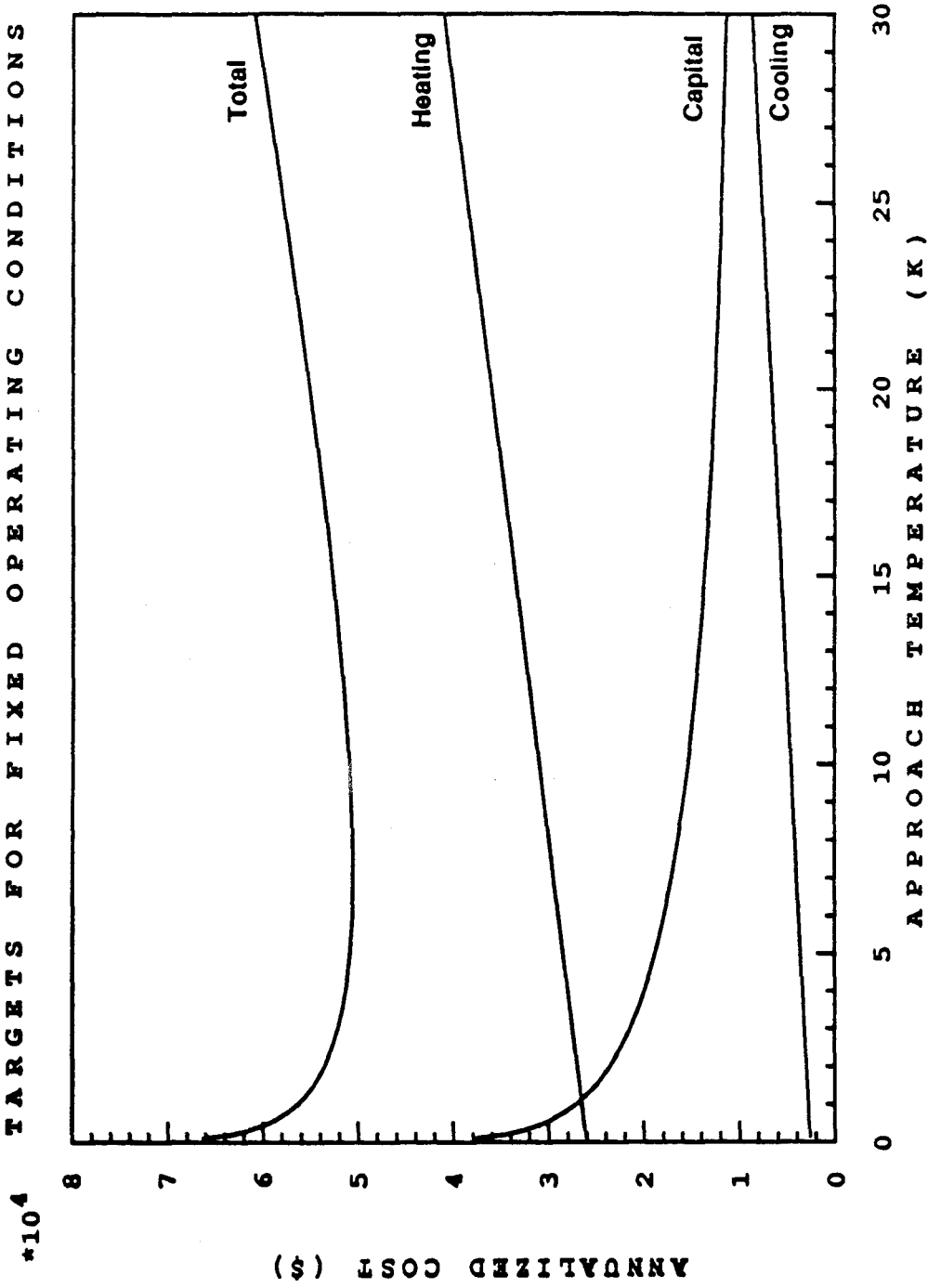

Figure 5.1: Utility, capital (area and number of units), and cost targets for fixed operating conditions parameterized in terms of ΔT_m.

5.2 The General Resilience – Cost Trade-off Problem

The general problem of predicting the trade-off between HEN cost and resilience might be stated as follows:

Given:

- *nominal supply temperatures, target temperatures, flow rates, and heat transfer coefficients (as a function of flow rate)*
- *acceptable ranges for the target temperatures*
- *known heat capacities*
- *temporal probability distributions for the uncertain supply temperatures, flow rates, and heat transfer coefficients (to take into account fouling as well as uncertainty in the nominal heat transfer coefficients), where several distributions with different spreads (e.g., size of uncertainty corresponding to two standard deviations) are given for each uncertain parameter*
- *utility and capital cost correlations for the exchangers, heaters and coolers*
- *costs of not being resilient (e.g., lost production, off-spec product, etc.)*

predict, before synthesis, a total annualized cost (TAC) target for the construction and operation of a HEN as a function of the different spreads in

the uncertainty probability distribution functions, where the TAC includes the cost of not being resilient. The optimum amount of resilience is that at which minimum TAC occurs.

According to this problem statement, several uncertainty distributions with different "spreads" should be given. The trade-off between cost and resilience is evaluated over these different size spreads. Actually, the problem statement could be made even more general by considering uncertainties in the heat capacities and in the cost data.

To solve this general resilience–cost trade-off problem, the following procedure might be used:

1. Choose several different HEN areas for which the corresponding heating, cooling, units and TAC targets will be calculated. [These HEN areas are used in place of ΔT_m to parameterize the HEN synthesis targets (e.g., Fig. 5.15).] These network areas should include the extra area installed in exchangers oversized to achieve resilience, as well as the area nominally required at each operating point.

2. For each temporal uncertainty probability distribution (with different spread), calculate a target for the number of units, and targets for the expected value of heating, cooling and TAC (where the TAC includes the cost of not being resilient), as a function of the parameter area. The optimum area and number of units, and expected values of heating and cooling, occur at minimum TAC.

3. Plot, as a function of the spread of the uncertainty distributions, the minimum TAC determined for each distribution. The optimum amount of resilience is the spread for which the smallest TAC occurs.

5.3 Procedure for Solving a Simplified Resilience–Cost Trade-off Problem

There are several difficulties with the general resilience–cost trade-off problem that cause the previous procedure to be, in general, intractable:

(1) While the process engineer may have a good estimate for the temporal distribution of a few discrete operating points (e.g., different production schedules required to satisfy a marketing campaign), the temporal distribution over a continuous range of operating conditions (e.g., due to uncertainties in the operating behavior of the surrounding process) can be very difficult to estimate. To avoid this difficulty, we specify a reference uncertainty range like that used to calculate the resilience target in Chapter 4 (with no specified temporal distribution for the conditions within this range), and calculate the trade-off between cost and the size of uncertainty ranges scaled with respect to this reference uncertainty range.

(2) The costs of not being resilient may be difficult to estimate compared to the difficulty of estimating capital and utility costs. To avoid this problem, we simply peform a sensitivity analysis on the cost of capital and utilities (excluding the cost of not being resilient) with respect to resilience, rather than minimizing total cost (including the cost of not being resilient). In particular, we seek the largest amount

of resilience for which the marginal TAC [the increase in TAC—based on capital and utility costs—per unit of increase in resilience (scale factor for the scaled uncertainty ranges)] remains acceptable.

(3) Uncertainties in heat transfer coefficients (especially as a function of flow rate) are much more difficult to handle than uncertainties in supply temperatures and flow rates (at least when using or extending any of the existing methods for targeting or synthesis of HENs for fixed or varying operating conditions). Thus we only consider the uncertainties in supply temperatures and flow rates, and not any uncertainties in heat transfer coefficients.

Thus, we solve a simplified resilience–cost trade-off problem in which we base the trade-off between TAC and resilience on uncertainty ranges scaled with respect to a reference uncertainty range, and where we examine marginal TAC excluding the costs of not being resilient. The following example illustrates one crude procedure for solving the simplified trade-off problem.

Example 5.1 Consider the nominal stream and cost data in Table 5.1. This is the same stream data as that used for the resilience target examples (Examples 4.1 and 4.2) in Chapter 4, except that the stream data are no longer shifted to account for ΔT_m. In these previous examples, we obtained a Class 1 resilience target of 2.87, based on a fixed ΔT_m of 10 K and a reference uncertainty range of

$$\Delta T_{h2}^S = \pm 10 \text{ K}$$

$$\Delta w_{h2} = \pm 0.5 \text{ kW/K}$$

Table 5.1: Nominal stream and cost data for Example 5.1.

Stream	*Supply Temperature* (K)	*Target Temperature* (K)	*Heat Capacity Flow Rate* (kW/K)	*Film Heat Transfer Coefficient* (kW/m^2 K)
H1	395	343	4.0	2.0
H2	405	288	6.0	2.0
C1	293	493	5.0	2.0
C2	353	383	10.0	2.0
Steam	520	520		2.0
Water	278	288		2.0

Heating utility cost: \$50/kW yr
Cooling utility cost: \$20/kW yr
Exchanger capital cost: $1100A^{0.65}$ \$, where A is in m^2

In other words, for this stream data (with $\Delta T_m = 10$ K), the largest Class 1 uncertainty range is

$$376.3 \leq \quad T_{h2}^S \quad \leq 433.7 \text{ K}$$

$$4.57 \leq \quad w_{h2} \quad \leq 7.43 \text{ kW/K}$$

In the current example, we calculate the resilience–cost trade-off based on the same reference uncertainty range as above. However, rather than using a fixed ΔT_m of 10 K, we parameterize the HEN synthesis targets in terms of area and allow ΔT_m to vary. To determine the resilience–cost trade-off, we proceed as follows:

Step 1: As a function of the uncertain supply temperatures and flow rates, calculate the heating and cooling targets corresponding to selected network areas. Figures 5.2–5.12 show, for several values of area between 34 and 100 m^2, heating target profiles as a function of uncertain parameters T_{h2}^S and w_{h2}. In these figures, the nominal operating point is indicated with an 'x'. The dashed rectangles represent different

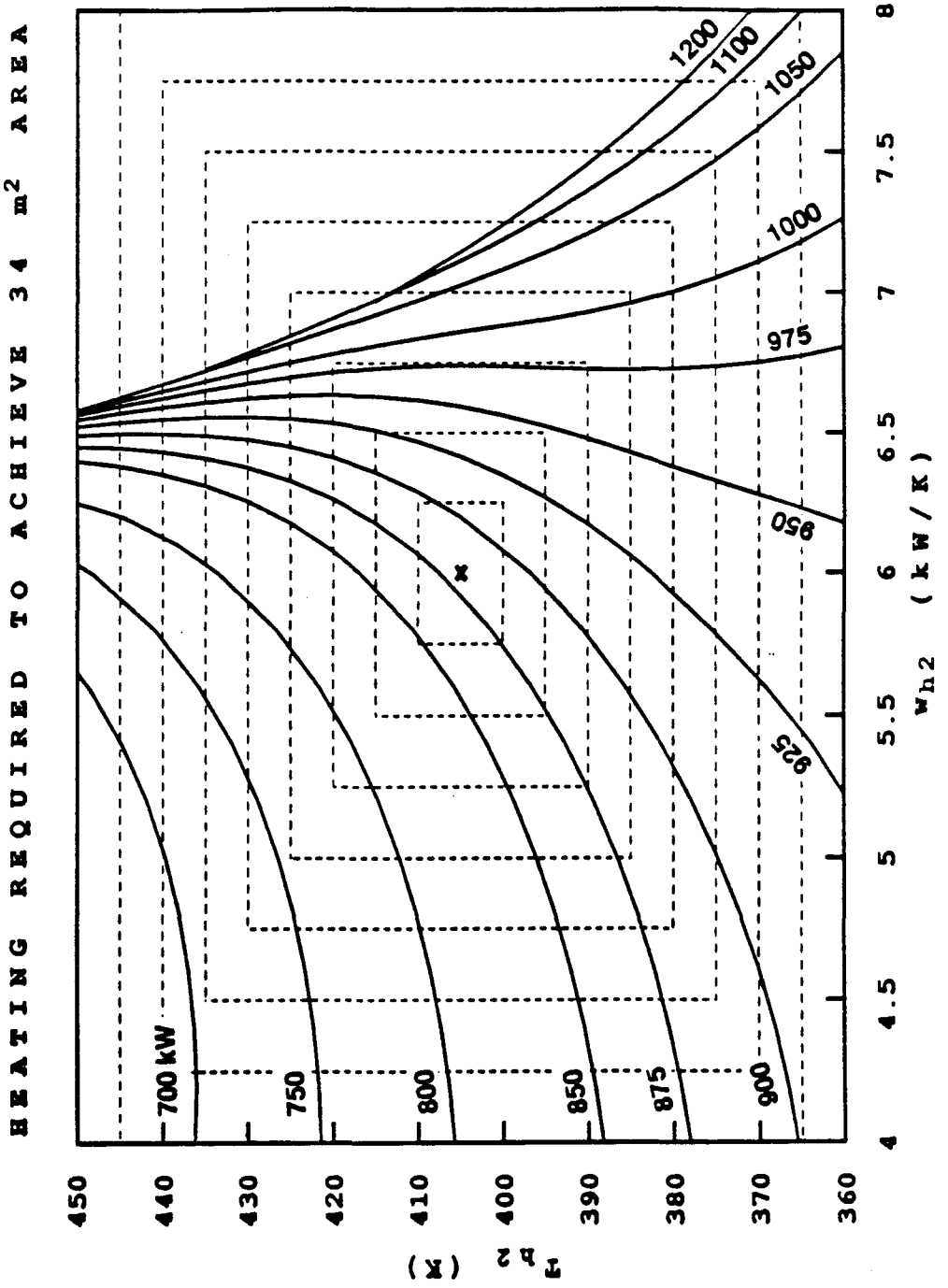

Figure 5.2: Values of heating target yielding an area target of 34m^2.

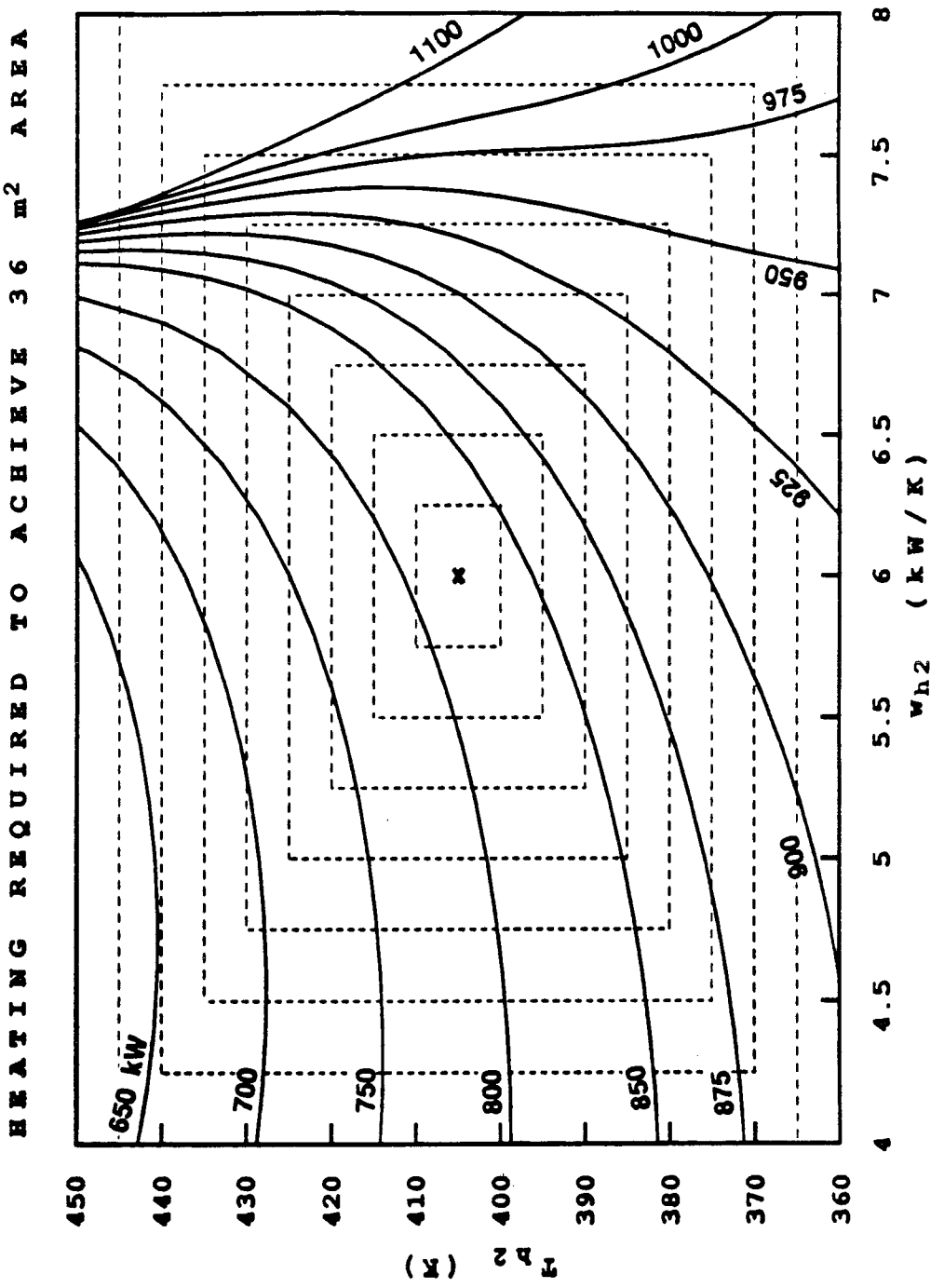

Figure 5.3: Values of heating target yielding an area target of $36m^2$.

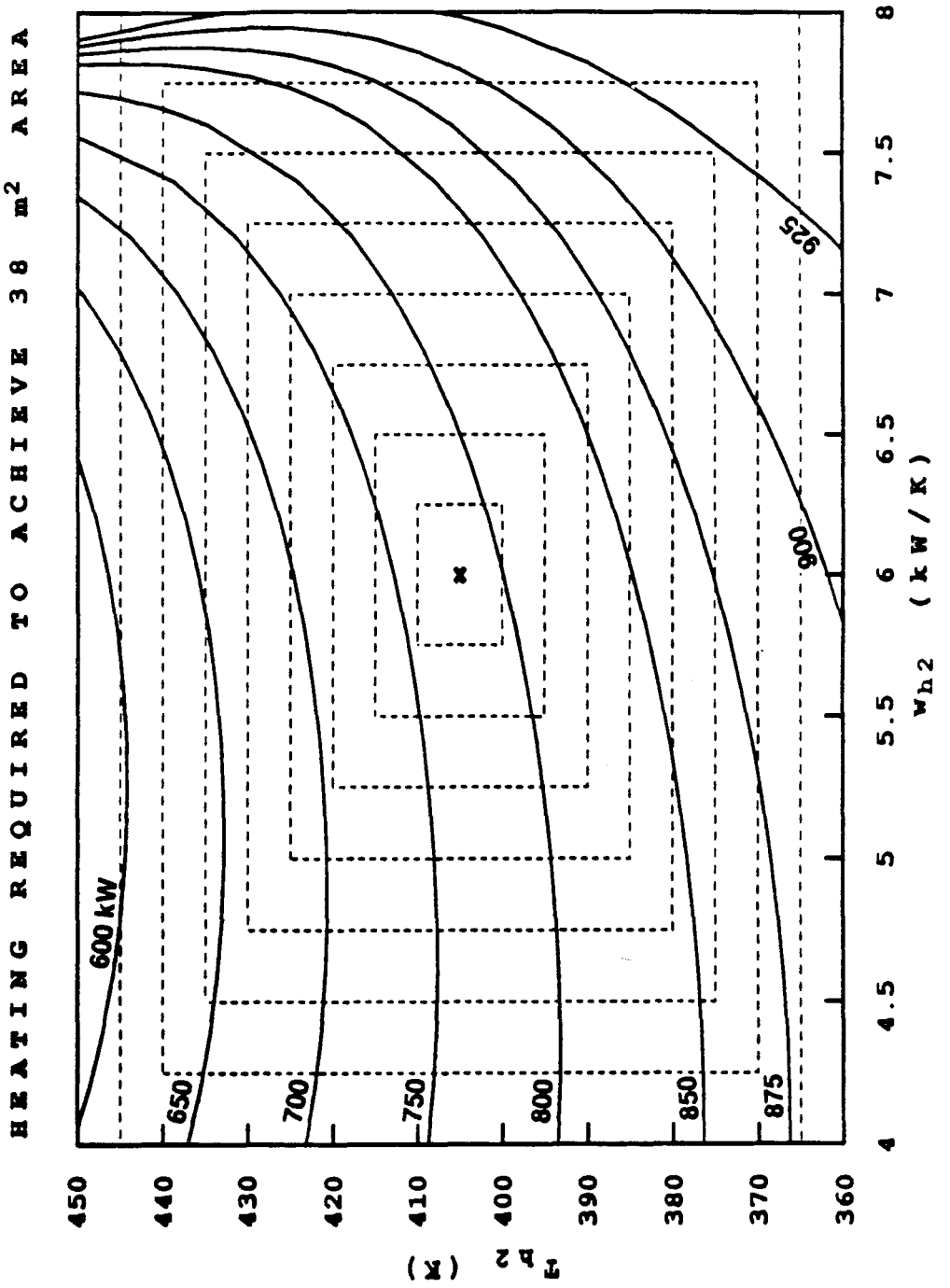

Figure 5.4: Values of heating target yielding an area target of $38m^2$.

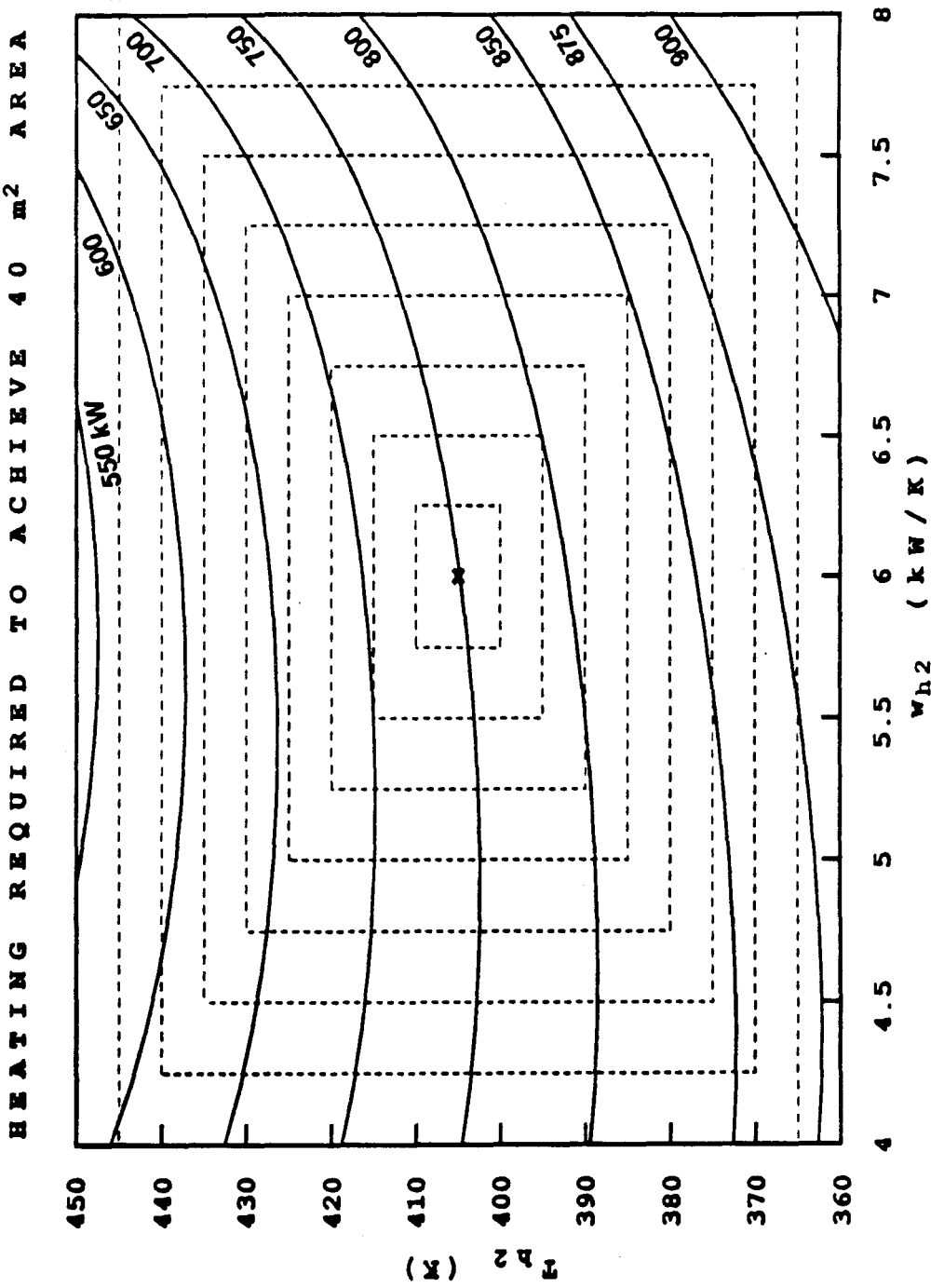

Figure 5.5: Values of heating target yielding an area target of $40m^2$.

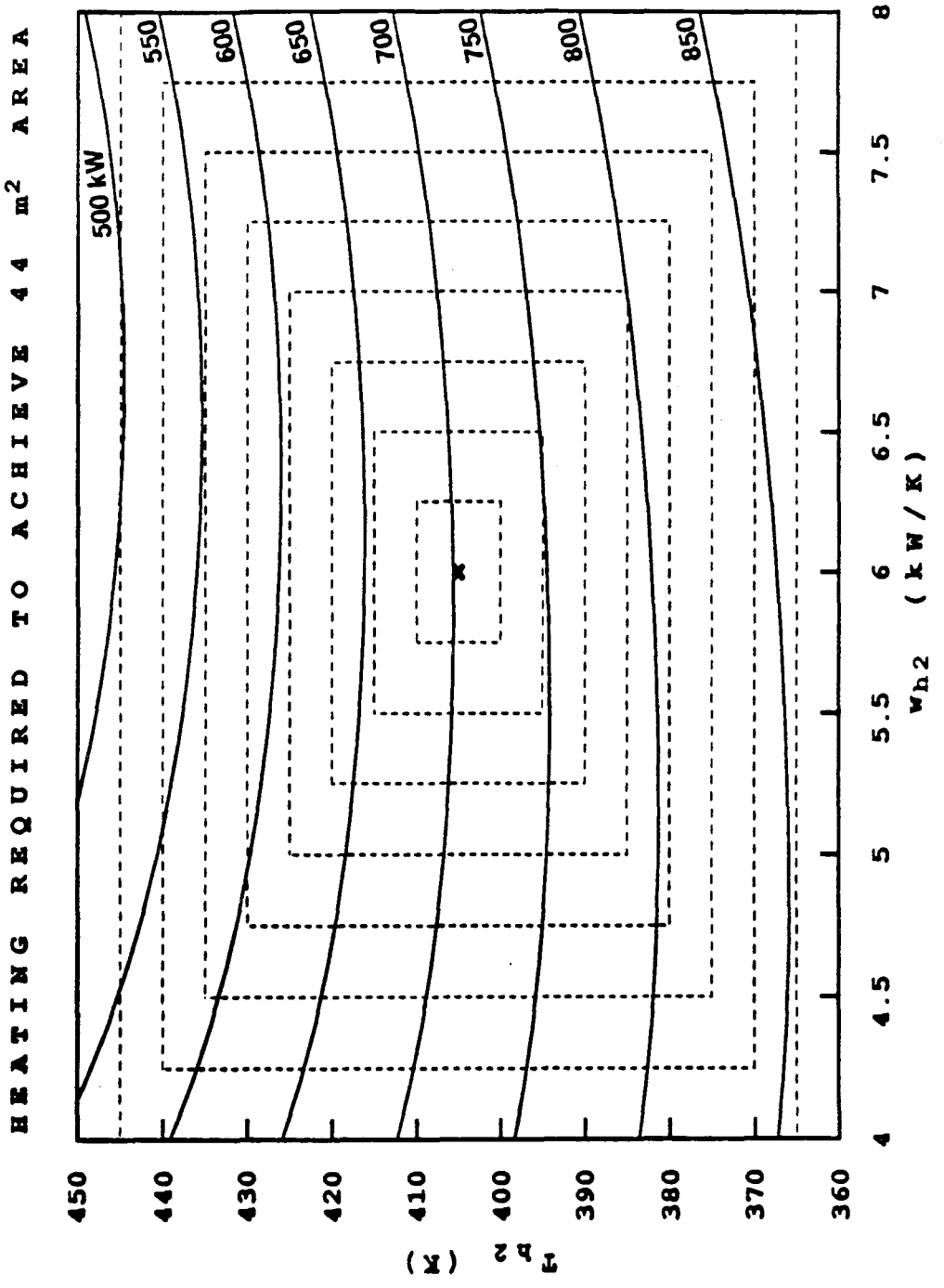

Figure 5.6: Values of heating target yielding an area target of 44m^2.

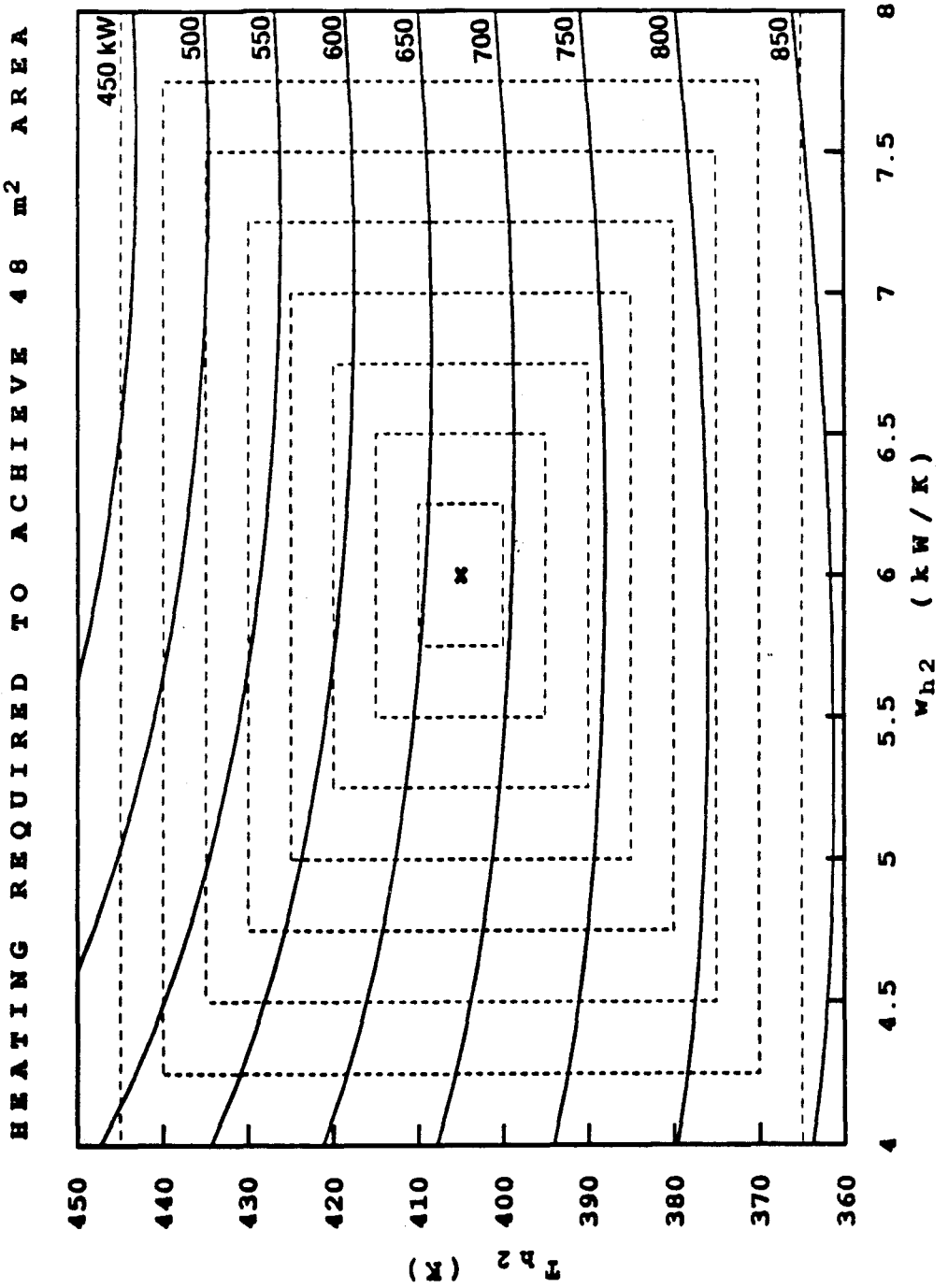

Figure 5.7: Values of heating target yielding an area target of $48m^2$.

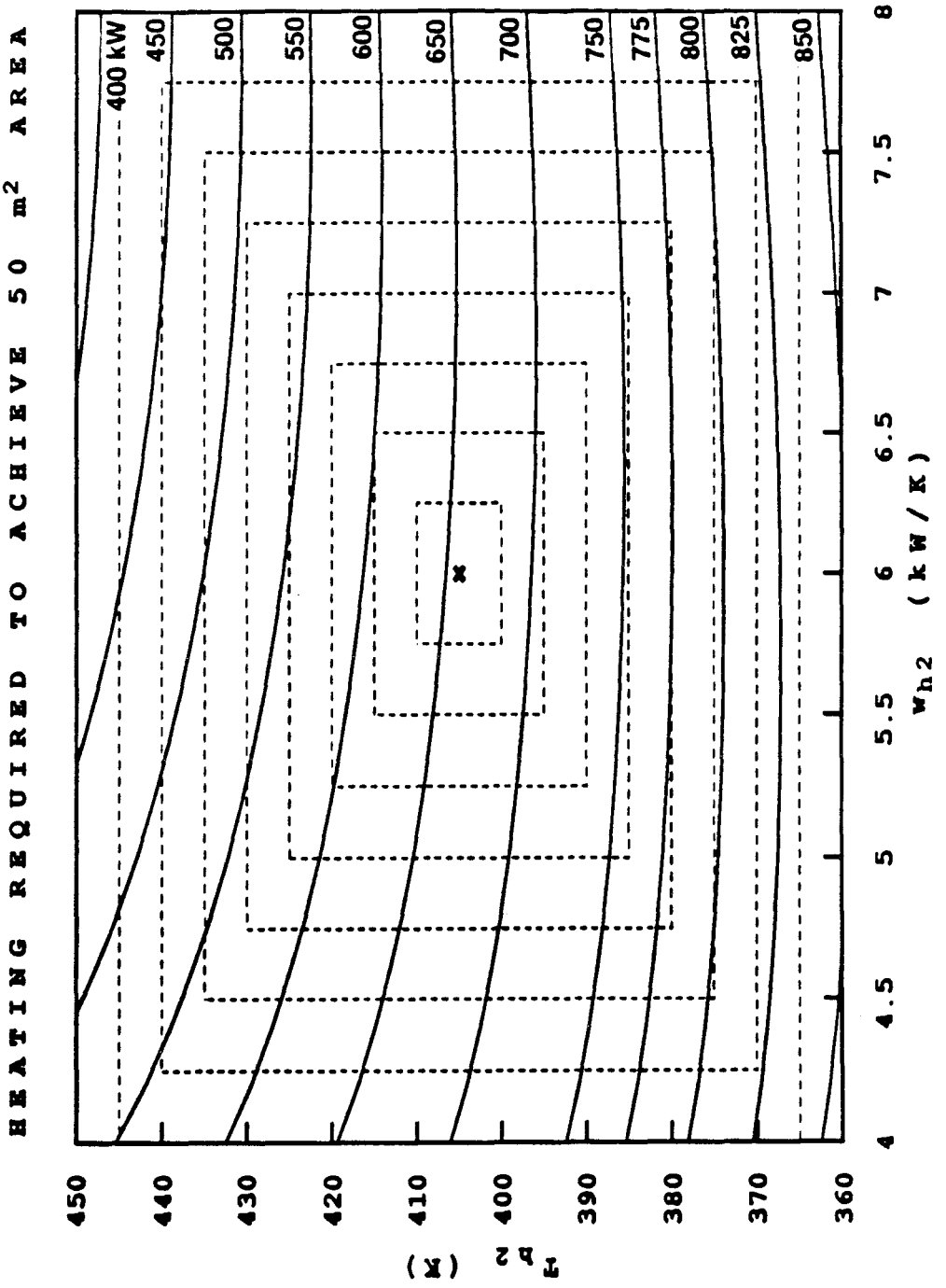

Figure 5.8: Values of heating target yielding an area target of $50m^2$.

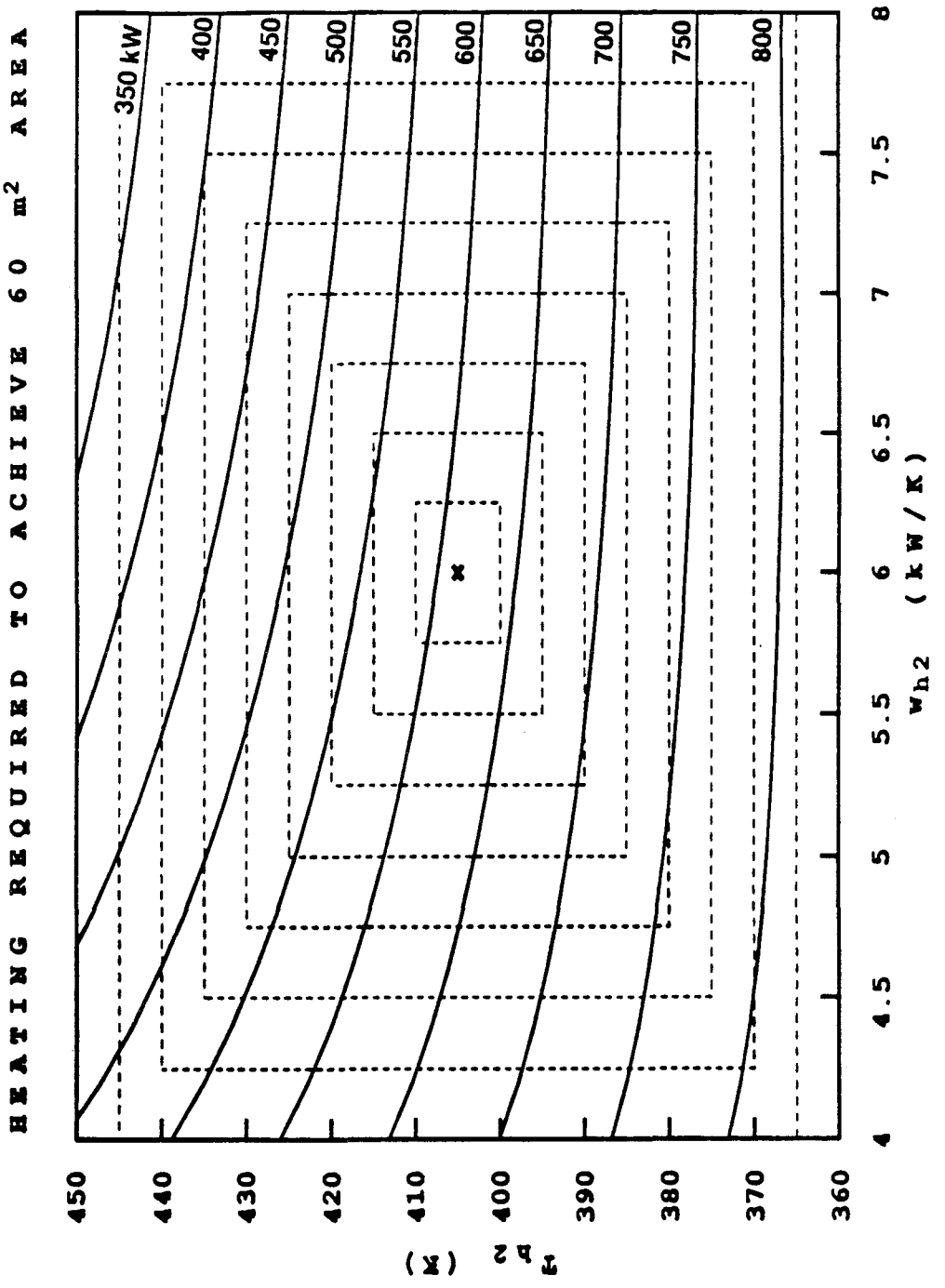

Figure 5.9: Values of heating target yielding an area target of $60m^2$.

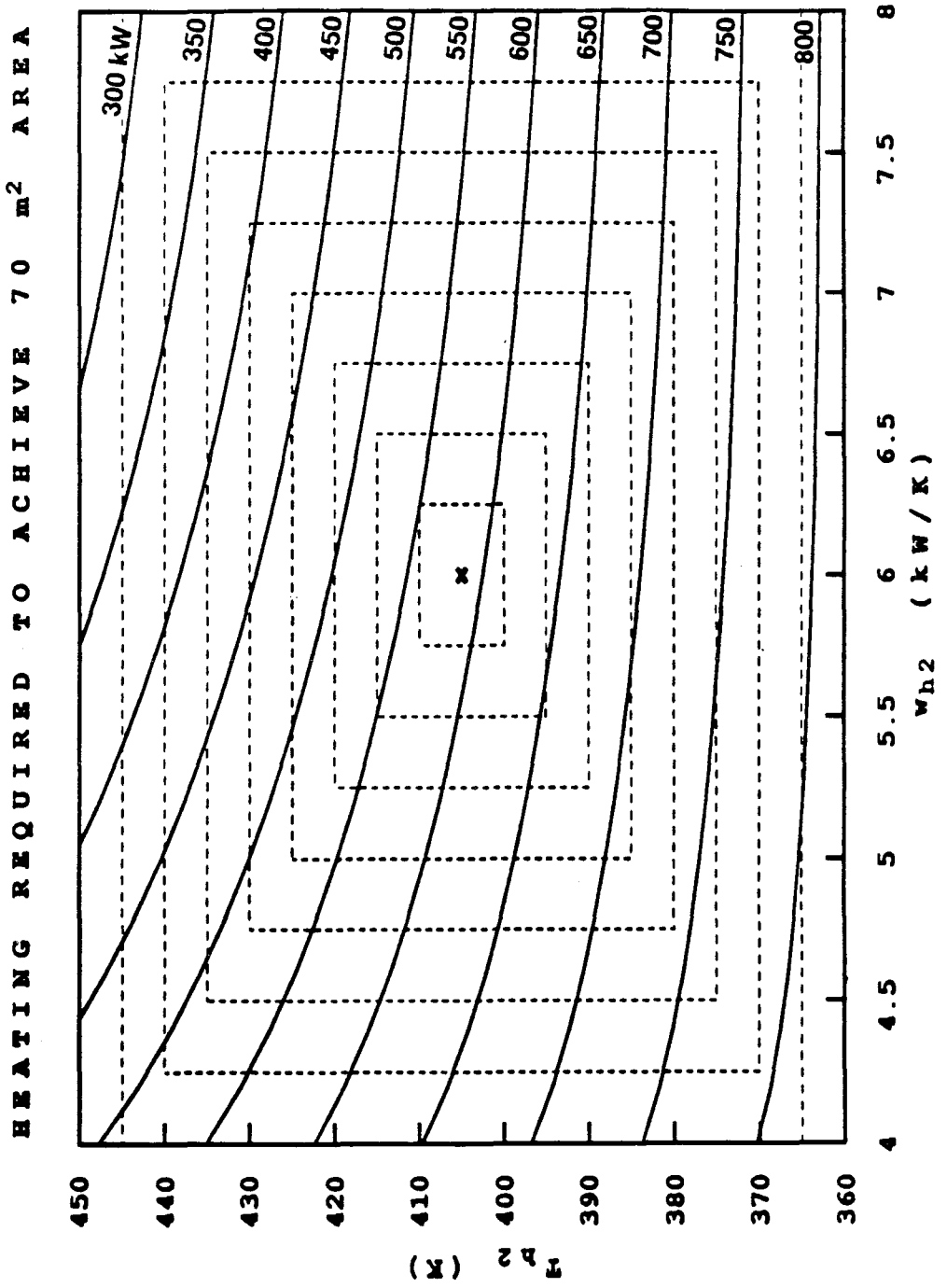

Figure 5.10: Values of heating target yielding an area target of 70m^2.

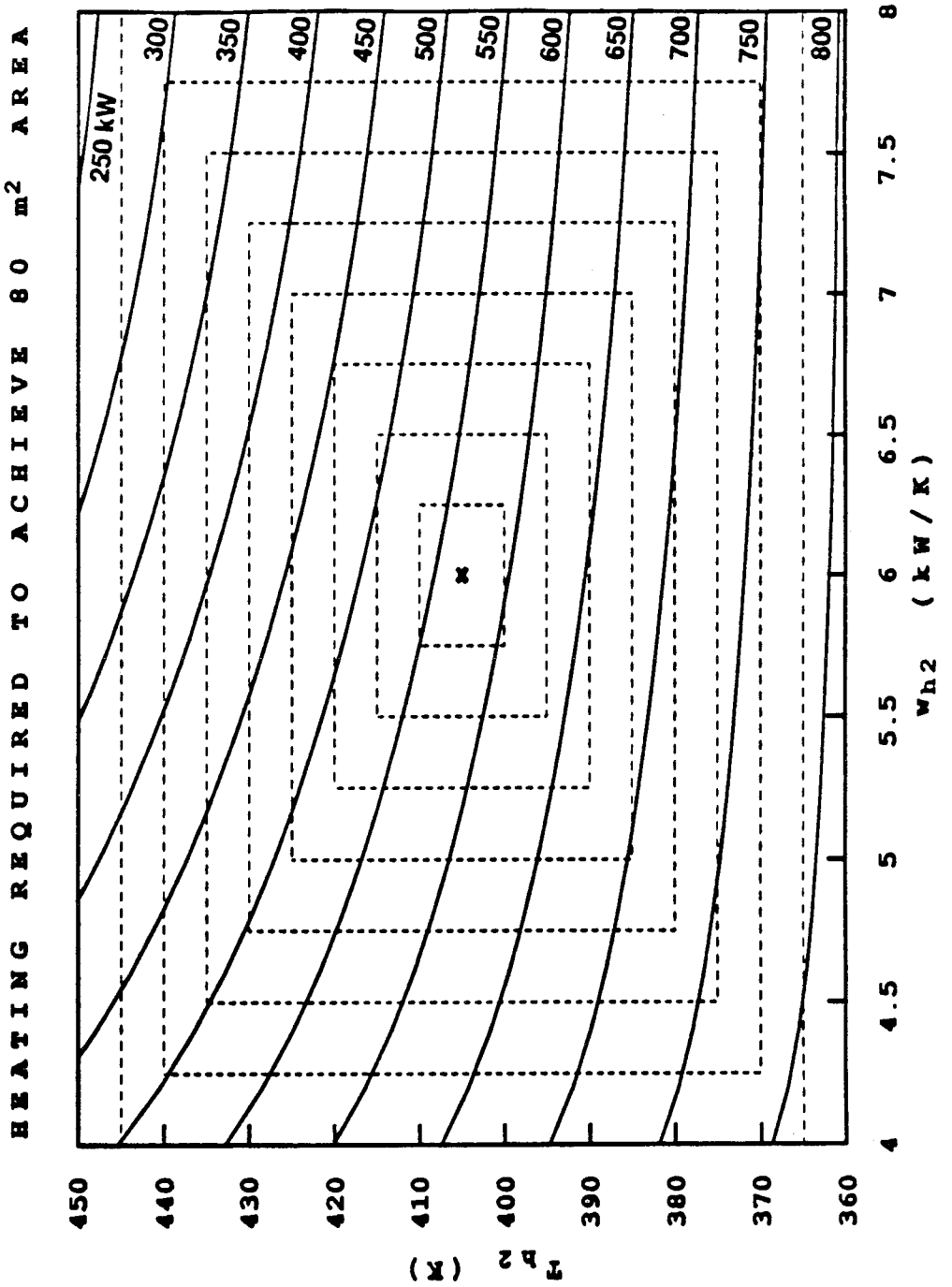

Figure 5.11: Values of heating target yielding an area target of $80m^2$.

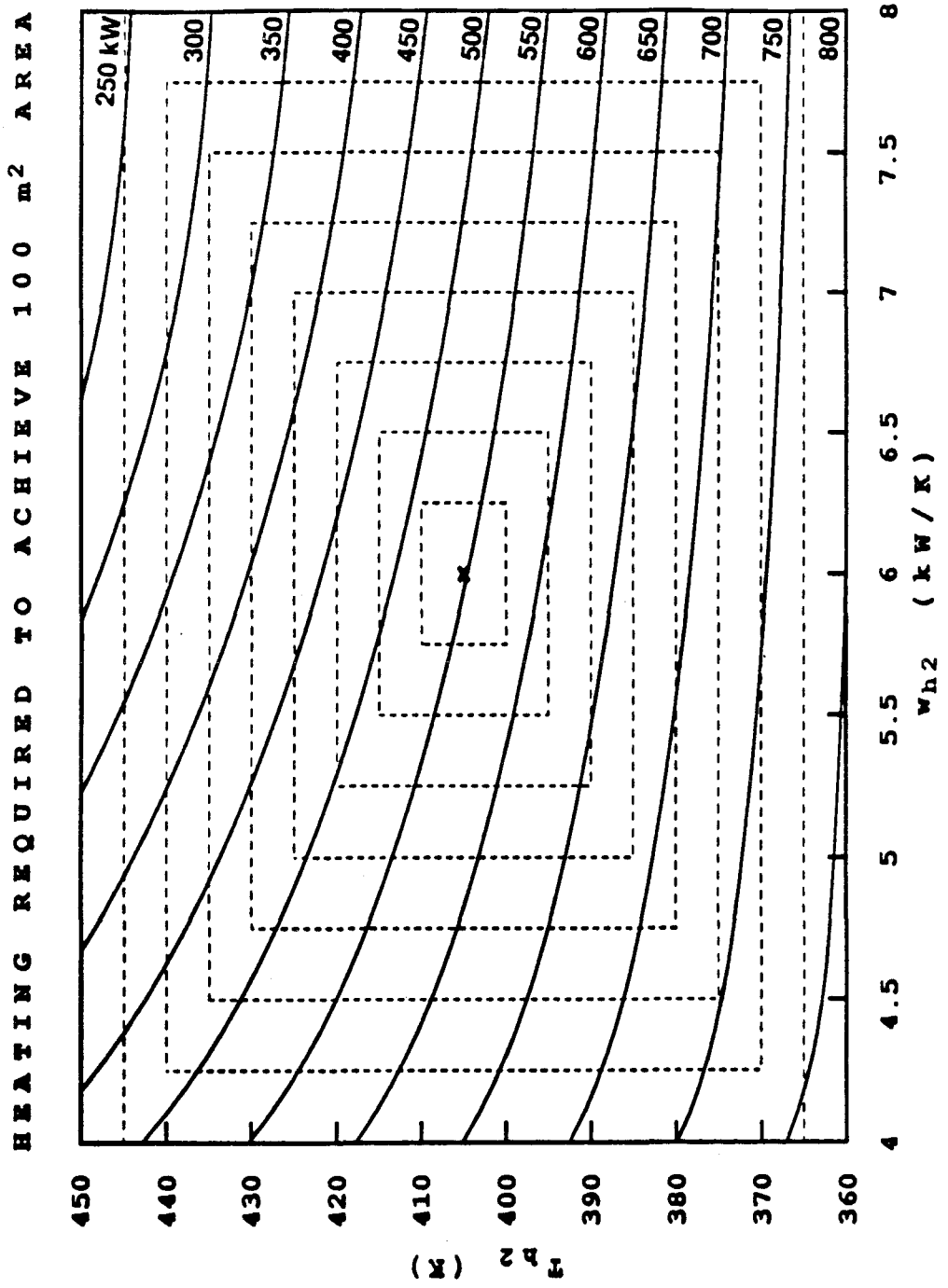

Figure 5.12: Values of heating target yielding an area target of $100m^2$.

size uncertainty ranges, scaled (by scale factor s) with respect to the reference uncertainty range. The heating profiles were determined by "inverse" area targeting—for given T_{h2}^S and w_{h2}, we determined by trial-and-error the amount of heating required to achieve the specified area target. (For simplicity, we use the composite-curve based area target rather than the NLP-based area target presented in Chapter 2.) For example, for each T_{h2}^S-w_{h2} point on the 800 kW heating curve in Fig. 5.2, the composite curve-based area target is 34 m^2 when 800 kW of heating is specified. In this example, heating targets greater than 1300 kW are not meaningful since zero process heat recovery occurs at these utility levels (i.e., for heating levels greater than 1300 kW, steam is sent directly to cooling water).

Step 2: Determine the maximum heating target (and the corresponding cooling target at the same operating condition) in each uncertainty range as a function of area. (Here, we are assuming that heating costs dominate cooling costs, and are using a worst case analysis for the heating cost.) Figures 5.13 and 5.14 show the maximum heating target, and corresponding cooling target, in each size uncertainty range as a function of area. In general, maximum heating occurs at a corner point of the uncertainty ranges in Figs. 5.2–5.12, except for a relatively quick transition from one corner point to another [e.g., as area increases from 48 to 50 m^2, maximum heating switches from the lower right corner point (T_{h2}^S = 375 K, w_{h2} = 7.5 kW/K) of the s = 3.0 uncertainty range in Fig. 5.7 to the lower left corner point (T_{h2}^S = 375 K, w_{h2} = 4.5 kW/K) of the same uncertainty range in Fig. 5.8]. The sudden change in cooling target in Fig. 5.14 occurs when the corresponding heating target changes from one corner point to another. Recall that for fixed ΔT_m, maximum heating

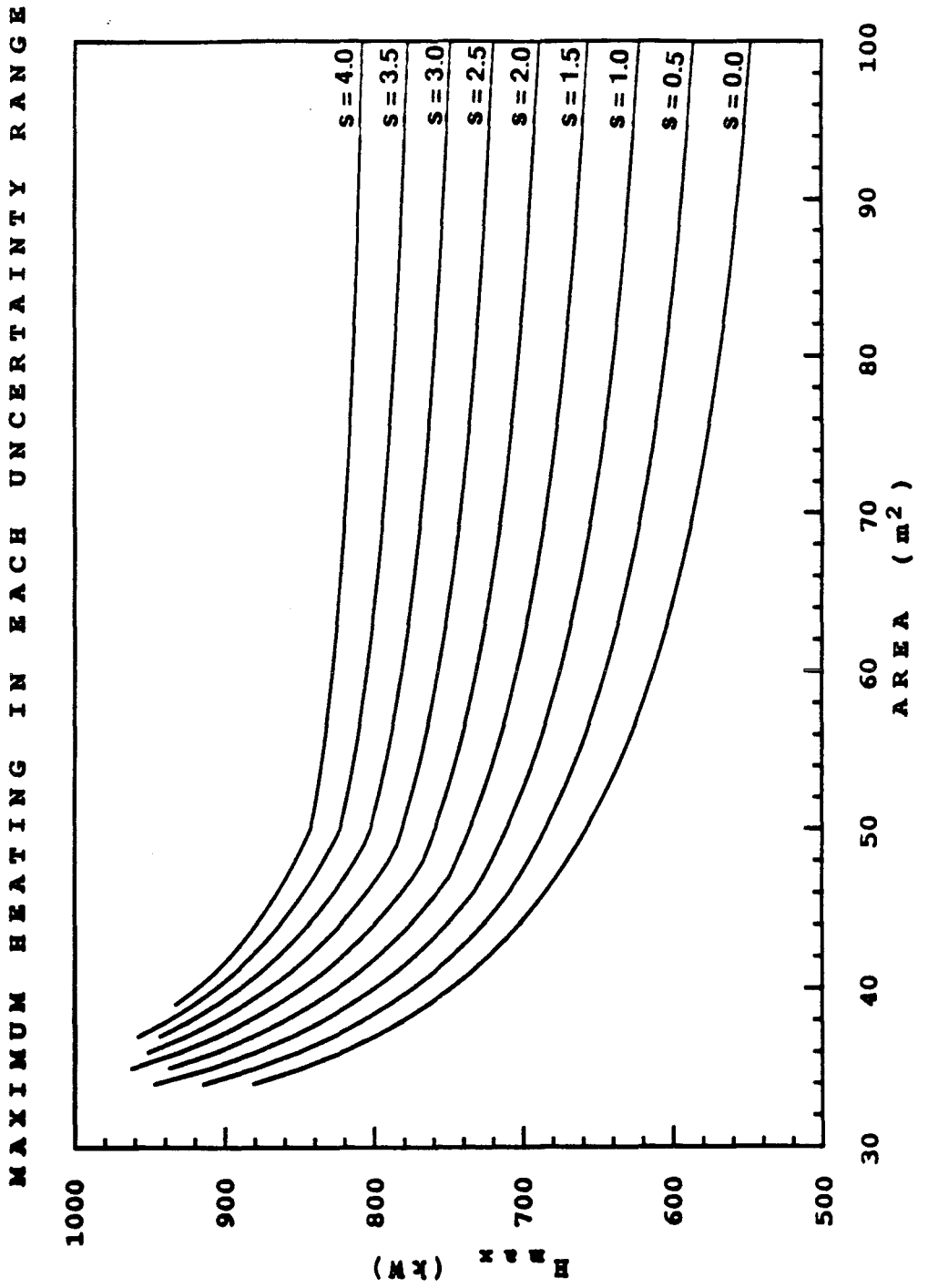

Figure 5.13: Maximum heating target in each size uncertainty range.

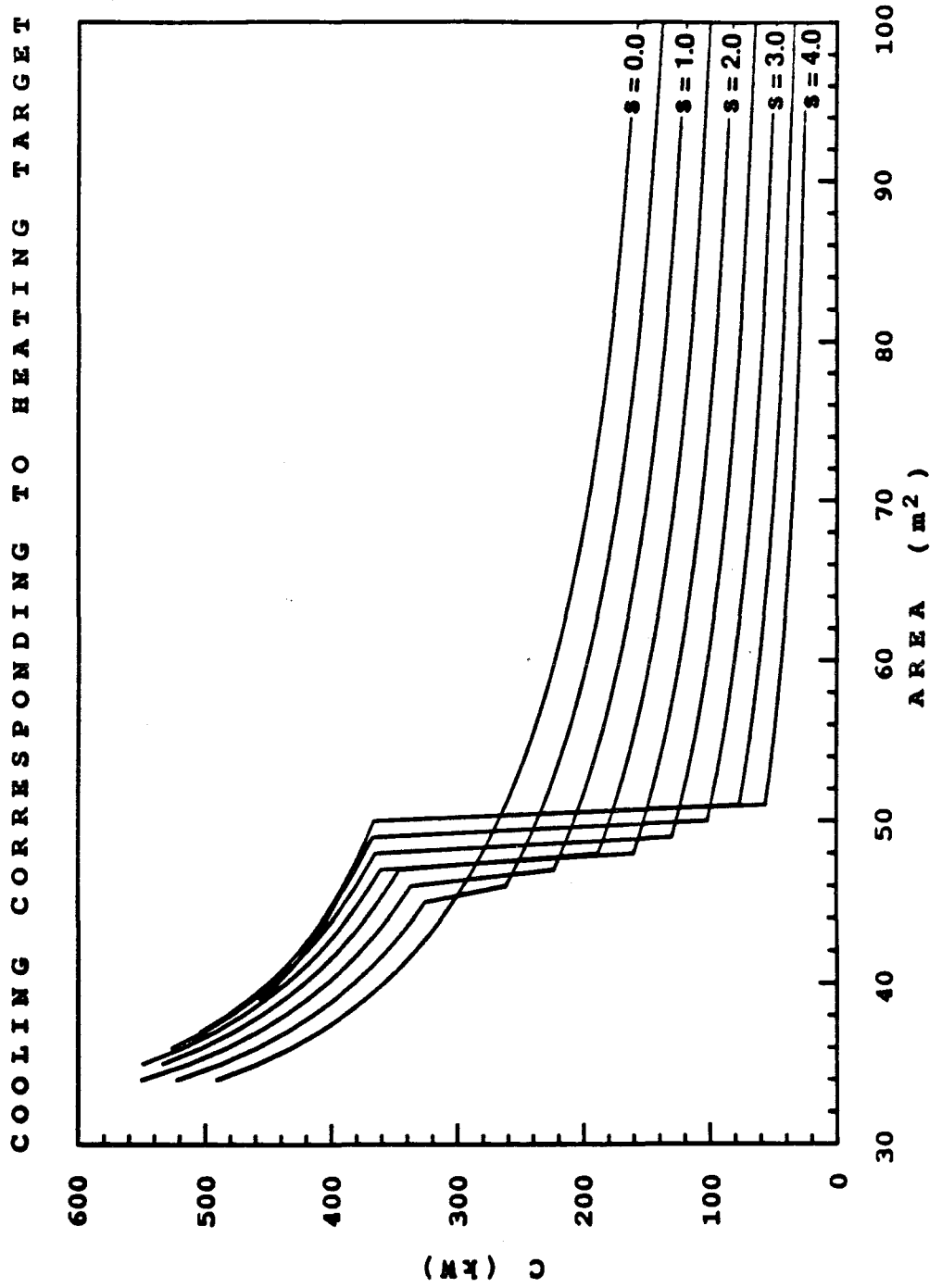

Figure 5.14: Cooling target corresponding to the maximum heating target in each size uncertainty range.

always occurs at a corner point, and always at the same corner point (the 'Case C' corner point, Section 4.3.2).

Step 3: Calculate cost targets (heating, cooling, annualized capital, and total annualized cost) for each size uncertainty range as a function of area. Figures 5.15–5.22 show these cost targets, where the TAC is based on the heating and cooling targets in Figs. 5.13 and 5.14 and the cost data in Table 5.1. For comparison, Fig. 5.23 shows the cost targets for nominal stream conditions. In each of these figures, the "cross hairs" indicate the minimum TAC and corresponding area. Note that in this cost analysis, we essentially require maximum energy recovery (minimum utility consumption) only at the worst case (largest heating target) point in an uncertainty range.

Step 4: Determine the cost–resilience trade-off. Figure 5.24 shows the minimum TAC, from Figs. 5.15–5.23, as a function of the scale factor s of each uncertainty range. As expected, the TAC target increases for larger uncertainty ranges. However, the TAC shows no sharp increase with increasing resilience and, in fact, the marginal TAC (the slope of the TAC plot in Fig. 5.24) decreases with increasing resilience. ■

Actually, the results of the previous example are disappointing. We had expected to see the marginal TAC increase with increasing resilience. At least two important factors were neglected in the example which, if taken into account, should reduce the concavity of the TAC–resilience trade-off curve in Fig. 5.24 (and possibly make the curve convex).

(1) Figures 5.2–5.12 consider only the *nominal* area required at each operating point; that is, these figures do not consider the extra area required in exchangers oversized to achieve resilience. For example, Fig. 5.2 considers HENs with a total

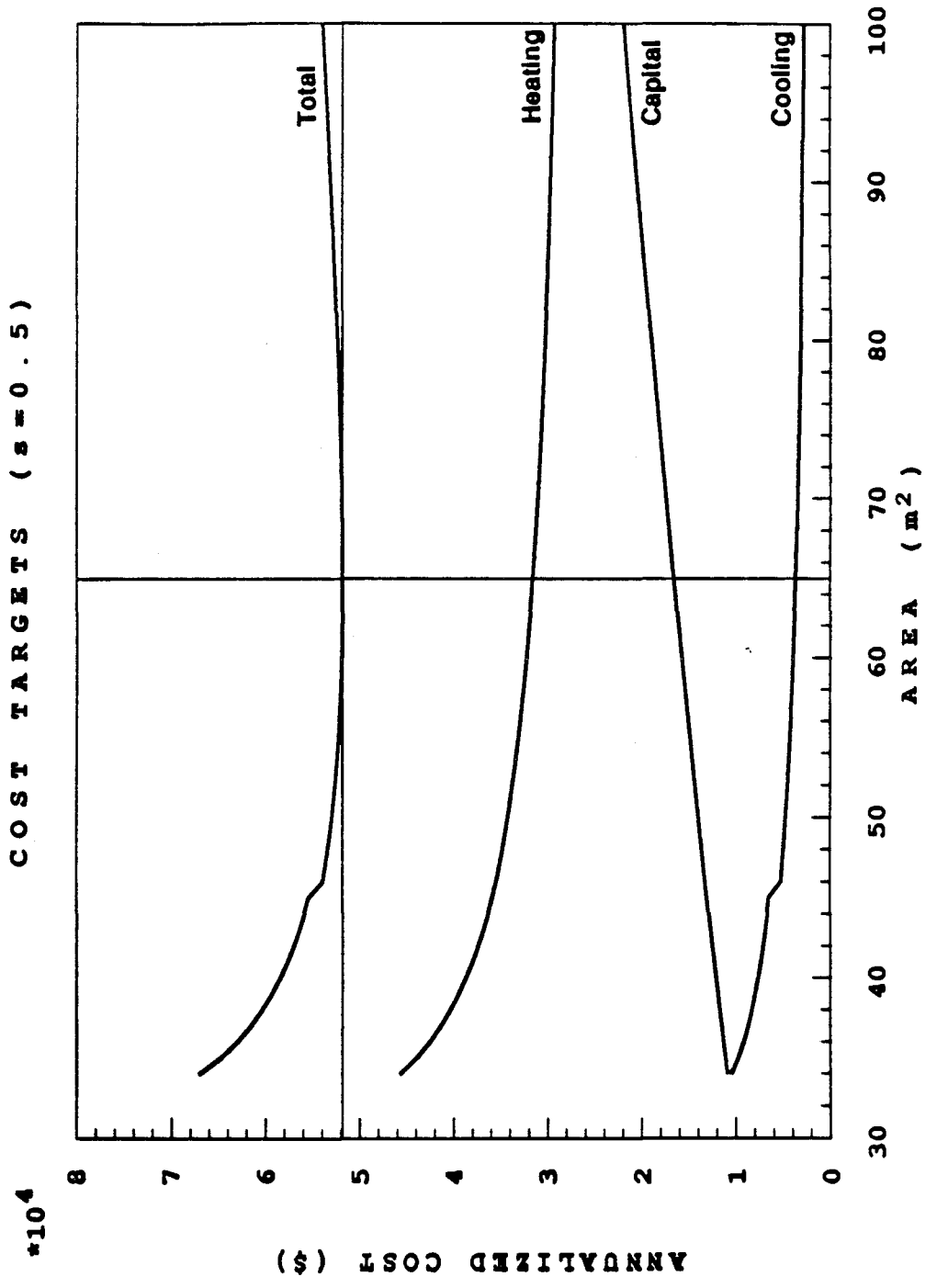

Figure 5.15: Heating, cooling, capital and total annualized cost targets for s=0.5.

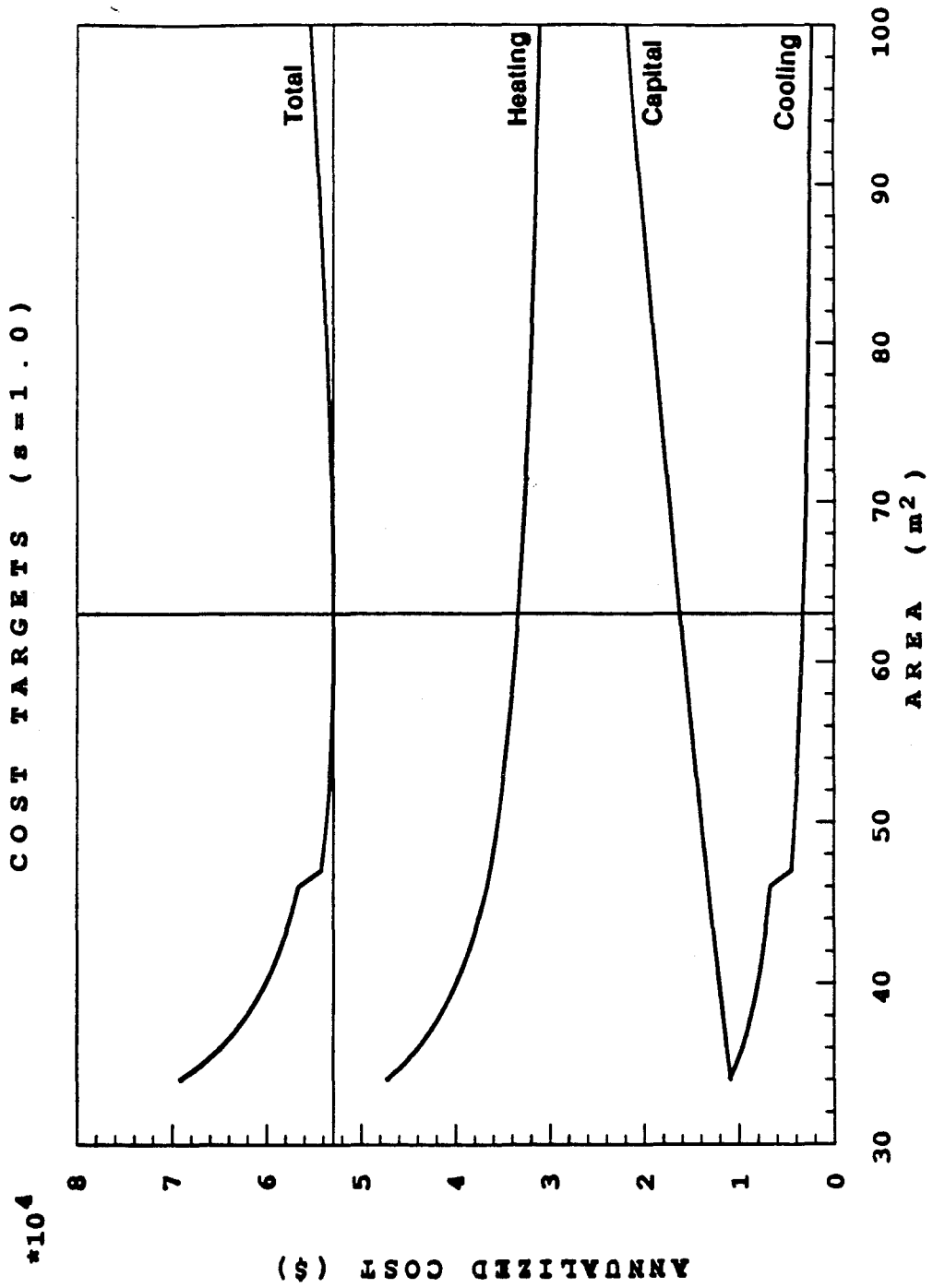

Figure 5.16: Heating, cooling, capital and total annualized cost targets for s=1.0.

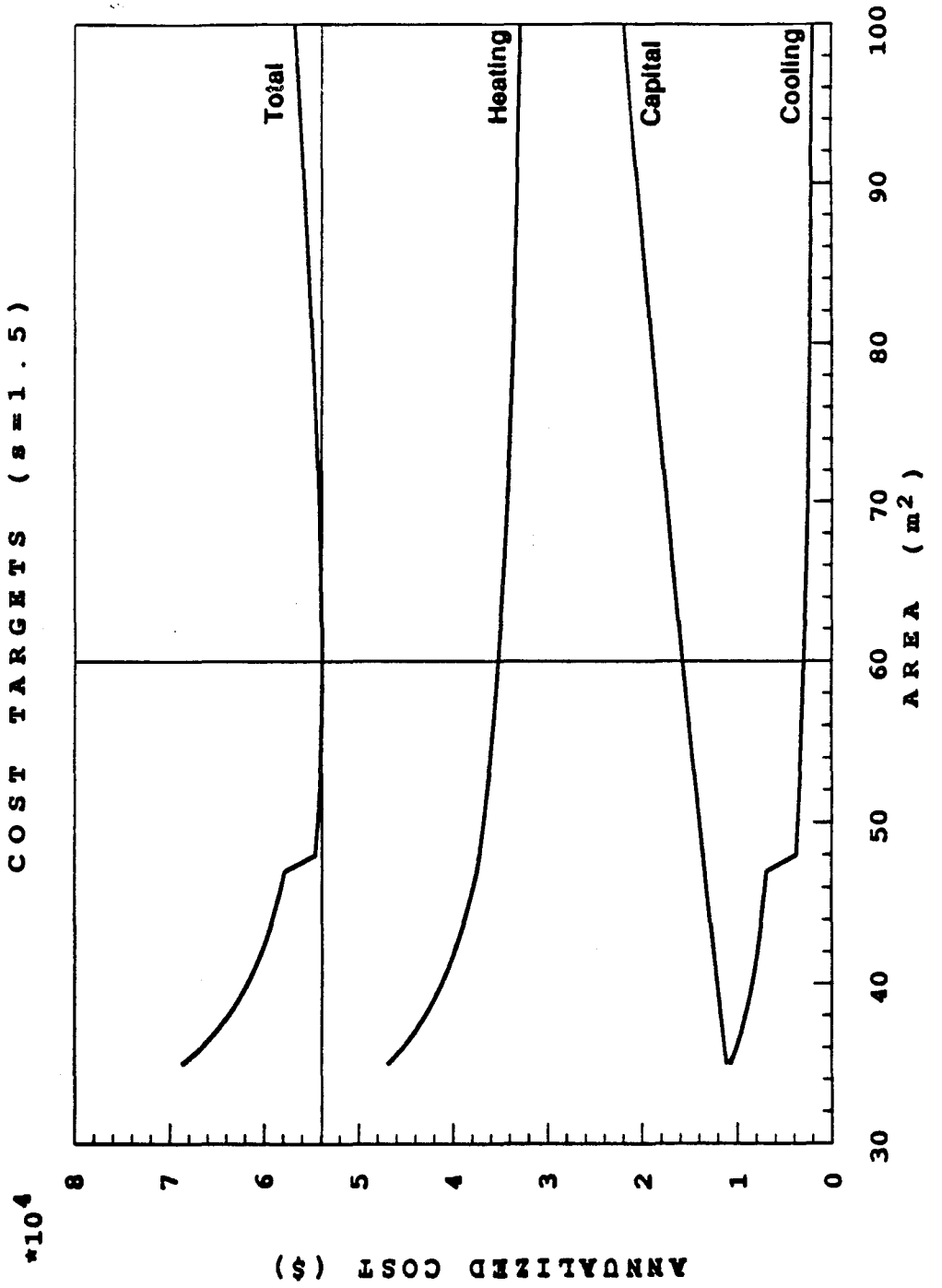

Figure 5.17: Heating, cooling, capital and total annualized cost targets for s=1.5.

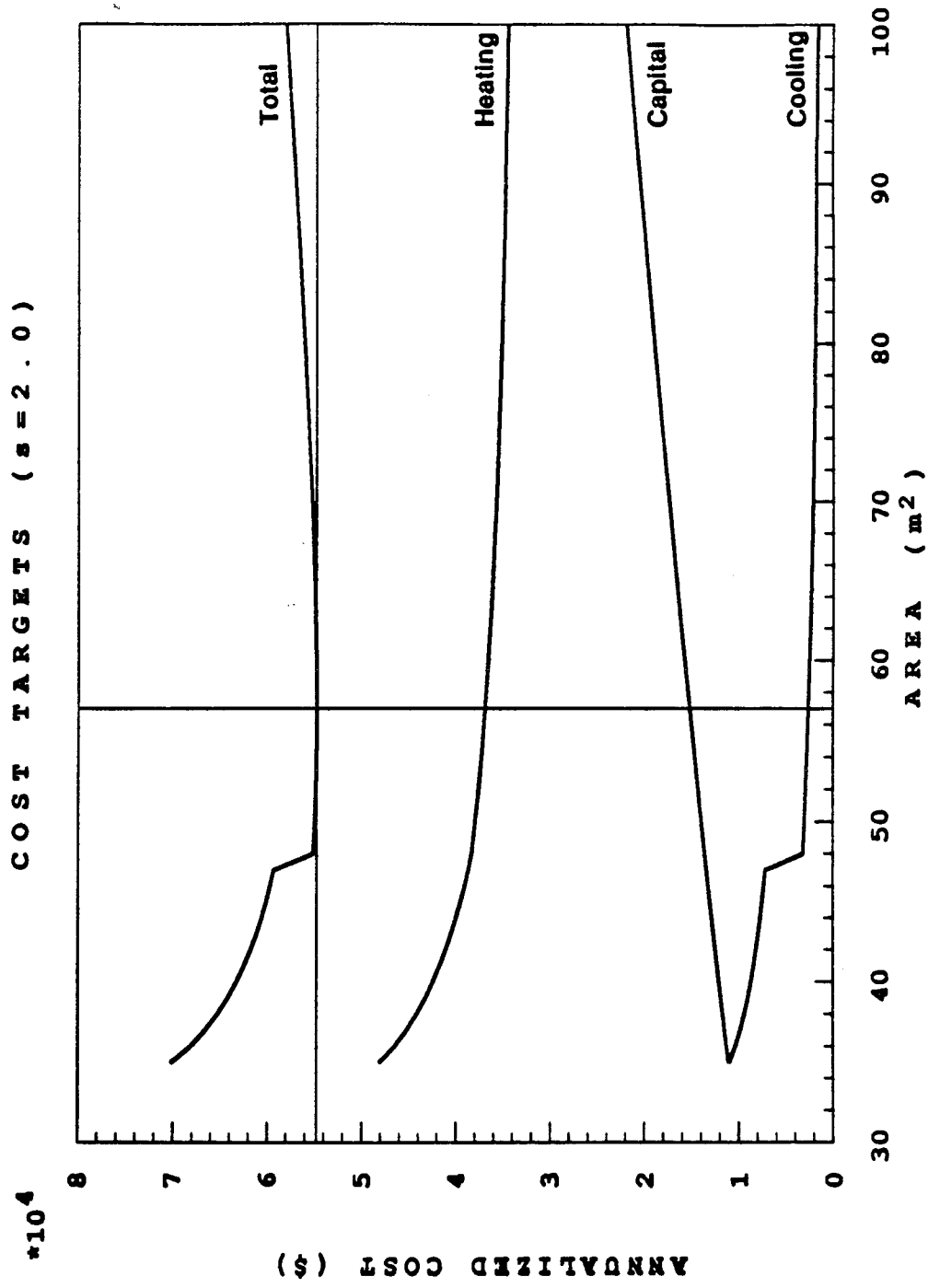

Figure 5.18: Heating, cooling, capital and total annualized cost targets for s=2.0.

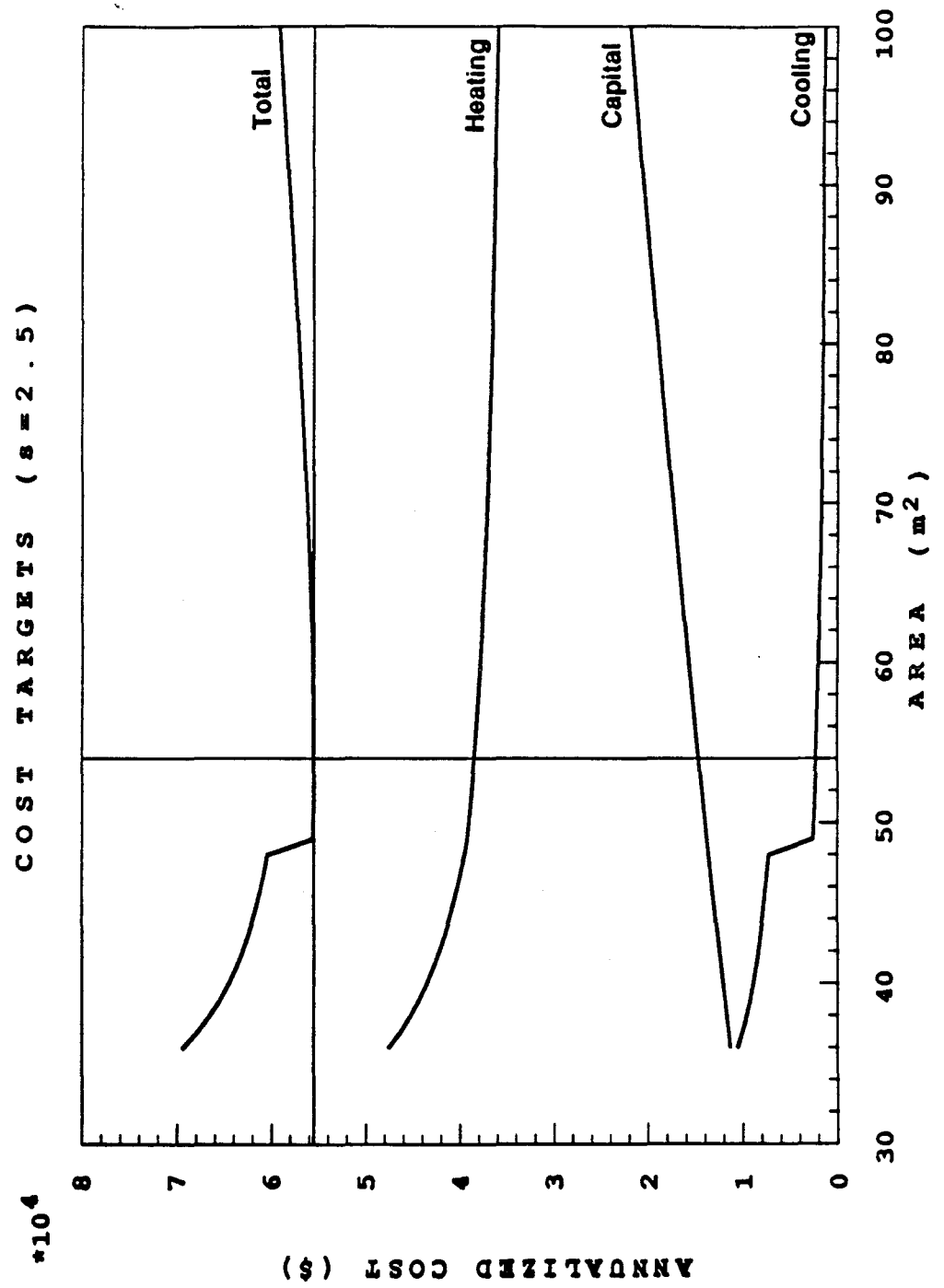

Figure 5.19: Heating, cooling, capital and total annualized cost targets for s=2.5.

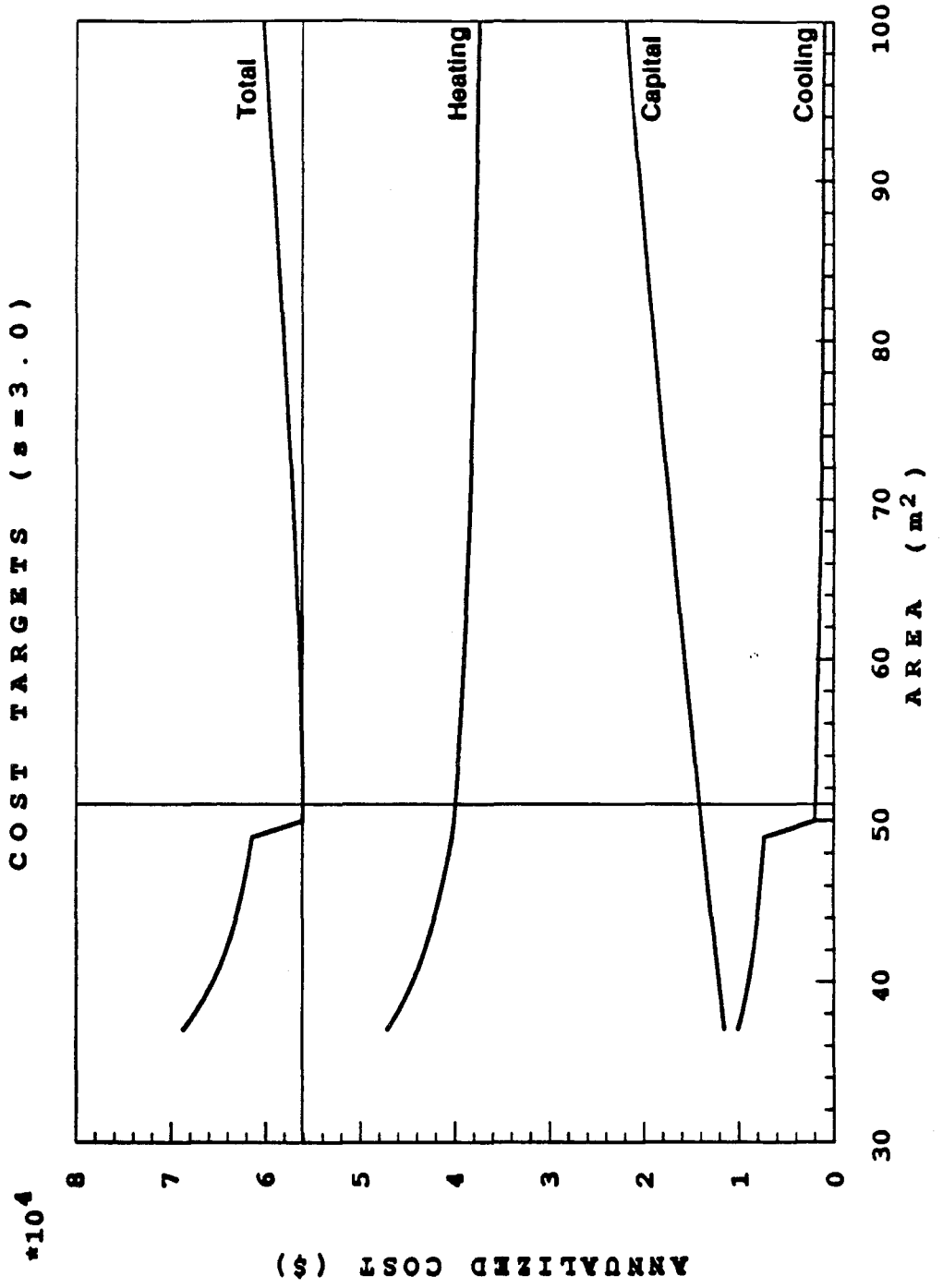

Figure 5.20: Heating, cooling, capital and total annualized cost targets for s=3.0.

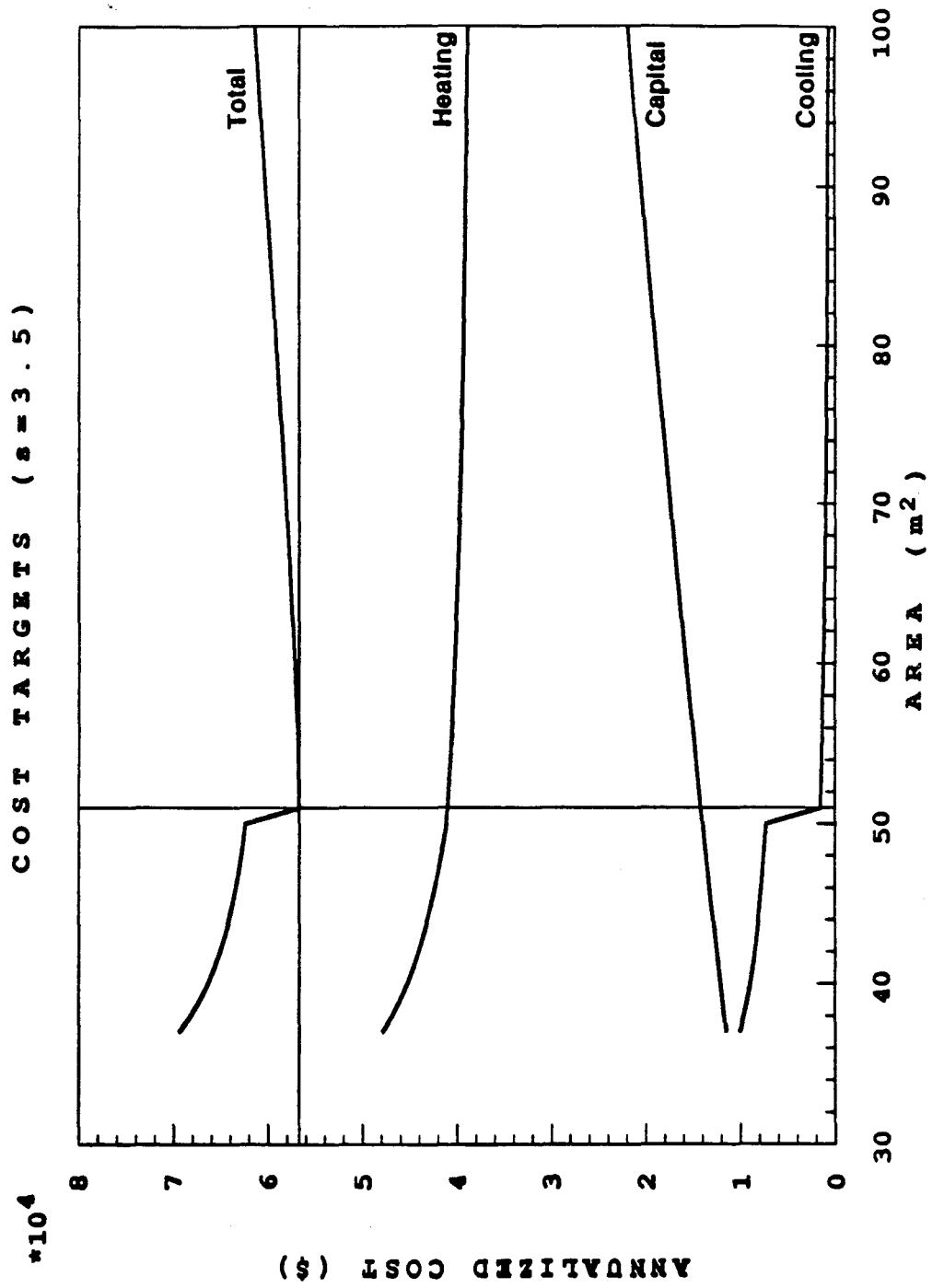

Figure 5.21: Heating, cooling, capital and total annualized cost targets for s=3.5.

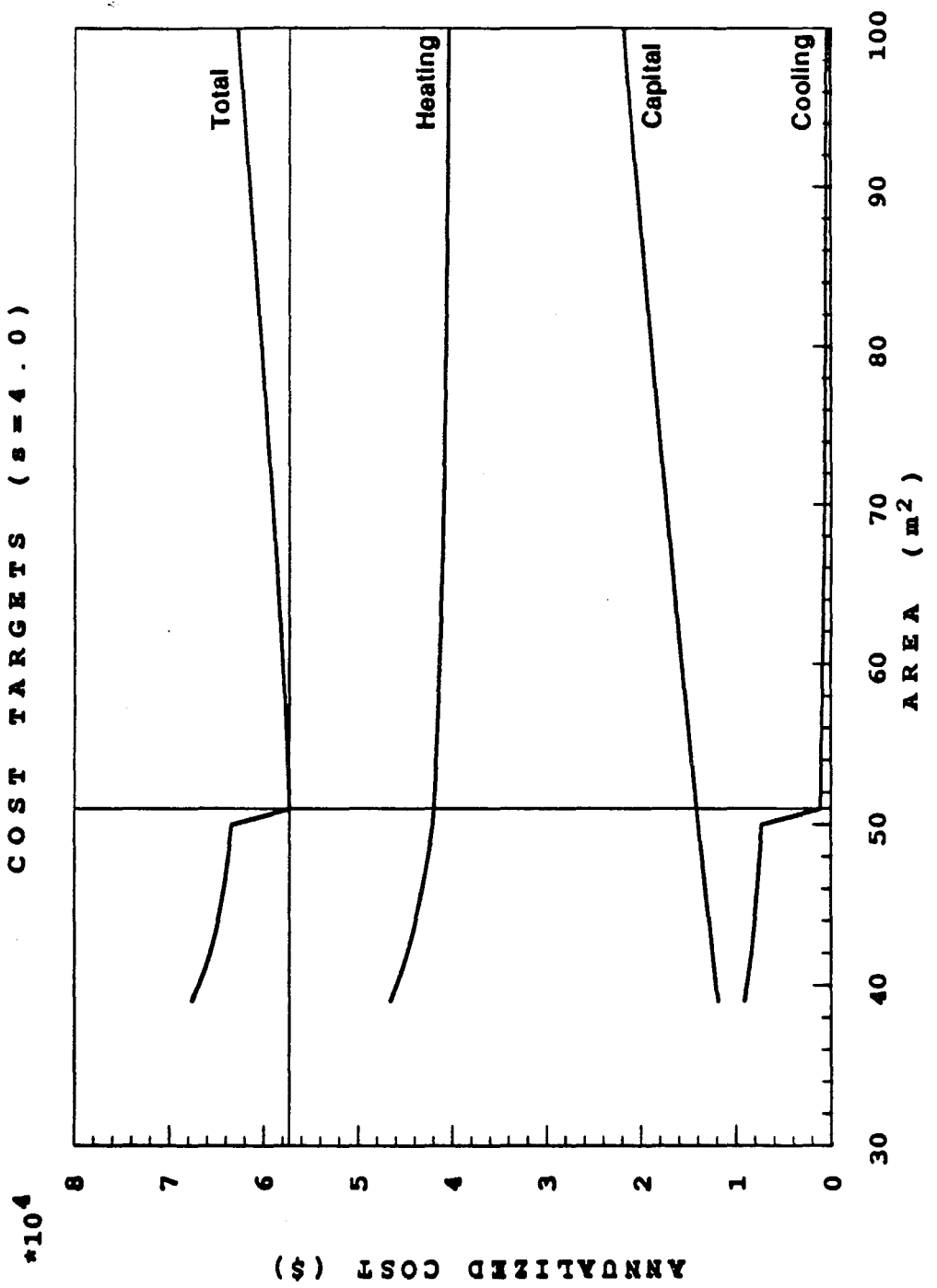

Figure 5.22: Heating, cooling, capital and total annualized cost targets for s=4.0.

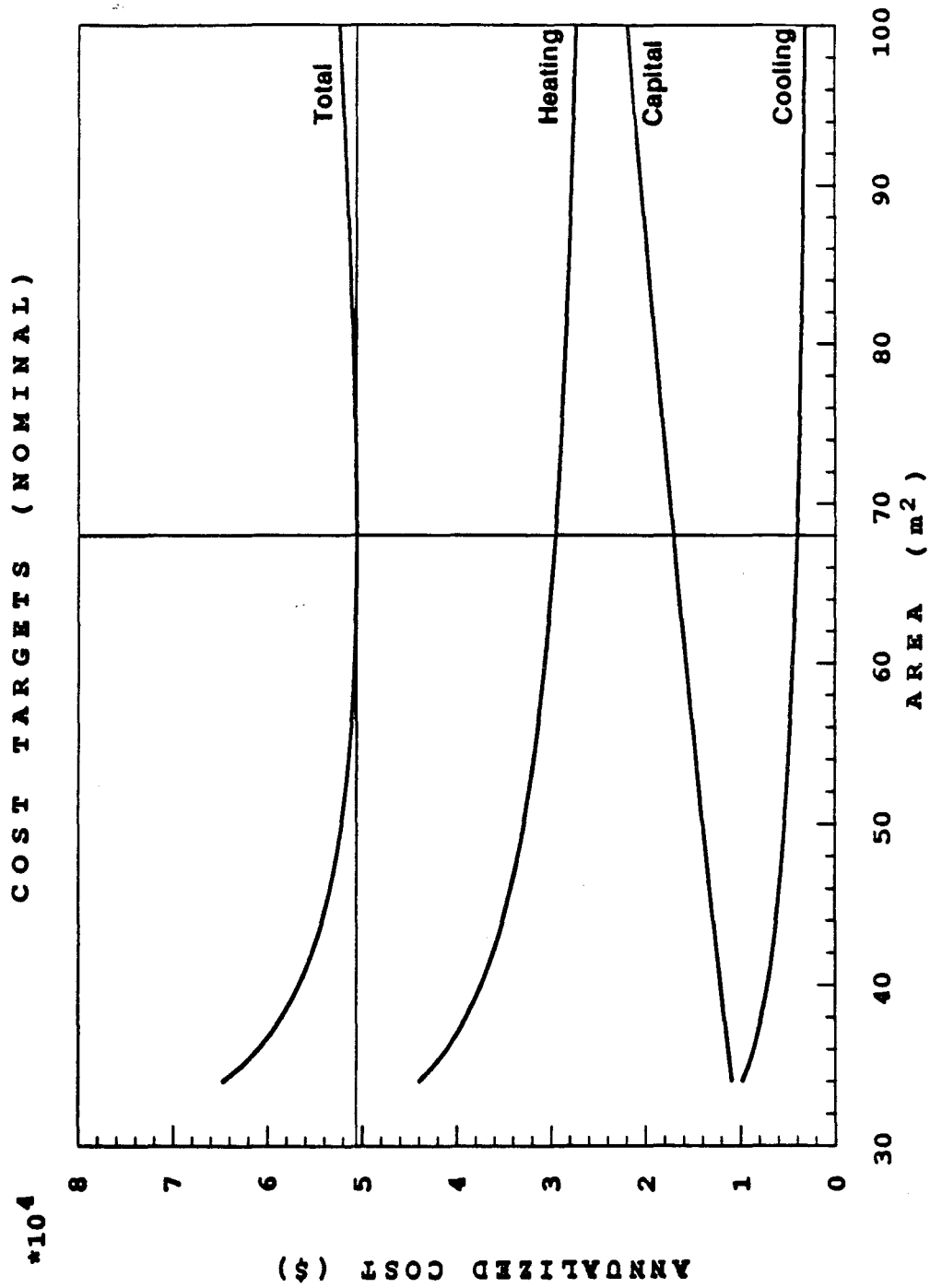

Figure 5.23: Heating, cooling, capital and total annualized cost targets for nominal operating conditions.

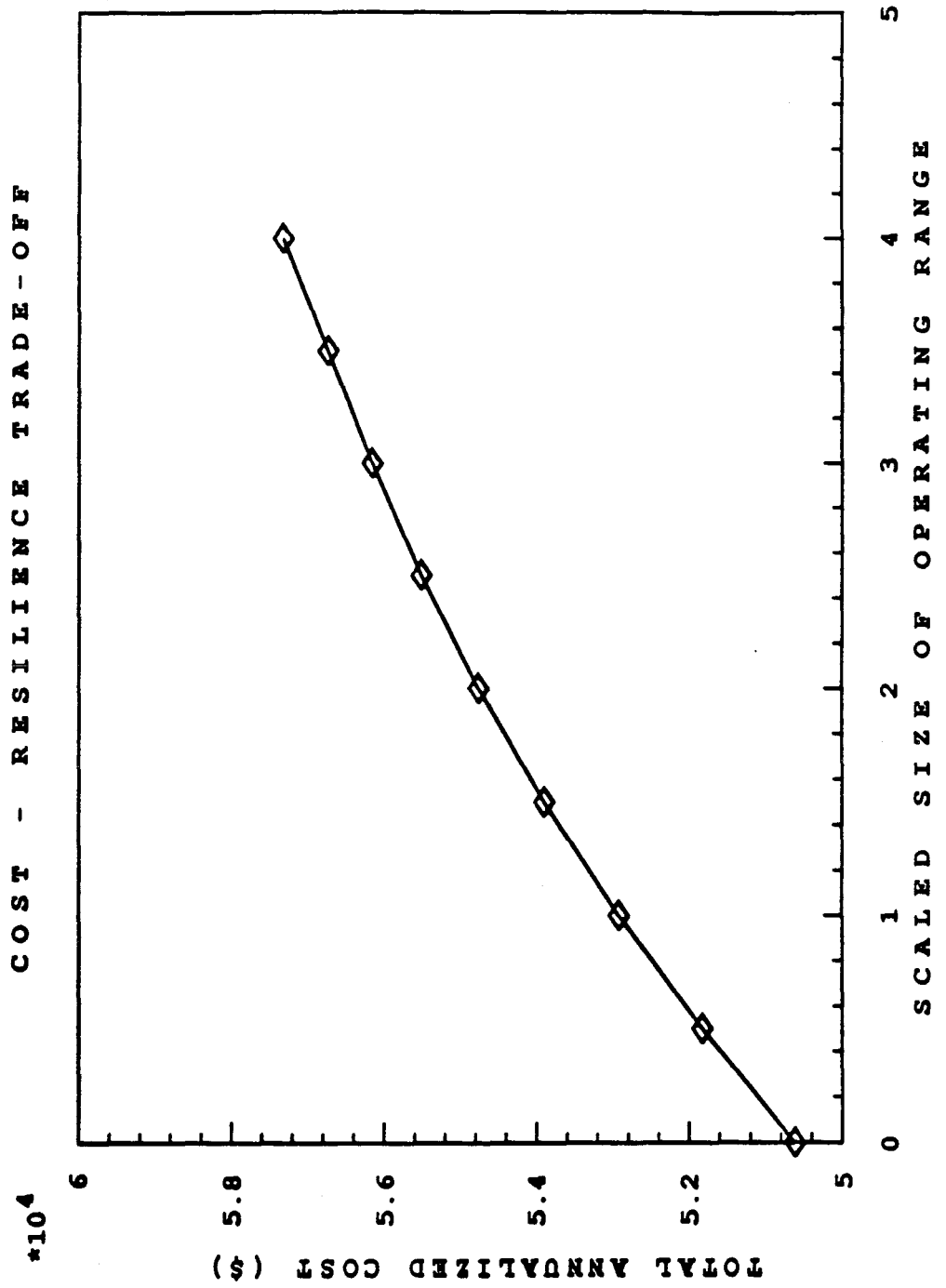

Figure 5.24: Total annualized cost target for different size uncertainty ranges.

area of 34 m^2, where this area can be redistributed among different exchangers as the "nominal" operating conditions change. This corresponds to different designs, with different areas, for each operating condition.

For a single resilient design, mathematically "redistributing" area among exchangers corresponds to changing the flow rates in bypasses around oversized exchangers. When mathematical area is moved from one exchanger to another, that area must physically be included in both exchangers (i.e., both exchangers must be oversized), and that area should be counted twice when costing the network. In the previous example, the error (not counting the extra area of oversized exchanges) increases as the size of the uncertainty range increases. Thus the area, hence TAC in Fig. 5.24, is increasingly underestimated as the specified resilience (scale factor s) increases. In fact, the optimal area shown in Figs. 5.15–5.23 decreases with increasing resilience.

An approximate upper bound on the total area required for a network to be resilient in a given uncertainty range can be obtained as follows: (1) by calculating composite curve-based area targets over a grid of operating points covering the uncertainty range, determine the maximum nominal area required throughout the range for each stream match (note that maximum area may occur at different operating conditions for each match); (2) add together the maximum areas required for each stream match to obtain an upper bound on the area required for the network. This procedure will generally overestimate the area required for a resilient HEN, since it does not take into account the fact that oversizing one match by a certain amount of area may save even more area in another match.

(2) Example 5.1 did not consider the number of units required for each size

uncertainty range. Extra units (beyond the number nominally required for each operating condition) are often required to achieve resilience, especially if the pinch jumps from one stream to another somewhere in the uncertainty range. Thus we expect step increases in the TAC as a function of uncertainty range size (Fig. 5.24) as the number of units suddenly increases.

For the simple example above (with only two uncertain parameters), one can superimpose pinch regions (regions of uncertain temperatures and flow rates where the same stream always causes the pinch, and where the stream populations above and below pinch are constant) in Figs. 5.2–5.12 by calculating composite curve-based area targets over a grid of parameters covering the uncertainty ranges. These pinch regions are similar to the regions in the "pinch behavior diagram" (Fig. 4.3) in Chapter 4, except that they should be determined for constant area, rather than for constant ΔT_m. By identifying the stream populations above and below the pinch in each of these pinch regions, one can determine the minimum number of units required to achieve the specified area in a given uncertainty range.

5.4 Summary; Suggestions for Future Research

In this chapter, we have introduced the use of HEN synthesis targets to predict, before synthesis, the trade-off between cost and resilience. We described an ideal procedure for analyzing the trade-off; however, because of difficulty in obtaining much of the required data (e.g., temporal uncertainty probability distributions), this procedure is, in general, impractical.

We also presented an example illustrating one crude procedure for predicting the cost–resilience trade-off. However, this procedure suffers a number of drawbacks:

- the extra area required for oversized exchangers is not considered;
- the increasing number of units required for larger uncertainty ranges is not considered;
- the graphical procedure is limited to problems with at most two uncertain parameters.

Research is needed to develop a general procedure for any number of uncertain parameters, for including the extra area of oversized exchangers, and for predicting the number of units required in a given uncertainty range.

At least two approaches to the units targeting problem (for any number of uncertain parameters) seem possible:

(1) Floudas and Grossmann (1987) use multiperiod optimization in conjunction with an active constraint strategy to target the number of units required for resilience, with fixed ΔT_m, in a specified uncertainty range when minimum utility consumption is required at selected discrete operating points. But the value of ΔT_m for minimum utility consumption changes with changing operating conditions when area is specified (as in Figs. 5.2–5.12). However, for varying ΔT_m, one still can guarantee feasible HEN operation thoughout an uncertainty range with the number of units given by Floudas' and Grossmann's algorithm if the smallest value of ΔT_m in the range is used in the algorithm. [This can be seen by considering variable ΔT_m in the proof in Appendix A of Floudas and Grossmann (1987).] Thus to determine a lower bound on the units

target for a given uncertainty range, one might use the lowest value of ΔT_m in the range. (For larger values of ΔT_m, fewer units cannot be used since tighter approach temperature constraints reduce the flexibility in choosing matches.) The difficulty is that this units target may be too conservative (i.e., may not reflect the effect of pinch shifts at higher ΔT_m), and the smallest value of ΔT_m may lie in the interior of the uncertainty range (especially when pinch shifts occur inside the range). It might be possible to locate the smallest value of ΔT_m by combining the composite curve-based area target with the active constraint strategy. The pinch location method of Duran and Grossmann (1986) might also be useful, especially for varying flow rates.

(2) Chapter 2 presented an area targeting NLP in which the number of matches (units) can be constrained. It might be possible to extend this area targeting NLP to variable temperatures and flow rates to determine the minimum number of units required to achieve a specified area target in a given uncertainty range. Floudas and Grossmann (1987) show that the utility targeting heat cascade (Section 2.3) can be extended to variable supply temperatures simply by defining temperature interval (TI) boundaries at the extremes of each supply temperature range. The area targeting heat cascade (Section 2.4.1) can be extended in the same manner. These extended heat cascades should be able to handle pinch shifts, since a shift in the pinch-causing stream merely causes the pinch location to change from one TI boundary to another; the utility and area targets can still be calculated from these heat cascades when the pinch location changes.

5.5 References

[1] Ahmad, S. and B. Linnhoff, Overall Cost Targets for Heat Exchanger Networks, paper presented at *IChemE Ann. Res. Mtg.*, Bath, U. K. (1984).

[2] Duran, M. A. and I. E. Grossmann, Simultaneous Optimization and Heat Integration of Chemical Processes, *AIChE J.*, **32**, 123 (1986).

[3] Floudas, C. A. and I. E. Grossmann, Synthesis of Flexible Heat Exchanger Networks for Multiperiod Operation, *Comp. Chem. Eng.*, **10**, 153 (1986).

[4] Floudas, C. A. and I. E. Grossmann, Synthesis of Flexible Heat Exchanger Networks with Uncertain Flow Rates and Temperatures, *Comp. Chem. Eng.*, **11**, 319 (1987).

[5] Jones, S. A., Methods for the Generation and Evaluation of Alternative Heat Exchanger Networks, Ph.D. Thesis, Eidgenössischen Technischen Hochschule (ETH), Zurich (1987).

Chapter 6

Conclusions

6.1 Conclusions and Suggestions for Future Research

The use of design targets for HEN synthesis is a very powerful approach to roughly optimize, before synthesis, the economic trade-offs between utilities, area, and number of units, and to "initialize" the solution of the HEN synthesis problem (e.g., to choose appropriate values for ΔT_m and the utility loads, to identify the stream populations above and below the pinch, and to decompose the synthesis problem at the pinch). The objective of this thesis has been to present improved targets for synthesis of HENs for fixed operating conditions, and new targets to synthesize resilient HENs for varying, uncertain operating conditions. In this thesis, we have presented:

- improved area and capital cost targets for synthesis of HENs for fixed operating conditions

- a resilience target to predict, given the nominal operating conditions and a fixed value of ΔT_m (or a range of values for ΔT_m), the largest uncertainty range for which a "practical" HEN (with few more units or stream splits than that required for nominal operating conditions) can be synthesized
- a procedure for predicting the trade-off between cost and resilience

In Chapter 2, we presented area and capital cost targeting NLPs which can be used to predict the trade-off between area and number of units for fixed operating conditions, and to rigorously predict area and cost targets even with unequal heat transfer coefficients. In particular, these NLPs can predict area and cost targets for HEN synthesis problems with constraints on the number of matches/units, forbidden matches, unequal heat transfer coefficients, and different capital cost laws for each stream match. In addition, by requiring the presence of selected matches with specific areas, area and capital cost targets can be calculated for revamp synthesis.

The solutions of the area and capital cost targeting NLPs provide an excellent starting point for synthesis of HENs achieving (within a few percent) the targets. In particular, the matches and heat loads given by the NLP solutions provide a good starting point for formulation and optimization of a HEN superstructure as used in the computer program MAGNETS (Floudas *et al.*, 1986). The "spaghetti" network corresponding to the NLP solutions also provides a good starting point for evolutionary development. However, the networks synthesized by MAGNETS often contain unnecessary bypasses which increase, slightly, the network area and cost. And use of evolutionary development to simplify the spaghetti structure is generally an *ad hoc* procedure. Research on more systematic methods to take advantage of the

matches, loads and temperatures given by the area and capital cost targeting NLP solutions could lead to improved algorithms for synthesis of minimum-area HENs with a wide range of heat transfer coefficients (e.g., HENs with phase change) and with restrictions on stream matches (e.g., due to safety, operability, start-up, or layout considerations, etc.).

Chapter 4 presented a Class 1 resilience target to predict the largest uncertainty range for which a practical HEN can be synthesized. This resilience target can also be used to predict whether trade-offs (in utilities, number of units, or size of uncertainty range) must be made in order to achieve resilience, and to identify the operating point and constraint most likely to limit resilience. For simple problems with few uncertain supply temperatures and flow rates, the Class 1 resilience target can be determined by plotting the composite temperature-enthalpy curves for different values of the uncertain parameters. For more complicated problems, the Class 1 resilience target can be calculated by an NLP which models the composite curves.

Finally, Chapter 5 introduced the problem of predicting, before synthesis, the trade-off between cost and resilience so that a process engineer can design for an economically "optimal" amount of resilience. We also presented a crude procedure for predicting this trade-off.

As summarized in Table 6.1, much research has been performed to develop HEN synthesis targets for fixed operating conditions. For fixed conditions, the process engineer can predict the trade-offs between utilities, area, and number of units, and can combine the targets to predict overall cost (total annualized cost target). These targets are correlated with each other by means of a common parameter, ΔT_m.

Table 6.1: Research on HEN synthesis targets for fixed and varying, uncertain operating conditions.

Synthesis Target	*Nominal HENs for Fixed Operating Conditions*	*Flexible HENs for Discrete Periods of Operation*	*Resilient HENs for a Range of Operating Conditions*
Utilities	Hohmann (1971) Raghavan (1977) Linnhoff and Flower (1978) Umeda *et al.* (1978) Papoulias and Grossmann (1983) Cerda *et al.* (1983) O'Young *et al.* (1988)	Floudas and Grossmann (1986) Jones (1987)	Floudas and Grossmann (1987) Chapter 5
Number of Units	Hohmann (1971) Cerda and Westerberg (1983) Papoulias and Grossmann (1983)	Floudas and Grossmann (1986)	Floudas and Grossmann (1987)
Area	Hohmann (1971) Nishida *et al.* (1971) Raghavan (1977) Nishimura (1980) Townsend and Linnhoff (1984) Chapter 2	Jones (1987)	Chapter 5
Cost	Ahmad and Linnhoff (1984) Chapter 2	Jones (1987)	Chapter 5
Resilience	(not applicable)	(not applicable)	Townsend and Morari (1984) Chapter 4

Much less research has been performed to develop synthesis targets for varying or uncertain operating conditions. The work of Floudas and Grossmann (1986, 1987) and Townsend and Morari (1984) is restricted to constant ΔT_m. However, the economically optimal value of ΔT_m varies as operating conditions change. The resilience target in Chapter 4 can be extended to a range of ΔT_m, but it is difficult to predict that range before calculating the resilience target. Jones (1987) parameterized the synthesis targets for flexible HENs in terms of area, and allowed ΔT_m to vary to satisfy given area. Jones (1987) calculated the utilities and area required to minimize total annualized cost (TAC) for a specified amount of flexibility. Because the synthesis targets for flexible (or resilient) HENs cannot be parameterized in terms of fixed (independent of operating conditions) ΔT_m, it is difficult to decouple the utility, area, and number of units targets. Instead, it is more natural to determine, simultaneously, the utility consumption, area, and number of units that minimizes TAC. Thus, even though Jones (1987) determined utilities and area simultaneously, we list his contributions as separate utility, area and cost targets in Table 6.1. Research is still needed to predict the number of units needed to satisfy given area and a specified amount of flexibility (i.e., given periods of operation).

A major goal of this research has been to extend the HEN synthesis targets to resilient HENs. For resilient HENs, the targets should also be parameterized in terms of area rather than ΔT_m. This is the approach taken in Chapter 5 to predict the resilience–cost trade-off. As for flexible HENs, it is more natural to determine the utilities, area, and number of units which simultaneously minimize TAC, rather than to calculate separate utility, area and units targets. To improve the targets for resilient

HENs, research is needed to develop:

- better methods to predict the minimum area needed to achieve resilience throughout a given uncertainty range, including the extra area required in exchangers oversized to achieve resilience
- methods to predict the minimum number of units needed to satisfy specified area throughout a given uncertainty range
- better methods to predict the resilience–cost trade-off which can handle an arbitrary number of uncertain supply temperatures and flow rates
- methods to include uncertainties in the heat transfer coefficients

Lastly, one final comment concerning the distinction between HEN resilience and flexibility. As defined by Grossmann and Morari (1983), resilience deals with *undesirable* changes and upsets. Thus steady-state resilience deals with long-term change (such as fouling) and uncertainty, and the ability to reach a new steady state after an upset. Flexibility, on the other hand, deals with the ability to adjust to *desired* changes, such as feedstock changes, product specification changes, etc. Thus, as noted in Section 4.1 [and in Jones (1987)], resilience generally deals with a continuous range of operating conditions (an uncertainty range), while flexibility generally deals with discrete operating conditions (periods of operation). The changes in operating conditions due to flexibility requirements are generally much larger than those due to process disturbances and uncertainty (resilience). However, many researchers seem to have applied resilience techniques to large operating ranges of the size required for flexibility, rather than of the size required to deal with process disturbances and

uncertainties. That is, they not only require a HEN to operate for the operating conditions associated with feedstock and product changes, etc., but also for intermediate operating conditions which might never be encountered. The situation more commonly encountered in the process plant is a combination of the flexibility and resilience problems—several discrete operating points occurring for different feedstocks, product specifications, etc., with relatively small uncertainty ranges surrounding each discrete point. Research is needed to deal with this combined resilience-flexibility problem.

6.2 References

[1] Ahmad, S. and B. Linnhoff, Overall Cost Targets for Heat Exchanger Networks, paper presented at *IChemE Ann. Res. Mtg.*, Bath, U. K. (1984).

[2] Cerda, J. and A. W. Westerberg, Synthesizing Heat Exchanger Networks Having Restricted Stream/Stream Matches Using Transportation Problem Formulations, *Chem. Eng. Sci.*, **38**, 1723 (1983).

[3] Cerda, J., A. W. Westerberg, D. Mason and B. Linnhoff, Minimum Utility Usage in Heat Exchanger Network Synthesis: A Transportation Problem, *Chem. Eng. Sci.*, **38**, 373 (1983).

[4] Floudas, C. A., A. R. Ciric and I. E. Grossmann, Automatic Synthesis of Optimum Heat Exchanger Network Configurations, *AIChE J.*, **32**, 276 (1986).

[5] Floudas, C. A. and I. E. Grossmann, Synthesis of Flexible Heat Exchanger Networks for Multiperiod Operation, *Comp. Chem. Eng.*, **10**, 153 (1986).

[6] Floudas, C. A. and I. E. Grossmann, Synthesis of Flexible Heat Exchanger Networks with Uncertain Flow Rates and Temperatures, *Comp. Chem. Eng.*, **11**, 319 (1987).

[7] Grossmann, I. E. and M. Morari, Operability, Resiliency and Flexibility—Process Design Objectives for a Changing World, paper presented at *2nd Int. Conf. on Found. of Computer-Aided Process Design*, Snowmass, CO (1983).

[8] Hohmann, E. C., Optimum Networks for Heat Exchange, Ph.D. Thesis, Univ. Southern California, Los Angeles (1971).

[9] Jones, S. A., Methods for the Generation and Evaluation of Alternative Heat Exchanger Networks, Ph.D. Thesis, Eidgenössischen Technischen Hochschule (ETH), Zurich (1987).

[10] Linnhoff, B. and J. R. Flower, Synthesis of Heat Exchanger Networks: I. Systematic Generation of Energy Optimal Networks, *AIChE J.*, **24**, 633 (1978).

[11] Nishida, N., S. Kobayashi and A. Ichikawa, Optimal Synthesis of Heat Exchange Systems: Necessary Conditions for Minimum Heat Transfer Area and Their Application to Systems Synthesis, *Chem. Eng. Sci.*, **26**, 1841 (1971).

[12] Nishimura, H., A Theory for the Optimal Synthesis of Heat Exchanger Systems, *J. Opt. Th. Appl.*, **30**, 423 (1980).

[13] O'Young, D. L., D. M. Jenkins and B. Linnhoff, The Constrained Problem Table for Heat Exchanger Networks, *Understanding Process Integration II*, IChemE Symp. Ser. 109, 75 (1988).

[14] Papoulias, S. A. and I. E. Grossmann, A Structural Optimization Approach in Process Synthesis—II. Heat Recovery Networks, *Comp. Chem. Eng.*, **7**, 707 (1983).

[15] Raghavan, S., Heat Exchanger Network Synthesis: A Thermodynamic Approach, Ph.D. Thesis, Purdue Univ., Lafayette, IN (1977).

[16] Townsend, D. W. and B. Linnhoff, Surface Area Targets for Heat Exchanger Networks, paper presented at *IChemE Ann. Res. Mtg.*, Bath, U. K. (1984).

[17] Townsend, D. W. and M. Morari, Resiliency of Heat Exchanger Networks: An Objective Compatible with Minimum Cost, paper presented at *AIChE Ann. Mtg.*, San Francisco (1984).

[18] Umeda, T., J. Itoh and K. Shiroko, Heat Exchange System Synthesis, *Chem. Eng. Prog.*, **74**, 7, 70 (July 1978).